

DESIGN OF RENEWABLE AMINES FOR PHOTOCHEMICAL CARBON DIOXIDE REDUCTION

EDWARD JAMES HOLLAND

A THESIS SUBMITTED FOR THE DEGREE OF DOCTOR OF
PHILOSOPHY

SCHOOL OF CHEMISTRY

CARDIFF UNIVERSITY

JANUARY 2014

TABLE OF CONTENTS

Table of Contents	ii
List of Figures.....	vi
List of Tables.....	x
Acknowledgements	xi
Abstract	xiii
Chapter 1 – Introduction	1
Global Warming.....	1
Evidence for Global Warming.....	1
The Climate Model	3
The Greenhouse Effect	7
Renewable Energy	11
Introduction.....	11
Types of Renewable Energy.....	11
The “Hydrogen Economy”	13
Photosynthesis	15
Introduction.....	15
Light Reactions	16
Dark Reactions.....	17
Lessons Learnt	18
Photochemical Water splitting	18
Introduction.....	18
Overview of Mechanism.....	19
Design Strategies	22
Visible Light Active Catalysts	22
Photochemical CO ₂ Reduction.....	24

Introduction.....	24
Semiconductor Catalyst.....	25
Molecular Catalysts	28
Chapter 2 – Previous Work.....	34
Introduction.....	34
Mechanisms of CO ₂ Reduction	35
Chapter 3 – Computational Methods.....	48
Quantum Chemistry	48
Formulation	48
Hartree-Fock.....	49
Post Hartree-Fock.....	51
DFT.....	53
Chapter 4 – Design of Renewable Amines.....	54
First Generation Amines.....	54
Introduction.....	54
Nitrogen Substituted Amines	55
Grob Fragmentation	57
Stabilised Amines	59
Second Generation Amines	61
Introduction.....	61
Radical Stabilisation Energy.....	62
Stabilising Substitutions	64
Phenyl Based Substituents	67
Rate Calculations	70
Introduction.....	71
Results	72
Conclusions.....	73

Photochemical Stability	73
Introduction.....	73
Alkene Addition	74
DMAP Based Amines	81
Introduction.....	81
Constrained DMAP Amines.	82
Conclusions.....	83
Chapter 5 – Synthesis of Renewable Amines	84
First Generation Amines.....	84
Synthesis of Amine Framework.....	84
Deoxygenation.....	86
Synthesis of DMAP Based Amines	97
Synthetic Routes.....	97
Addition to Ethers.....	99
Addition to Halides	101
Addition to Ketones.....	107
Conclusions.....	109
Chapter 6 – Computational studies on [3+4] Cycloadditions	110
Introduction.....	110
Literature Examples.....	112
Computational Study	116
Potential Energy Surface	121
Conclusions.....	122
Chapter 7 – Quantum Chemistry Interface - QCI	123
Introduction.....	123
Design Requirements	123
Technologies Used.....	125

Interface Design	127
Example Calculation	129
Implementation Details.....	131
Example Project.....	134
Conclusions.....	137
Epilogue.....	138
References.....	139
Appendix 1 – Experimental Details.....	150
General Experimental.....	150
<i>Tert</i> -butyl 11-azatricyclo[4.3.1.1 ^{2,5}]undecane-11-carboxylate	151
11-Methyl-11-azatricyclo[4.3.1.1 ^{2,5}]undecane	152
<i>Tert</i> -butyl 10-methylene-11-azatricyclo[4.3.1.1 ^{2,5}]undecane-11-carboxylate	153
(1 <i>R</i> ,4 <i>S</i>)-7-(Pyridin-2-yl)bicyclo[2.2.1]heptan-7-ol.....	154
(1 <i>R</i> ,4 <i>S</i>)-7-(4-(Dimethylamino)pyridin-2-yl)bicyclo[2.2.1]heptan-7-ol	155
6-Chloro-1-pyrrolidinocyclohexene ^[135]	157
<i>Tert</i> -butyl 10-oxo-11-azatricyclo[4.3.1.1 ^{2,5}]undec-3-ene-11-carboxylate ^[132]	158
<i>Tert</i> -butyl 10-oxo-11-azatricyclo[4.3.1.1 ^{2,5}]undecane-11-carboxylate ^[132]	159
(1 <i>R</i> ,4 <i>S</i>)-Bicyclo[2.2.1]hepta-2,5-dien-7-yl 2,2,2-trifluoroacetate ^[172a]	160
(1 <i>R</i> ,4 <i>S</i>)-7-(<i>Tert</i> -butoxy)bicyclo[2.2.1]hepta-2,5-diene ^[173]	161
(1 <i>s</i> ,4 <i>s</i>)-7-Chlorobicyclo[2.2.1]hepta-2,5-diene ^[172e]	162
(1 <i>R</i> ,4 <i>S</i> ,7 <i>s</i>)-Bicyclo[2.2.1]hept-2-en-7-ol ^[172b, c]	163
(1 <i>R</i> ,4 <i>S</i> ,7 <i>r</i>)-7-Iodobicyclo[2.2.1]hept-2-ene ^[172c]	163
(1 <i>s</i> ,4 <i>s</i>)-bicyclo[2.2.1]heptan-7-one ^[172d]	164
(1 <i>s</i> ,4 <i>s</i>)-7-Iodobicyclo[2.2.1]hepta-2,5-diene ^[172f]	165
Appendix 2 – Quantum Chemistry Interface Source Code.....	166
main.py.....	166
Classes.py	171

LIST OF FIGURES

Figure 1: Global Average Temperature.	1
Figure 2: Historic CO ₂ Records From Ice Core Data.	3
Figure 3: Global Energy Production by Source. Data from ^[38b, 39]	11
Figure 4: Global Renewable Energy Production in TWh. Data from ^[38b, 39]	12
Figure 5: Schematic Diagram of the Photosynthetic Z Scheme. Reproduced from ^[53]	16
Figure 6: The "Dark" reactions or The Calvin Cycle	17
Figure 7: Common semi-conductor bandgaps against water splitting redox potentials. reproduced from ^[62]	20
Figure 8: Mechanisms of Photochemical Processes in Semiconductors. Reproduced from ^[1]	21
Figure 9: Proposed Mechanism for Re based catalysts	29
Figure 10: Artificial Photosynthesis Schematic.....	34
Figure 11: Overall Artificial Photosynthesis.....	34
Figure 12: Enthalpy Profile for CO ₂ reduction with Triethylamine. Reproduced from ^[129]	36
Figure 13: Proposed Mechanism for H Atom transfer	37
Figure 15: Isotopic Labelling Studies on CO ₂ reduction with Triethylamine	39
Figure 16: Newly Proposed Mechanism for CO ₂ Reduction	40
Figure 17: Mechanisms for H Atom Loss from <i>n</i> -Butylamine Radical Cation	41
Figure 18: Tolerance of Bicyclic Amine to α Hydrogen Atoms	42
Figure 19: Mechanism of H/D Exchange in Bicyclic Amines	44
Figure 20: Retrosynthetic Analysis of Tricyclic Amine	44
Figure 23: Synthesis of Tricyclic Amine From Cycloaddition Product.....	46
Figure 24: CO ₂ Reduction and Renewal with Tricyclic Amine.....	47
Figure 25: Mechanism of CO ₂ Reduction in Tricyclic Amine.....	54
Figure 26: Mechanism of Grob Fragmentation	57
Figure 27: Mechanism of CO ₂ Reduction in Second Generation Amines	62
Figure 28: Graph of RSE Against Differences in Reaction Enthalpy ($R^2 = 0.822$)	66

Figure 29: Graph of RSE against Activation Energy	67
Figure 30: Reaction Parameters for Phenyl Substituted 2Nd Gen Amines (Kcal mol ⁻¹).....	69
Figure 31: Graph of Activation Energy against Reaction Enthalpy for a Series of Ph Substituted Second Generation Amines.....	70
Figure 32: Mechanism for Addition of Amine Radical cation to Alkene.....	74
Figure 33: Mechanism for CO ₂ Reduction in DMAP Based Amines.....	82
Figure 34: Formation of Enamine for Cycloaddition	84
Figure 35: Formation of Double Addition Product in Enamine Formation.....	84
Figure 36: Formation of Tricyclic Amine by [4+3] Cycloaddition.....	85
Figure 37: Hydrogenation of Cycloadduct.....	86
Figure 38: Schematic Representation of Wolff-Kishner Reaction	87
Figure 39: Mechanism of Wolff-Kishner Reduction.....	87
Figure 40: Kishner Scheme for Complete Reduction of Ketones.....	87
Figure 41: Wolff Scheme for Complete Reduction of Ketones.....	88
Figure 42: Huang–Minglon Modification to The Wolff-Kishner Reduction	88
Figure 43: Attempted Wolff-Kishner Reduction.....	90
Figure 44: Attempted High Pressure Wolff-Kishner Reduction.....	90
Figure 45: Attempted Formation of Tosyl Hydrazone	91
Figure 46: Proposed Mechanism for Clemmensen Reduction of benzophenone	92
Figure 47: Literature Example of Clemmensen Reduction in a Sterically Hindered System ...	93
Figure 48: Literature Example of Clemmensen Reduction in A Nitrogen Containing Compound	93
Figure 49: Clemmensen Reduction of Tricyclic Amine under Forcing Conditions.....	94
Figure 50: Optimised Clemmensen Reduction of Tricyclic Amine.....	94
Figure 52: Reduction of CO ₂ with Unsubstituted Tricyclic Amine	96
Figure 53: Schematic Tebbe Olefination	96
Figure 54: Tebbe Olefination of Tricyclic Amine	97
Figure 55: Attempted Synthetic Route to DMAP AMINes	97

Figure 56: Literature Example of Addition of Grignard Reagents to 7-OtBu-Norbornadiene	98
Figure 57: Production of Precursors From 7-OtBu-Norbornadiene	99
Figure 58: Synthesis of 7-OtBu-Norbornadiene	100
Figure 59: Attempted formation of DMAP Based Amine from 7-OtBu-Norbornadiene	100
Figure 60: Synthesis of 7-Chloro-Norbornadiene	101
Figure 61: Attempted Reactions from 7-Chloro-Norbornadiene	102
Figure 62: Finkelstien Reaction of 7-Chloro-Norbornadiene	103
Figure 63: Attempted Reactions from 7-Iodo-Norbornadiene	103
Figure 64: Synthesis of 7-Iodo-Norbornene	104
Figure 65: Attempted Synthesis of 7-Acteo-Norbornadiene	104
Figure 66: Possible Mechanisms of Formation of 7-Acteo-Norbornadiene	105
Figure 67: Synthesis of 7-Trifluoroaceto-Norbornadiene	105
Figure 68: Synthesis of Syn-Norbornene-7-ol	106
Figure 69: Mechanism of Alkene Reduction by LiAlH_4	106
Figure 70: Synthesis of 7-Iodo-Norbornene	106
Figure 71: Attempted Reactions with 7-Iodo-Norbornene	107
Figure 72: Synthesis of 7-Oxonorbornane	107
Figure 73: Reactions with 7-Oxonorbornane	108
Figure 74: Methylation of a DMAP Based Amine	109
Figure 75: Illustrative Retrosynthetic Analysis	110
Figure 76: Possible Cycloaddition Transition States	111
Figure 77: Products Formed from Possible [3+4] Cycloaddition Transition States	111
Figure 78: A Tethered Starting Material for [4+3] Cycloaddition	112
Figure 79: Literature Example of Amino Allyl Cation in Intramolecular [3+4] Cycloaddition	112
Figure 80: Literature example of Oxyallyl Cation in Intramolecular [3+4] Cycloaddition	113
Figure 81: Literature Example of a Intramolecular [3+4] Cycloaddition	113
Figure 82: Literature Computational Study of reaction between oxy-allyl cation and Pyrrole	114

Figure 83: Literature Example of a [4+3] Cycloaddition Studied by DFT	115
Figure 84: Equations Used to Calculate Global Electrophilicity Index	115
Figure 85: Formation of Amino Allyl Cation For Cycloaddition	117
Figure 86: Optimised Geometry For Chloride	117
Figure 87: Optimised Geometry For Amino Allyl Cation	118
Figure 88: Proposed Starting Materials For Synthesis of Second Generation Amines	119
Figure 89: Proposed Mechanims For [4+3] Cycloaddition.....	119
Figure 90: Reaction Profile For Synthesis of Second Generation Amines	121
Figure 91: Example Reaction Scheme for quantum chemistry interface	129
Figure 92: Example invocation of Quantum Chemistry interface	129
Figure 93: Example job submission with quantum chemistry interface.....	129
Figure 94: Example analysis of reaction with quantum chemistry interface	130
Figure 95: Example output from calculation analysis in quantum chemistry interface	131
Figure 96: Example reaction anaylsis in quantum chemistry interface.....	131
Figure 97: Example output from reaction analysis in quantum chemistry interface	131
Figure 98: Reaction Scheme for Diels Alder Calculations	135

LIST OF TABLES

Table 1: Global Warming Potential Data. Reproduced from ^[8c]	9
Table 2: Change in Greenhouse Gas Concentration Since 1750. Reproduced from ^[31]	9
Table 3: Isotopic Labelling Study Results.....	39
Table 4: Reaction Parameters for Tricyclic Amine (Kcal mol ⁻¹)	55
Table 5: Reaction Parameters for N Substituted Tricyclic Amines (Kcal mol ⁻¹)	56
Table 6: Reaction Parameters for Unsubstituted Tricyclic Amine (Kcal mol ⁻¹)	58
Table 7: Reaction Parameters for 7-Substituted Tricyclic Amines (Kcal mol ⁻¹)	59
Table 8: Reaction Parameters for Stabilised Tricyclic Amines (Kcal mol ⁻¹)	60
Table 9: Reaction Parameters for Second Generation Amine (Kcal mol ⁻¹)	64
Table 10: Reaction Parameters Substituted Second Generation Amines (Kcal mol ⁻¹)	65
Table 11: Results of Rate Constant Calculations at 298 K (S ⁻¹)	73
Table 12: Reaction Parameter for Cyclisation of First Generation Amine (Kcal mol ⁻¹)	75
Table 13: Reaction Parameters for Cyclisation of Second Generation Amine (Kcal mol ⁻¹)	75
Table 14: Reaction Parameters for Cyclisation of Alkene Constrained 2nd Gen Amines (Kcal mol ⁻¹)	77
Table 15: Reaction Parameters for Cyclisation of Amine Constrained 2nd Gen Amines (Kcal mol ⁻¹)	78
Table 16: Reaction Parameters for Cyclisation of Backbone Constrained Second Generation Amines (Kcal mol ⁻¹)	79
Table 17: Reaction Parameters for Cyclisation of Electronically Constrained Amines (Kcal mol ⁻¹)	80
Table 18: Reaction Parameters for DMAP Based Amines (Kcal mol ⁻¹)	82
Table 19: Possible Synthons For Production of DMAP Based Amines.....	98
Table 20: Reaction Parameters for Synthesis of Second Generation Amines (Kcal mol ⁻¹)	120
Table 21: Student Results Generated with Quantum Chemistry Interface (Kcal mol ⁻¹)	136

ACKNOWLEDGEMENTS

First and foremost I would like to thank Barry Carpenter, my supervisor, for taking me on as a student and his continued help and support both academically and personally. Over the last few years I have learnt a great deal from Barry and I'm glad I was given the chance to work with him.

As with any research project success would have been impossible without an excellent group of peers. I am very grateful for all members of the POC for both social and professional interactions. Jamie, Niek, Azzedine, Julia, Larry and Rob deserve a special mention, but it was a pleasure to work with everyone who visited the POC over the years.

No chemistry department would function without their support staff, but our staff not only managed to keep things running smoothly but also kept a jovial attitude throughout. Thanks to Rob and Robin for all their help with NMR and MS, to Gaz and Jamie for keeping us well stocked, to Alun, JC and Mal for keeping all our machinery in working order and finally to all the office staff for keeping the paperwork under control for us!

Finally I must thank all my friends and family for always keeping me motivated, without this I may never have finished writing! You have all been amazing over the last 7 years; I wouldn't have made it this far without you.

ABSTRACT

This thesis extends investigations into renewable amines for photochemical CO₂ reduction by the Carpenter group. This work is motivated by a desire to provide solutions for green energy production.

Modifications to the tricyclic amine, **20**, were studied computationally using DFT calculations. These studies suggest that there are no simple modifications to this class of amines that will offer significantly improved properties for CO₂ reduction. A second class of amines is then proposed in which radical stabilization groups can be introduced to promote the desired photochemistry. From this class of amines the phenyl derivative, **34**, was identified as the best candidate. Rate calculations predict that distonic radical cation formation will not present a bottleneck in the reaction scheme. A synthesis of this class of amines is proposed and supporting DFT calculations indicate that it is a viable synthesis. Using the leads from computational studies synthetic work was undertaken to find a synthetic route to amines, **14** + **66**. The routes developed are capable of producing the desired amines but need to be optimized for full-scale photochemical studies.

The final chapter presents a tool named Quantum Chemistry Interface that is designed mainly as a teaching tool for computational chemistry. It facilitates rapid generation of libraries of substituted molecules. It also understands a simple language for describing reaction steps to automate calculations of reaction thermodynamic parameters. Its utility is shown with a small project with an undergraduate student.

CHAPTER 1 – INTRODUCTION

GLOBAL WARMING

EVIDENCE FOR GLOBAL WARMING

Perhaps the most important challenge facing society today is one of climate change. The evidence for climate change is overwhelming, and although there is still much political scepticism from some quarters, the role of human activity is undeniable. Here is discussed the available evidence for climate change, these data have been drawn from numerous sources, some allowing measurement of ancient climates. This is particularly important as it allows deconvolution of human influence and natural climate change.

The most fundamental evidence for climate change is from direct measurements of global average temperature. Over a century of instrumental data have been collected by Hansen and co-workers who have then collated these data for analysis of global average temperature, the results of this study and others are shown in Figure 1.^[2] This graph shows that average global temperatures are rising; Hansen calculates an average current heating effect of 0.2 °C per decade, and 0.7 °C over the previous decade, which indicates a trend that the heating effect is accelerating. Care must be taken to question if this trend can be explained by natural climatic variation. Unfortunately surface temperature data has only been reliably collected for the last century so a direct comparison cannot be made; instead we must use “proxy” paleoclimate data. Analysis of these proxy data shows us that the earth is within 1 °C of its maximum during the last million years. The combination of these two metrics is evidence that the current rapid global warming effect is not part of a normal climatic cycle.

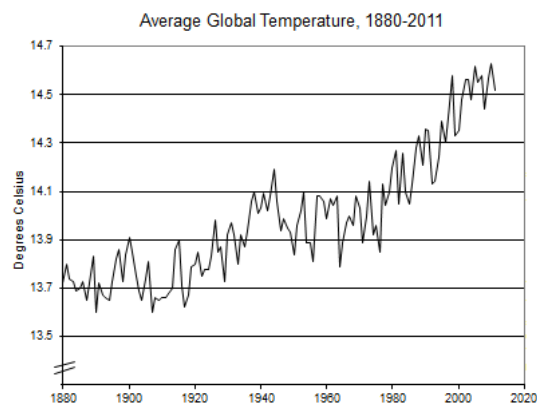


FIGURE 1: GLOBAL AVERAGE TEMPERATURE.

The Earth's surface is not the only place we can measure the heating effect, the oceans have also been undergoing a heating effect, albeit at a much slower rate than the surface temperature. Levitus^[3] reviewed this effect in 2009 and found a warming of approximately 0.1 °C since 1969 for the upper 2000 ft of water. This effect seems small when compared to surface temperature changes but we must consider that water has a significantly higher heat capacity than surface land, and there are many ocean currents redistributing the absorbed energy throughout the entire ocean depth. Further evidence can be found in the changes in sea level. These rises in sea level are indicative of a global warming due to thermal expansion and increased melt water. Data is available^[4] for sea levels over the last century: there has been a rise of around 17 cm in the last century, but the rate of change has doubled during the last decade. This acceleration indicates that the effect does not represent a normal climatic variation and supports rapid recent climate change. Confirmation of this evidence can be sought by considering the source of the extra water; thermal expansion alone cannot explain a change in sea levels of that magnitude so melt water must play a significant role. If melt water is a large factor then we should be able to observe reduction in global ice levels.

Measurements of the levels of ice globally all agree that immense amounts of ice are melting each year, and not being replenished in the colder seasons. NASA satellite data shows the Greenland and Antarctic ice sheets lost over 300 cubic kilometres between 2002 and 2006,^[5] this trend is repeated in almost all glacial areas as reported by Dyurgerov^[6] in 2005. The extent of Arctic ice cover is also in decline, falling by around 2.5% per decade. The combination of this evidence again supports a global warming hypothesis, and indicates that the rate of change is accelerating rapidly.

Perhaps the most important evidence for anthropogenic climate change is the atmospheric carbon dioxide level record.^[7] Analysis of Antarctic ice cores allows extremely accurate measurement of paleoclimate carbon dioxide levels by sampling trapped air pockets. The longest ice cores give data throughout an 800,000-year period during which carbon dioxide concentrations fluctuate between approximately 200 ppm (during ice ages) and 300 ppm (during interglacial periods). As shown in Figure 2 this has formed a fairly consistent pattern throughout ancient history, this situation starts to change after the last Ice Age, but it is not until the start of the industrial revolution that concentrations start to increase exponentially. By the 1950s atmospheric carbon dioxide levels had reached levels (over 300 ppm) not seen during the last 800,000 years, and the rate of change shows no sign of slowing. This evidence is particularly important as it allows direct comparison to paleoclimate datum; this means

we may refute the possibility of high atmospheric carbon dioxide levels being a normal feature of the Earth's recent climate. Furthermore these data sets not only provide us with evidence that anthropogenic climate change is a real effect but it also suggests a mechanism for the change: the greenhouse effect.

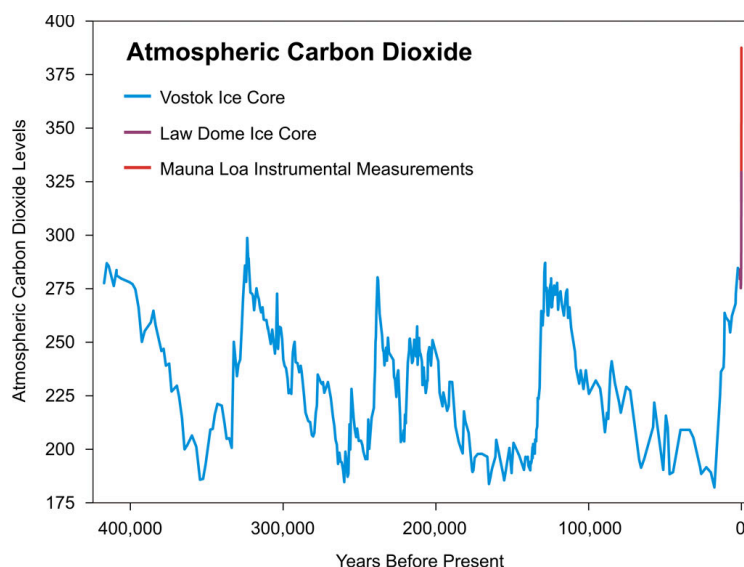


FIGURE 2: HISTORIC CO₂ RECORDS FROM ICE CORE DATA.

The preceding section briefly outlines the most important evidence for climate change, and provides compelling evidence that this climate change is beyond what should be considered normal variation of the climate system. However this can by no means be considered a complete review of the scientific literature around this subject, and interested readers are referred to the following references for a more complete analysis.^[8] The following quote is taken from the Intergovernmental Panel on Climate Change and concisely states the position of the scientific community as a whole

"Scientific evidence for warming of the climate system is unequivocal." – IPCC ^[8b]

THE CLIMATE MODEL

The issue of climate change is a complicated one, with many interacting factors, both natural and anthropogenic. This makes a complete analysis very challenging, and climate change prediction is an on-going research topic. Here is presented a simplified model for understanding the key processes of climate change.

Climate is a long-term statistical measure of the weather, that is, the temperature, humidity, atmospheric pressure, wind, precipitation and possibly other counts such as atmospheric particulate levels. A region's latitude, terrain, nearby water bodies and currents in both the air and the oceans, determine its climate. Climate change is defined as a statistically

significant change in overall weather patterns over an extended period, normally 30 years.^[9] The change could be a shift in the average, for example a slow increase of average temperatures, or a change in the distribution around the average, for example increased occurrences of El Niño events. Many use the term “climate change” to refer only to anthropogenic climate change. This however is inaccurate and should be avoided. It can become especially confusing when examining the causes of climate change as natural and anthropological causes are often intertwined in complex manners that may be inseparable.

Considering the earth as an equilibrium system in which energy is received from the sun and lost through radiative processes into space, then climate change is a consequence of an imbalance in these two processes. The change in global average temperature can be used as an indicator as to the extent of climate change. Weather is essentially a consequence of the uneven distribution of solar irradiance over the surface of the earth, and the constant struggle to reach equilibrium. So for a simplistic model of climate change we must consider factors that affect the levels of incoming or outgoing radiation, forcing mechanisms, and how the system reacts to these factors, typically called feedbacks. For example an external forcing mechanism could be a large volcanic eruption that releases a large volume of small particulates and the feedback would be a sudden cooling due to reduced radiation reaching the earth. Forcing mechanisms can be further categorized into radiative, affecting total amount of radiation, and non-radiative, affecting distribution of radiation.

Mechanisms of Global Warming

External forcing mechanisms are those that act from outside the climate system. The most significant external forcing factor is variation in the Earth’s orbit and is known as Milankovitch theory.^[10] Milankovitch proposed that changes in the orbit affected the distribution and amount of solar irradiance and this could be used to explain significant climatic events, for example Ice Ages.

The solar constant is a measure of the total solar energy flux over all wavelengths at a distance of 1 AU on a plane perpendicular to the incident rays. This is effectively a measure of the suns output without including factors such as Milankovitch cycles. The variation measured is around 0.1% and this is calculated to induce a temperature change of around 0.03 °C.^[11] Although this effect has often been reported in popular media close examination of the data suggests that this effect does not play a significant role in climate change.

Internal forcing mechanisms act from within the climate system, including factors such as geological changes, effect of ocean currents and atmospheric composition. These forcing

mechanisms are often dependent on the state of other parts of the climate system; so complicated relationships exist between them. This can lead to unpredictable changes in response to a forcing mechanism.

One of the most dramatic geological events is volcanic activity; during an explosive eruption masses of dust and gases are released into the atmosphere. Material expelled during an eruption can reach the stratosphere where it may persist for many years, and spread to cover the entire earth. The effect of a large volcanic event is two-fold, an immediate reduction in solar radiation due to reflection and a more long-term release of greenhouse gases. For typical eruptions the cooling effect is around $0.1 - 0.2\text{ }^{\circ}\text{C}$ ^[12] and lasts only a few years without supporting feedback. This is not a large enough effect to play a significant role in climate change. The release of greenhouse gases is also an important factor when considering the consequences of volcanic activity.

The oceans are hugely important in our climate system as they cover a large proportion of the earth's surface, and have a huge heat capacity; this means they can store an immense amount of energy and help to regulate climate change. The large currents that transport water globally throughout the oceans are known as thermohaline circulations and are driven by density gradients. ^[13] The gradient is formed by both changes in temperature and salinity. Other smaller currents exist but are driven by forces such as wind and tidal power and are typically only surface currents, in contrast to thermohaline currents that span the entire depth of the ocean. These deep ocean currents have a powerful moderating effect, as they contain huge volumes of water and circulation times can be several hundred years. This allows them to store immense amount of heat, and slow any rapid climate change.

The movement of tectonic plates is also an internal forcing mechanism, mostly due to position of mountain ranges and related volcanic activity. ^[14] The effects are either radiative or non-radiative respectively. It is important to recognize that the geological timescales involved in these processes are far too long to explain the sudden change in climate we have observed in recent years. Air currents are important machinery in distributing solar energy around the earth, so disruption of these currents may have worldwide effects. Ocean currents also play a large role in redistribution of solar energy, albeit on a much longer time scale than air currents, so the positions of the continents play a very similar role to that of the mountain ranges mentioned above. This effect is on huge geological time scales so offers little in the way of explanation of recent, rapid climate change.

The final forcing mechanism to be considered here is probably the most significant, variation in atmospheric composition. ^[15] The natural greenhouse effect is hugely important in regulating our climate, and it is likely without this effect Earth would have never become hospitable for human life. ^[16] However the greenhouse effect has a significant influence on amount of outgoing radiation, so can easily tip the balance towards a global warming situation. The greenhouse effect is discussed in more detail below.

Climate Feedback Mechanisms

As mentioned above, the forcing mechanisms are only part one of the story; the climate feedback responses are the link between forcing mechanisms discussed above and the climate we experience. These feedbacks can be split into positive feedback, which reinforces the original change, and negative feedback, which opposes the original movement. ^[8b] These feedback mechanisms can help explain extreme weather events that cannot be solely attributed to forcing mechanisms.

Global warming triggers a number of processes that create a positive feedback loop. One of most important feedback mechanisms is the release of carbon-based gases into the atmosphere from various sources. Carbon-based gases are often very powerful greenhouse gases, for example methane and carbon dioxide, and so their release increases the greenhouse effect. There are many frozen carbon sinks that are in danger of releasing huge amounts of volatile carbon compounds, including giant Siberian peat bogs, ^[17] underwater methane clathrate deposits, ^[18] dissolved carbon dioxide in arctic ice sheets. ^[19] There is also a mass of carbon stored in organic matter, such as forests, fossil fuel reserves, and peat bogs. Global warming can accelerate processes such as deforestation, desertification, peat decomposition and forest fires, all of which can contribute to the total carbon in the atmosphere at any given time. Intensive farming has also contributed a significant proportion of our greenhouse gas emissions when the whole food production chain is considered. ^[20]

Another important positive feedback mechanism is the Ice-albedo effect. ^[21] As ice is highly reflective, much of the radiation received in areas of high ice coverage is not absorbed. However, as this ice melts through global warming processes it is replaced by sea or land than is significantly less reflective. This creates a positive feedback loop in which a slight warming effect can be amplified. This effect is often cited as the reason for arctic temperatures rising more rapidly than the rest of the world.

There are also a number of negative feedback mechanisms we must consider; the most obvious is probably the blackbody radiation effect.^[22] According to the Stefan-Boltzmann equation the amount of radiated heat will increase with the fourth power of temperature, so as the Earth warms it will radiate more heat out to space. It is also expected that cloud cover can play a role in negative feedback loops. Surface warming increases evaporation, which in turn increases the amount of cloud cover. This cloud cover increases the albedo of the earth,^[23] reducing the amount of incoming radiation and producing a cooling effect from a heating cause.

Atmospheric carbon dioxide levels are modulated by Le Chatelier's principle, which, in this context, predicts that as carbon dioxide levels increase in the atmosphere the position of the equilibrium is expected to shift towards more carbon dioxide being dissolved in the oceans.^[24] It is predicted that on geological time scales approximately 75% of emitted CO₂ will dissolve into the oceans and seas.

It should now be clear why climate science can be such a complicated issue; we have only considered a simple model for climate change and already there are a staggering number of interactions. It is this complexity that has allowed those with ulterior motives to fudge the scientific facts and divert the attentions of policy makers. However the most striking conclusion from this model is that while human activity has certainly had a huge impact on climate change, the areas we have influenced are mostly limited to atmospheric composition and, less importantly, changing land uses. Therefore, if we wish to counter anthropogenic climate change then there is only one method within our reach: adjusting atmospheric composition to reduce the greenhouse effect. Given this conclusion it seems prudent to examine the processes involved in the greenhouse effect more closely.

THE GREENHOUSE EFFECT

The greenhouse effect is the name given to the global heating effect of gases trapped in the atmosphere. The “greenhouse” gases are transparent to short-wave solar radiation,^[8b] but absorb the longer wave radiation emitted by the Earth; the absorbed IR radiation is then reemitted in all directions causing a net heating effect when compared to situation in the absence of greenhouse gases. Although this effect has only become well known within the last few decades the phenomenon was originally proposed almost 200 years ago,^[25] and quantified by Arrhenius at the turn of the 20th century.^[26] The greenhouse effect is an important geothermal process; without which it is unlikely the Earth could support human life. If the Earth is modelled as a simple thermally conductive blackbody which reflects ~ 30%

of incoming radiation, then the predicted surface temperature is around $-18\text{ }^{\circ}\text{C}$.^[8b] The actual surface temperature is $33\text{ }^{\circ}\text{C}$ above this simple estimate; this difference is attributed to the greenhouse effect.

A greenhouse gas is defined as an atmospheric gas that absorbs and emits infrared radiation^[8b].^[8b] As discussed above, this property is what causes the heating effect. The major greenhouse gases in Earth's atmosphere include water vapour, carbon dioxide, methane, nitrous oxide and ozone.^[8b] The most abundant gases in the atmosphere are not greenhouse gases as cannot absorb IR radiation, and therefore can not retransmit trapped energy back to the earth's surface. However, some non-greenhouse gases can have an indirect effect. For example carbon monoxide can scavenge radicals that would otherwise react with methane decreasing its atmospheric lifetime.^[27] The atmospheric concentrations of these gases are dependent on the balance between emissions and sinks. Since the dawn of the industrial era the balance has been strongly shifted towards increasing emissions and increasing atmospheric concentrations.^[8b]

To assess the influence of a gas on the greenhouse effect we must consider more than just the concentration, we must also consider factors like atmospheric lifetime and its direct radiative effect. Atmospheric lifetime is defined as average time that a molecule of a particular gas lasts in the atmosphere between being released and removed from the atmosphere, through chemical reaction, deposition or moving out of the system. All greenhouse gases, except water vapour, are long-lived species that completely mix with the atmosphere and take years to be removed from the atmosphere.

We can define a variable, global warming potential (GWP),^[28] as a measure of the total influence of a particular gas on the total greenhouse effect. All GWPs are measured relative to carbon dioxide that is defined as 1 over all timeframes.^[29] GWPs are normally quoted over 20 year, 100 year and 500-year periods. A gas with high direct radiative effect and a short life time would have a high GWP over the 20 year period, but this would fall for the 100 year and 500 year case. Table 1 shows a table of GWPs of common greenhouse gases.^[30] It should be noted that carbon dioxide is regarded as the weakest greenhouse gas over all time periods, but we must take care to consider concentrations of each gas in the atmosphere. The highest GWP given is for perfluoroethane; however, its atmospheric concentration is only 3 ppt compared to 394 ppm carbon dioxide, and so it has a relatively small influence on global warming.

Species	Chemical formula	Lifetime (years)	Global Warming Potential (Time Horizon)		
			20 years	100 years	500 years
CO ₂	CO ₂	variable	1	1	1
Methane	CH ₄	12±3	56	21	6.5
Nitrous oxide	N ₂ O	120	280	310	170
HFC-23	CHF ₃	264	9100	11700	9800
Perfluoromethane	CF ₄	50000	4400	6500	10000
Perfluoroethane	C ₂ F ₆	10000	6200	9200	14000
Perfluoropropane	C ₃ F ₈	2600	4800	7000	10100

TABLE 1: GLOBAL WARMING POTENTIAL DATA. REPRODUCED FROM ^[8C]

Table 2 shows how atmospheric concentration of greenhouse gases have changed between 1750 and 1998,^[28, 31] and the total radiative forcing (a direct measure of the energetic effect of a process on the atmosphere) from each gas. It is clear from this table that carbon dioxide is the biggest contributor to the greenhouse effect. Now we have identified the key mechanisms for global warming (greenhouse effect), and understood the contributing factors to this mechanism we should seek to understand why there has been such an increase in greenhouse gases and what we can do to reverse the situation.

Gas	Pre-1750 tropospheric concentration	Recent tropospheric concentration	Absolute increase since 1750	Percentage increase since 1750
Carbon dioxide	280 ppm	392.6 ppm	112.6 ppm	40.2%
Methane	700 ppb	1874 ppb	1174 ppb	167.7%
Nitrous oxide	270 ppb	324 ppb	54 ppb	20.0%
Ozone	25 ppb	34 ppb	9 ppb	36%

TABLE 2: CHANGE IN GREENHOUSE GAS CONCENTRATION SINCE 1750. REPRODUCED FROM ^[31]

Since the dawn of the industrial revolution there has been a marked increase in all major greenhouse gases,^[32] as shown in Table 2. This is largely caused by increased energy

demands and increased industrial activity; natural greenhouse gas emission makes up less than 1% of total emissions today.

One class of greenhouse gases that is undeniably anthropogenic, is the halocarbons.^[33] These compounds were originally used as refrigerants, aerosol propellants, and industrial solvents. Unfortunately the high stability that makes them ideal for these purposes also ensures a long atmospheric lifetime of these gases. This coupled with their strong absorbances in the IR region make the halocarbons strong greenhouse gases with very high global warming potentials. The use of such chemicals is now strongly regulated and atmospheric concentrations are now falling. This is largely thanks to strong media attention into their ozone depleting properties and the Montreal Treaty.^[34]

Methane is an important greenhouse gas, and although its atmospheric lifetime is significantly shorter than carbon dioxide its global warming potentials is around 20 over a 100-year period. The most significant sources are natural gas extraction, intensive livestock breeding and landfills. Together these sources account for around 70% of total anthropogenic methane emissions. The remaining 30% of methane emissions are from sources such as rice farming, manure management, coal mining, wastewater treatment and petroleum infrastructure.

The most significant anthropogenic greenhouse gas is carbon dioxide. Lashof calculated that carbon dioxide contributes 80% of the warming effect of greenhouse gas emissions between 1980 and 1990, noting that this figure is 23% higher than the previous decade.^[35] Natural sinks have been balancing natural emissions sources for millennia. However recent anthropogenic emissions have tipped this balance. This has led to the increasing atmospheric carbon dioxide since around 1750. The main sources of anthropogenic CO₂ are the emissions from burning fossil fuels and cement production, which the IPCC report are together responsible for around 75% of the increased carbon dioxide concentrations since 1750.^[36] Changing land uses, such as deforestation, irrigation, and fertilisation, are have also contributed to increased CO₂ concentrations. Not only do these practices emit CO₂ they also reduce the ability of the land to act as a carbon dioxide sink.

Around 50% of carbon dioxide emissions come from transport fuels and power stations,^[37] another 20% comes from industrial processes, and the remaining 30% is from fossil fuel extraction, changing land uses and residential sources. From this evidence and that presented above it should be clear that our dependence on fossil fuels is the key factor in

the rapid climate change we are currently undergoing and the only hope in controlling it is to reduce emissions and sequester CO₂ from the atmosphere.

RENEWABLE ENERGY

INTRODUCTION

As presented in the previous chapter greenhouse gas emissions are the primary cause of global warming, and since demand for energy is unlikely to fall we must find ways of producing energy without producing more greenhouse gases if we wish to live sustainably into the future. In 2011 over 80% of the world's energy was produced from fossil fuels,^[38] as shown below in Figure 3. To replace the current non-renewable infrastructure with renewable alternatives they must be capable of operating at massive scale. This report now outlines the major renewable energy sources, how they are used today and how they could be used to mitigate the effects of global warming.

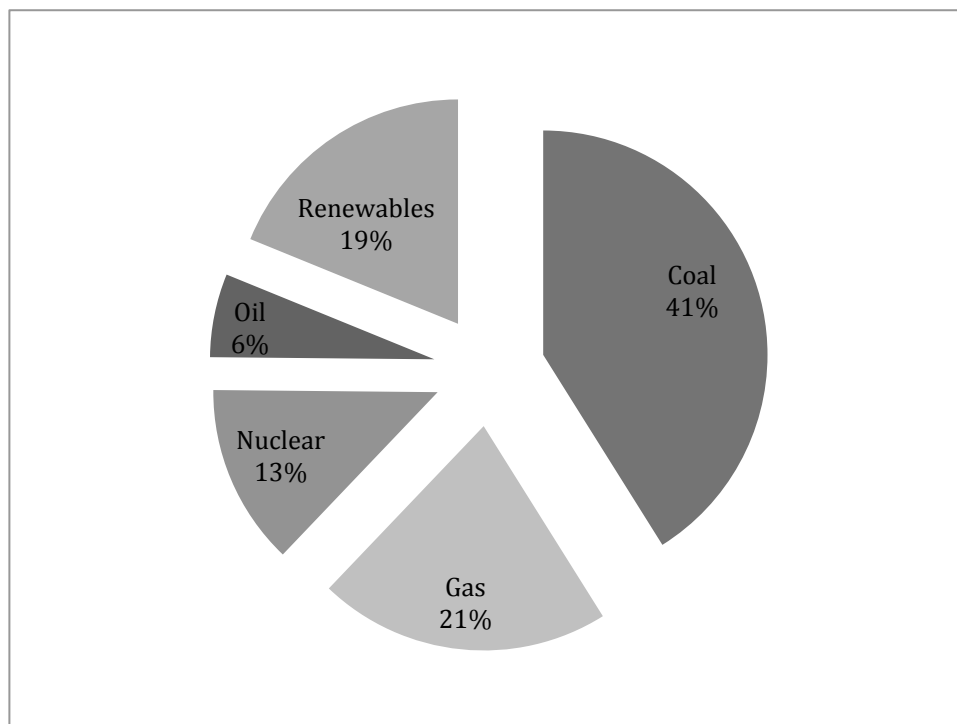


FIGURE 3: GLOBAL ENERGY PRODUCTION BY SOURCE. DATA FROM ^[38B, 39]

TYPES OF RENEWABLE ENERGY

The largest contributor to renewable sources is hydropower, at 16% of total energy production, Figure 4. Hydropower exploits the potential energy of stored masses of water to drive turbines, the massive scale of the plants needed to obtain economic feasibility make infrastructure costs huge. Hydropower stations sometimes flood huge valleys, which have

often been inhabited in past projects. The displacement of people has made these projects unpopular and concerns have been raised about the ecological impact on local wildlife. Most of the feasible products in developed countries have already been exploited.^[39] As such continued growth will require less economically developed countries to invest in significant projects.

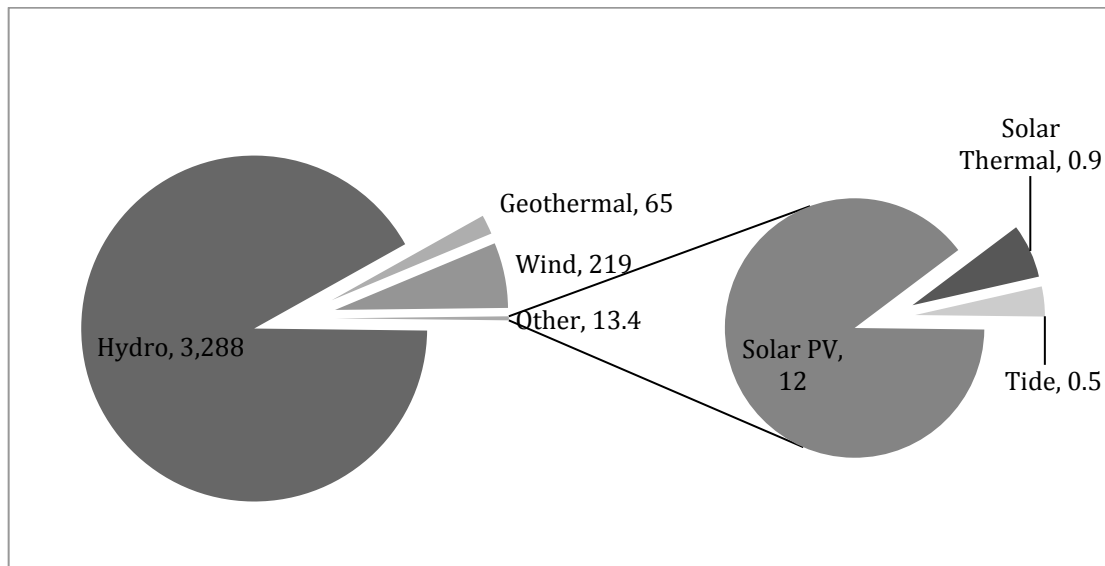


FIGURE 4: GLOBAL RENEWABLE ENERGY PRODUCTION IN TWH. DATA FROM ^[38B, 39]

Wind power is the process of collecting wind energy and converting it into more useful forms of energy. Typically wind energy is used to power turbines that produce electricity, which is fed into the national grid. Large-scale wind farms can contain hundreds of wind turbines, and are often placed offshore or in remote locations to minimise potential aesthetic objections. The main problem associated with wind power is the variable nature of wind currents,^[40] a network based mostly of wind energy would either have to devise methods of storing energy on scale or have backup generators for times of low wind. Not only are the on-going costs of wind generated electricity very low, the initial infrastructure costs are now lower per watt than traditional coal and gas fired power stations.^[41]

Although one of the smallest sources of renewable energy currently by far our largest renewable resource is the sun. The earth receives 3,850,000 exajoules per year energy in solar irradiation a year.^[42] At 10% collection efficiency approximately 0.1% of the Earth's surface would need to be covered by solar collectors to provide all the world's energy. This demonstrates the staggering amount of solar radiation we receive. How to effectively capture and convert this into useful energy is the challenge.

Current solar technology is broadly split into two categories namely: solar photovoltaics, which directly convert solar photons into an electrical current, and solar thermal technologies, which utilise the sun's energy to heat water; this hot water can then be used directly for heating or to generate steam for powering turbines.

Traditionally solar thermal energy has been the primary method of electricity production from solar sources.^[44] In giant solar plants, arrays of mirrors collect and concentrate the sun's energy into a central point. At this point the sunlight is concentrated to around 70 times ambient levels, this energy is used to heat water to steam, which is then used to drive turbines. Electricity produced at these plants is comparable in cost with traditional coal-fired electricity generation.

Photovoltaics are the types of solar cells that most people are familiar with, due to their appearance in consumer electronics. These cells directly convert solar photons into an electrical current. Typical commercial devices have efficiency between 5% and 20% but the latest research cells have been reported as up to 44% efficient.^[45] Photovoltaic cells have extremely low maintenance costs once installed so the electricity they produce can also be very cheap, depending on the infrastructure cost of installation. This balance between cost and efficiency still sees many inefficient amorphous silicon solar panels being installed today, although dye sensitised cells are starting to reach market.

THE "HYDROGEN ECONOMY"

These current renewable sources are competitive with traditional fossil fuel powered electricity production, however around a quarter of our total energy usage stems from transportation. Unless there is a revolution in battery technology it seems unlikely that electrically powered transport will become commonplace. This leads to the conclusion that the world will either remain dependent on oil reserves for transportation or we have to develop a new fuel for transportation.

The so-called "hydrogen economy" has often been proposed as the solution.^[46] The idea is fairly simple; replace fossil fuels with hydrogen gas. The main advantage to this is that the combustion of hydrogen only produces water as a product; this has obvious benefits when considering greenhouse gas emissions.¹ In most "hydrogen economy" models hydrogen is envisioned being consumed in fuel cells to provide electricity that can then be used to drive motors, but more traditional fuel based motors could also be designed.

¹ If one excludes water as a greenhouse gas, justification explained in more detail below

One issue often overlooked by proponents of a “hydrogen economy” is the energy density of hydrogen gas. There are two commonly quoted figures for energy density MJ/Kg and MJ/L,^[47] the first being weight based and the second volume based. If you consider hydrogen gas in the first measure you find the highest value of any common fuel (123 MJ/KG) this is mostly due to the sheer number of moles of hydrogen in a kilogram rather than a particularly weak H-H bond, or a tendency to form particularly strong bonds. If however you consider the second measure, based on volume, quite a different picture arises, the energy density is only 5.6 MJ/L compared with 34 MJ/L for petrol. This means that an equivalent engine would require 6 times the volume of hydrogen (pressurised at 800 bar) than petrol for a journey. If a global economy based on hydrogen becomes a reality then significantly more efficient engines would also need to be developed. Another concern is safety; while petrol certainly isn’t the safest fuel available, its risks are ones we have learnt to manage over the years we’ve used it. Highly pressurised hydrogen involves an entirely new set of risks that would have to be managed,^[48] development of hydrogen cylinders capable of withstanding high-speed car crashes would be vital.

For a “hydrogen economy” to be a green technology the hydrogen must be produced using renewable source of both energy and hydrogen. This means that the hydrogen must be eventually evolved from water. Plants in photosynthesis undertake the biggest scale water splitting on the planet, but plants have learnt that hydrogen isn’t a suitable fuel for their needs. So instead they funnel the electrons and hydrogen atoms derived from water splitting into carbon dioxide, thus producing carbohydrate fuels. While our energy needs wouldn’t be well served by mass scale carbohydrate productions perhaps we can take inspiration from natural photosynthesis and develop a carbon based, transportable fuel from carbon dioxide.

If we could develop an artificial photosynthesis that was capable of oxidising water and reducing carbon dioxide while producing a dense, transportable fuel then we could envision a carbon neutral economy based on solar irradiation.

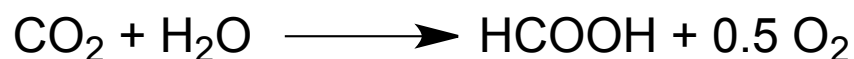
PHOTOSYNTHESIS

INTRODUCTION

Photosynthesis is the process by which plants capture the sun's energy and convert it into chemical energy, stored as carbohydrates.^[49] In total, the process takes carbon dioxide and water to produce sugars and oxygen. Although this process may appear simple it is actually a finely balanced system in which each part of the extremely complex machinery must play its role. This machinery has evolved over millions of years so the thermodynamics of each step drives the process forward. Almost all life depends on photosynthesis to provide the chemical energy used in respiration and aerobic life relies on the oxygen produced as a waste product in the reaction. There are innumerable different organisms that can photosynthesise but the key process is the same in almost all known cases. Light is collected in the light-harvesting centre; this energy is used to oxidise water and the electrons derived from water are then funnelled into carbon dioxide to produce organic compounds. This process first evolved around 3500 million years ago,^[50] and the fundamental process has changed little since. A complete discussion of photosynthesis is beyond the scope of this thesis, and so the focus will be on the lessons we can learn from natural photosynthesis to apply more generally to artificial photosynthesis.

In natural photosynthesis the overall reaction is split in to a number of smaller reactions,^[51] each with their own enzymatic machinery. This means that each step can be separately optimised with little effect on any of the other steps. It also means reactions that are kinetically unfavourable can be avoided by taking an alternative pathway.

Both water and carbon dioxide are very stable molecules so any direct reaction between them is likely to face a large thermodynamic barrier, so the first separation that the natural photosynthetic machinery makes is oxidation of water and reduction of carbon dioxide. The separate stages are normally known as the "light reactions", for water splitting, and the "dark reactions", for the production of fuels from carbon dioxide. The overall reduction of carbon dioxide by water is thermodynamically uphill. Even in the case of the two-electron reduction to formic acid, shown below, the reaction is endergonic by 270 KJ mol⁻¹. For the 4-electron reduction to glucose the situation is even more unfavourable being endergonic by 480 KJ mol⁻¹. By separating the reaction in to many steps photosynthesis can drive the unfavourable reaction forward with several photons.



LIGHT REACTIONS

The light reactions are, unsurprisingly, those reactions that are driven by the absorption of photons. The light reactions are summarized in the “Z Scheme”, shown below in Figure 5.^[52]

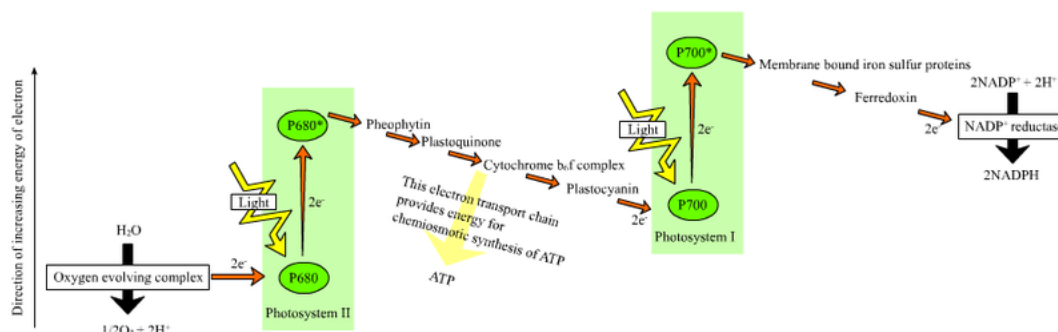


FIGURE 5: SCHEMATIC DIAGRAM OF THE PHOTOSYNTHETIC Z SCHEME. REPRODUCED FROM ^[53]

The reaction starts by the absorption of a visible photon in Photosystem II. This promotes an electron to an excited state that is then quenched by pheophytin.^[54] Pheophytin passes this electron along the electron transport chain in the process creating a proton gradient across the chloroplast membrane. Photosystem II is now deficient by one electron; this hole is filled by water oxidation in the oxygen-evolving complex. When the electron finally reaches Photosystem I much of its energy has been used in producing the proton gradient or irreversibly lost to the environment. Here a second photon is absorbed promoting the electron to a highly energetic state that passes through a short chain of electron acceptors before reducing ferredoxin. NADP⁺ reductase then uses two reduced ferredoxin molecules to reduce one NADP⁺ to one NADPH. The proton gradient developed during the electron transport chain is used to drive production of ATP. During these light reactions 2 photons are used to split water and produce two chemical energy stores, ATP and NADPH.

The oxygen-evolving complex is still shrouded in mystery with regards to exact mechanistic details but what is clear is that the active site contains 4 manganese atoms, 1 calcium atom and a tyrosine residue.^[55] It is thought that Photosystem II can excite the manganese cluster through various oxidation states, known as S states.^[56] The manganese cluster donates electrons to the oxidised Photosystem II, each time becoming more oxidised itself, until it reaches S₄. Once at S₄ the manganese cluster oxidises two water molecules, returning the cluster to its S₀ state and releasing oxygen and protons.

DARK REACTIONS

The second half of photosynthesis is known as the “dark reactions” or the “light independent reactions”, shown in Figure 6.^[57] This is the process in which ATP + NADPH are used to reduce carbon dioxide to organic molecules. This process is also known as the Calvin cycle and overall produces 3-carbon sugars that in turn can be converted into higher sugars and carbohydrates. The process starts with a 5 carbon sugar,^[58] ribulose-1,5-bisphosphate, the RuBisCO enzyme and one CO₂ molecule. The enzyme catalyses the carboxylation of ribulose-1,5-bisphosphate with carbon dioxide, this gives an unstable 6 membered sugar which quickly breaks down into two molecules of 3-phosphoglycerate. The 3-carbon sugars are then phosphorylated by ATP (from the light reactions) to produce 1,3-bisphosphoglycerate; these are then reduced by NADPH (again, from the light reactions) to give glyceraldehyde 3-phosphate. It is this glyceraldehyde 3-phosphate that goes on to produce complex sugars and carbohydrates. To complete the cycle, 5 of the 6 glyceraldehyde 3-phosphate produced are used to reform the 5-membered-ring sugar, ribulose-1,5-bisphosphate. This takes 3 molecules of ATP (once again, from the light reactions). In total 3 carbon dioxide molecules with 9 ATP and 6 NADPH are required to produce one molecule of glyceraldehyde 3-phosphate, 9 ADP, 9 inorganic phosphate and 6 NADH⁺.

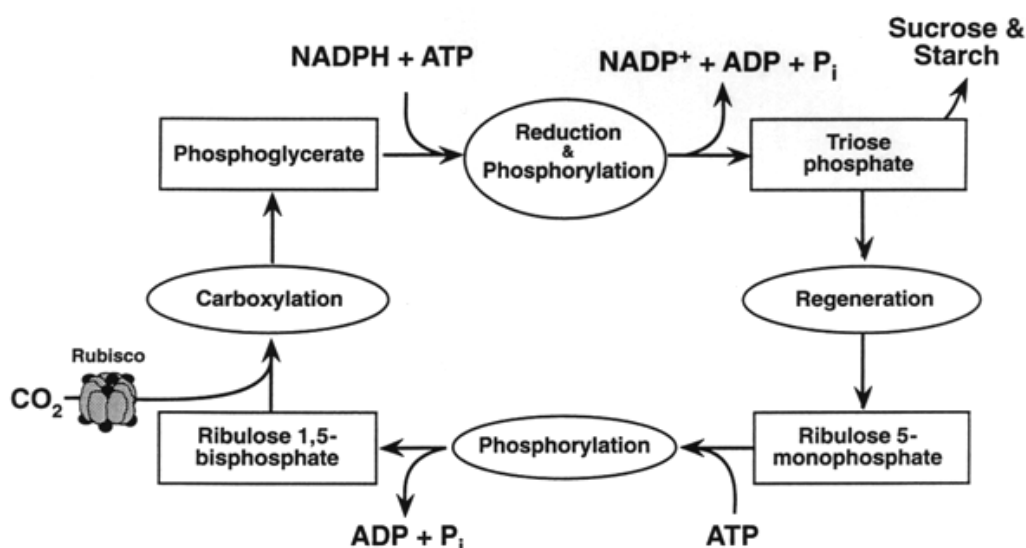


FIGURE 6: THE "DARK" REACTIONS OR THE CALVIN CYCLE

LESSONS LEARNT

Overall photosynthesis has taken carbon dioxide and water and utilised solar energy to convert them into high-energy fuels. As discussed in the previous section there are many reasons why an artificial mimic of this process would be beneficial, so we must ask the question: what lessons can we learn from natural photosynthesis? Firstly it is important to recognise that natural evolution is the product of millions of years of evolution and as such the machinery that makes this possible is vastly complicated. This complicated network of enzymes and proteins adapts itself for each step to ensure optimum conditions. It is worth highlighting at this point that natural photosynthesis has an efficiency that is typically less than 5%.^[59]

The first feature that is noticeable is the separation of water oxidation and CO₂ reduction.^[60] Water splitting occurs within the oxygen-evolving complex, the electrons derived from this are used to generate a renewable reducing agent (NADPH) and a high-energy fuel molecule (ATP). In separate steps carbon dioxide is fixed and converted into stable fuel molecules. The benefit of this separation are the avoidance of direct reaction of water and carbon dioxide, which allows the possibility of entirely different enzymatic frameworks to promote each reaction. The use of a renewable reducing agent allows the coupling of the two reactions without affecting the overall process. Another key feature of natural photosynthesis is the multi-photon nature of the process, 4 photons are used to generate the S4 state in the oxygen-evolving complex, and more photons are then used to boost the energy of the electrons in Photosystem I. It is this fact that allows photosynthesis to use visible light; any single photon process would require UV photons.

In summary natural photosynthesis suggests that we should separate the difficult reactions of water splitting and carbon dioxide reduction, couple them with a renewable reducing agent and design the process to utilise more than one photon

PHOTOCHEMICAL WATER SPLITTING

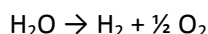
INTRODUCTION

The field of photocatalytic water splitting was founded by Fujishima and Honda in the early 70s with the observation that a photoelectrochemical cell with one TiO₂ electrode and another Pt electrode under UV irradiation and an external bias produces both hydrogen and oxygen gases.^[61] This seminal work proved the possibility of water splitting, and laid the groundwork for many years of research to come. Before we delve into the details of the

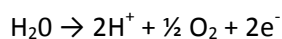
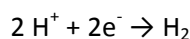
recent advances in this field it is important that we understand the physical processes involved.

Firstly it is worth highlighting that water is transparent to visible light, this may seem obvious, but it has an important consequence; no direct photochemical decomposition of water is possible with solar photons. As there is no hope of designing useful water splitting based on any excited state of water we must look for photocatalysts that can affect the water splitting in an indirect manner.

The overall equation for water splitting is given by:



However this reaction is actually the sum total of two separate reactions.



The reaction occurs by oxidation of water to molecular oxygen and protons; these protons are then separately reduced to molecular hydrogen using the electrons from the first process. The overall reaction is endothermic by 237 kJ mol^{-1} , so converts light energy to chemical energy. For this reason photochemical water splitting is often referred to as artificial photosynthesis.

OVERVIEW OF MECHANISM

Since the pioneering work of Fujishima and Honda, the vast majority of photochemical water splitting technology has been based around semiconductors. For this reason it is worth investigating the mechanism of water splitting with semiconductors and studying the thermodynamic constraints for a suitable photocatalysts. As with most applications of semiconductors the key process is the promotion of an electron from the valence band to the conduction band. In the case of photochemical water splitting, the promotion is effected by the absorption of a photon. This leaves a hole (h^+) in the valence band and a photoelectron (e^-) in the conduction band. These holes and electrons must then migrate towards the surface where they are available to interact with either water or protons. Charge recombination is an unproductive pathway that will be minimised in a successful catalyst.

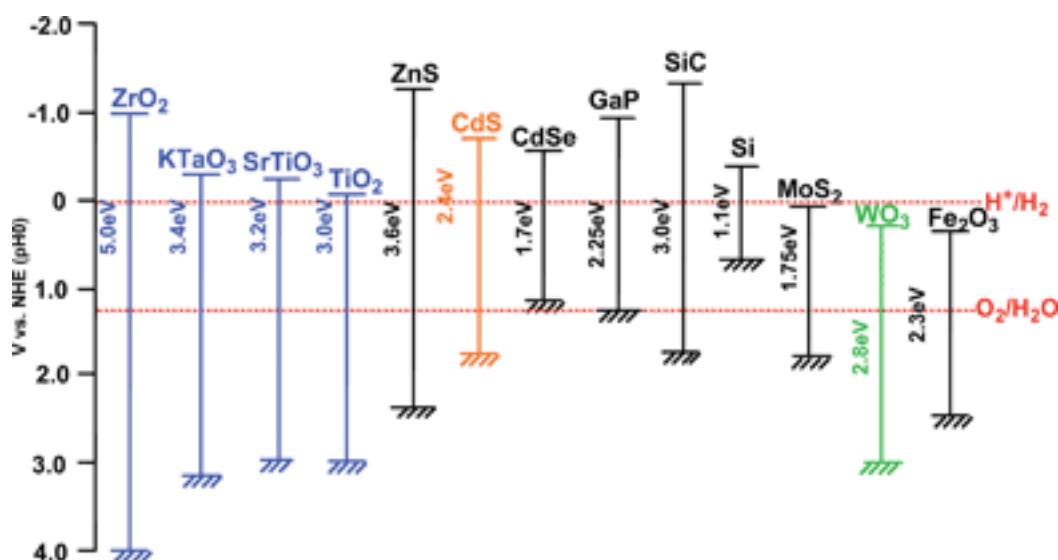


FIGURE 7: COMMON SEMI-CONDUCTOR BANDGAPS AGAINST WATER SPLITTING REDOX POTENTIALS. REPRODUCED FROM ^[62]

For successful proton reduction the conduction band edge of the photocatalyst must be higher than that of the standard hydrogen electrode (0.00 V), and for successful water oxidation the valence band edge must be more positive than 1.23 V. The above diagram, Figure 7, shows a variety of semi-conductors with appropriate band gaps to be considered for photochemical water splitting properties.^[62] This indicates that a successful photocatalyst will have band gap of greater than 1.23 eV, which corresponds to a wavelength of around 1000nm. This means that theoretically around 70% of solar photons would be available for water splitting; this of course implies that all this energy can be used effectively and none is lost to the environment. In practice successful catalysts normally have band gaps of around 2 eV.^[63] These thermodynamics constraints to catalyst design are fairly simple, and indicate a wide range of materials might be useful for photochemical water splitting but there are further constraints to bear in mind. The material should have good capacity for separating holes and electrons,^[64] it must minimise the recombination process,^[65] and reduce losses due to electron and hole transport.^[66] The kinetics of electron transfer at the solid liquid interface must be fast enough to compete with recombination and other unproductive reaction channels.^[67] Furthermore the photocatalyst must be resistant to photo-corrosion during the reaction, as well as being cheap and easy to synthesise.

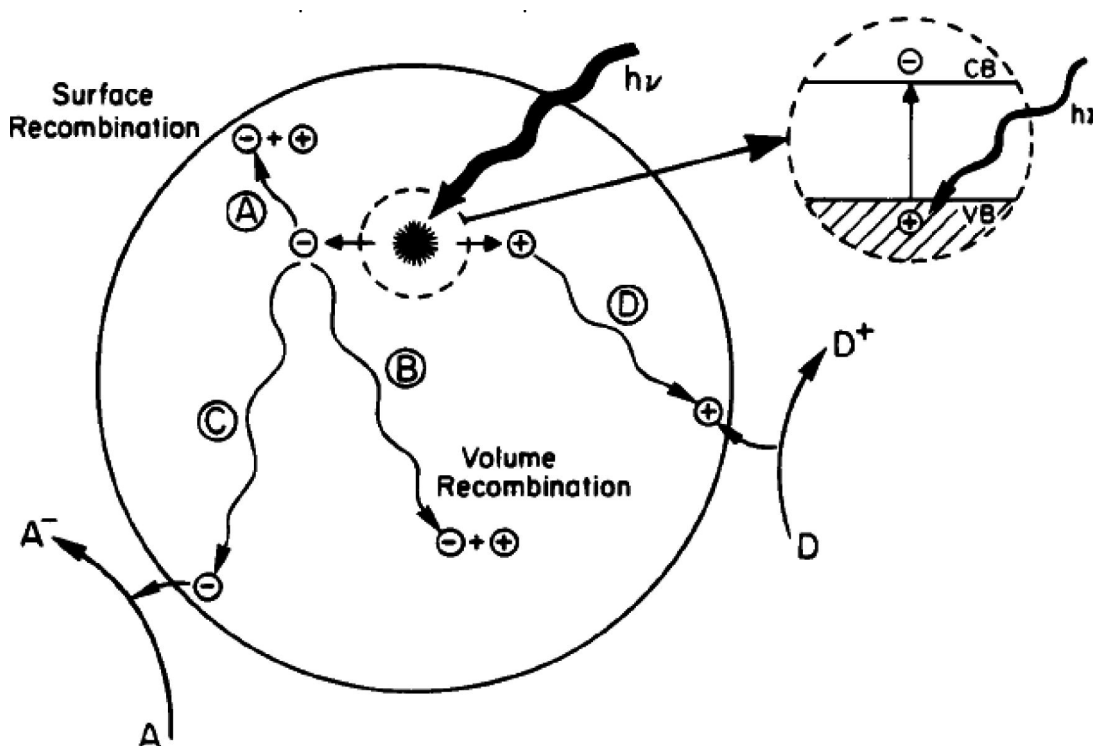


FIGURE 8: MECHANISMS OF PHOTOCHEMICAL PROCESSES IN SEMICONDUCTORS. REPRODUCED FROM ^[1]

The issue of charge recombination is fundamentally important if one wishes to design efficient photocatalysts, as this is the main unproductive pathway available to the excited photocatalyst. To understand how to reduce recombination rates it is important to understand mechanisms by which holes and electrons are produced, how they travel to the catalyst surface, how they react with molecules at the interface and finally how they can recombine. The diagram below, Figure 8, shows a simple schematic for the photochemical processes. In brief, a photon excites an electron in the bulk material and produces an electron-hole pair. The hole and the electron can then migrate through the bulk by repeated charge transfer reactions until they reach the surface where they can interact with molecules at the interface.

When an electron-hole pair is formed it is prevented from immediate recombination as the electron has the wrong energy. However there are many mechanisms by which electrons may lose this excess energy, they may emit a photon or they lose energy by processes akin to internal conversion and intersystem crossing. If this energy loss happens on a timescale shorter than electron-hole diffusion then recombination rates will be high. Defect sites can trap electron and holes for relatively long periods,^[68] this prevents them reaching the

surface where they do productive chemistry, and instead the trapped states dissipate their energy and eventually recombine. Particle size also plays an important part in this process.^[69] If the average radius of a semiconductor particle is smaller than the average diffusion length then a high number of electron-hole pairs should be available for productive photochemistry.

DESIGN STRATEGIES

Since the work of Honda,^[61] in the early 1970s, with UV light there have been many investigations into photochemical splitting with visible light but there have only been a handful of successful strategies.^[70] The band-gap engineering strategy involves manipulating the electronic structure of the semiconductor so that it can absorb in the visible region. This could involve doping the semiconductor with tiny amounts of impurities.^[71] This either provides access to energy levels normally within the band gap, or raises the top of the valence band. Both of these methods reduce the effective band gap. Another strategy has been to use two semiconductors in electrical contact with an offset bandgap.^[72] This mimics the “Z-scheme” found in natural photosynthesis allowing multiple photons to be absorbed to power the water splitting.^[73] A similar strategy uses semiconductor alloys in solid solutions;^[74] this method allows very fine control over band gap. A further strategy involves surface modification by deposition of metal catalysts;^[75] these catalysts can be designed for either H₂ production or O₂ production and they improve efficiency by reducing the activation barrier for reduction/oxidation of water and they also act as traps for electrons and holes from the photocatalyst. Dye sensitised semiconductors have also been investigated for water splitting;^[76] in these cases a dye excited state can inject electrons into the conduction band of the semiconductor.

VISIBLE LIGHT ACTIVE CATALYSTS

Before we embark on a journey through water splitting catalysts it is important to explain the use of sacrificial reagents when studying the photocatalytic activity of semiconductors. When developing catalysts sometimes one might want to isolate either the reduction or oxidation processes. To do this we provide a species than is more easily oxidised than water (typically methanol) or more easily reduced than protons (often silver nitrate) then one has effectively isolated the other process. This can help us in understanding catalyst designs but care must be taken, as the overall process may well be less efficient than the sum total of each half.

As previously mentioned Fujishima and Honda pioneered the field at the start of the 1970s with a TiO_2 catalyst,^[61] since then much work has focused on how to activate titanium based semiconductors to visible light.

Chemical doping of metal ions with partially filled d-orbitals ($\text{V}^{[77]}$, $\text{Cr}^{[72b, c, 78]}$, $\text{Fe}^{[79]}$, $\text{Co}^{[80]}$, $\text{Ni}^{[81]}$) into the semiconductor lattice results in a semiconductor with energy states in the TiO_2 band gap.^[82] These doped semiconductors show a visible-light response but have a very low activity for water splitting. A minor success story is TiO_2 doped with a combination of Sb V and Cr III which is capable of producing molecular oxygen with sacrificial AgNO_3 .^[83] Advanced ion implantation techniques show some success for H_2 production in TiO_2 thin films,^[78a, 84] although again this is under sacrificial conditions. The equipment cost of this method is also too high for any practical industrial application. Anionic doping of TiO_2 with nitrogen leads to catalysts with respectable oxygen evolution but very low H_2 production;^[85] again these measurements were taken under sacrificial conditions.

Catalysts can be made from titanium dioxide fused with various other metal oxides ($\text{SrO}^{[86]}$, $\text{La}_2\text{O}_3^{[87]}$, $\text{Sm}_2\text{O}_3^{[88]}$) and then ion doped. For example compare the band gap size of $\text{Sm}_2\text{Ti}_2\text{O}_7$ (3.5 eV)^[89] and its sulphur doped derivative $\text{Sm}_2\text{Ti}_2\text{S}_2\text{O}_5$ (2.0 eV). This catalyst shows potential in the decoupled half reactions under visible light, but fails to provide an overall water splitting catalyst.

Dye sensitisation of TiO_2 has been a much more successful strategy for water splitting than those discussed above; although successful overall water splitting cells still require an external bias for successful operation. A particularly impressive example is a case from Mallouk where a specially designed dye can simultaneously bind TiO_2 and a water oxidation catalyst.^[76c] The electrons are tunnelled from the water oxidation catalyst through the dye into the TiO_2 around the circuit, where an external bias is applied, to a Pt electrode that catalyses the reduction of protons to molecular hydrogen. Although this example still requires an external bias it proves that TiO_2 based overall water splitting is feasible, Mallouk suggests that dependence on an external bias could be solved with band gap engineering or a significant decrease in recombination rates.^[90]

Tantalates and Niobates are known to be very successful overall water splitting catalysts, however they require UV irradiation due to the large band gap (4.0-4.7 eV).^[91] The high activity of these catalysts is explained by the long lifetimes of electron-hole pairs due to easy migration between the MO_6 units. To reduce the band gap of these materials one may introduce partial substitution of nitrogen for oxygen into the matrix.^[87b, 92] This is very

successful in making visible region active catalysts; however there is no examples that can simultaneously split water and oxidise protons. The substitution causes degradation of the octahedral structure of catalyst, which extends the lifetime of the photo-generated holes and electrons..

An extension of this strategy is the use of metal oxynitrides, in particular d^{10} transition metals such as Ga^{3+} and Ge^{4+} . Maeda introduced this style of catalyst in 2005,^[74b, 93] when he constructed a solid solution between GaN and ZnO and found lower band gap energy than the parent semiconductors. The next year he discovered that inclusion of metal catalysts, in particular Rh and Cr, activated the system towards total water-splitting. This was the first report of a one stage, visible light, particulate photocatalyst for total water splitting, and its efficiency was around 2.5% at 420-440 nm irradiation. The Lee group published a similar catalyst in 2007 using a solid solution of ZnO and ZnGeN₂ loaded with RuO₂ nanoparticles,^[94] which was again found to be visible light active for total water splitting.

Abe recently reported a two-step Z-scheme based catalyst using an IO_3^-/I^- redox couple,^[72b, 95] where each semiconductor had preference to either IO_3^- reduction or I^- oxidation to allow the overall splitting reaction to occur. Kudo also reported the formation of an aggregate of two semiconductors,^[72a] which is another strategy for the development of Z scheme based photocatalysts.

The biggest success in photochemical water splitting has undoubtedly been the development of a low cost, earth abundant catalyst from the Nocera group.^[80, 96] They developed a cobalt phosphate water oxidation catalyst that forms in-situ. They then coupled this catalyst to a triple junction SiO₂ layer and a NiMoZn catalyst for proton reduction. Reported efficiencies reach almost 5% in the case of a wired photoelectric cell.

PHOTOCHEMICAL CO₂ REDUCTION

INTRODUCTION

As highlighted in the previous sections water splitting is only one half of photosynthesis; true model photosynthesis will also fix carbon dioxide. As CO₂ is a thermodynamically stable compound, its conversion into useful fuels will necessarily be endothermic. The energy necessary to drive this transformation in photochemical reductions is derived from incident photons. There have been many photocatalysts reported for carbon dioxide reduction and although various different strategies have been developed they all share some common traits. Firstly there must be a photosensitiser component that is capable of capturing

incident photons and initiating one-electron transfer. There must also be a catalyst that is capable of transferring one or more electrons to carbon dioxide to yield products. A variety of innovative catalysts, discussed in detail below, are capable of acting as both photosensitisers and reduction catalysts. A range of semiconductors, organic compounds, and metal complexes have been used as both photosensitiser and catalyst, and in one example an enzyme (CODH I) has also been used as reduction catalysts.^[97] Photochemical CO₂ fixation can be further subdivided into heterogeneous examples, typically effected by semiconductors, and homogenous examples, using organic compounds and metal complexes. As they were developed first, this section of the thesis begins with a discussion of semiconductor-based photocatalysts.

SEMICONDUCTOR CATALYST

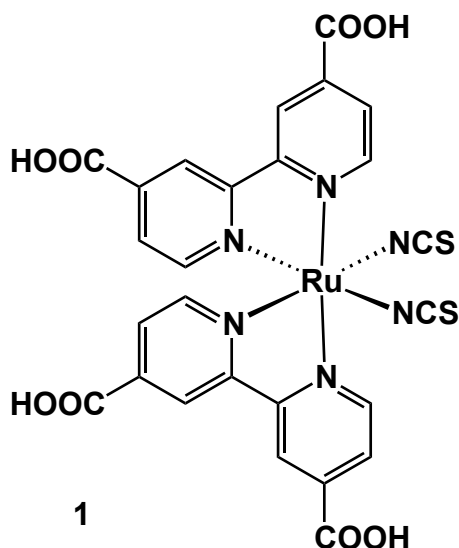
It was the pioneering work of Fujishima in the late 70s that first reported photochemical carbon dioxide reduction with water.^[61] He studied a number of catalysts including TiO₂, ZnO, CdS, GaP, SiC and WO₃ and discovered that the yield of methanol product was dependent on the conduction band energy. Semiconductors with more negative conduction bands were found to produce higher yields of methanol under UV irradiation. Around the same time Hemminger^[99] reported methane production from a photoelectrochemical cell with a single crystal SrTiO₃ semiconductor catalyst and Halmann reported the use of Zn doped GaP to produce a mixture of CO₂ reduction products.^[100] Inoue showed at the end of the 70s that semiconductor particles suspended in water could function as viable photocatalysts for CO₂ reduction.^[98] While these catalysts are impressive achievements they all require UV illumination and suffer from low turnover frequencies and numbers.

It was not long until “micro-photoelectrochemical cells” were developed by loading metals on to semiconductor particles. This was expected to result in improved catalysts as the metal centre could provide sites for CO₂ reduction and improve charge mobility within the semiconductor. Katzir and Kwiki discovered that RuO₂ loaded TiO₂ was a formic acid selective photocatalyst for CO₂ reduction,^[101] in the same year, 1984, Tennakone surveyed several metal loadings on TiO₂ and found Hg to be the most active.^[102] In early 90s Ishitani found that metal doping of TiO₂ significantly altered the selectivity of the catalysts,^[103] with metal doping favouring methane formation.

Several groups have also investigated Cu/TiO₂ systems for methanol formation and recent studies by Wu show the most active species for methanol formation is Cu₂O,^[104] and ESR studies by Yamashita observe photogenerated Ti³⁺ sites, CH₃ radicals and H atoms.^[105] The

last UV active semiconductor discussed here is ZrO_2 , without metal loading it is an extremely active photocatalyst for CO_2 reduction with water to CO .^[106] Unlike many of the previously mentioned systems it has an extremely long lifetime with no significant drop in activity over 20-hour irradiation. Metal doping ZrO_2 doesn't significantly alter the photophysical properties of the catalyst, but it can change the selectivity. This metal doping strategy works extremely well for improving catalyst turnover frequencies and numbers but does little to the visible light response. For any practical artificial photosynthesis we must develop catalysts that can make use of visible photons.

There has been much recent success in the development of dye sensitised solar cells, and this strategy can also be utilised for photochemical CO_2 reduction. The dye sensitisation method works by attaching a small band gap dye molecule (often a metal complex) to the semiconductor surface. When the dye molecule absorbs a photon it is excited to a triplet (which may then decay to a singlet state), this state can then transfer an electron into the conduction band of the semiconductor. This allows visible photons to inject electrons into the conduction band of wide band gap semiconductors. However care must be taken as the hole is left on the dye rather than in the semiconductor. An electron donor must fill this hole, but the energy of the hole is necessarily higher than that of the semiconductor and therefore has less oxidation potential. Regardless of this problem, successful dye sensitized photocatalysts have been developed. Ozcan who studied three dyes on TiO_2 semiconductors and found methane production from water- CO_2 mixtures under simulated day light was the first to use the dye sensitisation strategy in photochemical CO_2 reduction in 2007.^[107] This work was extended by Nguyen in the next year to use the commercial N3 dye, **1**,^[108] with metal loaded TiO_2 semiconductors. In this case it was found the rate of methane production doubled with the addition of the N3 dye.



More recently Zou has investigated the use of earth-abundant metals for dye sensitisation for CO₂ reduction. He found that a Cu Bipy complex^[109] with carboxylate modifications to ensure it binds to the semiconductor surface, is capable of reducing CO₂ under visible irradiation. This catalyst seems to have long-term stability to photolysis, but reduction products may slowly poison the catalyst as photocatalytic activity slows after around 20 hours of irradiation. Wang has taken a similar approach with CdSe quantum dots. The nano size of the CdSe dots increases their conduction band level to allow injection of electron into the TiO₂ conduction band.^[110] Photochemical CO₂ reduction is observed but the catalyst degrades as the quantum dots become oxidised.

The use of ion doped composite semiconductors has also been successful. Nguyen reported a Fe-Cu doped TiO₂ /SiO₂ catalyst which yields ethylene and other trace reduction products under concentrated sunlight. Dopant atoms are introduced using a sol-gel process, and their presence results in full visible light absorption.^[108] The overall energy efficiency for this system was reported to be 0.018% which despite being one of the most impressive figures reported for visible light semiconductor based catalysts is still far below the levels needed for a practical artificial photosynthesis. Other examples of this strategy include C-Fe doped LaCoO₃ from the Jia group^[111] and NiO/InTaO₄ which produces methanol from Pan and Chen.^[112] A Cu-TiO₂ /Molecular sieve composite has been reported to produce oxalic acid under visible light irradiation by the Subrahmanyam group.^[113] All these examples suffer from the low efficiency problems that plague semiconductor catalysts.

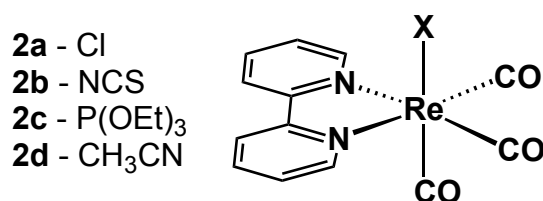
A recent breakthrough by Grimes has utilised N doped TiO₂ nanotube arrays with Cu cocatalysts.^[114] Nanotube arrays have recently become popular in many semiconductor applications due to their enhanced charge transfer properties, but it was Varghese and

Grimes who realised their potential for photocatalytic CO₂ reduction.^[114] Nanotube arrays have exceptionally high surface areas and so diffusion of molecules to the surface should be facile and the high number of surface sites allows increased catalysis compared to bulk materials. The walls of TiO₂ nanotubes are approximately 20 nm thick, and the average hole diffusion length in TiO₂ is 10nm so the electron-hole pairs are never generated far from the surface sites on which the relevant reactions occur.^[115] When synthesised with sufficient length nanotubes can also utilise parts of the spectrum only weakly absorbed in bulk TiO₂. These improved photophysical properties have a marked effect on quantum efficiency, with the reported value at 0.87%. This is the highest currently reported quantum yield for a semiconductor based visible light photocatalyst for CO₂ reduction.

MOLECULAR CATALYSTS

Metal Complexes

The discovery of molecular catalysts for CO₂ reduction happened in the early 80s when Lehn developed a Re catalyst, fac-Re(bipy)(CO)₃Cl, **2a**. This catalyst was visible light-active (>400nm),^[116] had the highest quantum yield, 0.14, known at the time and was CO-selective. Unfortunately because this type of catalyst is not a water oxidation catalyst (unlike most of the examples for semiconductors) and an electron source must be provided, in this case triethanolamine (TEOA), for the CO₂ reduction to proceed.



Many variations on this original catalyst have been studied; modifications have usually involved replacing the Cl- ligand. The most successful ligand replacements have seen Cl replaced with a more labile ligand. Replacement with the NCS- ligand, **2b**, provides a catalyst with a quantum yield of 0.30, over double that of the original catalyst.^[117] Use of the P(OEt)₃, **2c**, ligand enhances the quantum yield again to provide a catalyst with a quantum yield of 0.38.^[118] Unfortunately, this increase in efficiency has led to a concurrent decrease in the reported turnover number, 7.5 compared to 27 for the original catalyst. The increase in quantum yield for labile ligands suggests that loss of this ligand is important for determining the overall rate of CO₂ reduction. Variations on the Bipy backbone have also been studied, particularly 4,4-disubstituted bipyridines. The introduction of electron withdrawing

substituents is found to significantly hinder the catalytic activity of a given complex. This is indicative of a system in which the radical anion exists on the bipy ring. This radical anion is formed by triplet metal to ligand charge transfer followed by reductive quenching from amine. These one electron reduced species can be observed in solution.

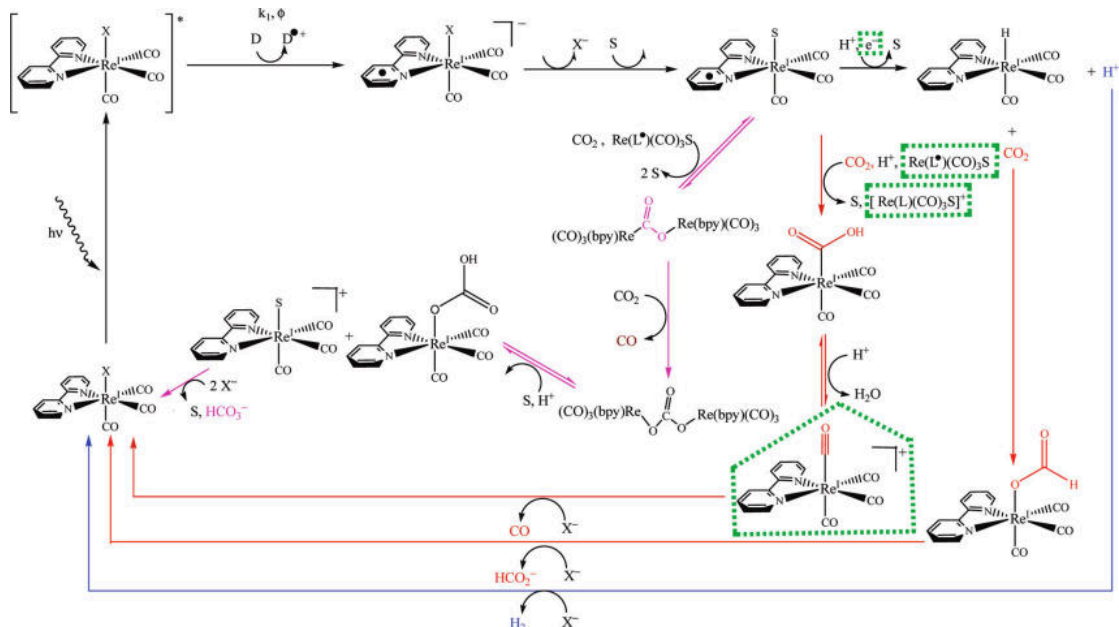
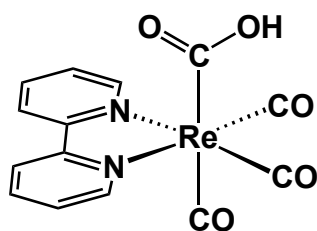
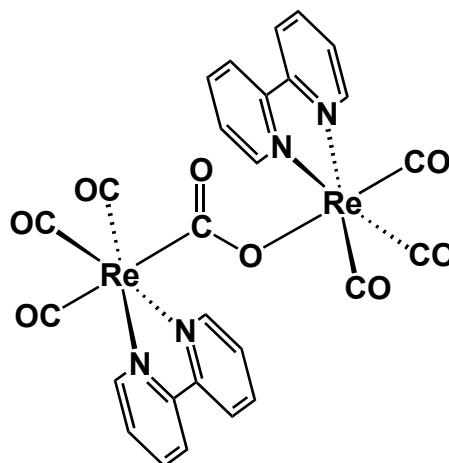


FIGURE 9: PROPOSED MECHANISM FOR RE BASED CATALYSTS

Although the mechanism of these catalysts is not fully determined, the current evidence suggests the following mechanism, shown in Figure 9.^[119] The Re catalyst absorbs an incident photon and becomes excited into its triplet MLCT state. This state is then reductively quenched by an electron donor (tertiary amine), this one electron reduced species can then lose a labile ligand to form a solvent complex. This solvent complex then forms an unknown adduct with CO₂, another equivalent of the one electron reduced species is then required to facilitate the 2 electron reduction of CO₂ to CO. Upon reduction, the CO₂ adduct falls apart, releasing the ground state solvent complex ready to reform the starting catalyst with the ligand lost earlier in the scheme. There are two proposed structures for the CO₂ adduct, shown below as **3** and **4**. The CO₂ bridged dimer, **4**, under irradiation in a CO₂ atmosphere gives a quantitative mixture of CO and CO₃²⁻. However carbonate has never been reported for any CO₂ reduction using these catalysts, and therefore more work is needed before confidence in this CO₂ adduct is achieved. The carboxylate complex, **3**, can lose OH⁻ to form Re(bpy)(CO)₄⁺ which is known to lose CO under irradiation forming the solvent complex. Again there has been no observation of this intermediate or its products. It would seem that neither of these proposed CO₂ adducts can form the full picture and more mechanistic work is needed in this area for future developments to occur.

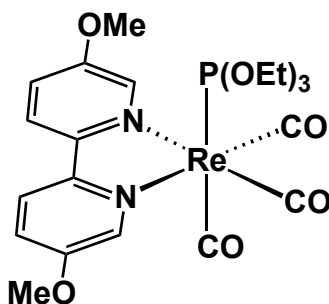


3



4

This mechanism suggests that improvements might be made with a mixture of catalysts; one to travel through the entire catalytic cycle and one to provide an additional reducing equivalent. Inoue reported a system in which he mixed 1:25 $[\text{Re}(\text{bipy})(\text{CO})_3(\text{CH}_3\text{CN})]^+$, **2d**, and $[\text{Re}(4,4\text{-(MeO)bipy})(\text{CO})_3(\text{P}(\text{OEt})_3)]^+$, **5**.^[120] The solvent complex was intended to give very fast access to the catalytic cycle and the phosphate complex was designed to have a long-lived excited state and persistent one electron reduced state. This strategy was extremely successful and results in a quantum yield of 0.59, the highest ever reported for any photochemical CO_2 reduction.

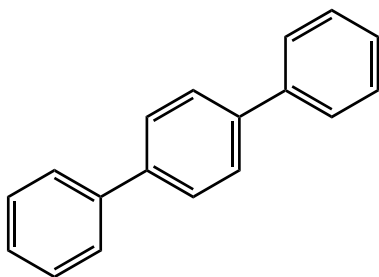


5

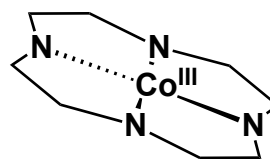
There have also been success stories with metallo-macrocycles, in particular iron and cobalt porphyrins. The main advantage of this type of catalyst compared to the Re catalysts above is the abundant nature of the metals involved. There is simply not enough Re in the Earth's crust to provide a significant amount of the world's energy; Fe on the other hand is cheap and readily available. Unfortunately all reported catalysts have required irradiation with wavelengths as short as 320 nm, which has negative implications for any industrial use.

However the turnover numbers reported for these catalysts are some of the highest known, so if the overall cost of the catalyst becomes more important than the total efficiency then these catalysts may become important. The mechanism of CO₂ reduction goes through a metal zero oxidation state, this extremely unstable state is produced by absorption of two photons and two reductive quenching procedures and finally a disproportionation.^[121] The second photon absorption is much less efficient than the first due to the weak extinction coefficient for the singly reduced species. The disproportionation step is also disfavoured meaning that there will only ever be a very small amount of the catalytically active species present, explaining the extremely low quantum yields.

A successful strategy is that of two component systems using PTP, **6**, as a photosensitiser and a Cobalt Cyclam catalyst, **7** as reduction centre. This system is reported to have a quantum yield of 0.13 and a turnover number around 500 with TEOA as sacrificial electron donor producing a mixture of CO and formate as products.^[122] This is an impressive quantum yield when compared to similar abundant metal catalysts mentioned above.

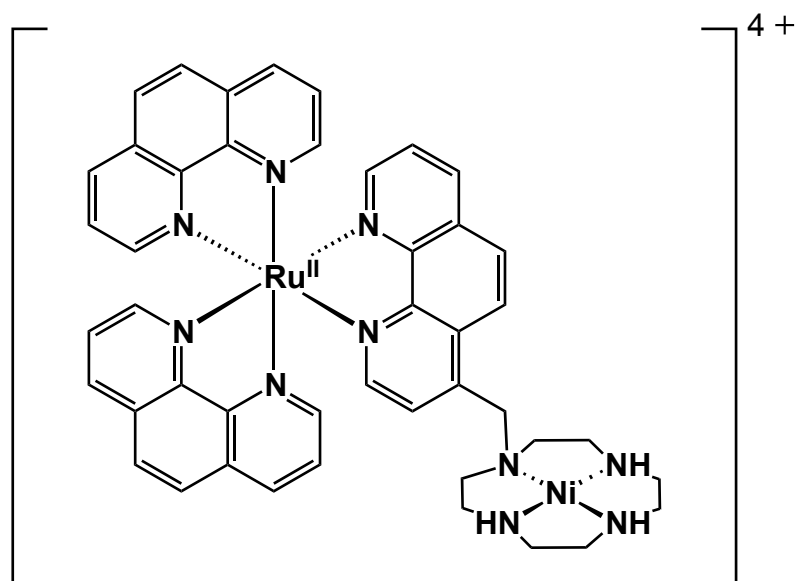


6



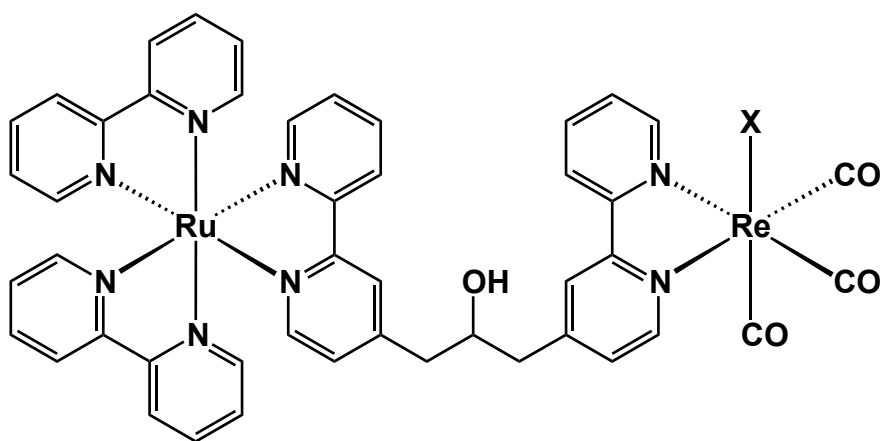
7

The next extension to the series of metal catalysts was the development of supramolecular complexes by Kimura in the early 1990s.^[123] The concept was simple, linking a molecule of photosensitiser and a molecule of catalyst through a bridge should increase the rate of electron transfer and therefore improve catalysis. The first example coupled a Ru photosensitiser and a Ni Cyclam complex through a methylene bridge between the ligands, **8**. Under irradiation with <350 nm light in a CO₂ atmosphere this catalyst can selectively produce CO. After prolonged photolysis this catalyst significantly out-performs the non-bridged equivalent, with the supramolecular catalyst system producing around 3 times the amount of CO. Although this strategy seems to be successful there are significant problems with catalyst degradation under photolysis.



8

Supramolecular complexes with Ru(II) and Re(I) centres have been the most successful with complex **9**^[124] significantly outperforming the non-bridged system with quantum yields of 0.12 and a 70 point jump in turnover numbers over the non-bridged variety. This complex was the first example of a supramolecular catalyst with high catalytic activity for CO₂ reduction, and the only reported improvement was the replacement of the Cl⁻ ligand for a P(OEt)₃ ligand with a quantum yield of 0.21, and a turnover number of 232.



9a - Cl
9b - P(OEt)₃

Organic Catalysts

Organic photocatalysts have received little attention in comparison to semiconductor or metal complex catalysts.^[121c-f, 125] This is most likely due to their poor CO₂ reducing properties and their unfavourable photophysical properties. However the Carpenter group has made extensive use of the PTP photocatalyst, **6**. Though UV irradiation is required, quantum yields are low and turnover numbers are often less than 5, the role of PTP in the mechanism is relatively simple when compared to metal catalysts and the formate produced is easier to detect than the CO produced by many other catalysts. We have already seen examples above where PTP has been used as a photosensitiser but Yanagida reported in 1992 that it could in fact also act as a photocatalyst itself.^[126] This is because the radical anion of PTP, produced by reductive quenching of its excited state by amines, has an extremely strong reduction potential of -2.2 V vs. NHE; more than enough to transfer its electron to CO₂ through an inner sphere mechanism. The PTP radical anion is also prone to further reduction to its dihydro form that deactivates its catalysis, explaining the low turnover numbers.

Other organic systems have also been investigated. For example Tazuke reported the CO₂ reduction by mixed systems of 1,4-dicyanobenzene or 9,10-di-cyanoanthracene with pyrene or perylene,^[127] However these systems undergo photocarboxylation reactions which deactivate the catalysts.

CHAPTER 2 – PREVIOUS WORK

INTRODUCTION

Direct $\text{CO}_2 + \text{H}_2\text{O}$ reaction is thermodynamically very unfavourable, and there has been only very limited success in developing systems which simultaneously reduce carbon dioxide and oxidise water. This leads one to question whether the two known chemistries could be coupled through a new reaction. From the discussion of photochemical carbon dioxide reductions above we have identified the use of a sacrificial electron donors. If a system could be developed in which the sacrificial electron donor was somehow made renewable then an artificial photosynthesis could be envisioned.

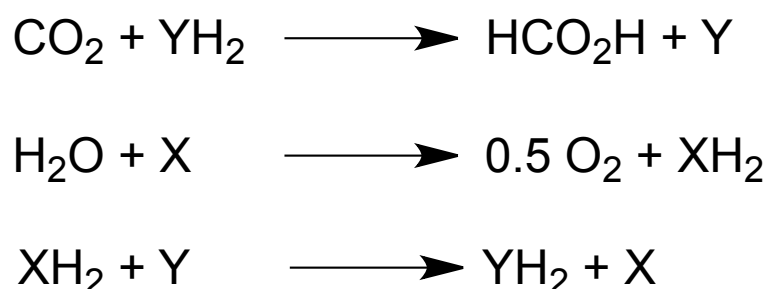


FIGURE 10: ARTIFICIAL PHOTOSYNTHESIS SCHEMATIC

The above scheme is a simple schematic to demonstrate how an overall total artificial photosynthesis could be constructed from two known reactions and a single new reaction.^[128] As discussed in the previous chapter there are many examples of the first two reactions but there is no known molecules for X and Y that will satisfy all three equations. For CO_2 reduction the Y reagent is typically a tertiary amine where the hydrogen atoms are on the alkyl side chains. The X reagent could be null in the case of true total photochemical water splitting, or could be a molecule such as a quinone in the case of transfer hydrogenations. The total of the above 3 reactions is shown in Figure 11.

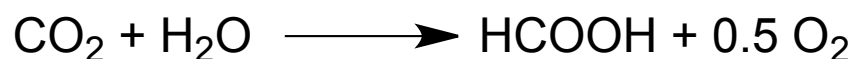


FIGURE 11: OVERALL ARTIFICIAL PHOTOSYNTHESIS

The separation of each step means that the process can utilise more than a single photon for its energetic requirements without the complexity of storing oxidation potential as in natural photosynthesis. It also allows us to consider reactions with mutually incompatible conditions, which is particularly advantageous when considering molecular CO_2 reduction catalysts that are often highly water sensitive.

To achieve the scheme shown in Figure 10 we must design an electron donor that is possible to renew in a separate step. As physical organic chemists we believe that design is best led by understanding and therefore the beginning of the project we focused on mechanistic studies of known photochemical CO₂ reductions.

MECHANISMS OF CO₂ REDUCTION

Spectroscopic Studies

Previous work by Yanagida in the early nineties,^[126] briefly mentioned above, identified PTP as an active photocatalyst for CO₂ reductions and the paper also describes some mechanistic studies to determine the electron transfer process involved in this reaction. They recognised that the excited state of PTP could be reductively quenched by the amine to give PTP radical anion and an amine radical cation. The rate constant for this process can be determined by fluorescence quenching measurements and is found to be close to the diffusion limit for the solvent $1.1 \times 10^{10} \text{ M}^{-1}\text{s}^{-1}$.^[122] Laser flash photolysis (LFP) experiments can detect the PTP radical anion signal in the UV region. Measurements in the presence and absence of carbon dioxide show that the radical anion is fairly long lived in the absence of carbon dioxide, but was found to decay with pseudo-first order kinetics when CO₂ is present. This supports a mechanism in which PTP radical anion transfers an electron to CO₂ returning PTP to its ground state and giving a one electron reduced carbon dioxide species.

It is worth noting at this point that LFP studies performed by a post doctoral researcher in the Carpenter group contradict some of the Matsuoka results. We believe that the fundamental mechanism is correct. However we have found the nature of the ion pairs can complicate kinetic analysis and have some evidence that the electron transfer really occurs through an inner sphere mechanism of a carboxylated PTP radical anion. This is briefly discussed later in this chapter.

Computational Studies

Based on Yanagida's results, indicating, that the reduction mechanism goes through a carbon dioxide radical anion and amine radical ion,^[122, 125-126] calculations were undertaken to determine how the C-H bond in formate is formed and from where the H atom is obtained.^[129] To assess the feasibility of relatively cheap calculations (DFT, MP2) one must compare results from these methods to high-level calculations or accurate experimental results. In this case the highest level of theory was complete basis set atomic pair natural orbital (CBS-APNO) in the gas phase, and single point CCSD based on DFT optimised geometries for solution phase calculation. The largest basis set considered tractable was aug-cc-pVDZ. Calculations at these levels provide the benchmark by which cheaper methods

can be calibrated. Overall MP2/aug-cc-pVDZ// MPWB1K/aug-cc-pVDZ was selected as the best model for study of large systems, though it is expected to systematically underestimate enthalpies by around 2 kcal mol⁻¹. Using this model, mechanisms of H atom transfer from Et₃N radical cation to CO₂ radical anion were explored. The results of the study are displayed in Figure 12 in the form of an enthalpy profile.

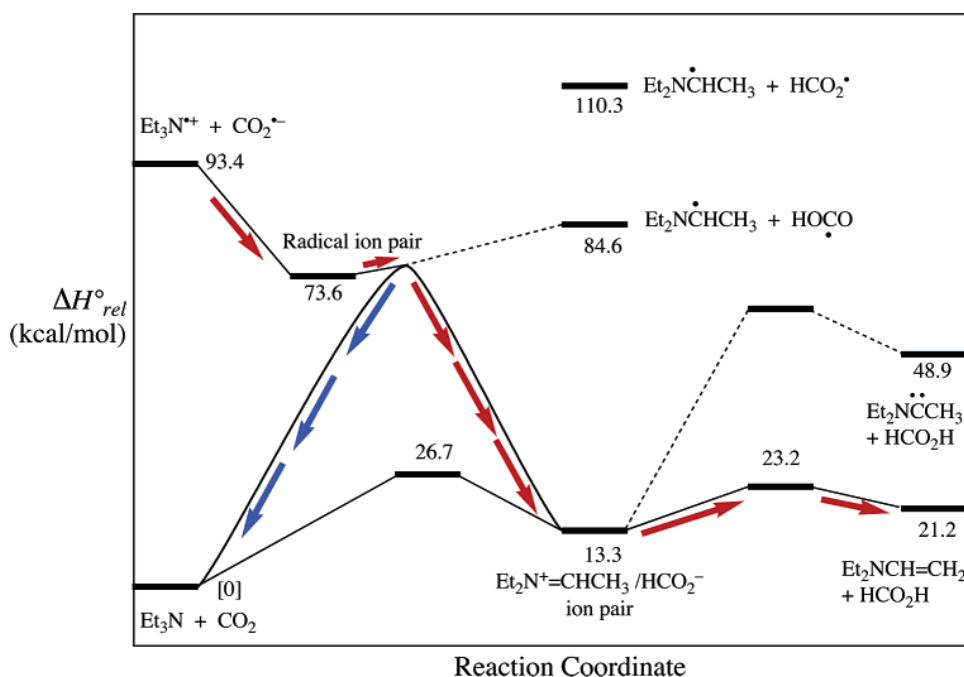


FIGURE 12: ENTHALPY PROFILE FOR CO₂ REDUCTION WITH TRIETHYLAMINE. REPRODUCED FROM ^[129]

The separated radical ions are found to be higher in energy than their ion paired state, so discussion of thermodynamics should be started from the radical ion pair for meaningful results. From this position it can be seen that only 2 H transfer reactions are exothermic, the double H transfer leading to an α amino carbene and the α hydride transfer. No transition state could be found for the double transfer pathway, indicating it either doesn't exist or it will be incredibly unfavourable. The hydride transfer reaction is found to be the most likely to occur. However the transition state for formation of Et₂N⁺=CHCH₃ and HCO₂⁻ was found to be closed shell, implying that the reactants were ground-state Et₃N and CO₂. For the photochemical reaction, there must be a surface crossing somewhere along the reaction coordinate, and there must be some barrier to unproductive electron back transfer.

A barrier to electron back transfer would be expected if the radical ion pair was in the so-called Marcus inverted region and calculations indicate that this should be the case, although an exact value for the barrier cannot be accurately calculated. Searching for conical intersections or surface crossings in solvent is particularly challenging and the inclusion of a

number of lone pairs involved during this reaction in the active space makes accurate calculations even more intractable. As a result the fairly low level cc-pVDZ//UB3LYP/aug-cc-pVDZ model calculations were chosen to achieve qualitative results on any possible surface crossings.

No surface crossing could be found along the reaction coordinate for direct transfer of the hydrogen between carbon atoms and the large gap between electronic states at the transition state indicates that is unlikely one exists. However if one considers the intrinsic reaction coordinate for proton transfer to the oxygen atom of CO_2 it is possible to locate a surface crossing from a singlet biradical state to a closed shell state. Linear synchronous transit calculations indicate that there likely exists a surface crossing that will lead to productive chemistry. To paint a picture in words: $\text{CO}_2^{\cdot-}$ approaches $\text{Et}_3\text{N}^{\cdot+}$ with an O atom facing the amine, if this ion pair starts to transfer a H atom to the O then a surface crossing will be found. From this surface crossing there are paths to both unproductive electron back transfer and productive CO_2 reduction chemistry. As the H transfer to O is endothermic it is disfavoured and so this path is not expected to complete. This series of calculations suggests that photochemical reductions of carbon dioxide with triethylamine abstract an H atom from the α position of the amine; the imine formed by this reaction can then have a proton abstracted by formate to yield an enamine and formic acid, Figure 13.

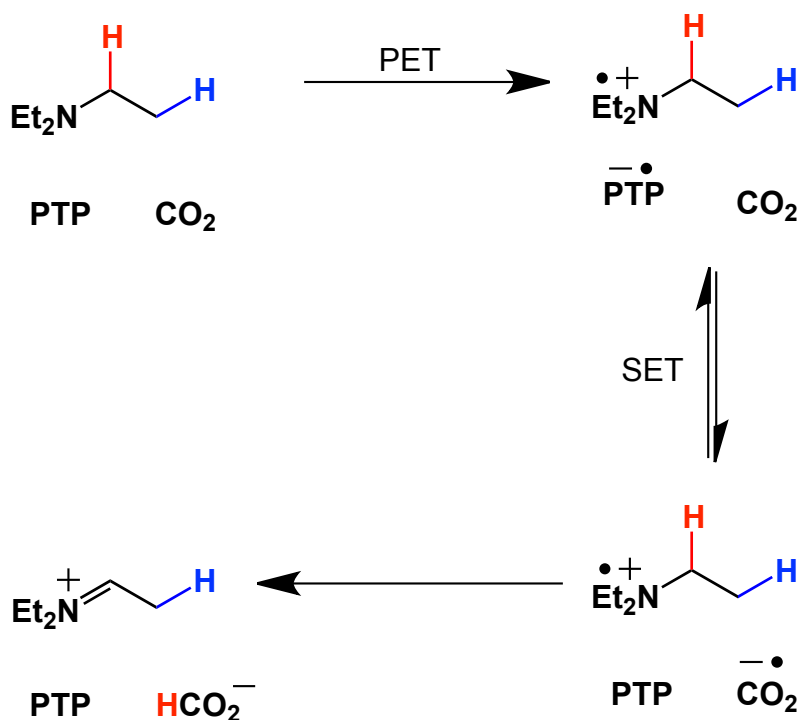


FIGURE 13: PROPOSED MECHANISM FOR H ATOM TRANSFER

Renewable Amines

Aza-Norbornane

Azanorbornane **10** was synthesised and was expected to be able to reduce CO₂; unfortunately no products were observed after prolonged photolysis, Figure 14. To further understand why this amine is not capable of reducing carbon dioxide laser flash photolysis experiments were undertaken.^[130]

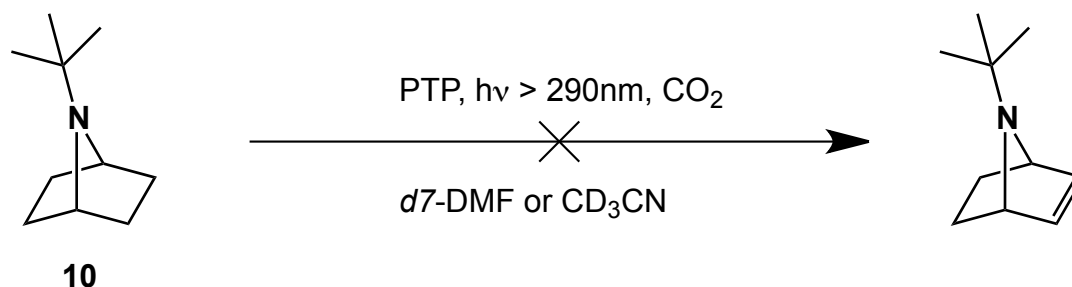


FIGURE 14: ATTEMPTED CO₂ REDUCTION WITH AZA-NORBORNANE ^[130]

The work by Yanagida previously mentioned followed the kinetics of PTP radical cation reacting with Et₃N, two peaks (440, and 470 nm) were assigned to PTP^{•+} and they were reported to decay with the same kinetics.^[126] When the same experiment with was tried with amine **10** a very different situation was found. The relative heights of the 2 peaks previously assigned to PTP^{•+} were different from those the Et₃N case, the kinetics for the decay of each peak was also different and the total lifetime for the radical cation was around a hundredth of that reported for Et₃N. This experiment forces us to reevaluate the assignments of Yanagida. The peaks cannot both belong to naked PTP^{•+} if the decay kinetics are different and the spectrum are amine dependent. TDDFT calculations confirm that there are no amine absorbances interfering with the spectra in this region. It seems likely the two observed peaks are therefore due to radical ion pairs. In the case of Et₃N it is thought that ground state Et₃N is capable of deprotonating the amine radical cation. This gives a neutral α amino radical and an Et₃NH⁺ ion. The ion pair therefore must be between PTP^{•+} and Et₃NH⁺. The important feature of this ion pair is that the Et₃NH⁺ is unable to accept an electron from PTP^{•+} having a full valence shell already. This prevents the electron back transfer from occurring in this ion pair and explains the long lifetime seen by Yanagida. It is not possible to deprotonate the radical cation of amine **10** so in this case the ion pair must be between PTP radical cation and amine radical anion. Electron back transfer in this radical ion pair is fast and this explains the 100 fold reduction in PTP^{•+} lifetimes. In the case of amine **10** the LFP signal returns to baseline indicating that no chemistry other than the back

electron transfer to occurring. Et₃N is an important part of the inner sphere electron transfer mechanism between PTP⁻ and CO₂; it would seem that amine **10** is not capable of fulfilling this role in CO₂ reductions. The conclusions of these experiments showed that the original calculations only revealed part of the picture.^[130]

Isotopic Labelling Studies

To probe the conclusions of these calculations an experiment was designed in which isotopically labelled Et₃N was synthesised and used in photochemical CO₂ reductions, Figure 15.^[130]

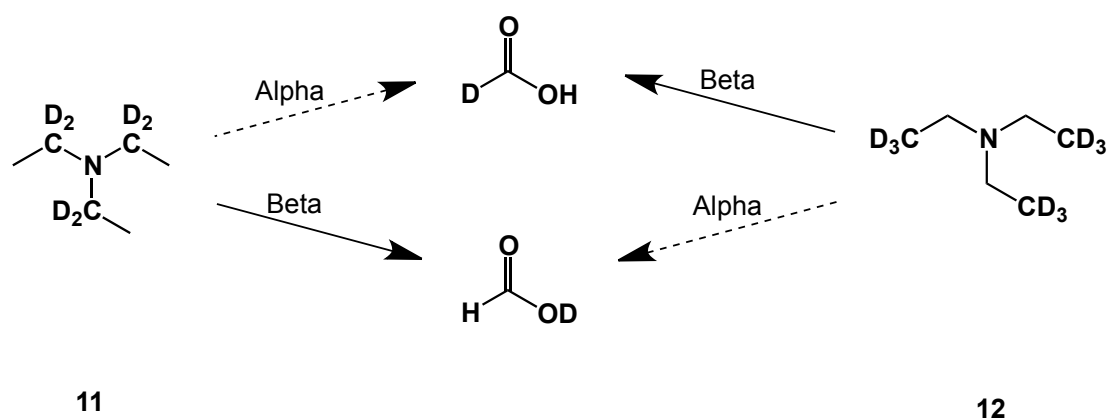


TABLE 3: ISOTOPIC LABELLING STUDY RESULTS

FIGURE 15: ISOTOPIC LABELLING STUDIES ON CO₂ REDUCTION WITH TRIETHYLAMINE

	2 hours	6 Hours
	[HCO ₂ ⁻]/[DCO ₂ ⁻]	[HCO ₂ ⁻]/[DCO ₂ ⁻]
N(CD ₂ CH ₃) ₃	2.9	1.85
N(CH ₂ CD ₃) ₃	0.51	0.88

Based on the conclusions from the previous set of calculations one would expect that for reactant **12** the main product would be DCOOH, and that for reactant **11** the main product would be HCOOD, however as shown in Table 3 we find that the situation is approaching the opposite result.

These experiments show that it is in fact the β hydrogen that is preferentially transferred to the carbon atom in CO_2 . The proposed mechanism is shown below in Figure 16

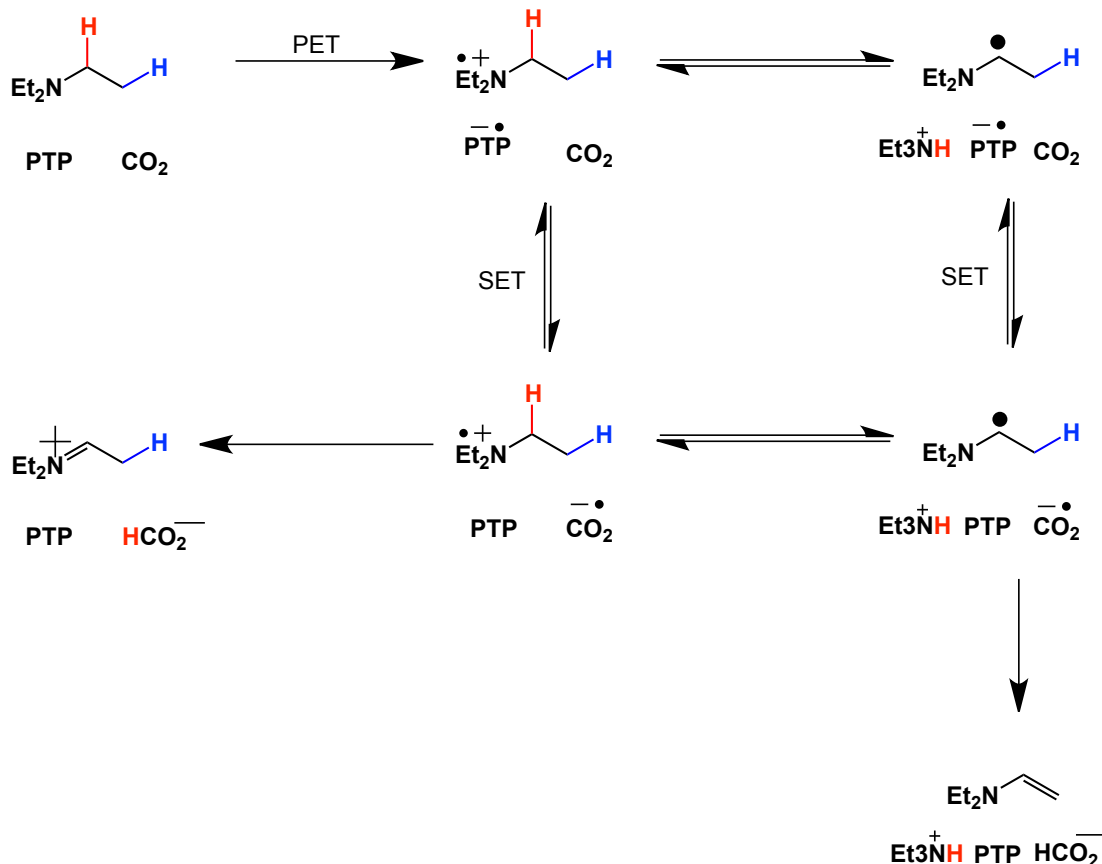


FIGURE 16: NEWLY PROPOSED MECHANISM FOR CO_2 REDUCTION

Mechanisms of H-Atom Loss

Given the weakening of the α C-H bonds in amine radical cations and the basicity of the reaction mixture in the systems studied a deprotonation mechanism is proposed,^[128, 131] shown in Figure 16. In this mechanism the α amino radical activates the β hydrogen for CO_2 reduction. This mechanism raises the question that if an α amino carbon centred radical can activate a hydrogen atom for CO_2 reduction chemistry then can other carbon-centred radicals do the same. If one could generate a carbon-centred radical away from the amine functionality then many of the decomposition pathways available to α amino radical cations would be closed. The next series of calculations were designed to probe this possibility.

As mentioned above amine radical cations have weak α C-H bonds, this is attributed to the formation of a C-N π bond compensating for the loss of the C-H bond. Given that C-N σ bonds are stronger than C-N π bonds one might expect a preference for cyclisation with concurrent H atom expulsion. An intramolecular H atom transfer could lead to a distonic

radical cation (one in which the charge and spin are separated). The distonic radical cation could then lose a distant H atom to CO_2 . The next series of calculations were designed to probe the mechanisms for H atom loss from amine radical cations.^[128]

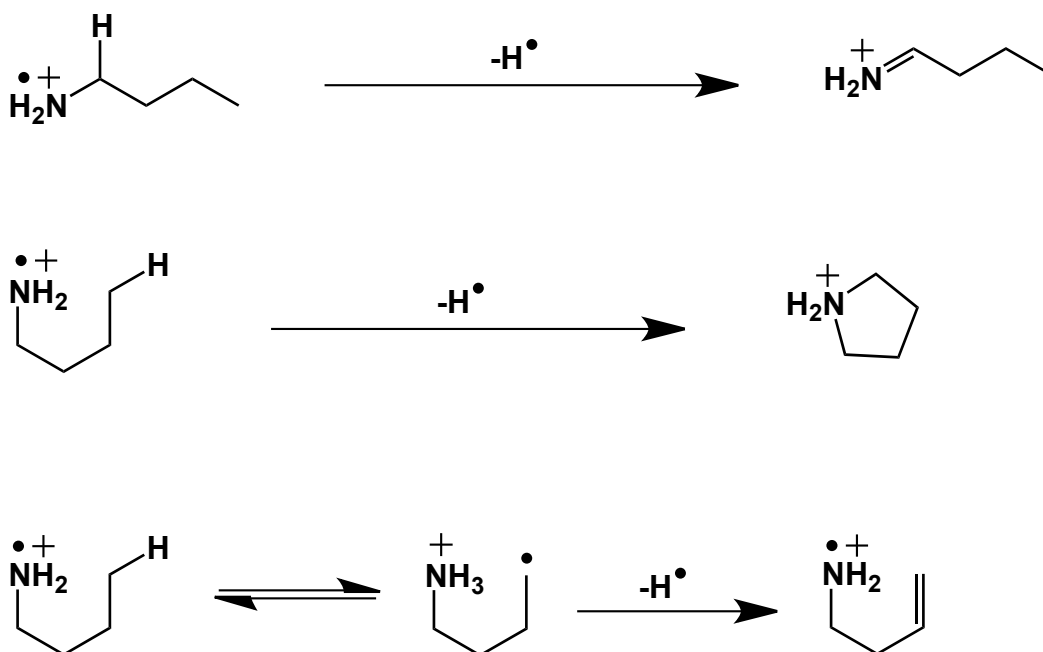


FIGURE 17: MECHANISMS FOR H ATOM LOSS FROM *N*-BUTYLAMINE RADICAL CATION

The reduction system was modelled by *n*-butylamine, Figure 17, as the simplicity of this model allows significantly higher-level calculations, the best model given the available computer power was judged to be (U)CCSD(T)/cc-pVTZ//((U)-CCSD/cc-pVDZ.^[129] Gas phase calculations on the 3 mechanisms shown in Figure 17 identified simple α H loss as the most favourable reaction kinetically, and the cyclisation product as the most thermodynamically stable.^[129] Unfortunately at this level of theory it was not possible to locate a transition state for the hydrogen transfer reaction, this is likely to be because it is “activationless”, a part from the conformational barrier to the reaction. These results are unlikely to represent an accurate description of the reaction in reality as the polar solvent would stabilise any open shell or ionic intermediates.

As PCM calculations were not feasible at the high level of theory used for gas phase calculations, a calibration study was undertaken to determine a suitable method for solution phase calculations and for studying large molecules.^[128] The high level results for the H atom loss mechanisms were used to calibrate the lower levels, (U)B3LYP/6-31+G(d,p), and (U)MP2/aug-cc-pVDZ. All stationary points used in the previous calculations were recalculated at these levels and the results compared. For the DFT level calculation there was found to be a systematic error of around 6 kcal mol⁻¹ for amine radical cations. This

error was fairly consistent for the amines studied and attributed to the self-interaction error. The MP2 calculations were also found to have significant errors in relation to the high level calculations, in this case however the discrepancy was not constant and the origin of this effect is less clear. UMP2 calculations typically suffer badly from spin contamination. For these reasons further calculations were run at (U)B3LYP/6-31+G(d,p) with a PCM model for acetonitrile. Solution phase calculations on the H atom loss mechanisms suggest that formation of the distonic radical cation is essentially activation-less and is predicted to be the most favourable reaction in the solution phase. Further calculations probe the possibility of a surface crossing along the reaction coordinate for direct hydrogen transfer from the distonic radical cation to the C atom in carbon dioxide. In total these calculations predict that an amine with a conformation holding a distant H atom close to the nitrogen centre should undergo H atom transfer chemistry quickly, this suggests that an amine with the correct conformation may well be able to tolerate the presence of α hydrogen atoms, Figure 18.

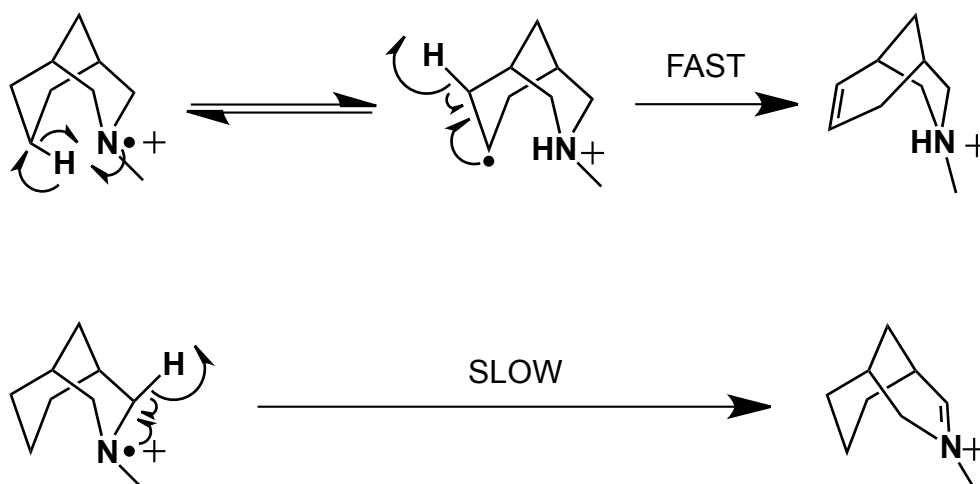
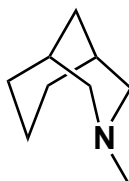


FIGURE 18: TOLERANCE OF BICYCLIC AMINE TO α HYDROGEN ATOMS

Bicyclic amine

These calculations laid the groundwork for the study of large amines that might be suitable for CO₂ reduction and suggested design features one might use for promotion of the desired chemistry. Deactivation of α H atoms by either removal or putting them at the bridgehead of small polycyclic rings is expected to help promote the formation of the distonic radical cation by reducing the number of back electron transfer pathways available to the molecule. Furthermore the inclusion of a rigid structure that holds an H atom near the nitrogen centre is expected to enhance the rate of this chemistry. An obvious way to remove α hydrogens is the use of aniline type amines; unfortunately these amines typically have significantly

endothermic H transfer reactions that preclude their use for distonic radical ion formation. As such the use of polycyclic aliphatic amines would seem the most sensible targets within the constraints set out above.



13

The amine originally studied is shown above, **13**, it was hypothesised that the bimolecular H transfer to CO_2^- would be slower than the unimolecular rearrangement and therefore the distonic pathway would dominate. DFT calculations found the enthalpy of activation for both cases is around 5 kcal mol^{-1} and the H atom transfer reaction is close to thermoneutral. These results support the conclusions from the earlier calibration study, and it is assumed that a similar surface crossing could occur in these systems.

It is important at this stage to refer back to our goal; we were planning to design a renewable reducing reagent by avoiding the reactive intermediates normally found in photochemical CO_2 reductions. The simulations predict that the reaction will produce an alkene as a stable final product on CO_2 reduction. We predict that this alkene will be stable under reaction conditions. If our predictions are correct and the chemistry is successful then we will have developed an amine that can be renewed by simple hydrogenation.

A post-doctoral researcher undertook synthesis of amine **13** and it was subjected to photolysis under a CO_2 atmosphere in the presence of PTP.^[130] Unfortunately, once again, no CO_2 reduction was found. This was presumed to be due to the loss of α H atoms, forming imine ions. To probe the mechanism for this reaction it was spiked with a small amount of D_2O (as a trapping agent). Surprisingly no trapped product was found but there had been complete H-D exchange in the α positions. This provides more evidence for α deprotonation occurring during the course of this reaction. The mechanism for this transformation is shown in Figure 19. This mechanism suggests that for a successful renewable amine we must deactivate the α hydrogens to deprotonation and we cannot rely on the kinetics of the H atom transfer to out-compete this chemistry.

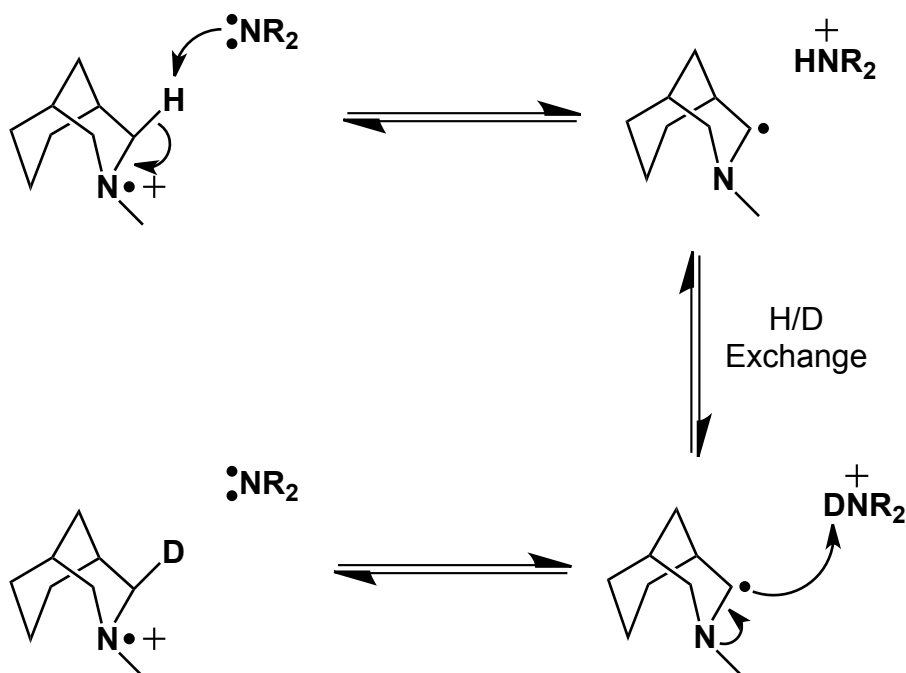


FIGURE 19: MECHANISM OF H/D EXCHANGE IN BICYCLIC AMINES

Tricyclic Amines

The removal of all α hydrogens from amine **13** is impractical, but if both α positions are joined with a methylene bridge then the remaining two α hydrogens are at bridgehead positions. These bridgehead hydrogen atoms should be unreactive due to poor hyperconjugation to stabilise the created charge as predicted in Bredt's Rule. The amine, **14**, is the optimised version of amine **13**. The author of this thesis undertook synthetic development of this amine during an undergraduate project^[132] and so only the final details are presented here.

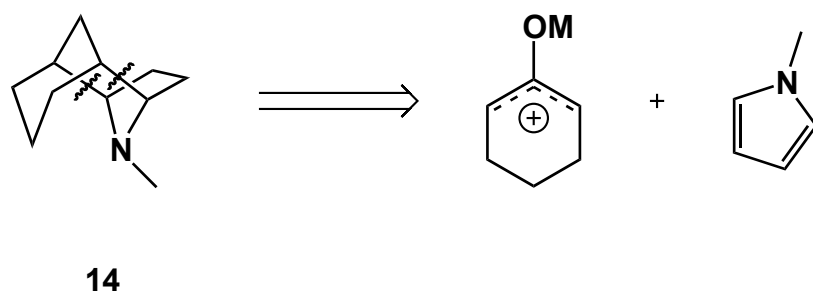


FIGURE 20: RETROSYNTHETIC ANALYSIS OF TRICYCLIC AMINE

Synthesis

The amine, **14**, was disconnected, as shown in Figure 20. This proposes synthesis through a [4 + 3] cycloaddition.² This style of cycloaddition is one of the few methods to access 7 membered ring systems, and is likely the only method suitable for construction of the tricyclic structure of the amine.^[133]

There has been much work on [4+3] cycloadditions and a complete review is not relevant at this stage. It is however worth mentioning that most reported [4+3] cycloadditions are reactions between oxyallyl cations and cis tethered dienes such as cyclopentadiene, furan and electron deficient pyrroles.^[134] To access amine **14** we coupled a cyclohexyl oxyallyl cation, and an N-alkyl pyrrole. Unfortunately pyrroles require strong electron withdrawing groups to disrupt their aromaticity enough to allow facile [4+3] cycloadditions, limiting our selection of suitable dienes. Literature examples typically use N-BOC pyrrole as a prototypical case,^[133] and given the ease with which BOC groups can be manipulated it was selected as a suitable diene to facilitate the cycloaddition.

Cyclic oxyallyl cations are relatively rare in literature compared to their acyclic varieties; typical precursors are α -brominated cyclohexanones that are reduced to oxyallyl cations in situ. Unfortunately when tested we were unable to produce useful cycloaddition products. The use of amino-allyl cations has also been reported for cyclic oxy-allyl equivalents. Chloro-enamines, such as **15**, can be treated with silver salts to generate amino-allyl cations, which then undergo facile cycloaddition reactions with N-BOC pyrrole. The literature preparation was successfully repeated, Figure 21, to generate the tricyclic structure, **16**.^[135]

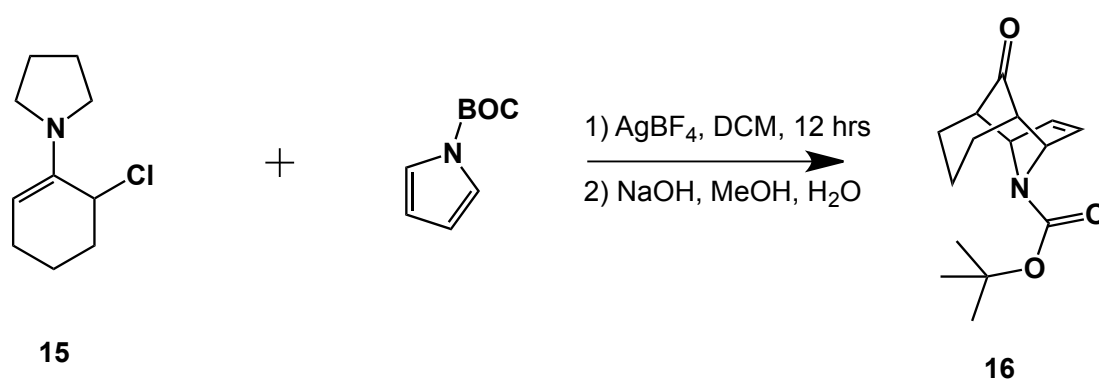


FIGURE 21: SYNTHESIS OF TRICYCLIC AMINE

² A note on naming conventions for cycloaddition reactions: [] indicate structural notation indicating the number of atoms, () indicates electronic notation indicating the number of electrons

The core of the amine was now built, but there were still many manipulations required to produce an amine suitable for photochemical studies. First, reduction of the alkene with hydrogen gas on Pd/C afforded an almost quantitative yield of ketone, **17**. The ketone could then be reduced with NaBH₄, without affecting the carbamate, to yield the alcohol. Methylation of this alcohol yielded a carbamate, **19**, one step away from amine, **20**. Very careful purification was undertaken after this step as purification of amines is often significantly more challenging than purification of their corresponding carbamates. The final step was reduction of the BOC group to a methyl. This step yielded an almost pure amine, and distillation over CaH₂ ensured complete purity and dryness. This “endgame” synthesis, Figure 22, was designed to access an amine suitable for photochemical studies within the time constraints of an undergraduate project, and did not yield the an optimal amine. The main body of text discusses in detail futher work to improve this synthesis.

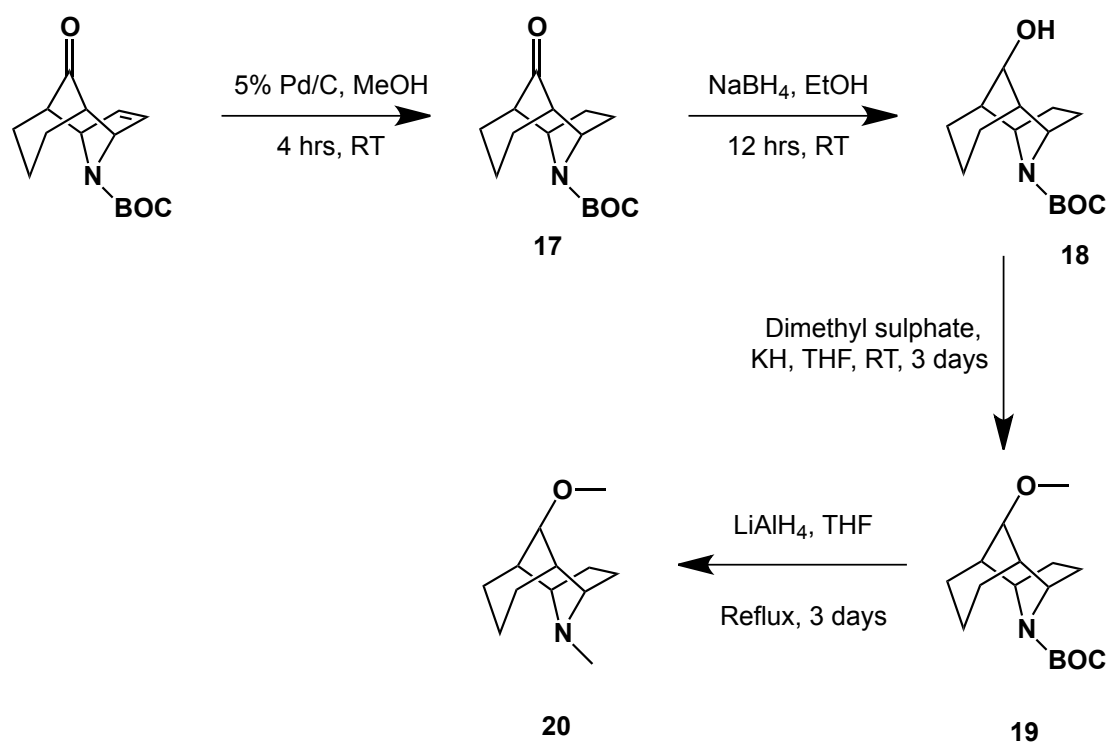


FIGURE 22: SYNTHESIS OF TRICYCLIC AMINE FROM CYCLOADDITION PRODUCT

CO₂ Reduction

Photochemical studies with amine **20** show that it was capable of reducing CO₂ to formate under photochemical conditions as shown in Figure 23.^[132] Confirmation that this amine was acting through the distonic radical mechanism was sought through identification of the alkene produced. An independent synthesis of the alkene **21** was undertaken by another group member.^[130] Results showed that alkene **21** is produced during photochemical CO₂ reduction with amine **20**. Furthermore it was shown that alkene **21** can be reduced with H₂

to yield the original amine.^[130] These experiments have proven that it is possible to design renewable amines for photochemical CO₂ reduction, and that in total an artificial photosynthesis scheme can be built on this basis.

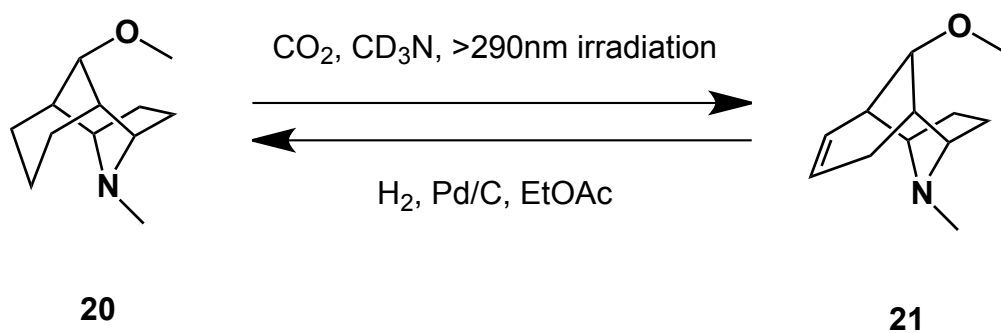


FIGURE 23: CO₂ REDUCTION AND RENEWAL WITH TRICYCLIC AMINE

CHAPTER 3 – COMPUTATIONAL METHODS

QUANTUM CHEMISTRY

Quantum mechanics tells us that all information about a system is contained within its wavefunction so in principle, given an exact wavefunction it should be possible to predict any observable property of the system. Unfortunately it is neither possible to construct an exact wavefunction or exactly solve the complex equations that form solutions.

All is not lost though; there are many different simplifications that can be made which allow solutions to be calculated. Computational chemistry could well be considered the art of making the correct simplifications to allow meaningful prediction of the chemical system you are interested in. The simplifications chosen strongly affect the accuracy of the final result so great care must be taken to ensure the validity of any results obtained.

Unlike in experimental chemistry we are not bound by the limits of what can be synthesised in a laboratory or what our equipment can measure. We can study molecules that would be too reactive or short lived for traditional methods and we can even characterise transition states. Computational chemistry is bound only by the size of our computers (and our imaginations). During the last 3 decades there have been huge advancements in both the speed of computers and the methods used, this has opened up the field for many new applications and led to a huge surge in computational chemistry.

It is now common for computational chemists to successfully predict novel chemistry and experimentalists are increasingly explaining their results in terms of computational chemistry. The literature is now full of examples of practical uses of computational chemistry, which pays testament to the founders of the field and the general utility of the method. A full discussion of computational chemistry could, and indeed does, fill many textbooks so this thesis will endeavour to only focus on core principles and those details that are particularly important in terms of this project.

FORMULATION

The Schrödinger equation describes how the quantum state of a system evolves over time, it can be considered the quantum equivalent of Newton's second law of motion. The equation is shown below where Ψ is the wave function of the quantum system, and \hat{H} is the Hamiltonian operator

$$i\hbar \frac{\partial}{\partial t} \Psi = \hat{H} \Psi$$

Application of this equation to molecular systems predicts stationary states, or standing waves; these are the atomic and molecular orbitals that chemists are familiar with. As these states do not evolve over time it is possible to simplify Schrödinger's equation to a time independent form.

$$E\Psi = \hat{H}\Psi$$

This equation allows us to calculate the total energy of a system given its wave function and applying the Hamiltonian operator to it. The Hamiltonian operator tells us how the total energy is built up from the kinetic and potential energy of all the constituent particles of the system.

$$\hat{H} = T_N + T_e + V_{nn} + V_{ne} + V_{ee}$$

In a molecular system the energy is composed of the kinetic energies of all the nuclei (T_N) and all the electrons (T_e), plus the potential energy associated with the interactions between each pair of particles: that is, each pair of nuclei (V_{nn}), each nucleus – electron pair (V_{ne}), and each pair of electrons (V_{ee}). The so called “quantum many body problem” is that of solving for the many interacting particles in equations such as the above. It is this problem that can only be solved numerically, and for large systems we must also make simplifications to allow the calculation to be tractable with modern computers.

There are many different simplifications we can make to get solutions to the Schrödinger equation; one of the most fundamental simplifications is known as the Hartree-Fock method. Although not particularly accurate on its own it forms the basis for most high-level approaches and acts as a good example of the principles of computational chemistry.

HARTREE-FOCK

The Hartree-Fock Method makes several approximations to simplify the calculation.^[136] Firstly the Born-Oppenheimer approximation is employed so that the kinetic energy of the nuclei falls out of the Hamiltonian and the nucleus-nucleus potential energy becomes a constant.^[137] Relativistic effects are completely ignored. The wave function is assumed to be approximated by a linear combination of basis functions, typically orthogonal gaussian functions. The term basis set refers to a particular set of functions used to approximate a set of orbitals, gaussian functions are often chosen due to the ease in which they can be integrated. A further assumption is that the wave function can be adequately described by a single Slater determinant; this can fail in bond breaking reactions and open shell singlet molecules, where there is more than one possible electron configuration. The most serious

assumption in Hartree-Fock is the mean field approximation, which assumes each electron only interacts with the mean effect of the other electrons rather than treating them as individual particles. This causes Hartree-Fock to ignore correlation between electrons completely.

With these approximations in place it becomes possible to calculate energy from a wave function constructed from a gaussian basis set. However the initial guess wave function might not be the best wave function to describe the system. If we could somehow test the accuracy of the energy compared to other wave functions we could iteratively optimise the wave function until the best fit was found. Fortunately the Variational Principle tells us that the Hartree-Fock method can never underestimate the energy of a system,^[138] so we know the lowest calculated energy must be the most accurate. So the Hartree-Fock algorithm is an iterative process that optimises a wave function to produce lowest energy possible within the framework of the assumptions explained above. The optimised wave function can then be used to calculate many properties including thermodynamic quantities and spectroscopic properties.

Of the assumptions described above only 3 are considered significant problems for the study of most chemical systems, and methods have been developed to overcome them in various ways. Firstly considering all electrons to exist in doubly occupied orbitals makes it challenging to study molecules with an uneven number of electrons, or having singlet biradical nature. One method to address this problem is restricted Open Shell Hartree-Fock (ROHF) that considers all orbitals as doubly occupied except those containing unpaired electrons. This causes problems in the mean field approximation, as it is not accurate to assign the same mean-field to electrons with different spin, but when we assign all paired electrons to the same orbitals this is effectively what we are doing. Unrestricted Hartree-Fock (UHF) assumes that all electrons occupy their own orbital; this solves the problem created in ROHF but introduces the problem of spin contamination. This means that excited states with higher spin multiplicities are contaminating the ground state.

The remaining two assumptions both cause Hartree-Fock to ignore electron correlation, the interaction between electrons. Electron correlation comes in two flavours, dynamical and non-dynamical. Dynamical correlation relates the interactions between moving electrons, this is ignored in Hartree-Fock due to the mean field assumption. Non-dynamical correlation occurs when more than one electron configuration is needed to accurately describe the system; this is impossible to describe properly using only a single Slater determinant. The

methods used to recover this electron correlation energy are called Post-HF methods and are described in detail below.

POST HARTREE-FOCK

Dynamical correlation is recovered by methods such as Møller-Plesset theory (MP),^[139] configuration interaction methods (CI)^[140] and coupled cluster theory (CC).^[141] A complete discussion of these methods and their strengths and weaknesses is beyond the scope of this thesis and so only the core principles of each method will be discussed.

MP perturbation theory is a specific implementation of Rayleigh–Schrödinger perturbation theory. Perturbation theory teaches that a complicated system can be modelled by applying a perturbation to a simpler known system. In this case the known system is the HF waveform and the perturbation is an operator to calculate correlation potential. This is shown in the following equation, where λ is an arbitrary parameter to be optimised, \hat{H} the Hamiltonian, and \hat{V} the perturbation.

$$\hat{H} = \hat{H}_0 + \lambda \hat{V}$$

The new waveform can then be expressed as terms of an infinite power series, as shown in the following equation.

$$\Psi = \lim_{n \rightarrow \infty} \sum_{i=0}^n \lambda^i \Psi^{(i)}$$

As such the energy can be expressed as:

$$E = \lim_{n \rightarrow \infty} \sum_{i=0}^n \lambda^i E^{(i)}$$

Brillouin’s theorem states that any combination of a ground-state waveform and a singly excited waveform can be expressed within the ground state waveform and therefore the initial optimisation of the ground state will find the lowest energy possible. In terms of MP theory this means that terminating the series at the first term will yield no improvement in energy. However MP2, MP3 and MP4 (where the number indicates where the power series is terminated) are commonly used methods for recovering dynamical correlation.

CI methods start with the Slater determinant from HF, as the ground state, excitations from this ground state are then considered. Each possible excitation from the ground state is called a configuration state function (CSF). The overall wave function is then expressed as a linear combination of CSFs. In the limiting case where all CSFs are considered the

Schrödinger equation is solved exactly within the framework of the chosen basis set and the Born-Oppenheimer approximation. However the number of CSFs required for a full CI calculation very quickly becomes extremely large and therefore the method is intractable for anything other than very small molecules. A common simplification is to only consider a certain level of excitations, typically limited to singles and doubles only (CISD). Again Brillouin's theory applies so considering only single excitations will not improve the total energy.

Coupled cluster methods are similar in concept to CI methods, however the excitations are generated through a cluster operator, T . T acts on the HF waveform to produce all excitations as a power series, this series can be truncated at the desired level. While this may seem to have no advantage over the conceptually simpler CI method, CC is a size-consistent method unlike truncated CI. This means that the total energy of two infinitely separated particles is the same as the sum of the energies of the two particles calculated separately. To understand why this occurs in truncated CI methods consider two non-interacting hydrogen molecules. If the system is studied at CISD, the total energy of two separated molecules will not total that of the molecules calculated separately. This is because the first calculation will fail to include double excitations on both molecules simultaneously, to capture equivalent excitations it would need to include quadratic interactions. The Pople group developed a method known as quadratic configuration interaction (QCI) that includes additional interactions to ensure size consistency.^[142]

Coupled cluster calculations are typically faster than their CI equivalent so they typically allow higher-level terms to be included. CCSD calculations are possible with relatively large system but CCSDT and CCSDTQ are possible only for small systems. CCSD(T), where the parenthesis around the T indicate the triples are calculated through perturbation, is almost as accurate and feasible for much larger systems. CCSD(T) has often been called the gold standard for quantum chemistry.

Methods designed to recover non-dynamical correlation are called multireference methods. They abandon the single reference Slater determinant that has been used either to generate all the excitations, or as the only Slater determinant in all the methods discussed above, as a single Slater determinant can never accurately describe two different but almost degenerate electronic configurations. These methods are particularly important when dealing with systems that contain either partially broken bonds (such as TS structures), or singlet biradicals. This is because of the various nearly degenerate electronic configurations needed to properly describe these phenomena. Multireference methods involve an optimisation of

linear combinations of Slater determinants on top of one of the previously described methods. This increases the complexity of the calculations significantly above the non-multireference versions described above and so the systems studied can only be very small.

DFT

Density functional theory (DFT) is an entirely different approach to solving the Schrödinger equation than the methods discussed above, instead of working upwards from the basic principles of quantum mechanics, DFT works from the top down. The founding principle of DFT states that there is a one-to-one correspondence between the electron density of a system and its energy. If one considers that the electron density is essentially the square of the wave function this conclusion should be clear.

Within the framework of Kohn-Sham DFT the kinetic energy of the electrons can be calculated exactly, so the only unknown is the exchange-correlation energy.^[143] Unfortunately it is not possible to calculate the exchange-correlation exactly so it must be approximated. Typically the local density approximation (LDA) allows estimation of the energy by assuming each electron only interacts with the mean field of all the other electrons. Two functionals are needed within LDA, the exchange functional and the correlation function. In DFT the density functional converts a wave function into an electron density that in turn produces energy. Many functionals have been published for both exchange and correlation, the most famous of which is BLYP.^[144] This comprises of the Becke exchange functional, and the Lee, Yang + Parr correlation functional. A common variation on this functional is mixing a certain percentage of HF into the waveform; this improves results by reducing the self-interaction error, where an electron interacts with itself in the mean field. This variation is so common it has been given a general naming scheme “AXB” where A is the exchange functional, X the number of parameters involved in the mixing, and B the correlation functional, this gives rise to functional names such as B3LYP^[144] and MPW1PW91^[145]. DFT is one of the most commonly use electronic structure methods today, and as such is a still an on-going research area. Recent functionals aim often aim to reduce the self-interaction energy, or describe non-covalent interactions more accurately.

CHAPTER 4 – DESIGN OF RENEWABLE AMINES

FIRST GENERATION AMINES

INTRODUCTION

Following from the work discussed in the previous chapters it was thought important to undertake computational studies to help design more efficient amines for CO₂ reduction. Previous computational work led the group to its first successful amine, this chapter builds on this work.^[132]

The first area selected for study was basic modification of the substitution patterns to the amine **20** previously synthesised by the author. Information from such a study could be used to guide the syntheses of second-generation amines.

The modifications detailed in this chapter around all led from the understanding of the reaction route shown below in Figure 24.^[128, 132] The modifications seek to improve the overall rate for CO₂ reduction and total quantum efficiency .

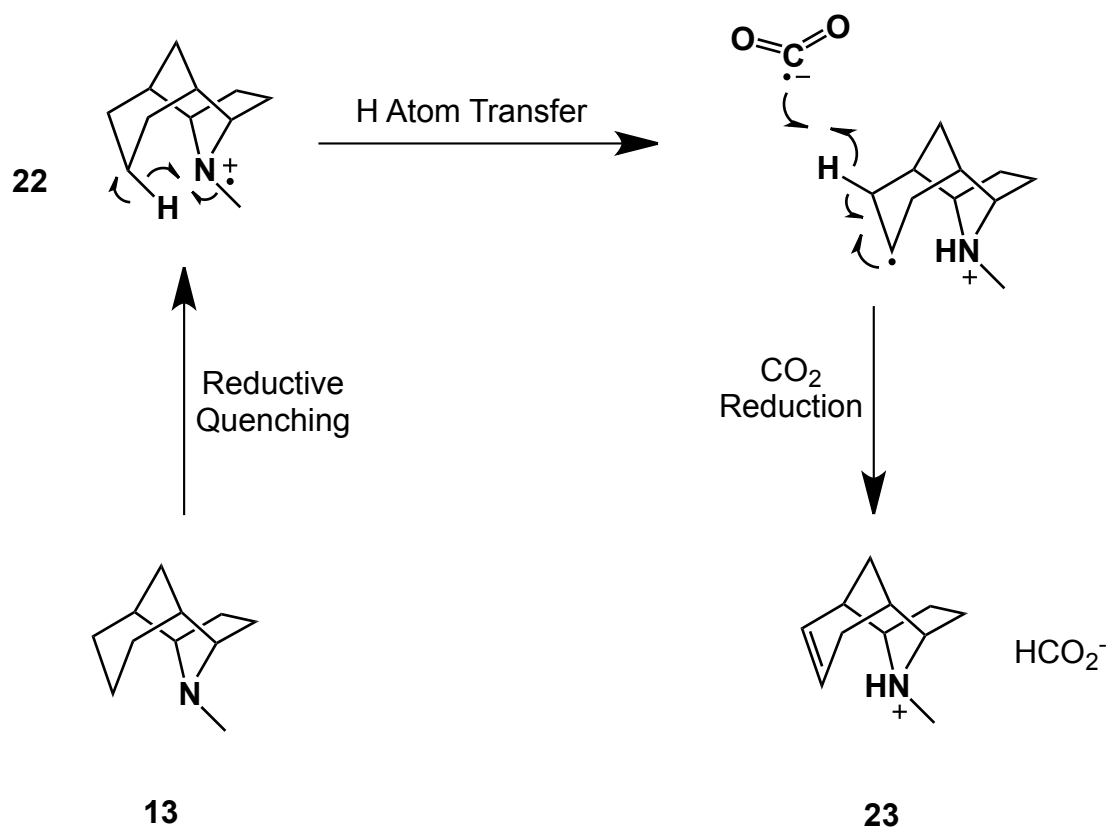


FIGURE 24: MECHANISM OF CO₂ REDUCTION IN TRICYCLIC AMINE

First the neutral amine, **13**, undergoes a charge transfer reaction with some excited state photocatalyst producing the amine radical cation, **22**. This can then undergo the hydrogen transfer reaction to produce the distonic radical cation. This molecule can then donate a hydrogen atom to CO₂ radical anion to produce the alkene and formate. Previous calculations within the group tell us there is a barrier to unproductive electron back transfer reactions from the distonic radical cation as the system falls well within the Marcus inverted region.^[129] We seek amines that undergo transformation into the distonic radical cation extremely quickly, this should be the case for reactions with low activation barriers that are exothermic or thermoneutral.

First, the thermochemistry for hydrogen transfer in amine **20** was calculated, because this amine had been experimentally shown to reduce CO₂ and therefore served as a useful benchmark for evaluating any further changes to the system. As can be seen from the results in, Table 4, the overall reaction is computed to be almost thermoneutral. The error in the calculations is likely to be larger than the predicted enthalpy of reaction. The reaction barrier of 7.20 Kcal mol⁻¹ is around the value expected for a reaction involving very little reorganisation in its transition state and suggests the reaction is likely to be fast. These results correspond well to the overall chemistry that has been previously observed experimentally.

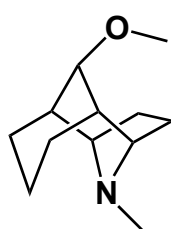
	ΔG^\ddagger	ΔH
20	7.20	1.33

TABLE 4: REACTION PARAMETERS FOR TRICYCLIC AMINE (KCAL MOL⁻¹)

NITROGEN SUBSTITUTED AMINES

From previous work it was known that unproductive H/D exchange reactions are possible with α H atoms on the amine. In the amine **20**, α H atoms within the cyclic structure were deactivated by making them bridgehead positions. However, the methyl group still has accessible hydrogen atoms for unproductive chemistry, this could reduce the overall quantum yield of the total CO₂ reduction.

The three molecules below, **23-25**, were chosen for study, as their lack of α H atoms on the nitrogen substitution should increase the quantum yield.

As shown in Table 5, the introduction of a phenyl substituent had a considerable impact on the reaction thermochemistry. This was expected due to the calculations reported by the group however it served as a useful example of the utility of the calculations to reveal poor substitution choices.^[128] In this case it is likely that the radical cation structure is significantly stabilised by delocalisation of the single electron around the phenyl ring. This would have a net effect of increasing the enthalpy of reaction and activation energy.

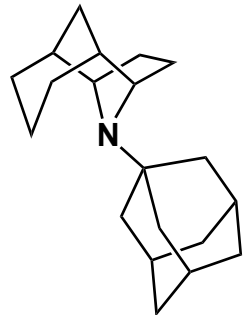
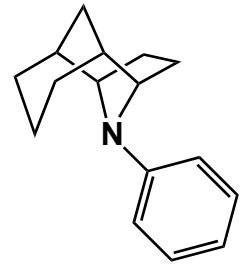
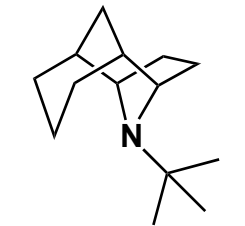
	ΔG^\ddagger	ΔH
 <p>23</p>	9.55	5.21
 <p>24</p>	19.13	17.30
 <p>25</p>	3.68	-0.89

TABLE 5: REACTION PARAMETERS FOR N SUBSTITUTED TRICYCLIC AMINES (KCAL MOL⁻¹)

The adamantane substitution, **23**, was chosen due to its famously inert structure, this should reduce the possibility of any side reactions occurring which could increase the amount of productive chemistry that can occur. As shown by the calculations this substitution has a minimal effect on the overall thermochemistry, the activation energy has risen by 2.35 kcal

mol⁻¹ and the enthalpy of reaction rose by almost 4 kcal mol⁻¹. While these increases are small, the relative increase is fairly large, and may influence the overall CO₂ reduction chemistry more significantly than the magnitude might suggest. We must also consider how such a large substitution will affect other chemical properties; the solubility of such a large non-polar group in the typically polar solvents used in CO₂ reductions is questionable. However there is no simple method to determine such properties accurately without resorting to experiment.

The introduction of the tert-Butyl group, **25**, had a more desirable effect on the overall thermodynamics, calculations predict an exergonic reaction, although we must take care not to forget that the error in such DFT calculations is often around 5 kcal mol⁻¹. The activation energy also decreased from the reference system; this suggested that reaction would be faster in this system. Coupling the faster rate of H transfer and the reduced number of unproductive pathways this molecule is predicted to be a significantly more efficient amine for CO₂ reduction and as such would be a valuable target for any further synthesis.

GROB FRAGMENTATION

The next series of modifications are based around replacing the OMe group in amine, **20**. The motivation to remove this group is to avoid the possibility of a Grob fragmentation. This is a reaction, illustrated below in Figure 25, in which a 1,4 elimination occurs. The reaction normally occurs in molecules with 2 heteroatoms in the 1 and 4 positions to facilitate the charge transfer steps and is particularly common in rigid polycyclic systems.^[146] In this case the tricyclic system would be broken leaving a cyclic amine, **26**, useless for CO₂ reduction chemistry.

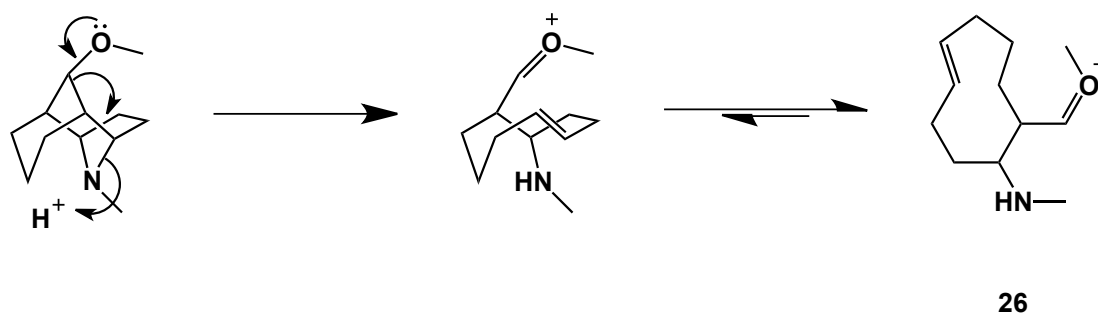


FIGURE 25: MECHANISM OF GROB FRAGMENTATION

The initial calculations were carried out on amine **13**, where a single H atom has replaced the OMe group. This provided a system that removes the possibility of a Grob fragmentation

without adding any additional complexity. As can be seen below in Table 6 the overall thermodynamics of the system were found to be very similar to those for the OMe substituted version, **20**. This showed the desired chemistry was not significantly affected by the presence of the OMe group and provided confidence that further modifications in the same position could lead to further improvements.

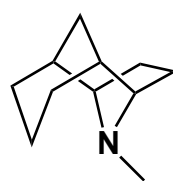
	ΔG^\ddagger	ΔH
	7.31	3.38
13		

TABLE 6: REACTION PARAMETERS FOR UNSUBSTITUTED TRICYCLIC AMINE (KCAL MOL⁻¹)

We next considered two molecules where the OMe group had been replaced with an alkyl group, these molecules are potentially available through Wittig type chemistry. This should be considered an alternative method of removing the oxygen atom remaining from the cycloaddition. As Table 7, shows, the overall change in thermochemistry is negligible; both reactions showed an almost thermoneutral pathway and low activation barriers. The simplest case, methyl substituted **22**, had similar activation energy to its parent amine **20**. This suggested the molecule is likely to also reduce CO₂ at a similar rate to its parent, but not be depleted by the Grob fragmentation.

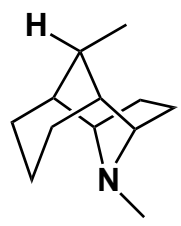
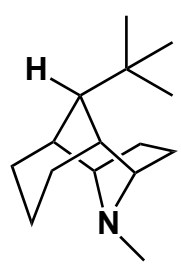
	ΔG^\ddagger	ΔH
 27	6.89	1.12
 29	4.71	1.18

TABLE 7: REACTION PARAMETERS FOR 7-SUBSTITUED TRICYCLIC AMINES (KCAL MOL⁻¹)

STABILISED AMINES

The final two molecules based on parent amine **20** aim to stabilise reaction products through delocalisation of the spin around a phenyl ring. The molecules shown below, **30** and **31**, have phenyl rings β and α to the radical we wish to stabilise and the results are shown in Table 8. For the β -substituted version of this molecule, **30**, it was not possible to locate the transition state but it was possible to predict the reaction is endothermic by almost 5 kcal mol⁻¹. This is not unexpected as a radical β to a phenyl group is not expected to gain any stabilisation through delocalisation. This substitution should however promote the transfer of an H atom to CO₂ radical anion; unfortunately it was not possible to make accurate predictions about this chemistry using the available computational models.

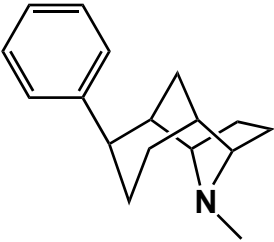
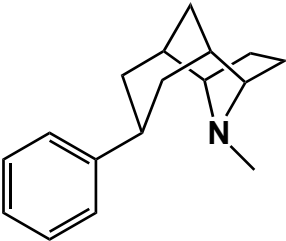
	ΔG^\ddagger	ΔH
 30	N/A	4.72
 31	2.81	-7.26

TABLE 8: REACTION PARAMETERS FOR STABILISED TRICYCLIC AMINES (KCAL MOL⁻¹)

The second molecule of this type is the α -substituted version, **31**, it was hoped that the phenyl group would stabilise the distonic radical cation. In this case the reaction was found to be exothermic by almost 7 kcal mol⁻¹, this suggests that the product is stabilised significantly compared to its parent. The kinetics are likely to remain fast as the activation energy is still only around 3 kcal mol⁻¹. These calculations suggest that amine **31** will rapidly form a distonic radical cation, this predicts a low rate of electron back transfer. If the stabilisation of the radical cation has not raised the barrier to H-atom transfer significantly this amine should be suitable for productive CO₂ reduction chemistry. It is unfortunately not possible to accurately study the H-atom transfer chemistry within the framework of our DFT model and the system is too large to calculate reaction parameters with higher-level methods.

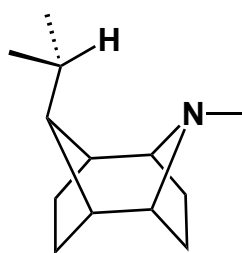
However, another issue to be considered for the last 2 molecules concerns stereochemistry. In both cases, the calculations were conducted on the epimer with the phenyl ring pointing away from the reactive centre, however the sterically accessible face for hydrogenation of the alkene will produce the wrong epimer. In the case of the α amine, **31**, this would result in a complete deactivation of the CO₂ reducing properties of the molecule.

It seems clear that the parent amine, **20**, is not suited to modifications that aim to stabilise the distonic radical cation and as such it seems prudent to study a series of molecules that are capable of such a stabilisation without eroding the other properties of the molecule.

SECOND GENERATION AMINES

INTRODUCTION

From previous work within the group it was known that the hydrogen transfer reaction is fast for structures involving a 6 membered transition state,^[128, 147] and from the previous calculations within this project we know stabilising the distonic radical cation is important to ensuring efficient formation of the distonic radical cation. It is also important to ensure that we do not introduce stereochemical issues that could influence the overall scheme for CO₂ reduction as illustrated above. Furthermore it is important we retain the rigid structure that holds the amine in the correct conformation for the reaction. Considering all these factors, the following amine, **32**, was designed.



32

The design of amine **32** has moved the H atom due to be transferred out of the rigid ring structure, onto a freely rotatable group. This allows us to keep to optimum conformation for the transfer while allowing us to introduce stabilising groups without the potentially negative stereochemical issues addressed above. The explicitly shown hydrogen in structure **32** is the atom that would be transferred during the formation of the distonic radical cation. The following diagram shows the full mechanism that this class of amine is likely to react through, Figure 26.

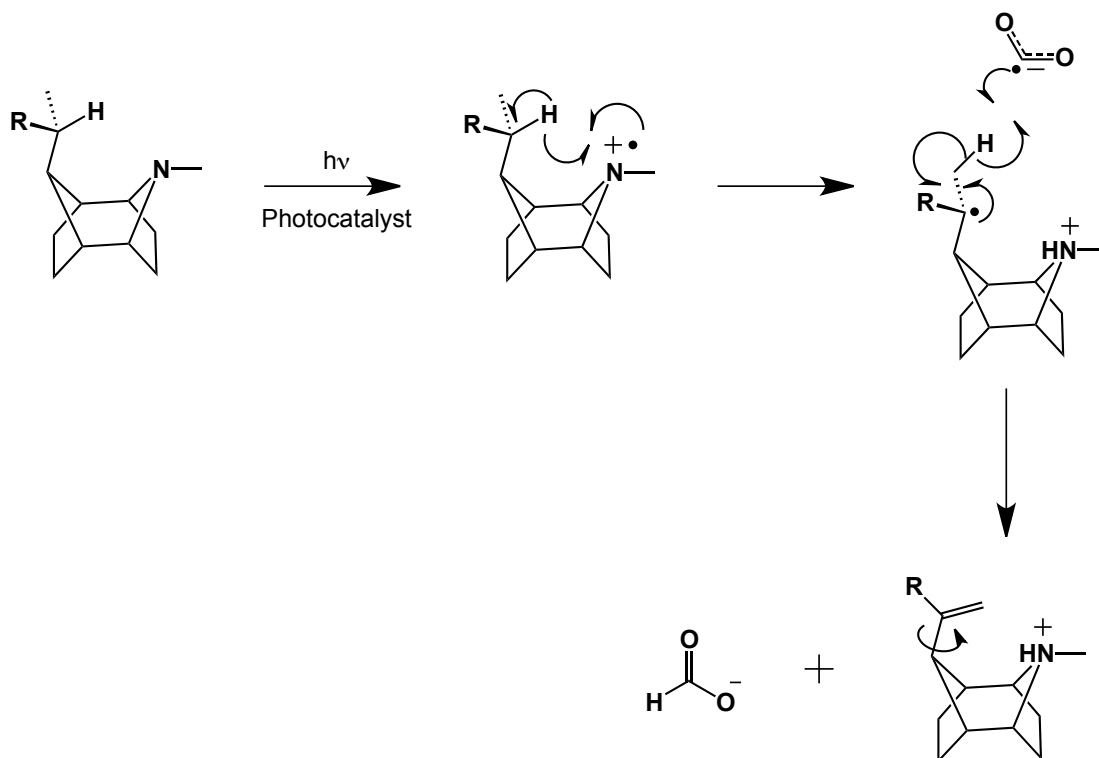


FIGURE 26: MECHANISM OF CO₂ REDUCTION IN SECOND GENERATION AMINES

The R group should be freely substitutable for any group that will not interfere with the photochemistry or the subsequent CO₂ reduction chemistry. The next section of this thesis aims to identify the optimal substitution pattern to enhance formation of the distonic radical cation.

RADICAL STABILISATION ENERGY

Before launching into an in depth study of the how best to stabilise the distonic radical it is worth discussing the background of the subject. Many people have studied the stability of carbon-centred radicals and the vast majority use the radical stabilisation energy (RSE) as a convenient measure of the relative effects of substituents. The RSE is defined as the enthalpy change of the reaction between a methyl radical, and the closed shell parent of the substituted molecule in question. This effectively compares the relative stability of reference methyl radical and the radical in question or, to describe the concept in another way, it is a comparison of the relative bond dissociation energies of the closed shell parent compounds. This is a thermodynamic measure of radical stability and does not account for kinetics. Neither does it account for the varying C-H bond strengths in the parent compounds, the effect of this is often small due to similar C-H bond strengths across a wide range of hydrocarbons. This assumption can often fail in the cases of very polar molecules or in cases where steric effects have become significant. It is also possible to change the reference

compound to more substituted molecules such as ethane, propane and isobutane; which can be more appropriate for cases where the radical of interest is not a primary radical. There are some alternative schemes for calculation of RSE that aim to reduce some of these deficiencies by considering dimeric structures which reduce polar effects but introduce steric effects. However each are fraught with their own problems and in meta studies do not typically perform better.^[148] A vast number of RSE energies have been reported in literature and with careful consideration, we can use these values directly in the study of new radicals. The RSEs used in this project have been determined computationally using high level *ab initio* calculations (at the G3(MP2)-RAD level), the study which published these results shows the wider applicability of their results through comparison of almost 200 test cases to various bond dissociation energies and Mulliken spin densities.^[148]

There are various mechanisms by which a radical centre can be stabilised; the key is to reduce the orbital density of the lone electron on any particular atom. This reduces the accessibility of the radical to undergo further reactions, and therefore rendering it stabilised. The first and most simple mechanism is the inductive mechanism in which the density of the radical is pulled away from its main centre. This can be seen by the positive RSE of the CH₂F group, meaning this radical is more stable than the methyl radical. CHF₂ and CF₃ show negative radical stabilisation energy due to strong C-H in the closed shell parents and the ability of F substituents to act as both a σ -acceptor and a π -donor.^[149] The second effect is delocalisation of the radical; this can spread the density of the SOMO across a number of atoms. In the case of a benzyl radical the SOMO can be delocalized across the entire ring structure, giving rise to a RSE of around 14.6 kcal mol⁻¹^[150].^[148] This is around twice as powerful as the inductive effects in a tert-butyl radical. The final mechanism of stabilisation considered is lone pair donation, this is effectively a charge transfer reaction that spreads the spin across another atom and generates a zwitterion. These effects can also be combined and may produce synergetic effects, this has been reported especially for peptide radical species.^[150]

The applicability of the RSEs from the above study to the case of the distonic radical cations studied during this project may well be questioned on several levels. Firstly it is unlikely that the H atom BDE in the parent amine radical cation is modelled well by a simple hydrocarbon radical BDE because the amine C-H bond has been purposely weakened to promote the desired chemistry. Secondly the steric effects of a rigid ring system are bound to have an influence on the stability of the distonic radical cation. Additionally there will be large polar effects from the positively charged nitrogen atom held in close proximity to the radical in

question. However despite these concerns it is expected that the general trend predicted by the RSEs is likely to hold true in our system. The first series of calculations performed seek to confirm this assumption.

STABILISING SUBSTITUTIONS

The first step in the investigation of this class of amines was to calculate the properties of the base molecule, **32**. This allows us to determine if the overall scheme was a viable route for CO₂ reductions. Table 9 shows that activation energy was improved over the first generation amine, **20**, and formation of the distonic radical cation was exothermic from the localized radical cation. This suggested that the new class of amines are suitable for the desired CO₂ reduction chemistry and warrants further investigation of the stabilisation of the distonic radical centre.

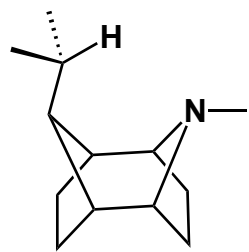
	RSE	ΔG^\ddagger	ΔH
	5.49	2.00	-2.63
32			

TABLE 9: REACTION PARAMETERS FOR SECOND GENERATION AMINE (KCAL MOL⁻¹)

Using a series of substituents chosen from a published list of RSEs,^[148] filtered for examples expected to be suitable for photochemistry and stable to hydrogenation, a library of calculations was compiled.^[148] The enthalpies of activation and formation of distonic radical cation against the published RSE values are given in, Table 10. The results are also presented in a graphical format in Figure 27 and Figure 28.

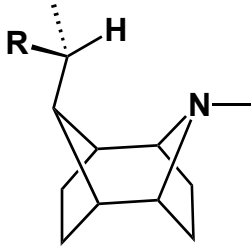
32 - Me 33a - CFH₂ 33b - CF₂H 33c - CF₃ 33d - CN 33e - OMe 34 - Ph		RSE	ΔG^\ddagger	ΔH
32		5.49	2.00	-2.63
33a		3.94	7.20	0.70
33b		2.46	8.63	1.53
33c		1.84	8.79	3.24
33d		11.58	7.11	-5.39
33e		8.72	1.73	0.15
34		16.31	3.20	-5.47

TABLE 10: REACTION PARAMETERS SUBSTITUTED SECOND GENERATION AMINES (KCAL MOL⁻¹)

Before discussion of the results in relation to CO₂ reduction it is worth assessing the utility of RSE values in predicting the stabilising effect of substituents on the distonic amine radical cations. Plotting the difference in reaction enthalpy of a substituted amine and the base amine, **32**, against the RSE value of the substituent showed a correlation ($R^2 = 0.82$), Figure 27. Although the correlation is not strong a general trend relating RSE values to reaction enthalpies seems clear. This trend allowed us to select substituents for more detailed study that does not rely on accurate predictions from the RSE value.

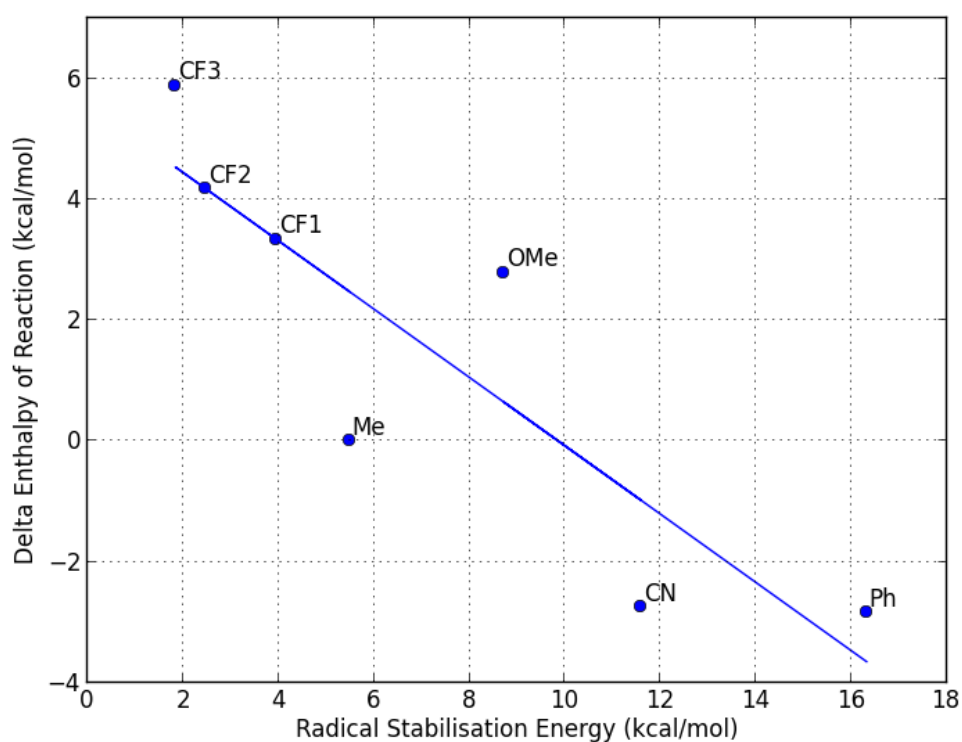


FIGURE 27: GRAPH OF RSE AGAINST DIFFERENCES IN REACTION ENTHALPY ($R^2 = 0.822$)

Analysing the same data set but plotting the activation enthalpy against the RSE leads to two conclusions. Firstly electron-withdrawing substituents are destabilizing to the formation of the distonic radical cation and electron-donating substituents are strongly stabilising. Secondly, the key observation from this series of calculations is those substituents capable of delocalizing the spin across several atoms are highly stabilising. The low activation energy of **33e** does not follow the expected trends for electron withdrawing substituents this supports the conclusion that delocalisation of the radical is a particularly effective stabilisation method.

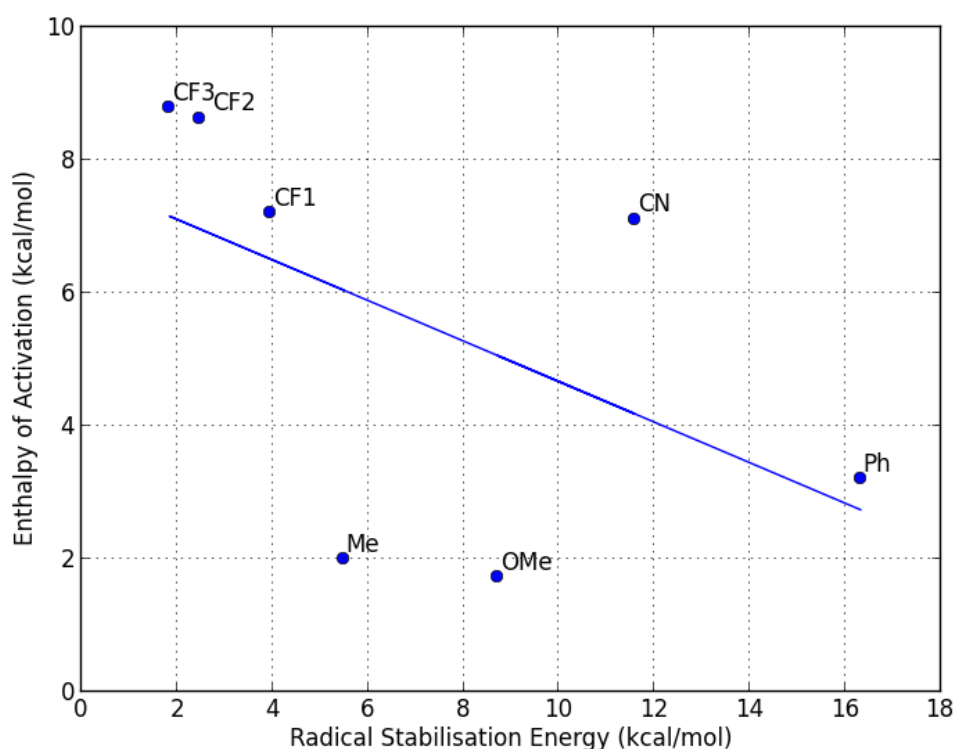


FIGURE 28: GRAPH OF RSE AGAINST ACTIVATION ENERGY

These results led to the conclusion that the best substituents to promote the desired formation of the distonic radical cation are those with strong delocalisation properties. This class of substituents gives rise to amines that undergo extremely fast formation of the distonic radical cation, which should in turn lead to low rates of electron back transfer. This is due to the combined influence of both low activation energies and almost thermoneutral or exothermic reaction enthalpies. This class of delocalising substituents may well influence the ability of the distonic radical to transfer an H-atom to CO₂ radical anion, unfortunately it was not possible to accurately study this effect within the framework of our DFT model.

PHENYL BASED SUBSTITUENTS

When considering suitable substituents for CO₂ reduction chemistry we must consider not only efficient formation of the distonic radical cation but also the stability of the molecule throughout the scheme. Firstly the molecule must be stable to irradiation across a wide range of wavelengths, it should not undergo unwanted electron transfer reactions that may lead to undesirable side reactions. It should also be stable to the hydrogenation conditions required to return the alkene to the initial amine required for CO₂ reduction.

The above considerations ruled out any molecules containing alkene or alkyne groups, as these would not tolerate the hydrogenation conditions. This is unfortunate as some of the

highest reported RSE values are those for di-allyl substituents. The substituents with highest degree of delocalisation that will also be stable to hydrogenation are phenyl-based fragments. However we must take care not produce a substituent with electronic properties that are likely to interfere with the photochemistry. As such it seems that a simple phenyl substituent is likely to be the most appropriate substituent for this particular chemistry.

As shown in the above graph, Figure 28, a simple phenyl substitution produced an amine with low activation energy, $3.2 \text{ kcal mol}^{-1}$, and a negative enthalpy of reaction. This suggested that CO_2 reduction chemistry from this amine would be efficient. However it is possible that a substituted phenyl ring could provide an even more suitable amine, that is one with a thermoneutral reaction enthalpy. To investigate this possibility three substituted phenyl rings were investigated, *p*-fluoro **36**, *p*-methoxy **37** and *p*-cyano **35**. These were chosen as a representative model of an electron withdrawing, electron donating and delocalising substituents while being unresponsive to irradiation. The thermodynamics parameters calculated for these species are presented alongside the phenyl case below, Figure 29. As can be seen the activation energies of each of the molecules are similar, with a slight tendency for electron withdrawing substituents to have higher values. The enthalpy of reaction is within $2.71 \text{ kcal mol}^{-1}$ for all cases studied, with no clear tendency for particular electronic properties to show values closer to zero. These results suggested that the electronic properties of the ring have a much smaller influence on radical stabilisation than the rings ability to delocalise spin around itself. As shown in these molecules modification to the phenyl substituent shows little improvement in overall thermodynamics of the reaction.

overall scheme. The studies on the electronic properties of these phenyl-based substituents suggest that all substituents are centred closely on a point, Figure 30. This suggests that additional substitution plays little role in the overall photochemistry. This leads to the overall conclusion that a simple, unsubstituted phenyl ring is the overall the most suitable substituent for stabilising the formation of the distonic radical cation in this class of amines. Ideally one would hope to find an amine with extremely low activation energy for the forward reaction, with a slight exothermic nature to retard the backwards reaction.

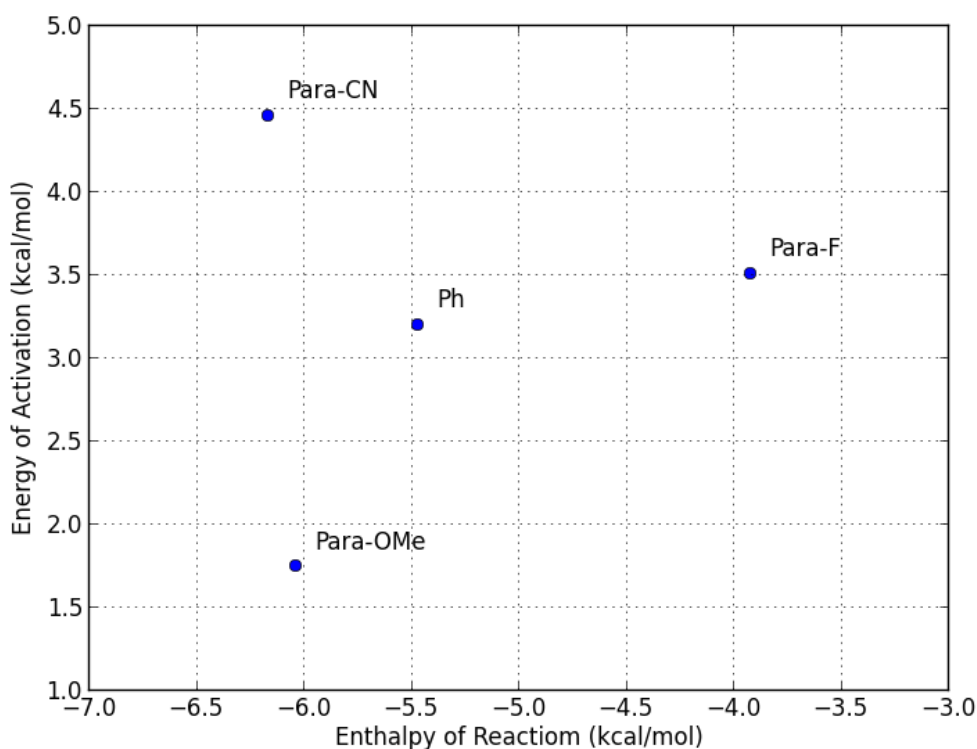


FIGURE 30: GRAPH OF ACTIVATION ENERGY AGAINST REACTION ENTHALPY FOR A SERIES OF PH SUBSTITUTED SECOND GENERATION AMINES

RATE CALCULATIONS

When one examines the potential energy surface for phenyl-substituted amine, **34**, it is clear that the thermodynamic barrier to reaction is extremely low and that the distance moved by the H atom to the transition state is extremely small. Reactions of this nature are often extremely fast due to contribution from quantum tunnelling; the following sections aims to determine if second generation amines have a tunnelling component to their rate constant with direct dynamics calculations.

INTRODUCTION

Quantum tunnelling is a phenomenon predicted by the laws of quantum mechanics that allows particles to pass through barriers that they would classically be unlikely to cross. Quantum tunnelling correctly predicts many observations that are inexplicable by classical mechanics such as nuclear decay, some properties of semiconductors and the possibility of scanning tunnelling microscopes.

This effect can be explained by combination of the Heisenberg uncertainty principle and particle-wave duality. If one considers a potential energy well with high walls but narrow wall thickness then it can be shown that the wave function of a particle within the well could have a non-zero density outside the well, thereby predicting that a certain number of particles will be able to tunnel through the barrier even though they have insufficient energy to pass over the top of the barrier. The ability to pass through barriers without passing over the traditional transition state ensures that some chemical reactions will display rates much faster than that predicted by standard transition state theory.^[151] There have been many examples of such reactions directly observed in the chemical literature; in recent years examples of heavy atom tunnelling have also been found.^[152]

Tunnelling Corrections to Rate Calculations

Classical Transition State Theory (CTST) can predict reaction rates from knowledge of the potential energy surface. It achieves this by assuming a “quasi-equilibrium” between reactants and the transition state (also called activated complex), and that once the system reaches the transition state saddle point it can either collapse back to reactants or undergo productive chemistry. The rate at which products are formed from the transition state can be determined by considering the vibrational modes along the reaction coordinate. Classical Transition state theory (CTST) correctly predicts the rate constants of many reactions. It should be clear from this brief outline of CTST that it will not accurately predict rates of reactions with a significant quantum tunnelling component as the key assumption expects the reaction coordinate to pass over the maximum barrier to reaction. Wigner derived separable approximation for including quantum effects that is normally known as the Wigner tunnelling correction.^[153] It allows crude estimation of the tunnelling portion of a reaction modelled by CTST.

If one wishes to calculate accurate rates in reactions that involve a tunnelling component it is critical to consider alternative reaction pathways that can avoid crossing through a traditional transition state. It can be shown that wave functions decay exponentially while inside barriers. In the simple case, of low curvature, to find the optimum tunnelling pathway

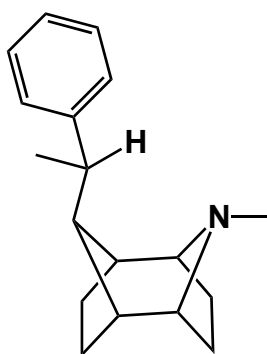
one must find where the barrier height and width are both at a minimum. However in the case of high curvature between the reactant potential energy surface (PES) and the product PES we must also consider how this will influence optimal tunnelling paths in this case we must optimise to straight and short tunnelling paths.^[154]

A complete analysis of the cases above requires a complete PES for both reactants and products within the reaction area. This is intractable for anything but the simplest systems; so approximate methods must be used to allow facile calculation of complex systems. Direct dynamics simplifies this method by following the IRC (intrinsic reaction coordinate) from the transition state of the reaction and examining the potential for tunnelling at each step. This can be extremely accurate in cases of low curvature, where there are unlikely to be tunnelling pathways off the IRC. However in cases of high curvature one must also consider the possibility of “corner cutting” that may avoid most if not all of the points considered in a typical IRC calculation. In high curvature cases it is often better to concentrate calculations around the equilibrium geometry of the reactant and product.^[151b, 155]

As described above the nature of such calculations can become extremely complicated and can require many electronic structure calculations to provide enough detail about the reaction potential energy surface to provide accurate rate information. Thankfully programs such as PolyRate abstract most of this effort away from the end user and allow calculation of reaction rates including tunnelling corrections with just coordinates for the reactant, transition state and products.^[156]

RESULTS

Due to the expensive nature of accurate rate calculations it was only possible to study a single step of a single molecule and the calculations had to be run without solvent model. The chosen molecule was amine, **34**, as this has been selected as the most appropriate molecule for overall CO₂ reduction in the previous set of calculations.



34

The reaction studied is the formation of the distonic radical cation from the localised parent radical cation amine. Three tunnelling approximations were considered (Wigner, zero curvature and small curvature) as the additional cost of each additional tunnelling approximation is small in comparison to the overall cost of the calculation. As can be seen in the results below, Table 11, the reaction is predicted to be incredibly fast even without considering the tunnelling pathways.

The forward reaction is shown to have a tunnelling component at 298K with predicted reaction rates doubling when small curvature tunnelling is considered. The reverse reaction is shown to be substantially slower than the forward reaction indicating that a significant amount of the distonic radical cation should exist during the course of the reaction. It is also worth noting that the rate of formation is above typical rates of diffusion in solvent, this suggests that the rate-limiting step in this reaction will not be formation of the distonic radical cation.

Forward Rates				
	None	Wigner	Zero Curvature	Small Curvature
TST	1.40E+11	1.86E+11	1.93E+11	2.24E+11
Backward Rates				
	None	Wigner	Zero Curvature	Small Curvature
TST	7.60E+06	1.01E+07	1.05E+07	1.22E+07

TABLE 11: RESULTS OF RATE CONSTANT CALCULATIONS AT 298 K (s^{-1})

CONCLUSIONS

The above calculations suggested that amine **34** would be an efficient molecule for the photochemical CO_2 reductions. Unfortunately calculations can only take us so far, so we must design a feasible synthesis for such amines. A proposed route to this amine is suggested in Chapter 5 and calculations performed to determine its feasibility.

PHOTOCHEMICAL STABILITY

INTRODUCTION

An important part of designing an effective system for photochemical CO_2 reduction is that all the molecules involved should not undergo side reactions. This would prevent the reaction slowing down over time due to depletion of the starting materials. From previous

work in the group we know that amine **20** is stable under photochemical conditions long enough to produce detectable levels of formate. As we can detect the alkene in the reaction mixture we know that this alkene must also be stable to the reaction conditions. When evaluating amines such as, **32**, we must also consider the stability of the produced alkene.

ALKENE ADDITION

The alkene, **38**, is susceptible to reductive quenching reactions with an excited state photocatalyst just as its parent alkane was. This would produce a highly reactive amine radical cation in close proximity to an alkene system; it is possible that a cyclisation reaction could occur, Figure 31. This would render the amine inactive to hydrogenation and therefore remove it from the overall reaction scheme. The following section studies this possibility and attempts to propose manners by which the possibility of such a reaction could be reduced or moved entirely.

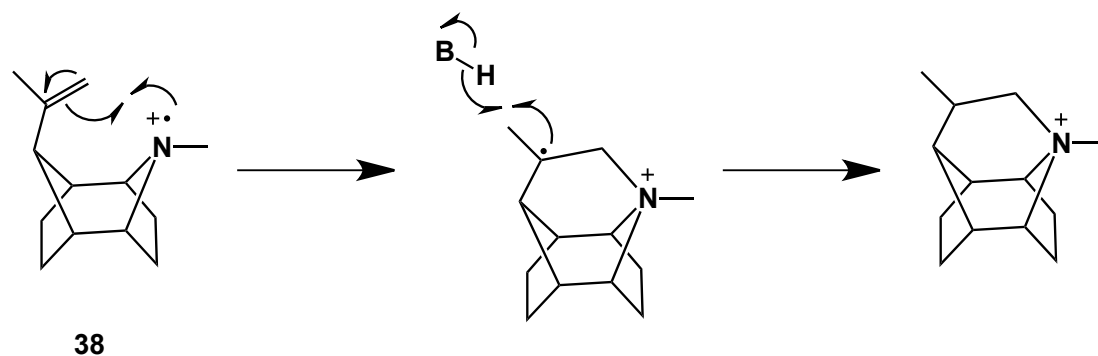


FIGURE 31: MECHANISM FOR ADDITION OF AMINE RADICAL CATION TO ALKENE

We already know from previous experimental work that amine **20** is fairly stable to any possible alkene addition chemistry so we first calculated the reaction thermodynamics for this case.^[132] This acts as a valuable comparison between computational and experimental results for future calculations. The calculated reaction enthalpy showed the reaction to be exothermic by 5.40 Kcal mol⁻¹, Table 12. Unfortunately, despite extensive searching, it was not possible to locate a transition state for this reaction. This likely means that the transition state exists on a saddle point so shallow that the convergence criteria used to locate transition states are inadequate. This suggested that the reaction would face very little barrier from the correct conformation, however this conformation could still lie well above the equilibrium geometry on the potential energy surface.. In this reaction it seems unlikely that there is a large enough barrier to reaction to baffle normal algorithms, so it is presumed that the transition state lies within a shallow saddle point and the barrier to reaction is mostly conformational.

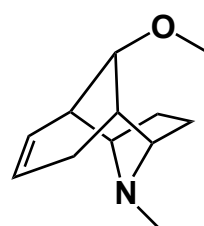
	ΔG^\ddagger	ΔH
	N/A	-5.40
21		

TABLE 12: REACTION PARAMETER FOR CYCLISATION OF FIRST GENERATION AMINE (KCAL MOL⁻¹)

The previous calculations suggest that amines with rigid structures holding the amine radical cation in close proximity to the alkene are likely to face more significant problems with unwanted side reactions during CO₂ reduction reactions. As the second-generation amines discussed in the previous section are significantly more constrained than the first-generation amines this problem is likely to be more manifest in this class of amines. The reaction thermodynamics were calculated for the base second-generation amine, **38**, but again it was not possible to locate a transition state. The overall reaction enthalpy was found to be 0.01 kcal mol⁻¹. Although it was not possible to locate the transition state, the barrier to reaction was assumed to be low.

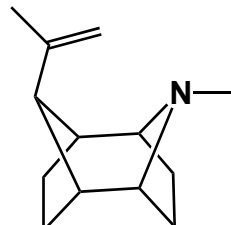
	ΔG^\ddagger	ΔH
	N/A	0.01
38		

TABLE 13: REACTION PARAMETERS FOR CYCLISATION OF SECOND GENERATION AMINE (KCAL MOL⁻¹)

The following section aims to qualify the problem in second-generation amines and evaluate some methods by which the problem could be reduced. Based on the understanding that the main barrier to reaction is likely to be conformational, most designs aim to hold each reactive moiety away from the other and in one case we aim to solve the problem with electronic effects.

The molecules described below were all examined to determine the likelihood of them undergoing alkene addition chemistry. In all cases extensive searches for the relevant transition state were undertaken but only in a handful of cases were we successful.

Alkene Constrained Amines

The first method investigated was to hold the alkene away from the amine centre with additional constraints. This involved an extra hydrocarbon backbone that reduces the ability of the alkene to move towards the centre of the molecule.

Both these molecules aim to reduce movement in the alkene by pinning it back on itself, as is shown in Table 14. The first molecule, **39**, shows enthalpy of reaction of $-7.77 \text{ kcal mol}^{-1}$ however in this case we were unable to locate a transition state. In fact all attempts to locate the transition state collapsed to product, this again supports a hypothesis of very shallow saddle points.

The transition state search for the second molecule, **40**, successfully found a stationary point in a gas phase calculation, $0.45 \text{ kcal mol}^{-1}$ above the starting material. The imaginary frequency is only $174.43i \text{ cm}^{-1}$ which indicates that the saddle point is extremely flat; this confirms our assumption that the barrier to reaction is mostly conformational in this class of reactions. It also goes some way to explaining why the search for transition states was often unsuccessful in this section.

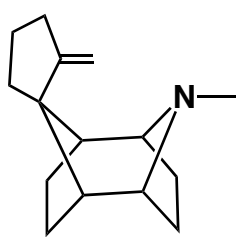
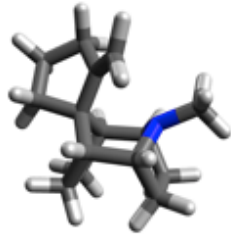
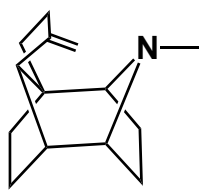
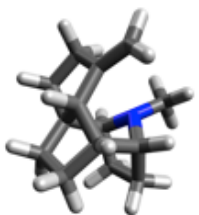
		ΔG^\ddagger	ΔH
		N/A	-7.77
39			
		0.45	-11.36
40			

TABLE 14: REACTION PARAMETERS FOR CYCLISATION OF ALKENE CONSTRAINED 2ND GEN AMINES (KCAL MOL⁻¹)

In both cases the thermodynamics of the CO₂ reduction chemistry seemed mostly unaffected. These parameters were calculated in solution phase in order to allow comparison to other second-generation amines. Activation enthalpies for formation of distonic radical cation were found to be 6.02 kcal mol⁻¹ for **39** and -0.15 kcal mol⁻¹ for **40**, and reaction enthalpies were again found to be almost thermoneutral, 1.18 and -1.58 kcal mol⁻¹ respectively.

Amine Constrained Amines

The second method investigated was to restrain the amine from moving towards the alkene; this used an additional hydrocarbon backbone to hold the amine group in place. These molecules take a similar “pinning back” strategy to the previous pair of molecules, except we now held the amine in place.

In neither case was it possible to locate a transition state between reactants and products in either gas or solution phase. As such the following calculations were performed in solution phase, Table 15. In the cyclopentyl case, **41**, the search again collapsed into product on each attempt, and the overall reaction enthalpy is found to be almost exactly thermoneutral at -0.01 kcal mol⁻¹. The cyclohexyl case, **42**, was found to be more significantly exothermic,

-11.76 kcal mol⁻¹ and the transition state search did not collapse to product or reactant. This suggests there is some barrier to this reaction however it is still likely to be small.

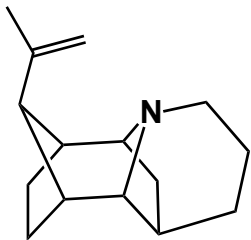
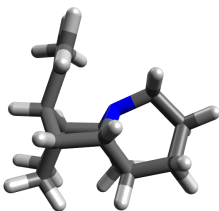
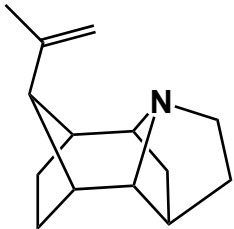
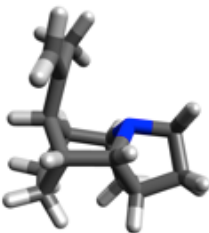
		ΔG^\ddagger	ΔH
  41		N/A	-11.76
  41		N/A	-0.01

TABLE 15: REACTION PARAMETERS FOR CYCLYLISATION OF AMINE CONSTRAINED 2ND GEN AMINES (KCAL MOL⁻¹)

The CO₂ reduction chemistry of the cyclohexyl case, **42**, was found to be favourable with activation energy for formation of distonic radical cation of 3.30 kcal mol⁻¹ and an overall reaction enthalpy of -1.87 kcal mol⁻¹ calculated in solution phase.

Backbone Constrained Amine

The molecules below were designed to make the entire backbone structure more rigid in hope that the reduced flexibility would prevent close proximity of the alkene and amine radical cation, Table 16. In both cases it was possible to locate a solution phase transition state for these molecules, the activation energy has been calculated at -0.49 and 2.54 kcal mol⁻¹ respectively. While negative activation energy is a physical impossibility the error in such calculations is much larger than the magnitude of the activation energy, this suggests we have a low positive activation energy. The imaginary frequencies were found to be 144.31i cm⁻¹ and 228.10i cm⁻¹ suggesting a shallow nature of the saddle point and supported the conclusion of a high rate constant for the reaction. The reaction enthalpies are predicted to be -9.15 kcal mol⁻¹ for the hexyl case, **43**, and -3.99 kcal mol⁻¹ for the pentyl case, **44**. The pentyl case showed the most promising result so far but a barrier of that magnitude is unlikely to prevent the reaction occurring.

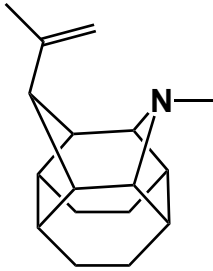
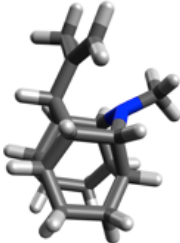
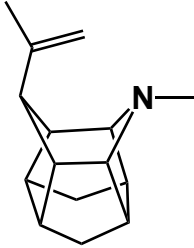
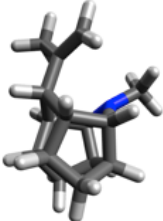
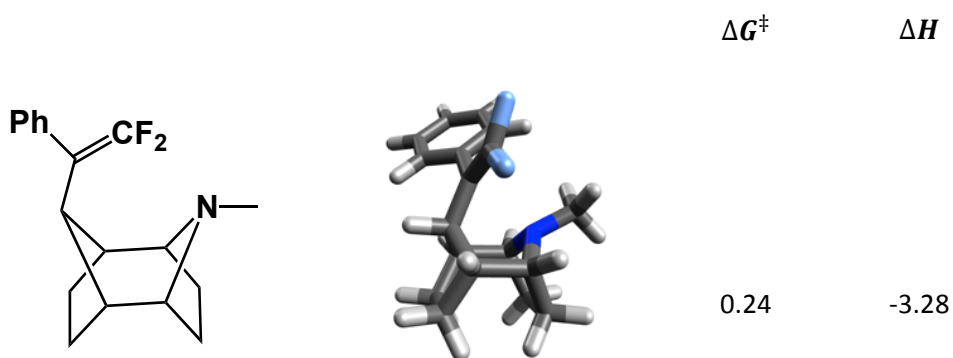
		ΔG^\ddagger	ΔH
		-0.49	-9.15
43			
		2.54	-3.99
44			

TABLE 16: REACTION PARAMETERS FOR CYCLISATION OF BACKBONE CONSTRAINED SECOND GENERATION AMINES (KCAL MOL⁻¹)

The thermodynamics of CO₂ reduction chemistry are still favourable for the hexyl case, **43**, with activation energy for formation of distonic radical cation of 5.92 kcal mol⁻¹ and an enthalpy of 0.96 kcal mol⁻¹. It was not possible to determine overall CO₂ reduction properties for the pentyl case as stationary points for the relevant transitions states could not be found

Electronically Constrained Amines

The final method tested was one in which the constraints take the form of electronic influences that should prevent the reaction. In the case discussed below the first step of the alkene addition would create a radical destabilised by a CF₂ group, which should be disfavoured according to the RSE values discussed previously in this chapter. The phenyl group is present to ensure that the productive formation of the distonic radical cation is still facile despite the presence of the electron-withdrawing group.



45

TABLE 17: REACTION PARAMETERS FOR CYCLISATION OF ELECTRONICALLY CONSTRAINED AMINES (KCAL MOL⁻¹)

In the final molecule studied it was not possible to locate a solution phase transition state, but we were more fortunate in the gas phase. The saddle point was found to sit 0.24 kcal mol⁻¹ above the reactant and again the imaginary frequency, 174.81i cm⁻¹, indicated the flat nature of the potential energy surface in this region. The reaction enthalpy was calculated as -3.28 kcal mol⁻¹ in the solution phase. This strategy meets with limited success, and the presence of two electron-withdrawing groups α to the H atom transferred to CO₂ will affect the CO₂ reduction chemistry.

DMAP BASED AMINES

INTRODUCTION

Previous unpublished work within the group involves high-level calculations on pyridine and dimethylamino-pyridine (DMAP) based amines.^[130] This work has shown that, while pyridine based amines do not possess an appropriate surface crossing to allow productive CO₂ reduction chemistry, DMAP based amines do. This work was undertaken by another group member and has yet to be published so a complete discussion of the method and results is beyond the scope of this thesis. However with the knowledge that DMAP based amines should be suitable for CO₂ reduction chemistry we can start to study constrained DMAP amines.

The initially proposed DMAP amine is based on a norbornane structure, **46**. This structure should hold the amino radical cation above the ring structure of the norbornane unit, which should facilitate rapid H atom transfer. Calculations on this molecule show that the optimum geometry for the ground state, **46**, holds the nitrogen atom away from the H atoms we wish to transfer. This suggests that even with a rapid H transfer reaction there would still be a significant barrier to reaction coming from the conformational change required.



46

By restricting the rotation of the DMAP moiety it is thought the desired chemistry could be promoted. The remaining calculations in this section aim to address this problem by calculation of activation energies, and reaction enthalpies of a series of molecules that join the aromatic ring to the norbornane ring in two places.

The preceding set of calculations suggest that the second-generation amines are at risk of undesired cyclisation reactions. It seems that design choices that favour CO₂ reduction chemistry also promote the destructive alkene addition chemistry. A number of strategies are outlined to reduce this problem however none of them have met with particular success. These issues must be overcome for any amine intended for industrial applications

CONSTRAINED DMAP AMINES.

The following section details calculations on DMAP based amines that are constrained with an additional ring structure holding the aromatic ring perpendicular to the bottom of the norbornane ring. The molecules were all presumed to follow the normal mechanism for distonic radical cation formation, as shown in Figure 32.

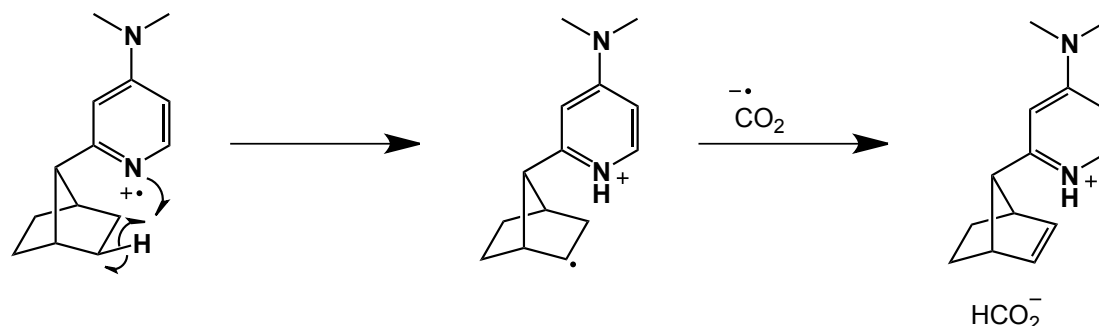


FIGURE 32: MECHANISM FOR CO₂ REDUCTION IN DMAP BASED AMINES

A series of constrained DMAP based amines have been studied and the results for formation of the distonic radical cation are shown below in Table 18.

n = 0 - 47a n = 1 - 47b n = 2 - 47c n = 3 - 47d n = 4 - 47e		ΔG^\ddagger	ΔH
47a		15.11	-4.92
47b		10.25	-4.04
47c		12.12	-1.39
47d		12.63	-6.79
47e		13.64	-2.51

TABLE 18: REACTION PARAMETERS FOR DMAP BASED AMINES (KCAL MOL⁻¹)

The trend in calculated activation energies does not agree with the presumption that a structure holding the N atom above the H atom will result in fast, favourable reactions. It is possible that the introduction of the tether is influencing the reaction more than initially expected. The tether could be introducing additional strain into the transition state and therefore increasing its energy. These calculations suggest that introducing an additional

ring to tether the DMAP moiety may not be a fruitful approach to facilitate the desired chemistry. This leads to the conclusion that a non-constrained DMAP based amine may well be suitable for photochemical CO₂ reduction and that it worth investigating experimentally..

CONCLUSIONS

This chapter has studied variations on the first generation amine, **20**. This investigation was unable to find a simple substitution pattern that was predicted significantly improved properties for CO₂ reductions. On this basis a series of second-generation amines, based on amine **32**, were examined for improved properties. This class of amine could be substituted with radical stabilizing groups to promote formation of distonic radical species. It was found that phenyl substituted amine, **34**, will rapidly form distonic radical cation and it was predicted that quantum tunneling will play a role in the fast rate of this reaction. However this new class of amines is not without their own problems; it is predicted that this class of amines will undergo photochemical cyclisation reactions that would deactivate them to further CO₂ reductions. Finally a series of constrained DMAP based amines were investigated for torsional properties, unfortunately the study was inconclusive at the level of calculation feasible within the constraints of this project.

CHAPTER 5 – SYNTHESIS OF RENEWABLE AMINES

FIRST GENERATION AMINES

SYNTHESIS OF AMINE FRAMEWORK

The work in this section leads on directly from the work reported in the previous chapter and has been guided by the calculations reported in the previous chapter. While the original development of the synthetic procedures towards the tricyclic amine **13** was performed before the work described in the present thesis, the synthesis had to be optimised for large scale. The first section of this chapter reports the efforts to scale the synthesis of the core framework of amine **20**.

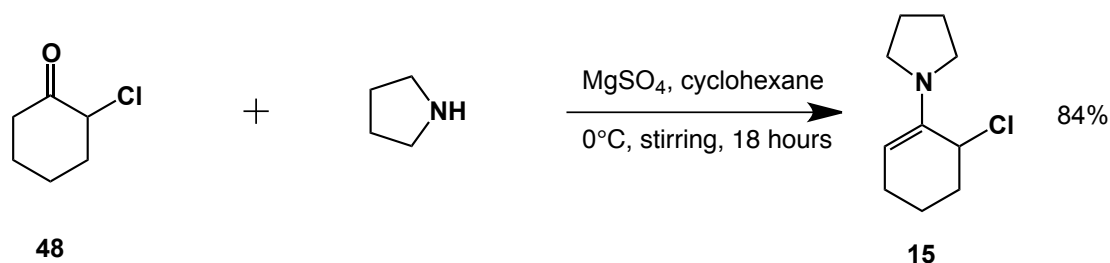


FIGURE 33: FORMATION OF ENAMINE FOR CYCLOADDITION

The first step in the synthesis is production of the enamine, **15**, which acts as a precursor to the amino-allyl cation in the cycloaddition.^[135] Previously, synthesis of this precursor enamine, shown in Figure 33, had been plagued by the formation of the double addition product, as shown below in Figure 34. While this reaction is only a side reaction, which occurs much slower than the enamine production, it reduces the overall yield of suitable amino-allyl precursor. The double addition product does not seem to interfere with the cycloaddition reaction directly, but it certainly complicates purification.

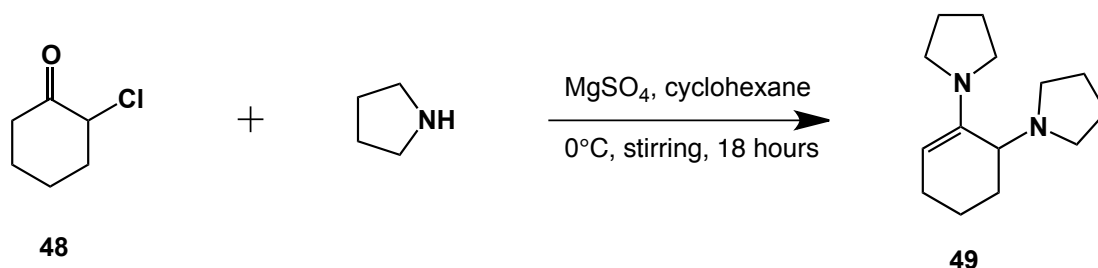


FIGURE 34: FORMATION OF DOUBLE ADDITION PRODUCT IN ENAMINE FORMATION

This reaction was scaled to 100 g 2-chlorocyclohexanone. Initially only 2 equivalents of pyrrolidine were added slowly with stirring. The reaction was monitored with GCMS and

more amine slowly added at 0°C until complete consumption of **48** was observed. At this point none of the double addition product, **49**, was observed. It was discovered that the double addition product forms during the work up procedure. This was probably occurring when the reaction mixture was being concentrated. The boiling point of the reaction solvent is lower than that of the pyrrolidine. This caused an increasingly high concentration of amine, eventually high enough to add to **15**. It was found that maintaining a temperature of 0°C throughout the work up minimised the formation of the double addition product, with optimal cases only producing trace amounts of this diamine, **49**.

The enamine **15** can then be used as an amino-allyl cation precursor.^[135] Treatment of this enamine with silver salts abstracted the chloride ion, leaving a delocalised cation, which acts as the two-electron component in the cycloaddition. N-BOC pyrrole is the four-electron component, the BOC group being required to withdraw electrons from the ring system disrupting the aromaticity enough to allow facile cycloaddition. The reaction scheme is shown below in Figure 35. Scaling of this reaction was particularly troublesome, initial tests produced large amounts of black tar from which isolation of product was arduous. It was found that the efficiency of stirring during these reactions was vitally important; for large-scale reactions sufficient stirring could only be accomplished by overhead mechanical stirring. When conditions were optimum, crystals were produced directly from the hydrolysis reaction and these could be purified by recrystallization. Less optimal conditions led to black tar which required column chromatography to obtain a pure product. Yields were consistently lower for experiments producing tar rather than crystals.

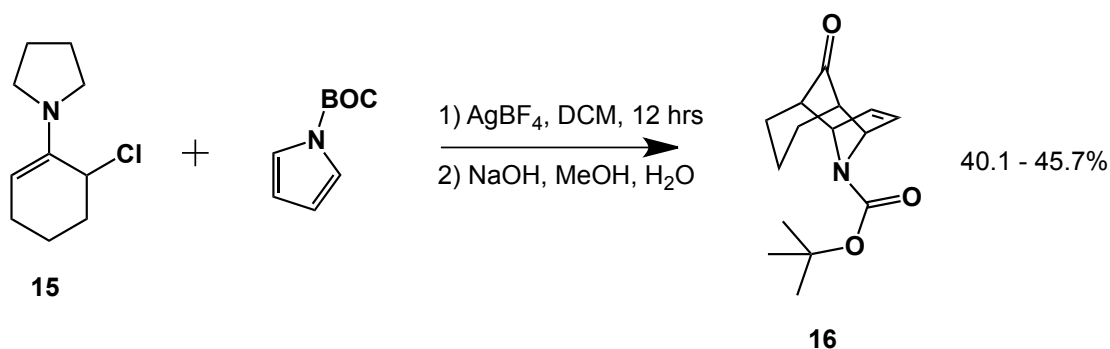


FIGURE 35: FORMATION OF TRICYCLIC AMINE BY [4+3] CYCLOADDITION

Scaling of the hydrogenation reaction was, unsurprisingly, simple. Run at scales of up to 25 g this reaction was found to be almost quantitative in yield and purity. The reaction scheme is shown below in Figure 36.^[132]

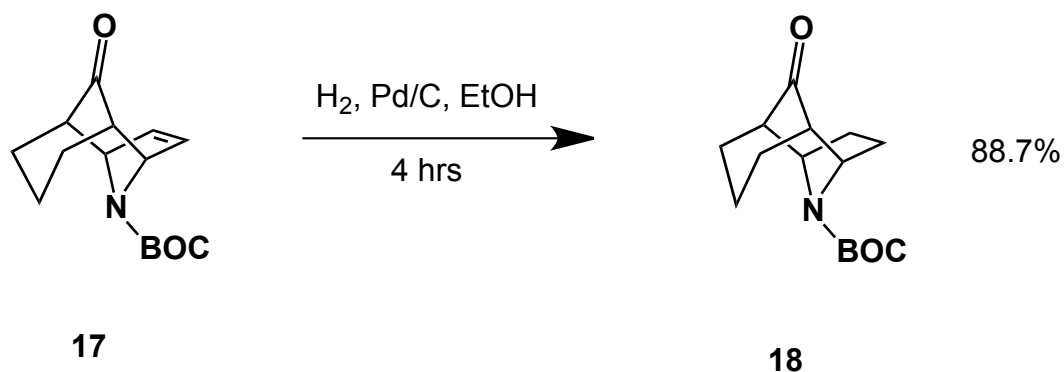


FIGURE 36: HYDROGENATION OF CYCLOADDUCT

DEOXYGENATION

Calculations, reported in the previous chapter, indicate that the OMe group in amine **20** is undesirable so methods of removing it were sought. To minimise the possibility of any additional reactive pathways it would seem that the best substitution for the carbonyl group would be a complete reduction to the parent alkane. There are two main methods of reducing ketones to alkanes reported in the literature, Wolff-Kishner and Clemmensen reductions.^[157]

Wolff-Kishner

The Wolff-Kishner reaction has seen use throughout organic chemistry for a number of years and is often used in aliphatic systems. Given the literature precedent for this reaction working on related systems significant synthetic effort was spent investigating various conditions and modifications to this reaction.^[158]

Literature Review

Introduction

The Wolff-Kishner reaction was first discovered as a method to deoxygenate ketones at the beginning of the 1900s.^[157b, c, 159] Since then it has become the ubiquitous method of reducing various ketones into their parent alkanes. The reaction has received much attention throughout the years and a number of modifications have been made to the original procedure,^[153] but the essence of the method has never been lost.

The reaction takes a carbonyl compound, normally a ketone, and hydrazine as its feedstock and produces a fully reduced alkane and nitrogen gas as its products. This is illustrated below in Figure 37.

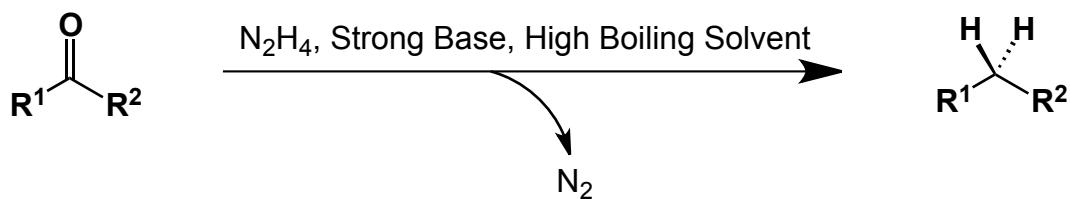


FIGURE 37: SCHEMATIC REPRESENTATION OF WOLFF-KISHNER REACTION

The Wolff Kishner reduction proceeds through the formation of a hydrazone, and then the thermal decomposition of this intermediate in the presence of base to produce the alkane. The mechanism for this transformation is shown below in Figure 38, with some proton transfers being condensed into single steps.

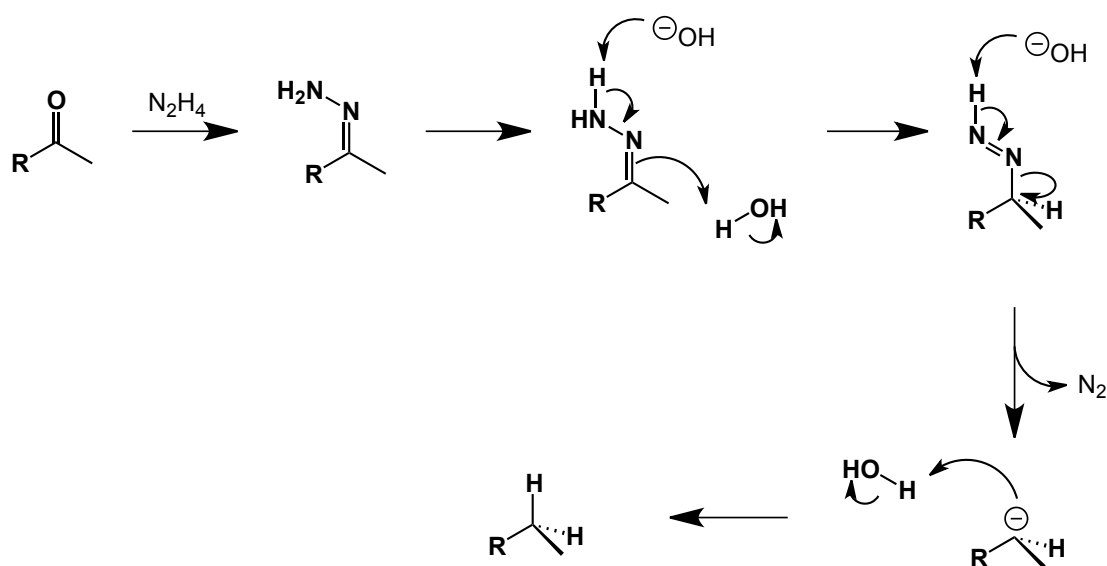


FIGURE 38: MECHANISM OF WOLFF-KISHNER REDUCTION

This review will first outline the original procedure and the most common modifications, before detailing some recent literature surrounding compounds with similar structures to the target amines **17** discussed in this chapter.

History + General Methods

Both Kishner and Wolff discovered the procedure independently, and published within a year of each other.^[160] Although each chemist's procedures were different the overall reactions were fundamentally the same.

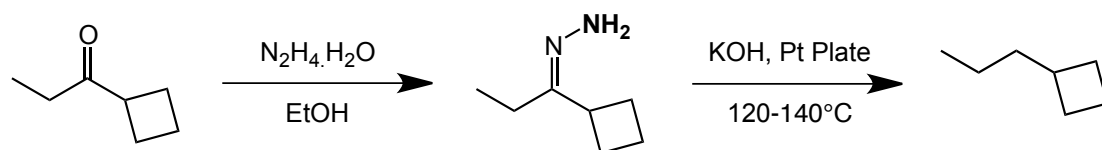


FIGURE 39: KISHNER SCHEME FOR COMPLETE REDUCTION OF KETONES

The Kishner process was first published by Kasansky who developed a process whereby a hydrazone dropped onto a mixture of hot potassium hydroxide and platinized porous plate would produce the corresponding alkane, Figure 39.^[161] The Wolff procedure involved heating the hydrazone in a sealed tube with sodium hydroxide to the same result, Figure 40.^[160b] Both methods gave similarly high yields.

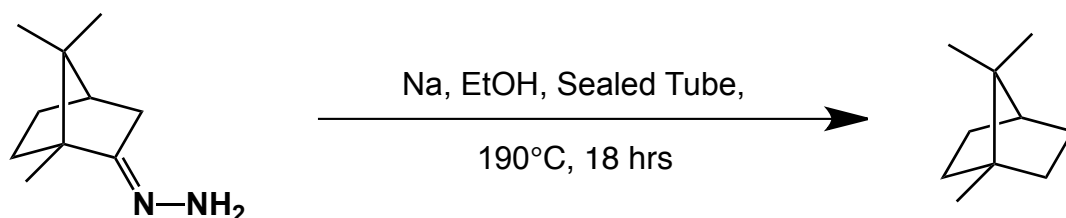


FIGURE 40: WOLFF SCHEME FOR COMPLETE REDUCTION OF KETONES

These classic procedures are rarely seen in modern literature due to the prevalence of some common modifications. The first of these modifications was introduced during the late forties by Huang–Minglon, Figure 41.^[157b, c] He realised that original procedures involving a preformed hydrazone were inconvenient and sought to design a method that avoided this step. His use of a high boiling solvent has two benefits. Firstly it allows facile formation of the initial hydrazone by continuously removing water from the reaction. Secondly it avoids the need for a high-pressure environment by utilising a solvent with a reflux temperature high enough to drive the reaction to completion. Due to its ease of utility, this one pot method has now become a common feature in literature, overtaking the original procedures in terms of citations.

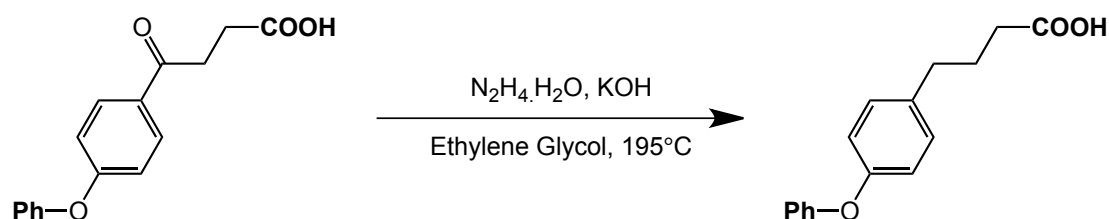


FIGURE 41: HUANG–MINGLON MODIFICATION TO THE WOLFF-KISHNER REDUCTION

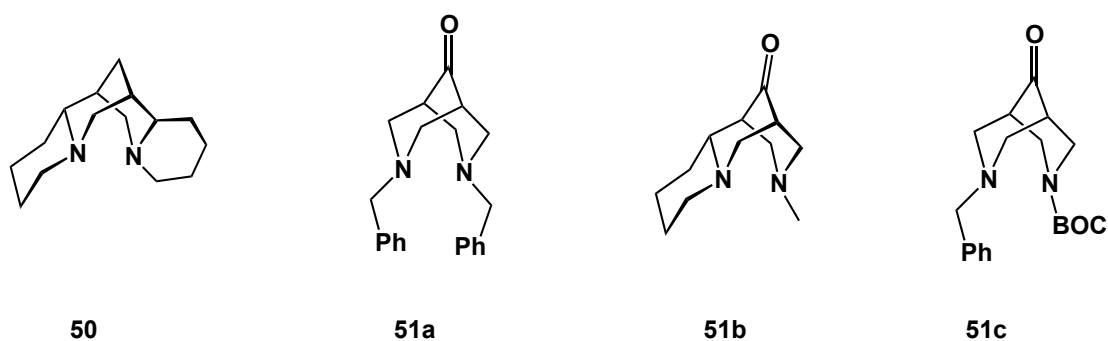
The above methods all involve the use of strong bases to facilitate the decomposition of the hydrazone; this limits the capacity of these methods in compounds with sensitive chiral centres. In particular compounds with racemisable proton centres near carbonyl functionalities are prone degradation due to H exchange reactions. To avoid the use of strong bases a method has been developed where the starting material is a tosyl-hydrazone, this can then be decomposed under reducing conditions. This avoids both the use of strong bases and high temperatures that can both contribute to the decomposition of the starting

materials. This modification first appeared in literature in the mid sixties and has since been used when one wishes to effect a deoxygenation of an acid/base sensitive carbonyl compound.^[162]

Despite the prevalence of the Wolff-Kishner reaction there has been no major developments in its application for many years. This could well be considered testament to the solid foundation of this reaction. However this has resulted in relatively little attention from modern chemistry in terms of comprehensive reviews of the topic. For further reading on the topic the classic *Comprehensive Organic Synthesis* is suggested.^[163] For more details on the mechanistic aspects of the reaction the reader is referred to the 1968 paper from Szmant.^[159]

Related Reductions

An extensive literature search has been unable to find examples of Wolff-Kishner reductions in related tricyclic carbocycles; this is not unexpected as examples of compounds similar in structure to amine, **20**, are extremely rare. However during the course of the search many examples of Wolff-Kishner reductions in closely related bicyclic systems were uncovered. Sparteine is a naturally occurring alkaloid, **50**, with a structural core very similar to the target amine. Sparteine has been studied as an antiarrhythmic agent, but more recently related compounds have found many applications as chiral scaffolds in both organic and inorganic chemistry. Synthesis of such amines invariably involves the reduction of a ketone such as those shown below, **51a-c**. In all literature examples Wolff-Kishner protocols have successfully reduced these ketones in high yields to their parent alkane.^[158] The success of this methodology in very similar compounds to amine, **17**, suggested that a similar procedure could prove fruitful on route to this amine.



In the literature mentioned above no special procedures were needed to effect the complete reduction of the carbonyl groups. However it should be noted that amine **17**

shows a significantly more crowded environment which may block the Bürgi–Dunitz angle for nucleophilic attack on the carbonyl group.

Experimental Results

Firstly the classic Wolff-Kishner reaction was tested with tert-butanol as solvent, as shown in Figure 42. This reaction was entirely unsuccessful, with no trace of product or hydrazone produced after 18 hours reflux. Replacement of *t*BuOH with triethylene-glycol under the same condition also failed.

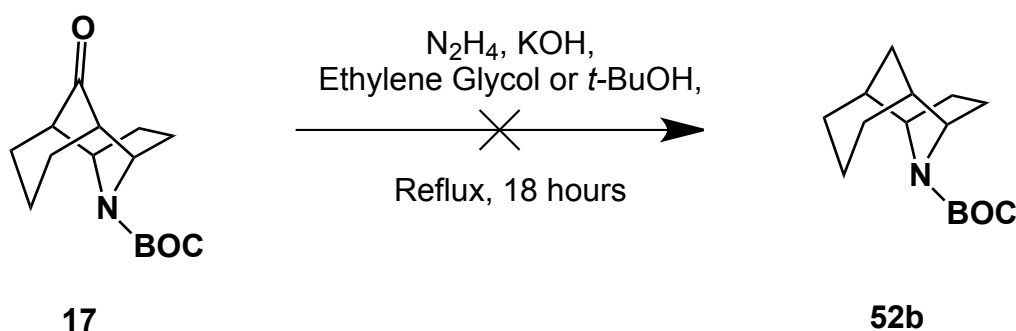


FIGURE 42: ATTEMPTED WOLFF-KISHNER REDUCTION

To further increase the heat available for this reaction the next modification examined the use of pressure tubes. Both *t*BuOH and triethylene-glycol were tested as solvents in pressure tubes at 200°C. This modification was also unsuccessful, Figure 43; again no products or hydrazone could be detected by GCMS or NMR.

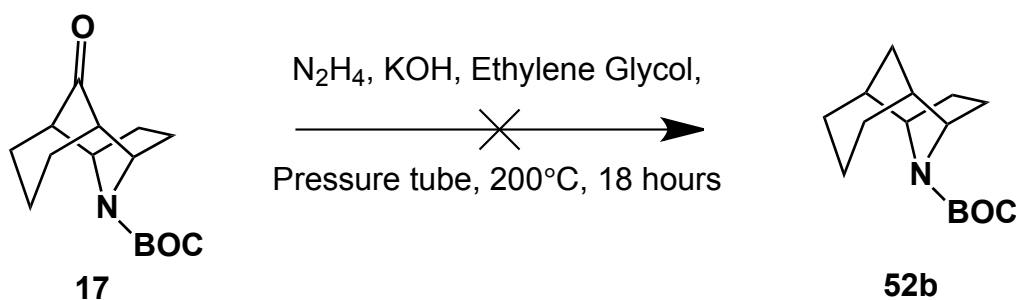


FIGURE 43: ATTEMPTED HIGH PRESSURE WOLFF-KISHNER REDUCTION

The final modification tested was the use of tosyl hydrazine Figure 44; this reagent is normally reserved for base sensitive molecules as the hydrazone can be reductively cleaved. No formation of hydrazone was observed during this reaction, indicating that all Wolff-Kishner methods are unsuccessful on ketone, **17**.

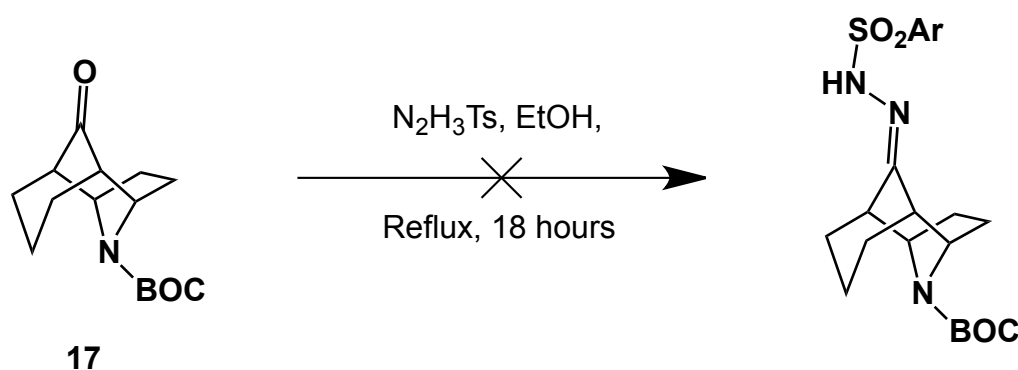


FIGURE 44: ATTEMPTED FORMATION OF TOSYL HYDRAZONE

The failure of all Wolff-Kishner reactions on this substrate was likely due to the sterically hindered nature of the ketone. The Bürgi–Dunitz angle is the trajectory that an incoming nucleophile must attack a ketone for efficient overlap with the ketone anti-bonding orbital. In amine **17** the Bürgi–Dunitz angle was extremely sterically hindered in both directions, one side from the methylene bridge and the other from the cyclohexyl ring. This means that attack of this ketone by nucleophiles would require geometries far away from their equilibrium positions. This would suggest that Wolff-Kishner reactions on ketone **17** are intrinsically kinetically unfavourable. In all the above procedures starting material was recovered and no evidence of BOC removal was found by either GCMS or NMR spectroscopy.

Clemmensen Reduction

The Clemmensen reduction is the other named reaction for reduction of ketones to alkanes. Unlike the Wolff Kishner reaction it is run under strongly acidic conditions and typically is reported for ketones with stabilising features, such as α benzene substituents. The main exception to this is in steroid synthesis.^[164] In many cases aliphatic steroidal ketones are reduced to the corresponding alkanes.

The Clemmensen reduction has developed very little since its discovery 100 years ago,^[157a] this shows the strength of the method over a wide range of reactions. Clemmensen discovered the reaction while attempting reductions of alkyl-aryl ketones from Friedel-Crafts acylation reactions. He found that the reduction was effective when the ketone was treated with Zn-amalgam in the presence of hydrochloric acid. The mechanism of the reaction has been debated over the years and no proposed mechanism has been able to explain all outcomes of Clemmensen type reductions. An extensive study of the reduction of benzophenone was published in 1990 and proposed a mechanism that explains some observations not predicted by previous mechanisms, shown in Figure 45.^[165] The mechanism

has two pathways, both involve a mixture of radical and ionic processes and share a common intermediate. One pathway starts with single electron transfer from the zinc metal to the carbonyl forming a Zn-O bond and a carbon radical, then a second electron transfer event, protonation and attack from HCl yields the common intermediate, chlorodiphenylmethane. A single electron transfer event followed by chloride ion loss from this intermediate yields the diphenylmethyl radical. Protonation of this radical leads to the fully reduced diphenylmethane. A second pathway is also proposed that starts with the dichlorination of benzophenone in acetic acid producing dichlorodiphenylmethane. This can be reduced by zinc metal to produce its radical cation, which then losses a chloride ion to product a chlorodiphenylmethyl radical. Protonation of this radical produces the common intermediate chlorodiphenylmethane.

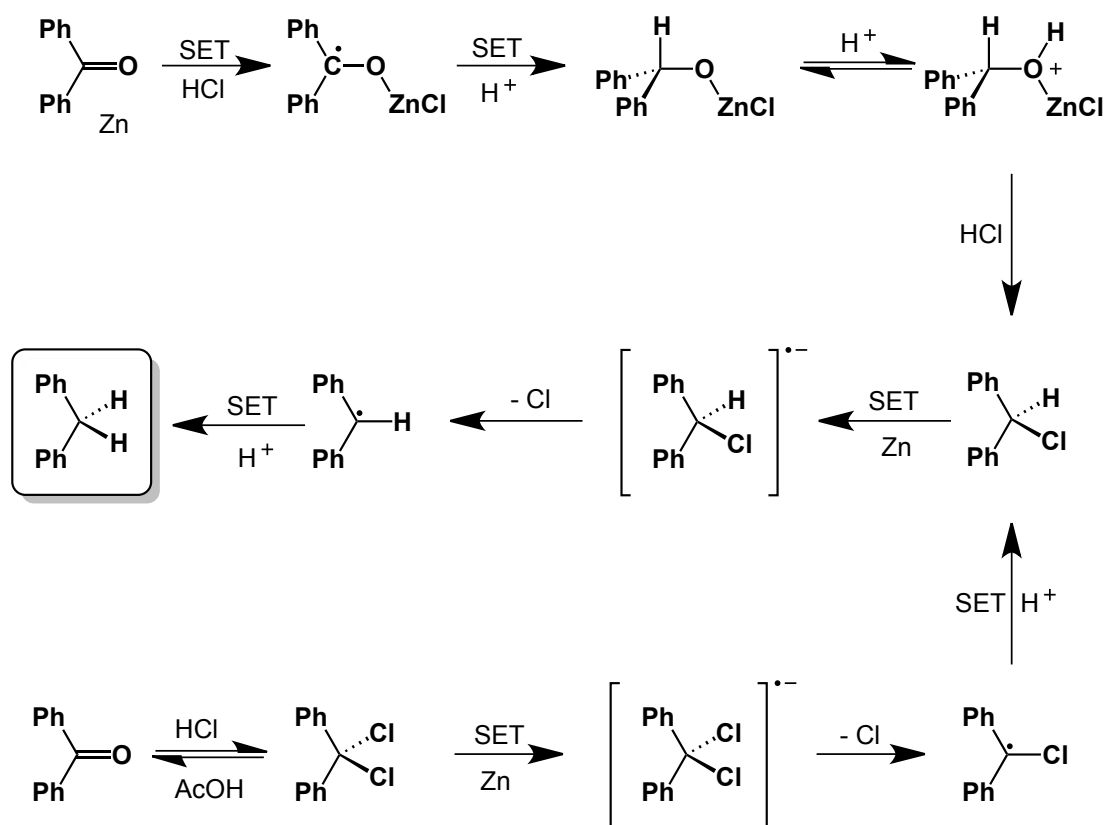


FIGURE 45: PROPOSED MECHANISM FOR CLEMMENSEN REDUCTION OF BENZOPHENONE

It is also possible to reduce aliphatic ketones with the Clemmensen reduction, although typically greater success is found when plain zinc powder is used over an amalgam. The majority of cases reported in literature focus around the reduction of unwanted ketones in steroid type molecules.^[166] While these examples prove the ability of the Clemmensen

reduction to reduce unstabilized ketones they do not provide good model compounds for the target amines.

Unfortunately no literature examples of directly related compounds could be found, however it was possible to find two examples that indicate that this reaction may prove itself fruitful on route to target amine, **20**. Firstly an example of reduction in a highly sterically crowded environment was found,^[167] Figure 46. The success of this reaction indicates that Clemmensen reductions do not require an unhindered Bürgi-Dunitz approach angle as found for the Wolff-Kishner reaction above.

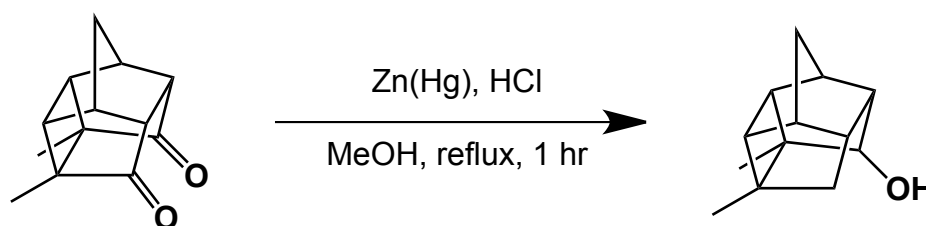


FIGURE 46: LITERATURE EXAMPLE OF CLEMMENSEN REDUCTION IN A STERICALLY HINDERED SYSTEM

The second related example, Figure 47, shows the applicability of this method to ketone containing nitrogen groups within the same molecule.^[168] The yield of this reaction is relatively low, 57%, which suggests that reduction of such aliphatic ketones is not particularly favourable and side reactions can play a significant role during the reaction. It is worth noting the benzamide is not affected by the reduction condition.

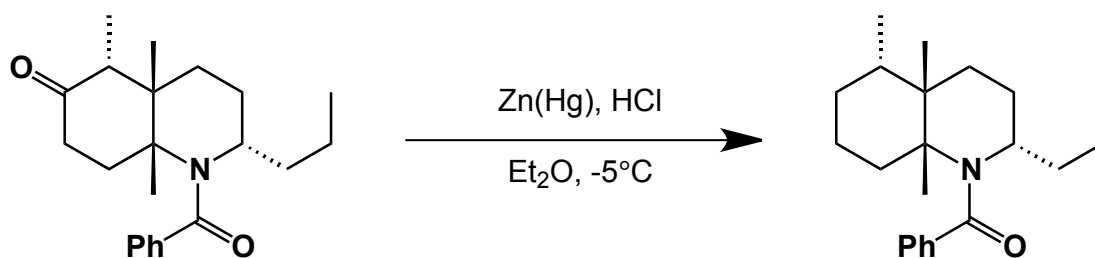


FIGURE 47: LITERATURE EXAMPLE OF CLEMMENSEN REDUCTION IN A NITROGEN CONTAINING COMPOUND

The above examples suggest that the Clemmensen reduction may prove a useful reaction on route to target amine **13** and that it is worth investing synthetic effort to investigate such a scheme.

Results

Reported Clemmensen reductions typically dissolve ketone into a saturated solution of HCl/diethyl ether; zinc metal is then added in one portion and the resulting alkane is produced in high yields in short reaction times.^[168] When ketone, **17**, was treated under

these conditions a trace of reduction product, **52a**, was found. This result was promising as with the previous procedure no product could be detected in any reactions. These conditions were then modified to force the reaction to completion. Instead of using a saturated solution of HCl in ether, dry HCl gas was continuously passed through the reaction vessel and zinc metal was added to the solution periodically. Under these conditions, shown in Figure 48, reasonable conversion to product was found, but the reaction was still far from complete.

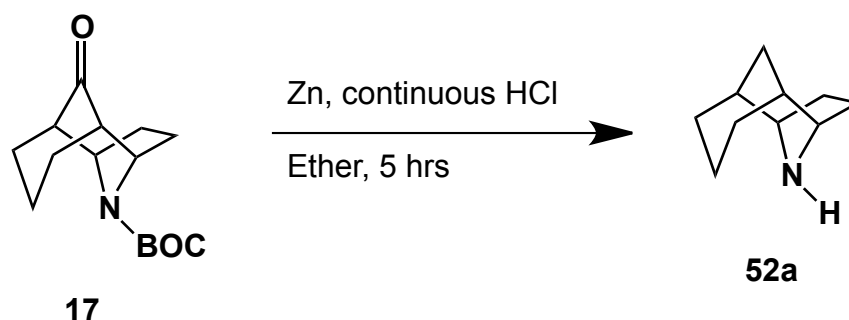


FIGURE 48: CLEMMENSEN REDUCTION OF TRICYCLIC AMINE UNDER FORCING CONDITIONS

To further optimise the reaction four solvents were investigated: diethyl ether, dioxane, acetic anhydride and ethyl acetate. Acetic anhydride was found to be a poor solvent, with no reaction being observed; the other 3 reactions were found to give similar reaction rates. Inspection of the crude NMR spectra from the reaction mixture with each of the 3 solvents that yield product show that ethyl acetate gave the cleanest reaction mixture. Dioxane and diethyl ether both showed product but were contaminated with significant impurities. This could be due to reactions between intermediate radical species and the ethereal solvent.^[169]

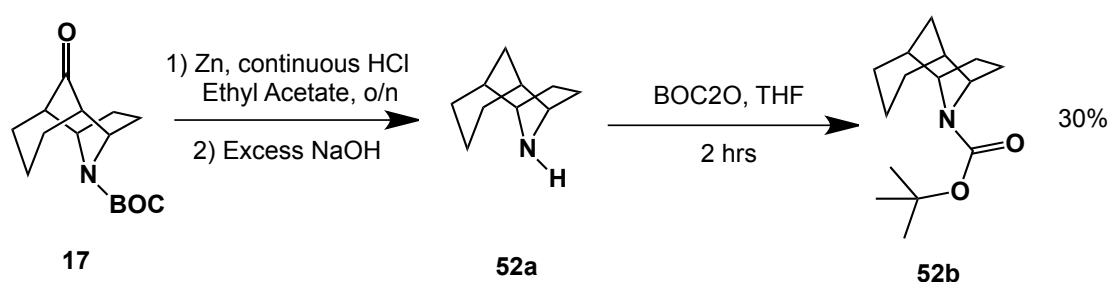


FIGURE 49: OPTIMISED CLEMMENSEN REDUCTION OF TRICYCLIC AMINE

The optimised conditions for this reaction are shown in Figure 49. It is important to make note of the use of a vast excess of base during the workup, use of stoichiometric base led to the formation of solid zinc oxides which trapped some of the product, **52a**, significantly reducing yields. Excess base caused the formation of zincates from zinc oxide, which are water-soluble and therefore do not trap product. During scaling of this reaction it was found

to be impossible to continue the reaction to completion, this could be due to formation of water impeding progress. Total conversion was found to be around 30%. During this reaction the BOC group was cleaved, and so had to be introduced again to facilitate purification, 52b.

This product was now only a reduction step away from an amine suitable for photochemical studies, Figure 50. As during the previously reported works this carbamate was selected as the optimal product for final purification. This is because the final step should be very clean, and amines are notoriously difficult to purify. The product was purified by column chromatography, however the final product was not completely pure. GCMS analysis shows a small peak with a mass two less than that of the parent carbamate.

Initially it was thought that this impurity was a simple alkene carried over from the previous steps. However hydrogenation condition used previously had no effect on the GCMS peak observed, furthermore bromination and dihydroxylation also had no effect. This would seem to indicate that this peak did not belong to an alkene. At this point purification by HPLC was considered. Partial separation could be achieved using analytical columns, however using semi-preparative columns no separation could be observed. NMR was unable to identify the nature of the impurity, due to its low concentration and the overlapping nature of most peaks.

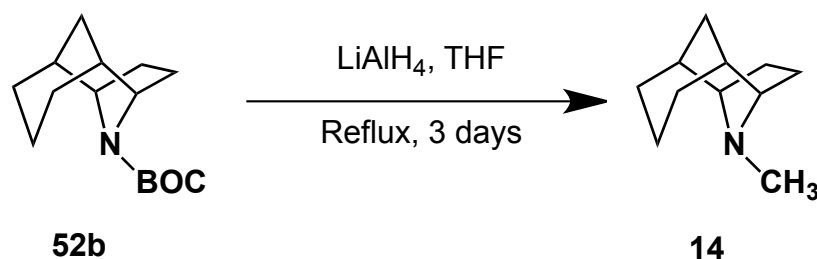


FIGURE 50: REDUCTION OF BOC GROUP TO FORM FINAL TRICYCLIC AMINE

The difficulties purifying this compound, **14**, made it unsuitable for serious photochemical studies as it would be impossible to determine if any alkenes found in the reaction mixture were a product of the CO_2 reduction process or as a result of the impurities present. However preliminary photochemical studies were undertaken as shown in Figure 51. Although the results of this experiment cannot be used to draw quantitative conclusions it was clear that formate was being produced with this amine. Given the similar nature of this amine, **14**, to amine, **20**, it seems likely that it was reducing CO_2 through the distonic radical mechanism.

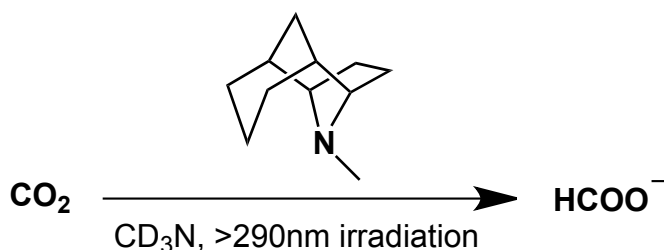


FIGURE 51: REDUCTION OF CO_2 WITH UNSUBSTITUTED TRICYCLIC AMINE

Tebbe Olefination

Functionalising a ketone is the most common way to remove them during synthesis; this is the strategy used in amine, **20**. In the case of amine, **20**, OMe was synthetically easy to access so was an attractive option during a short undergraduate project. Due to the possibility of a Grob fragmentation occurring during the use of the amine in the photochemical CO_2 reduction, this substitution is non-optimal and so functionalization that also removes the oxygen atom would be preferred. However, the results from the Wolff Kishner reaction indicated that addition of nucleophiles to this ketone might be difficult.

With these constraints in mind the Tebbe reaction was considered. This reaction methylenates ketones, as shown in Figure 52. This reaction proceeds from a Schrock carbene and likely undergoes a [2+2] cycloaddition reaction the ketone and then cycloreversion to produce the product. This reaction bears many similarities to the Wittig reaction, but does not involve any nucleophilic addition to the ketone.

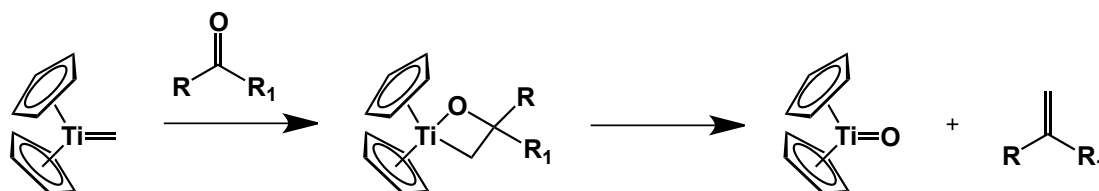


FIGURE 52: SCHEMATIC TEBBE OLEFINATION

Treatment of ketone **17** with commercially available Tebbe's reagent produced an alkene in high yield. The resulting alkene was then purified by column chromatography to yield **54**.

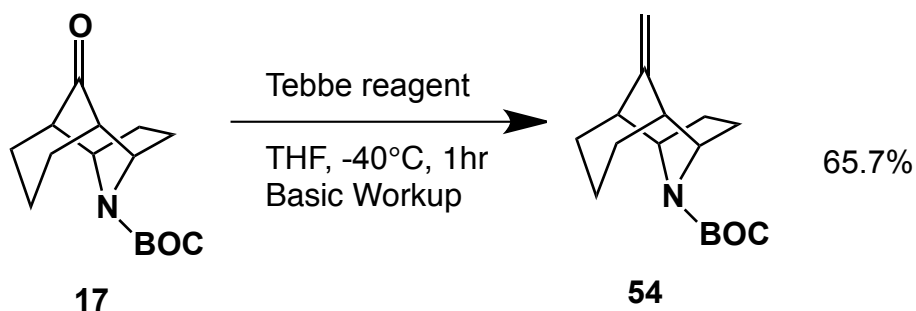


FIGURE 53: TEBBE OLFENATION OF TRICYCLIC AMINE

SYNTHESIS OF DMAP BASED AMINES

Synthesis of the DMAP based amine **46**, introduced in the previous chapter, was first attempted during an undergraduate project. Disconnecting the bond between the norbornane and the DMAP units leads to two possible routes. As part of an undergraduate project the group investigated the possibility of a nucleophilic aromatic substitution route to target amine **46**, however this was entirely unsuccessful, Figure 54. The alternative route is investigated here.

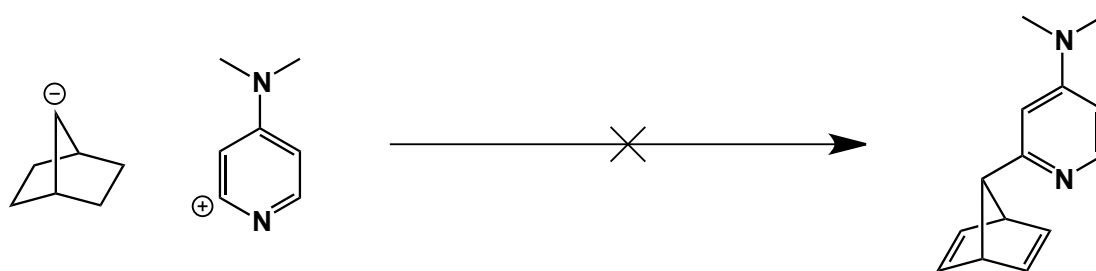


FIGURE 54: ATTEMPTED SYNTHETIC ROUTE TO DMAP AMINES

SYNTHETIC ROUTES

The alternative strategy that is investigated in this report involves an aryl nucleophile attacking a 7-norbornane electrophile. The synthons for this disconnection are shown in Table 19, and possible synthetic equivalents are listed.

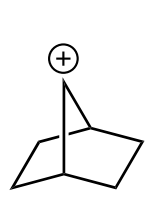
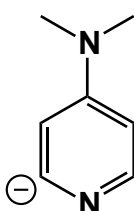
	
Cl	MgBr
Br	Li
I	Cuprate
OTs	Zn
OMs	
C=O	
OtBu	

TABLE 19: POSSIBLE SYNTHONS FOR PRODUCTION OF DMAP BASED AMINES

The first five synthetic equivalents suggest in Table 19 are typical electrophiles, however the OtBu group last in the list may seem unusual. The inclusion of this synthetic equivalent into the list is based on reports by Newton that treatment of tert-butyl ether, **55**, with phenyl Grignard reagents produces the corresponding addition product, shown in Figure 55.^[170] This seemingly unusual reaction is probably facilitated by the relatively high stability of 7-norbornadienyl carbocations.^[171]

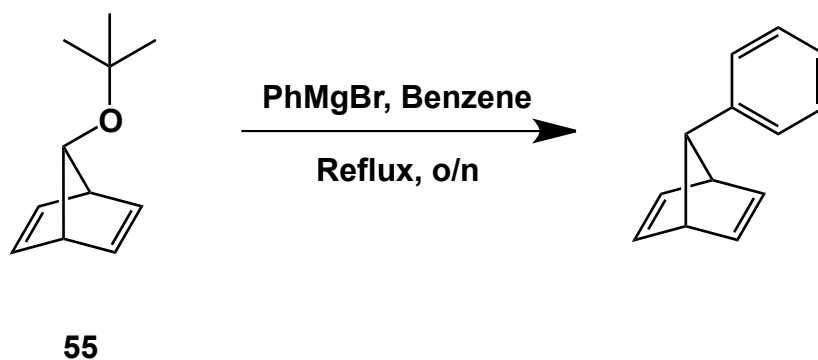


FIGURE 55: LITERATURE EXAMPLE OF ADDITION OF GRIGNARD REAGENTS TO 7-OTBU-NORBORNADIENE

Not only is tert-butyl ether **55** a possible synthetic equivalent for the desired reaction it is also a precursor to all the other synthetic equivalents listed above as shown in Figure 56.^[172]

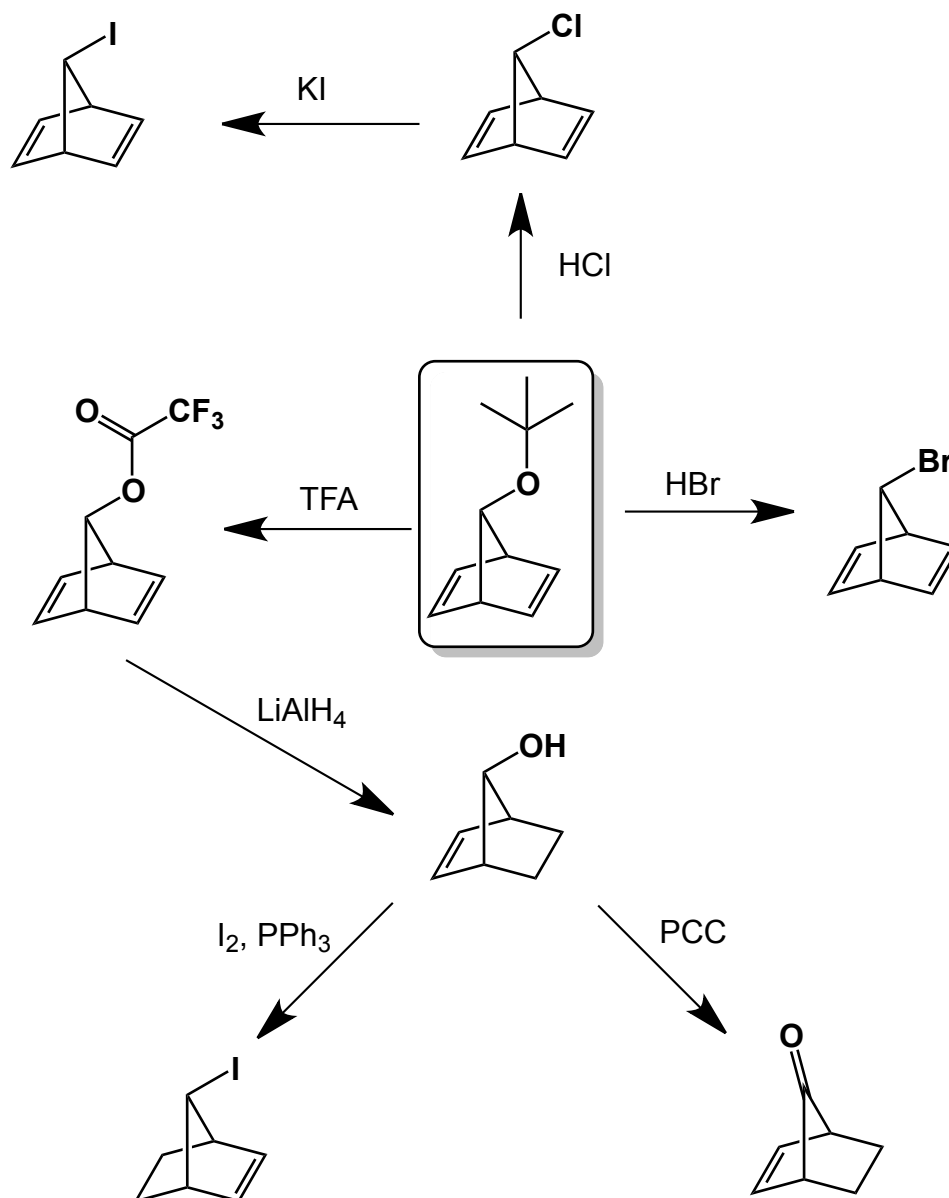


FIGURE 56: PRODUCTION OF PRECURSORS FROM 7-OTBU-NORBORNADIENE

ADDITION TO ETHERS

Synthesis of the tert-butyl ether, **55**, was possible in a single step from commercially available starting materials, as shown in Figure 57.^[173] The total yield from this reaction was poor at only 23% but the starting materials are cheap and purification simple so this reaction was performed on a large scale to provide ready access to 7-substituted norbornanes. It is worth noting that other methods for accessing these structures involve several synthetic steps including the use of both chlorine and ethylene gases.

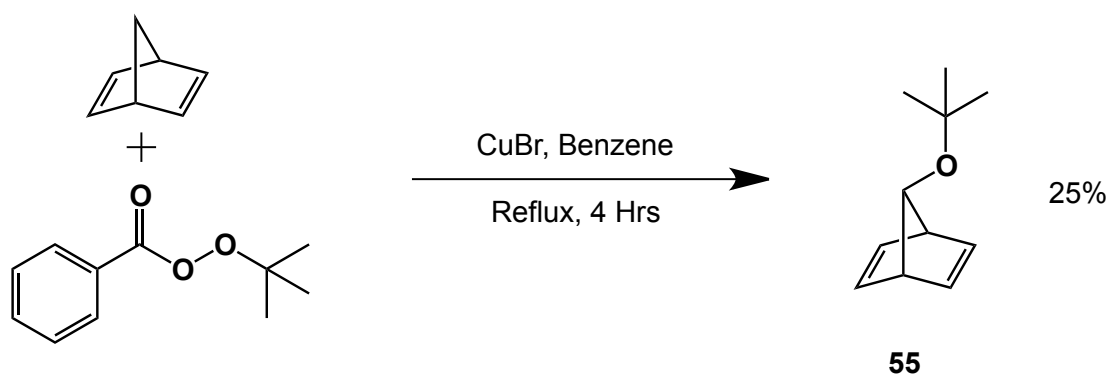


FIGURE 57: SYNTHESIS OF 7-OTBU-NORBORNADIENE

Using the method report by Newton for the addition reaction both DMAP-MgBr and Pyr-MgBr were tested, shown in Figure 58.^[170] These reactions both failed to produce any product, and so the literature report was tested to ensure the viability of the chemistry. The chemistry was successful when commercially available PhMgBr was used as nucleophile; this raised concerns that the formation of the pyridine based Grignards was problematic.

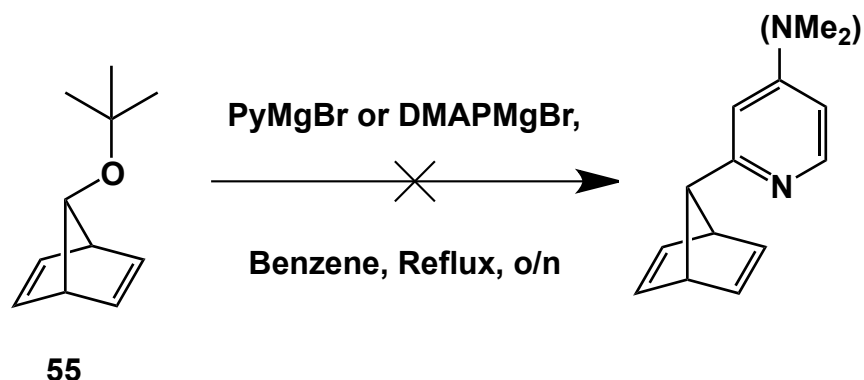


FIGURE 58: ATTEMPTED FORMATION OF DMAP BASED AMINE FROM 7-OTBU-NORBORNADIENE

Five methods of Grignard formation were investigated and the resulting products were used as nucleophiles in reaction, Figure 58. The first two methods are classic Grignard formations where a magnesium atom inserts itself into the C-Br bond. A small amount of activator, either DIBAL or dibromoethane, was added to initiate the reaction. These activator molecules attack the surface of the metal exposing unoxidised atoms required for the reaction to proceed. The third method involved a transfer reaction from isopropyl Grignard in the presence of LiCl. This method appeared to be entirely unsuccessful during all tests even though it was reported for related systems. The fourth method utilised Rieke magnesium, a finely divided metal powder produced by reduction of magnesium halides with alkali metals. This method produced high quality Grignards but was extremely water sensitive and required the use of reactive metals such as potassium. The final method of

Grignard formation tested was transmetallation. Formation of the aryl lithium reagent followed by transmetallation with MgBr_2 produced high quality Grignards that added cleanly to benzaldehyde, higher yields were seen for *t*-BuLi over *n*-BuLi. Due to the ease of handling butyl lithium reagents compared to potassium metal required for the Rieke procedure, the transmetallation procedure was selected for future Grignard formations. Unfortunately none of the Grignards tested above could be successfully added to tert-butyl ether **55**. The starting ether could be recovered from the final reaction mixture, which indicates that there is no reactive channels open to ether **55** and pyridine based Grignards. This could be rationalised by considering the electron deficient nature of the pyridine ring deactivating the MgBr. Given this conclusion one may well predict a more reactive electrophile may prove successful.

ADDITION TO HALIDES

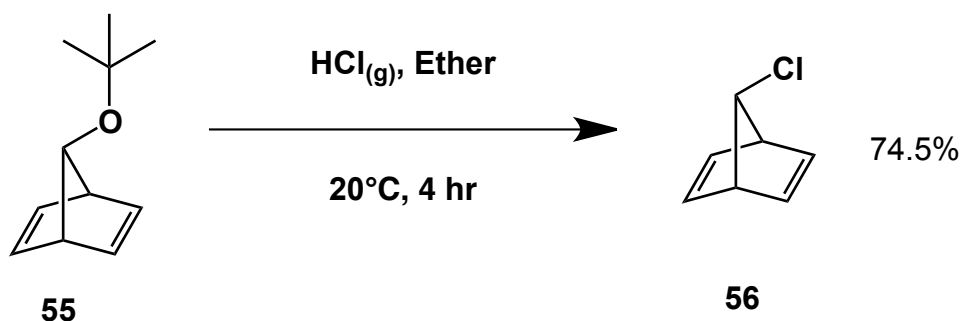


FIGURE 59: SYNTHESIS OF 7-CHLORO-NORBORNADIENE

Synthesis of 7-chloro-norbornadiene, **56**, was possible with treatment of the tert-butyl ether, **55**, with HCl gas as shown in Figure 59.^[172e, 174] This follows the literature report of Newton, and similar yields were found. Due to the difficulties with previous additions to norbornane electrophiles the chloride was first tested with commercially available nucleophiles, Figure 60.

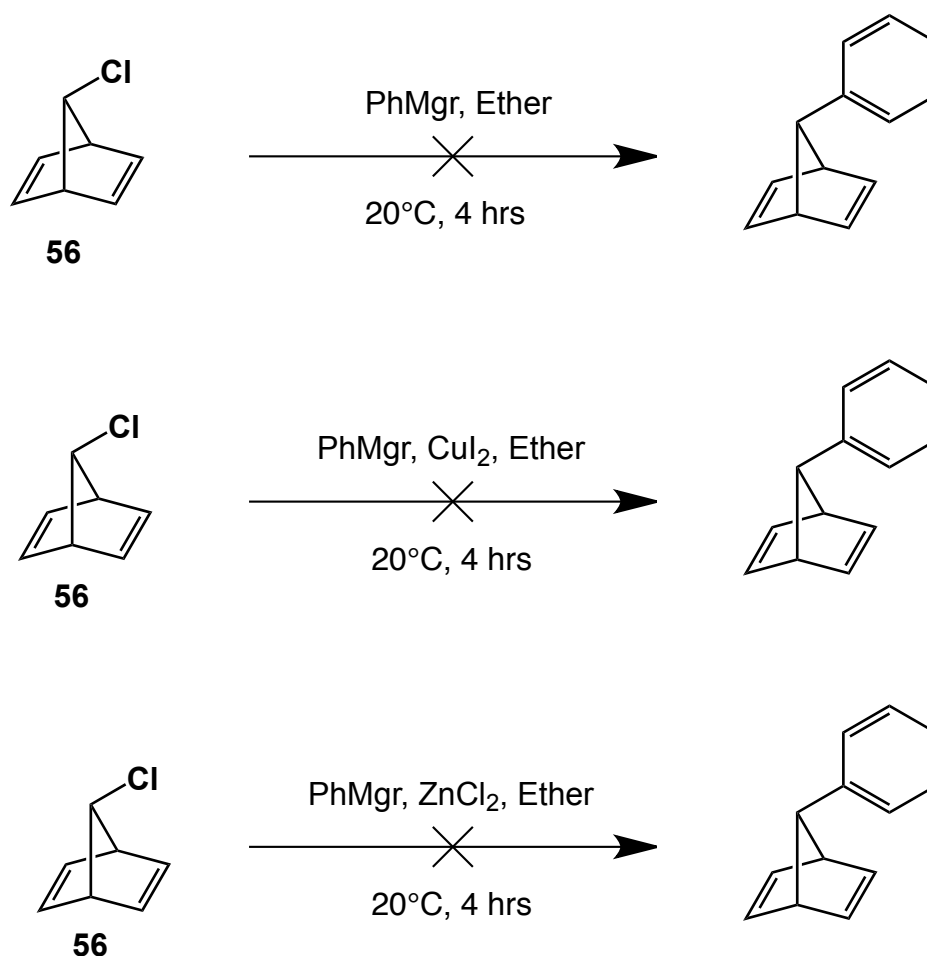


FIGURE 60: ATTEMPTED REACTIONS FROM 7-CHLORO-NORBORNADIENE

These reactions all produced biphenyl, presumably as oxidation products of the organometallic reagents. The reaction likely proceeds through a single electron transfer from the organometallic to the chloronorbornadiene producing metal chloride, phenyl radical and 7-norbornadienyl radical. It is likely the biphenyl is formed by combination of two phenyl radicals. The high stability of 7-norbornadienyl radical could go some way to explaining the lack of productive chemistry in this reaction.^[171] However given that no products were found in these reactions it was decided that further synthetic work on chloronorbornadiene was unlikely to yield final products and therefore this route was considered a dead end.

Next the iodide derivative was investigated as electrophile, the presumption being that it should be more reactive than the chloride due to the weaker C-I bond relative to the C-Cl bond. Synthesis of the iodide, **57**, from the chloride, **56**, was possible using the Finkelstein reaction, Figure 61.^[172f] This named reaction exploits the difference in solubility between KI and KCl in acetone. The equilibrium is driven towards the iodide as the KCl falls out of solution when produced.

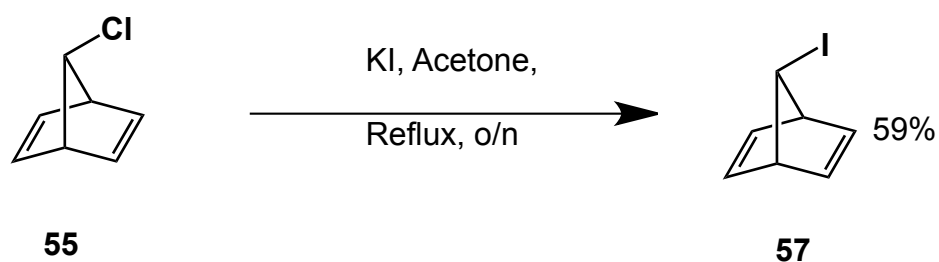


FIGURE 61: FINKELSTIEN REACTION OF 7-CHLORO-NORBORNADIENE

Although this reaction was successful the reflux conditions required to drive the reaction forward also caused degradation of the product. Given the unstable nature of this compound purification was not attempted but a crude sample was used as a test electrophile, as shown in Figure 62. The failure of both of these reactions was not considered sufficient evidence to abandon this route as the impurities could well be interfering with the reaction.

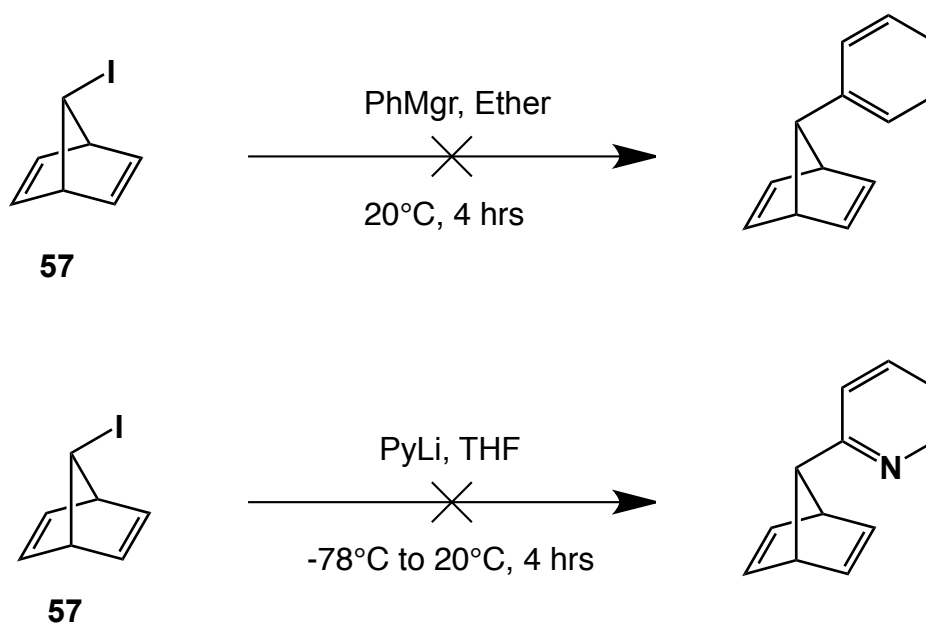


FIGURE 62: ATTEMPTED REACTIONS FROM 7-iodo-NORBORNADIENE

An alternative route to a 7-iodo norbornane derivative was sought. The literature reports that syn-7-iodonorbornene is accessible from syn-norbornene-7-ol in the presence of triphenylphosphine and iodine.^[172c] The syn-alcohol can be produced by LiAlH₄ reduction on the acetate structure, **58**, which is in turn available from the tert-butyl ether. This scheme is shown below in Figure 63.

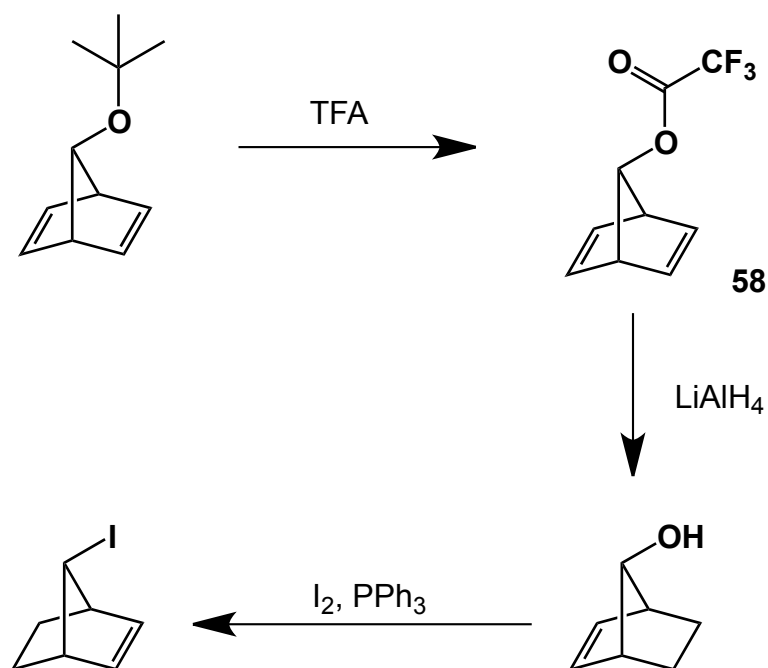


FIGURE 63: SYNTHESIS OF 7-iodo-NORBORNENE

Formation of the acetate, **59**, from the tert-butyl ether, **55**, in literature reports utilises perchloric acid.^[172c] This is an extremely strong oxidising acid, whose salts are often explosive. A method to produce an equivalent acetate was sought. First the reaction was tested under the conditions shown in Figure 64.

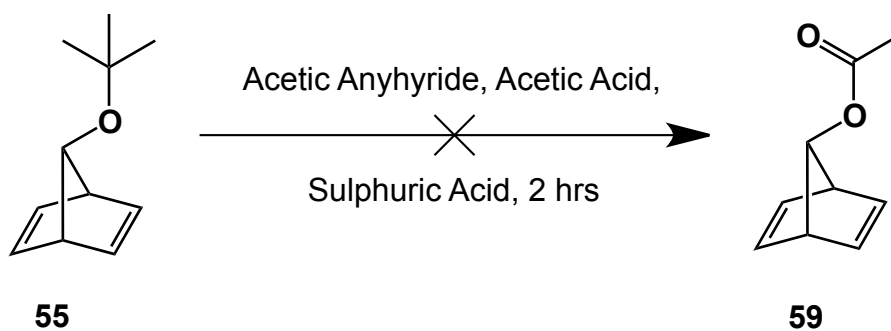


FIGURE 64: ATTEMPTED SYNTHESIS OF 7-ACETO-NORBORNADIENE

This reaction afforded no products, which is presumably due to the pH of the reaction mixture not being low enough to allow formation of the 7-norbornadienyl cation in sufficient quantity, Figure 65.

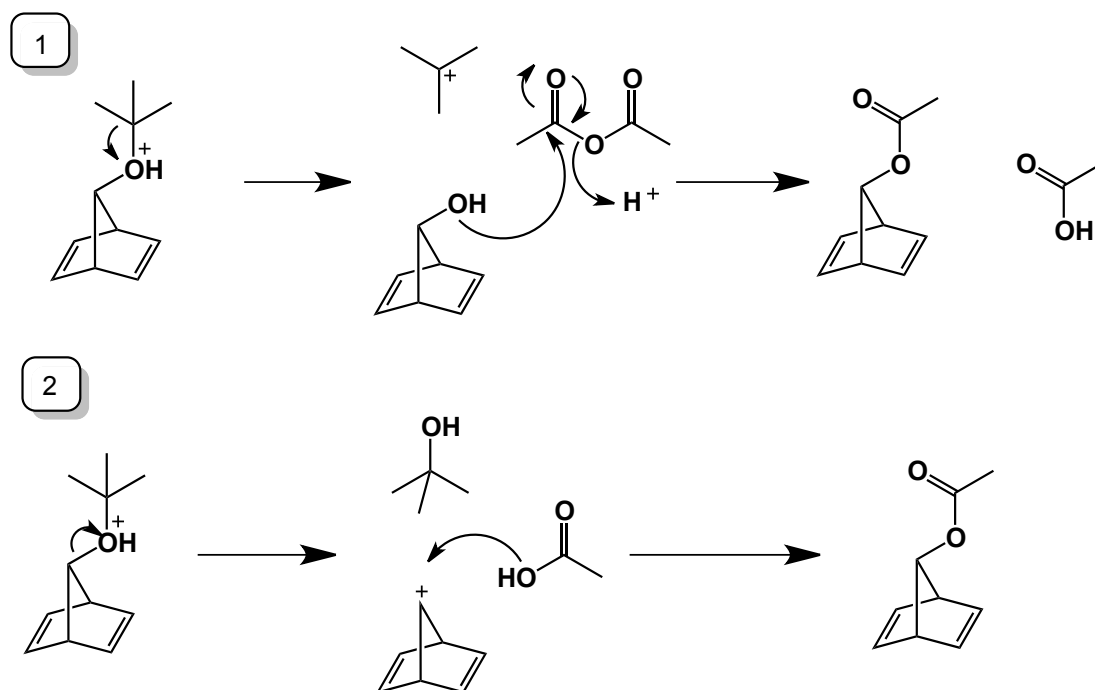


FIGURE 65: POSSIBLE MECHANISMS OF FORMATION OF 7-ACTEO-NORBORNADIENE

Trifluoroacetic acid has a significantly lower pKa than the first ionisation of sulphuric acid or acetic acid and so might be a strong enough acid to facilitate the formation of the 7-norbornadienyl carbocation. An NMR test reaction with *d*-trifluoroacetic acid in *d*-chloroform was run and almost complete conversion was observed.^[172a] Further investigations found the optimal conditions for large-scale versions of this reaction were solvent free, as shown below in Figure 66. Care must be taken during workup as the final product has fairly high water solubility.

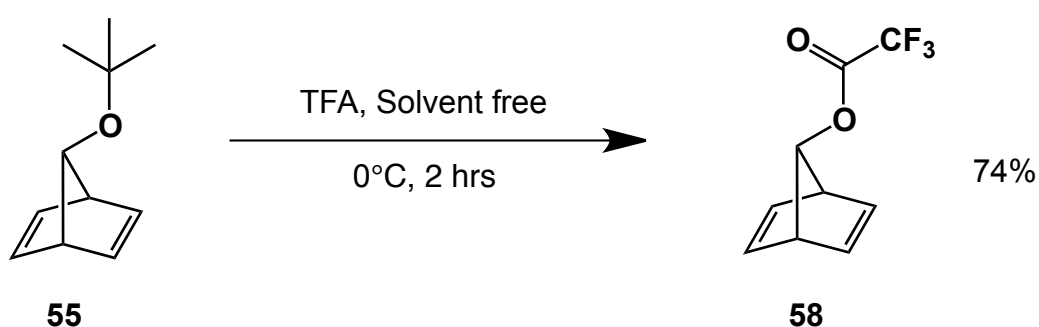


FIGURE 66: SYNTHESIS OF 7-TRIFLUOROACETO-NORBORNADIENE

Reduction of acetate, **58**, yielded the syn alcohol as shown in Figure 67.^[172c] The reaction mechanism follows typical LiAlH_4 pathways to produce the alcohol and then is capable of effecting reduction of a double bond, as shown in Figure 68.

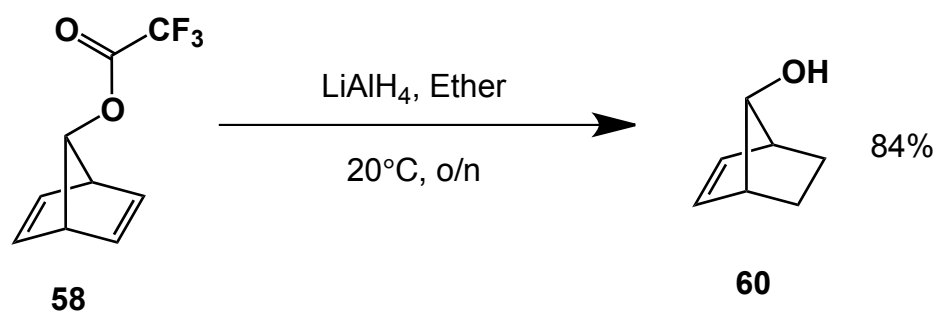


FIGURE 67: SYNTHESIS OF SYN-NORBORNENE-7-OL

This mechanism has been shown to follow a similar pathway to the more well-known propargyl alcohol reduction studied in detail by Corey.^[175] The cyclic aluminium structure is cleaved during work up to yield the product. The formation of the C-Al bond on hydride addition seems to prevent any rearrangement reactions that could otherwise occur.

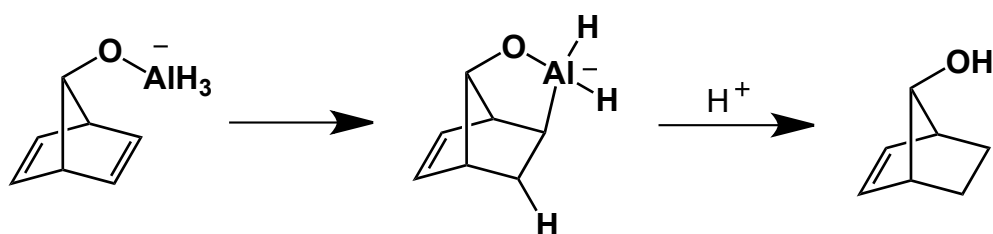


FIGURE 68: MECHANISM OF ALKENE REDUCTION BY LiAlH_4

Production of the iodide was trivial from the alcohol, **60**, following Figure 69.^[172c] However separation of the triphenylphosphine oxide produced during the course of the reaction required purification by column chromatography. This procedure allowed production of a product free from impurities. The pure product, **61**, obtained was then used as an electrophile for three pyridine based nucleophiles, as shown below in Figure 70.

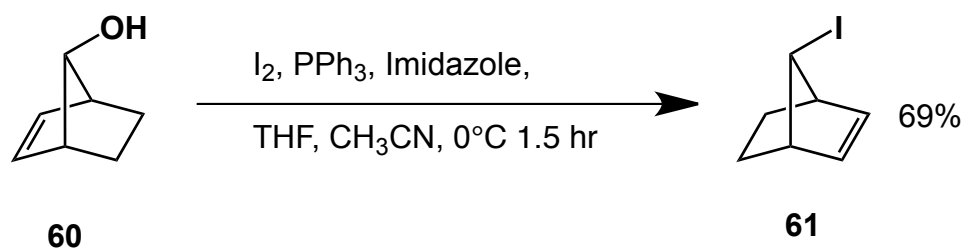


FIGURE 69: SYNTHESIS OF 7-iodo-NORBORNENE

Failure of the following reactions would seem to indicate that 7-halo norbornane derivatives are not reactive to pyridine-based Grignards or lithium reagents, Figure 70. This conclusion is somewhat surprising and may be due to a poor quality source of THF. Unfortunately when the THF problems were uncovered there was insufficient time to redo the key experiments in this section.

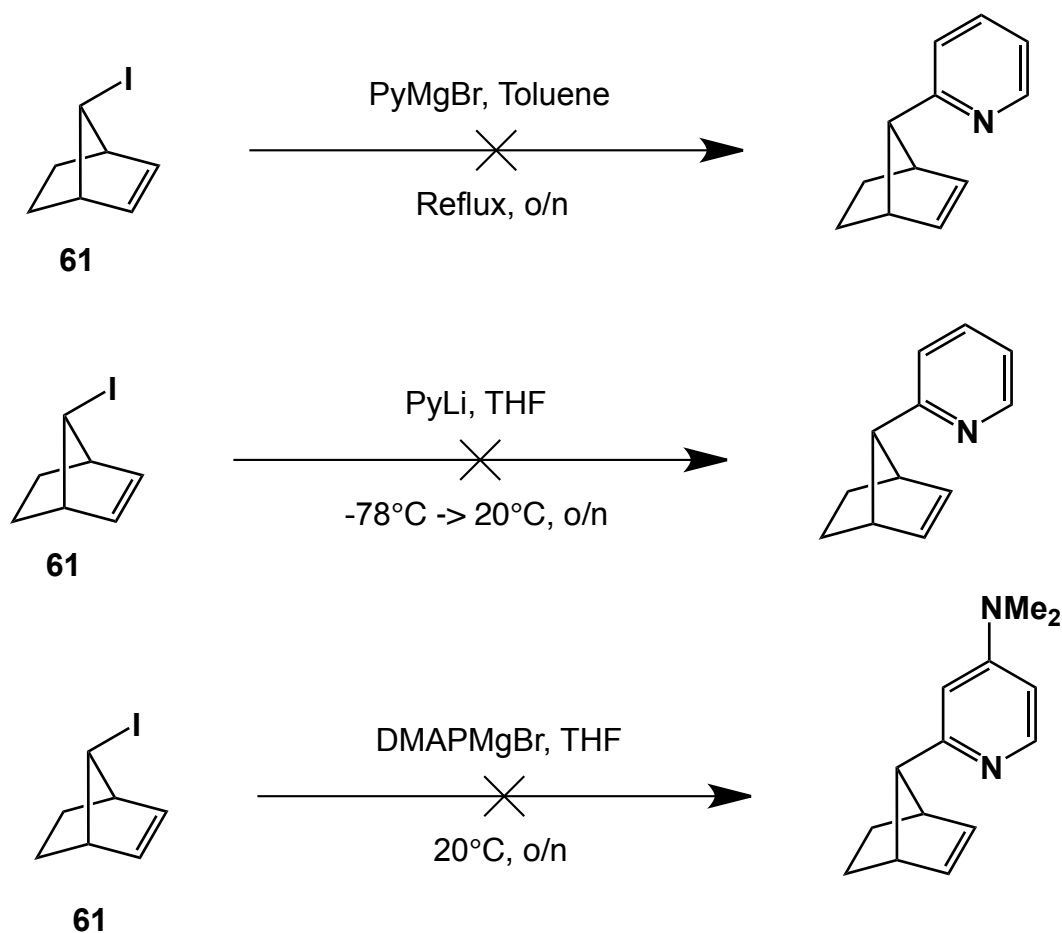


FIGURE 70: ATTEMPTED REACTIONS WITH 7-iodo-NORBORNENE

ADDITION TO KETONES

Referring to the list of synthons discussed at the beginning of this section, Table 19, it should be apparent from the synthons already investigated that other similar synthons are unlikely to produce a viable reaction for production of DMAP based amines. The possibility of an addition reaction to a ketone has not yet been investigated and will likely give the most facile reaction. Synthesis of 7-oxonorbornane, **63**, can be achieved, as shown in Figure 71, by reduction of alkene, **62**, followed by oxidation of the alcohol. Total yield of the ketone is 63%, but care must be taken to achieve a yield this high as the product is fairly volatile.^[172d]

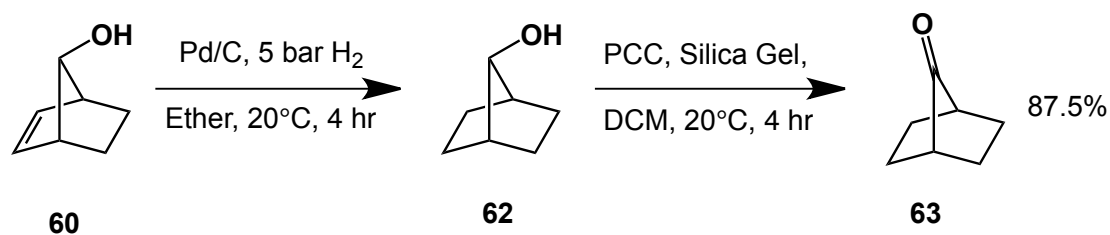


FIGURE 71: SYNTHESIS OF 7-OXONORBORNANE

Addition of pyridine based Grignards and lithium reagents to this ketone were then tested, and the results summarised in Figure 72. All these reactions were successful, producing compounds, **64** and **65**, in good yields. Examining the results from these initial test reactions shows that DMAP-Li was the most successful nucleophile for 7 oxonorbornane. The reaction mixture could be easily purified by recrystallization to yield a pure product.

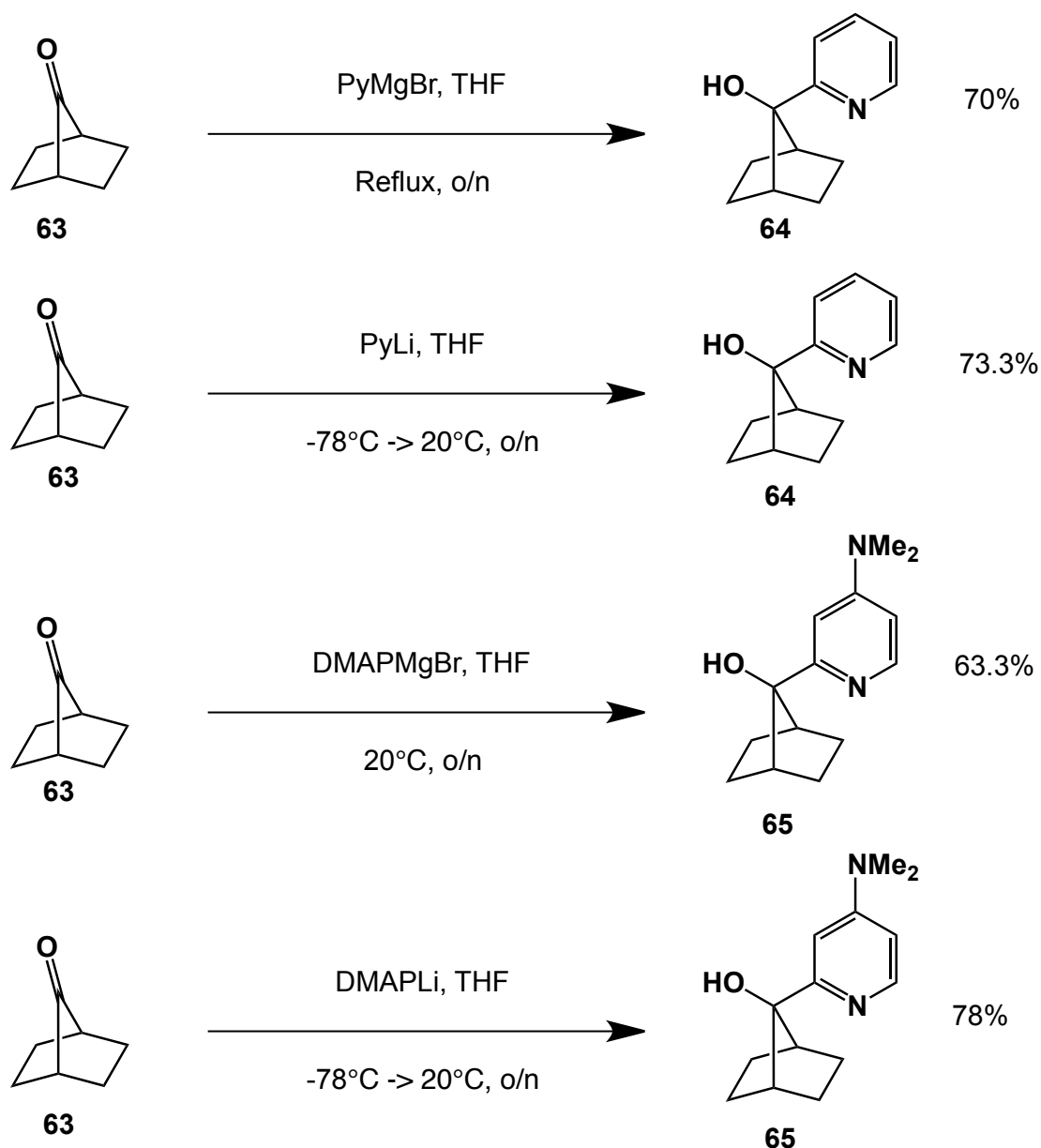


FIGURE 72: REACTIONS WITH 7-OXONORBORNANE

Before photochemical studies are possible we must methylate the oxygen atom as shown in Figure 73. Unfortunately this methylation does not proceed cleanly and purification was not possible during the time constraints of the project. It is likely that optimisation of this step, or perhaps purification by preparative HPLC would yield a product suitable for studies on the photochemical reduction of carbon dioxide.

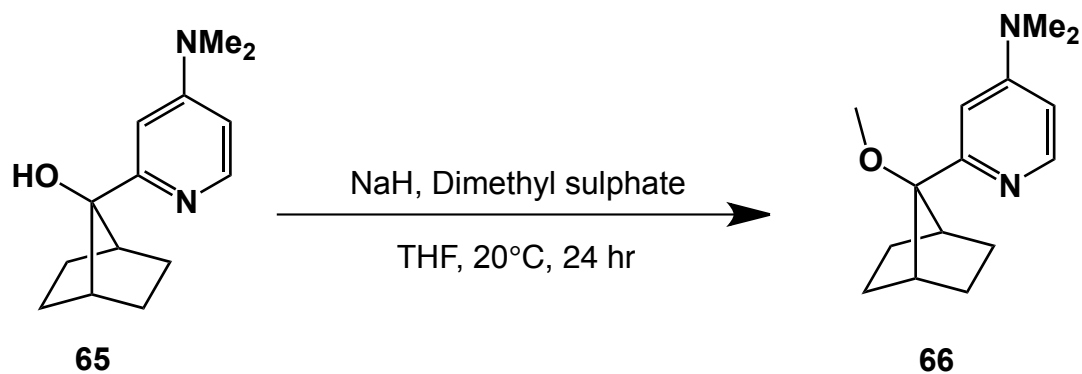


FIGURE 73: METHYLATION OF A DMAP BASED AMINE

CONCLUSIONS

This chapter has focused on the synthesis of amines for CO₂ reduction. First we investigated variations on amine, **20**. These modifications were aimed at removing the O atom that may cause Grob fragmentation. Of the two methods found to remove the O atom the Tebbe reaction was found to be most successful, it is thought this is due the lack of any S_N2 type chemistry in the mechanism. Whilst the Clemmensen reduction could produce product the rate was extremely slow and the final product was contaminated with an impurity that could not be removed by the author. The second half of the chapter details the synthesis of DMAP based amines, a successful route was found to amine, **66**, but the time limitations prevented optimization of the synthesis. Future work could optimize this synthesis and undertake photochemical studies.

CHAPTER 6 – COMPUTATIONAL STUDIES ON [3+4] CYCLOADDITIONS

INTRODUCTION

As reported in the previous chapter the syntheses of amines with suitably constrained backbone structures have proved difficult to achieve. Given that the second-generation amines investigated computationally in chapter 4 have even more constrained backbones than amines previously synthesised by the [3+4] cycloaddition methodology it would seem sensible to embark on a computational study. The study aims to calculate the most appropriate manner by which to synthesise amines similar to **32**.

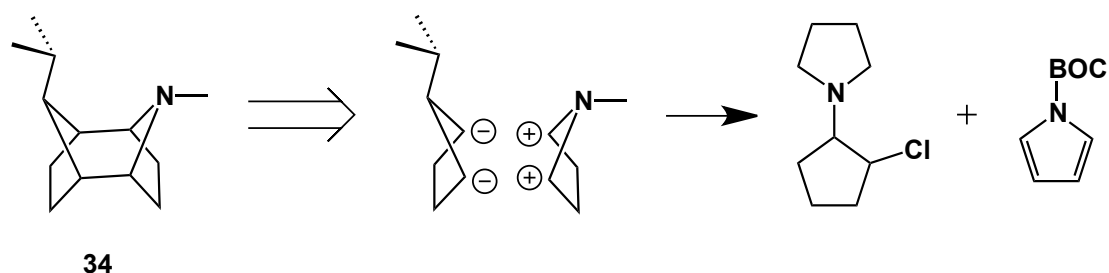
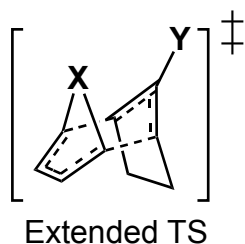
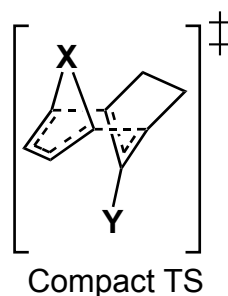


FIGURE 74: ILLUSTRATIVE RETROSYNTHETIC ANALYSIS

The starting materials proposed in the above retrosynthetic analyses, Figure 74, takes no account of the known stereochemistry of [3+4] cycloaddition reactions and only serves as a reference for the following discussion of this subject. It is important to recognise the influence the shape of the transition state in a cycloaddition reaction has on the final product. In such cycloadditions there are normally two possible transition state configurations, the chair-like extended TS, Figure 75-a, and the boat-like compact TS, Figure 75-b. These two cases are illustrated below in Figure 75. The factors affecting the preferred transition state structure complex are often hard to identify. Much experimental and computational work has focused on shedding light on this problem.^[134a, 176] The conclusions of which are broadly discussed below and in further detail later in the chapter.



a



b

FIGURE 75: POSSIBLE CYCLOADDITION TRANSITION STATES

The ratio of products is highly dependent on the nature of the reactants and reagents however the extended TS pathway can often be favoured by the use of highly electrophilic oxyallyl species and to a lesser degree by the use of cyclic dienes.^[177] For the weakly electrophilic species proposed in the above retrosynthesis, Figure 74, these trends predict a preference for the compact transition state. The compact transition state for these starting materials will inevitably lead to a high proportion of the incorrect stereoisomer. This is shown below in Figure 76 where it can be seen that the compact TS leads to a product with a trans relationship between the heteroatoms. As a consequence, it seemed fruitful to explore alternative synthetic approaches that could force the stereochemical outcome of the reaction.

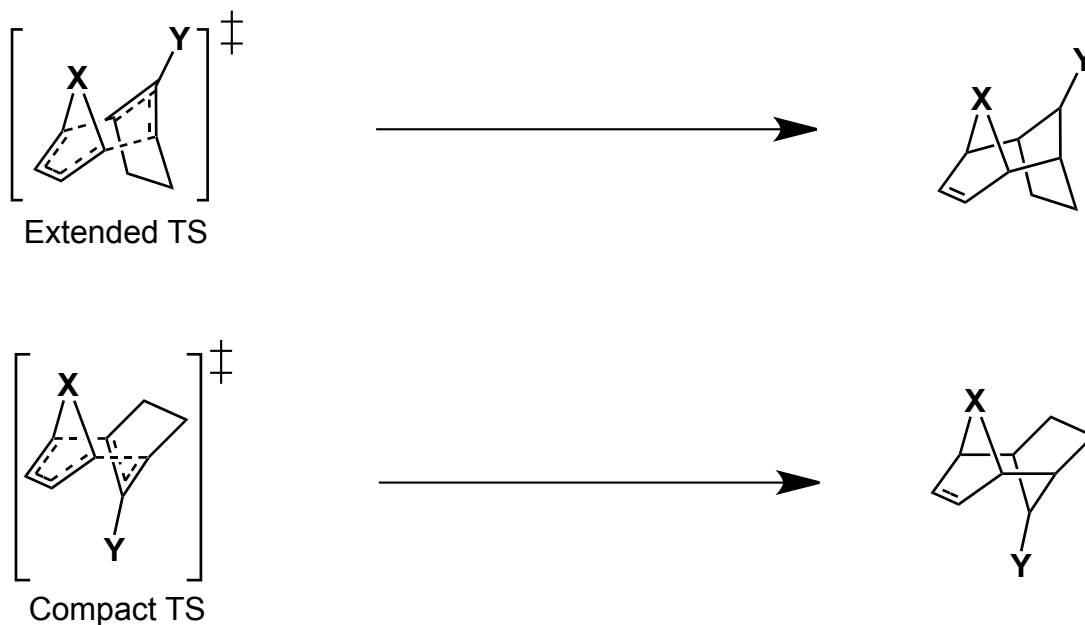


FIGURE 76: PRODUCTS FORMED FROM POSSIBLE [3+4] CYCLOADDITION TRANSITION STATES

An intramolecular cycloaddition, as shown in Figure 77, would force the configuration of the transition state and therefore the product regiochemistry. There has been reported numerous intramolecular [3+4] cycloadditions, however examples with cyclic oxyallyl cations or aminoallyl cations are rare.^[134a, 178]

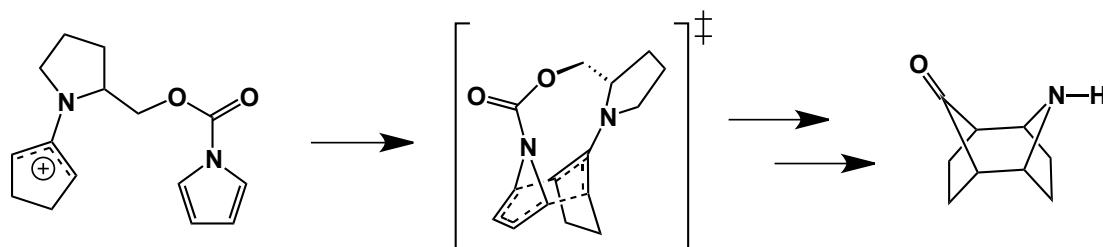


FIGURE 77: A TETHERED STARTING MATERIAL FOR [4+3] CYCLOADDITION

LITERATURE EXAMPLES

Shipman and co-workers are the only group to have reported an aminoallyl cation being utilised for an intramolecular cycloaddition.^[179] They described the generation of an aminoallyl cation from alkylidene aziridines by Lewis acid. This method of generation is very different to the reductive conditions previously used in this group but still provides evidence the proposed cycloaddition reaction, Figure 78, is a plausible route to the second-generation amines. Shipman utilises a furan ring as diene as it is known to be a better diene for dipolar cycloadditions than pyrrole. The reported 67% yield for this reaction is high so even a less efficient reaction with pyrrole may prove feasible

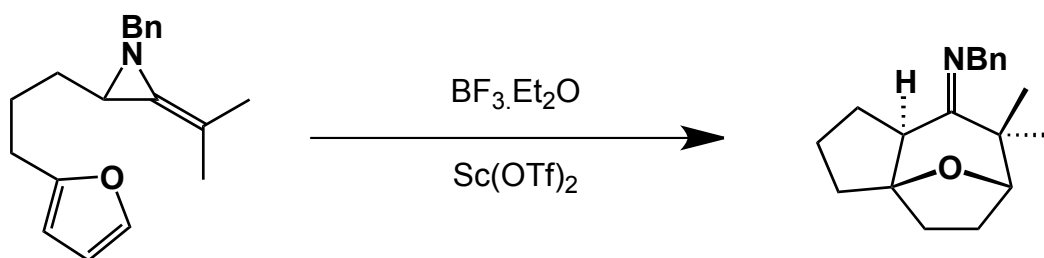


FIGURE 78: LITERATURE EXAMPLE OF AMINO ALLYL CATION IN INTRAMOLECULAR [3+4] CYCLOADDITION

In the early 1990s Harmata reported one of the first reliable intramolecular [3+4] cycloaddition reactions.^[134b, 180] He reported a stable precursor that under treatment with a Lewis acid would generate oxy-allyl cations suitable for [3+4] cycloaddition reactions, as shown in Figure 79. A collaborative computational study with Schreiner used DFT to assess the mechanism for the reaction and rationalise the observed product ratios.^[181] This shows

that it is possible to get qualitative results from B3LYP calculations that provide insight into the energetics of such reactions.

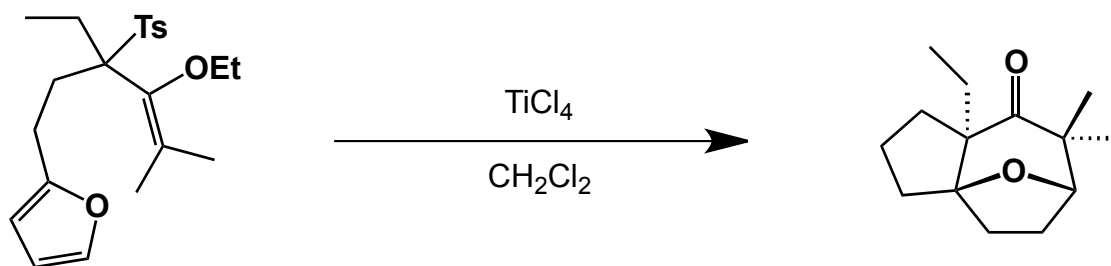


FIGURE 79: LITERATURE EXAMPLE OF OXYALLYL CATION IN INTRAMOLECULAR [3+4] CYCLOADDITION

Reports of intramolecular cycloaddition that contain a cyclic oxy-allyl cation are even more rare. In the early nineties Harmata reported several reactions using cyclic oxy-allyl cations.^[134b, 182] At that time no computational studies were undertaken. However, several years later Harmata collaborated with Cramer for computations on a related system,^[177b] Figure 80. The calculations used MP2 single-point energies on HF-optimised geometries; this approach was selected due to the tendency of DFT to over-delocalise charge and spin.^[183] It was noted that the results of these calculations were qualitatively correct, but the exact product ratios could not be accurately predicted..

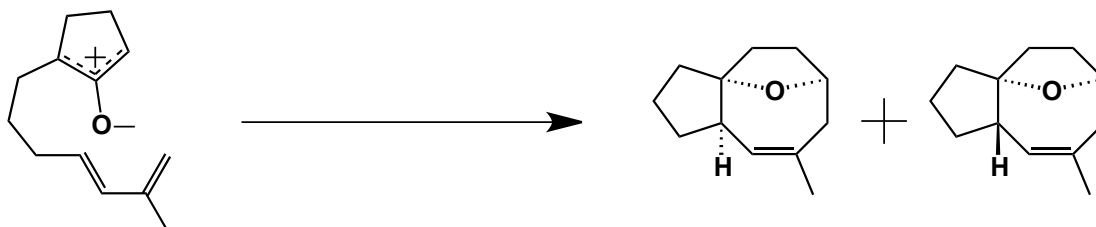


FIGURE 80: LITERATURE EXAMPLE OF A INTRAMOLECULAR [3+4] CYCLOADDITION

The number and scope of computational studies into intramolecular [3+4] cycloadditions has been fairly limited. This can be attributed to the high cost of suitable level calculations on relevant systems, this is exacerbated by not only the large size of the systems but the complicated electronic structure of the mechanisms. It is often necessary to include biradical structures in calculations that are rarely accurately described by DFT and require very large basis sets.

What lessons can we learn from the literature of intermolecular cycloadditions? The electronic properties of intra or inter molecular reactions should be largely the same in either case. Typically in intramolecular reactions, you expect lower entropy of activation but

higher activation energy. This can occur due to strain or suboptimal orientation introduced by the tether.

In the late 1990s Cramer took a computational approach to mechanistic studies on [3+4] cycloaddition with oxyallyl cations.^[176b] In particular the study focused on the how the nucleophilicity of the diene influenced the mechanism of the cycloaddition. As expected, the study found that weakly electrophilic dienophiles require strongly nucleophilic dienes in order to undergo cycloaddition reactions and that weakly nucleophilic dienes (such as pyrrole) have a propensity to undergo acylation reactions rather than cycloadditions. The study used both B3LYP and MP2 calculations throughout and found them to be in qualitative agreement in all but a few cases despite the known issues with DFT over-delocalising both charge and spin. The most relevant reaction studied was that between hydroxyallyl cation and pyrrole. It was found, by both DFT and MP2, that the reaction would not proceed to cycloaddition products but instead would be trapped at the acylation stage due to the highly stable intermediate (which could then capture a proton to yield a stable product) as shown in Figure 81. This study suggested that we should be able to reliably determine the possibility of the proposed cycloaddition even if we were not able to calculate accurate reaction barriers.

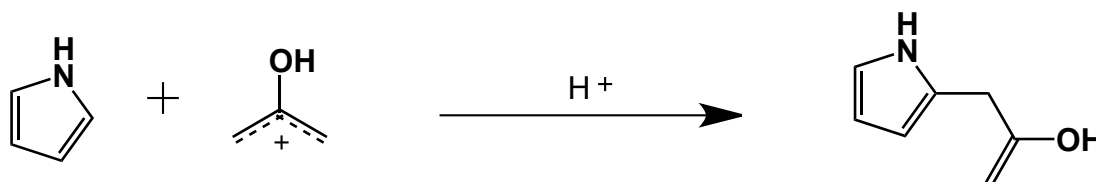


FIGURE 81: LITERATURE COMPUTATIONAL STUDY OF REACTION BETWEEN OXY-ALLYL CATION AND PYRROLE

Domingo studied cycloadditions of 2-(trimethyl silyloxy) acrolein with furan under Lewis acidic conditions.^[184] The reaction has very different electronic properties to the reaction studied by Cramer above as the 3 atom component is significantly less electrophilic than the hydroxyl allyl cation. In fact comparisons were drawn between the title reaction, Figure 82, and Diels Alder reactions involving acrolein.^[185] The difference in electrophilicity of the reacting partners indicated that the reaction should follow a polar pathway. The study confirmed this and then went on to show that this causes a concerted asynchronous [3+4] cycloaddition reaction. There is a significant amount of charge transfer between the oxyallyl cation and dienophile in the transition state, again typical of a polar reaction. Aminoallyl cations such as the proposed amine will have relatively low electrophilicity indexes and as

such the methods used in this study should also apply well to our system. Further studies by Domingo in related system also use B3LYP as their main functional.^[186]



FIGURE 82: LITERATURE EXAMPLE OF A [4+3] CYCLOADDITION STUDIED BY DFT

Many groups have used the global electrophilicity index to predict the feasibility of cycloaddition reactions.^[177a, 187] Several indexes can be defined from the DFT one-electron energies of the LUMO (ϵ_L) and the HOMO (ϵ_H) to chemical potential, chemical hardness and finally electrophilicity power, Figure 83.^[188]

$$\mu \approx \frac{\epsilon_H + \epsilon_L}{2}$$

$$\eta = \epsilon_L - \epsilon_H$$

$$\omega = \frac{\mu^2}{2\eta}$$

FIGURE 83: EQUATIONS USED TO CALCULATE GLOBAL ELECTROPHILICITY INDEX

The parameter μ , is the electron chemical potential as defined by Parr,^[189] this a measure of how the energy of a molecule changes with the number of charge or how the molecule responds to charge transfer. The chemical hardness (η) defines the willingness of the system to undergo the change described by the chemical potential.^[189] As such a good electrophile will be characterised by high values for μ and low values for η . The electrophilicity power (ω) measures the stabilisation when a system acquires an additional electronic charge.^[190] Domingo uses this as a direct comparison for electronegativity between differing molecules and assumes that bad electrophiles will be good nucleophiles. These assumptions are not globally acceptable but seem to allow prediction of accurate reaction rates in the systems he has studied. Many would object to a global electrophilicity scale based on ground state electronic structure and would instead suggest a system based on kinetic analysis of reference nucleophiles reacted with many electrophiles.^[191]

Perez and Domingo used this index to rationalise the rates of (1,3) dipolar cycloaddition reactions.^[177a] They determined that reactions with a very polar character would display high rate constants. They explain this by counter-example. Reactions with little polar character

have similar HOMO and LUMO energies for both reactants and proceed through a concerted mechanism. This concerted mechanism implies a later, more product-like, transition state. This requires more rearrangement and is therefore higher in energy and the reaction rate is then slow. We then must conclude that reactions with a high polar character will have an early transition state, and a high rate constant of reaction.

While this method has found application in literature and has been found to be suitable for qualitative rate prediction in many cases, it is unlikely to be helpful in this case. Due to the generalisation of mechanisms that is made during the assumptions of this method, it is likely that this reaction occurs by a stepwise ionic process rather than a sigmatropic process assumed by this analysis. It has previously been reported that pyrrole has a very low ω value (0.31),^[187b] and nitrogen substituted dienophiles are predicted to have high values of ω (N-Methylmethylen ammonium cation = 8.97)^[177a]. This indicates that global electrophilicity index analysis would predict a high reaction rates for related reactions. This prediction does not match our experimental results for cycloadditions involving pyrrole and its derivatives, where only a single successful reaction has been found. For these reasons it was determined that a more accurate description of the potential energy surface was required to make reliable predictions about the synthetic feasibility of such reactions.

COMPUTATIONAL STUDY

Based on the conclusions discussed in the preceding literature review it was determined that to accurately determine the feasibility of scheme Figure 76, the mechanism must be determined and the relevant stationary points should be calculated. This would allow us predict reaction enthalpies for each step of the predicted mechanism and assess this as a possible thermal step. The B3LYP functional was selected due to its relatively low cost and success in literature examples discussed above. The moderately large 6-31+G(d,p) basis set was chosen to ensure that the cationic intermediates were modelled as accurately as possible but within a reasonable time frame.

Following an analogous procedure to that used for the synthesis of the first generation amines the proposed starting material would be treated with AgBF₄. This would abstract a chloride ion from the starting material, **67**, and yield the amino allyl cation, **68**, ready for cycloaddition, Figure 84. This step is presumed to follow an ionic mechanism as it is known that silver chloride is produced as a product in such reactions. The creation of a cation at this stage seems to indicate that the cycloaddition mechanism would proceed by an ionic

mechanism. While this assumption may not be entirely correct, if a reasonable ionic mechanism pathway can be found there is no reason to suspect it would be incorrect.

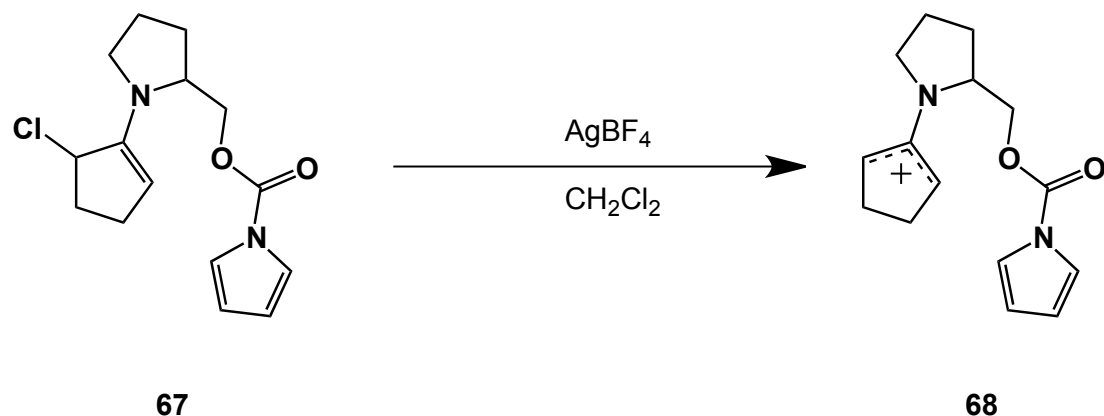


FIGURE 84: FORMATION OF AMINO ALLYL CATION FOR CYCLOADDITION

It was anticipated that calculation of various stationary points on the potential energy surface would allow us to determine whether the reaction proceeds through a concerted or stepwise mechanism. The magnitude of the activation barriers and the thermochemistry of the overall reaction should allow us to predict the synthetic feasibility of the reaction.

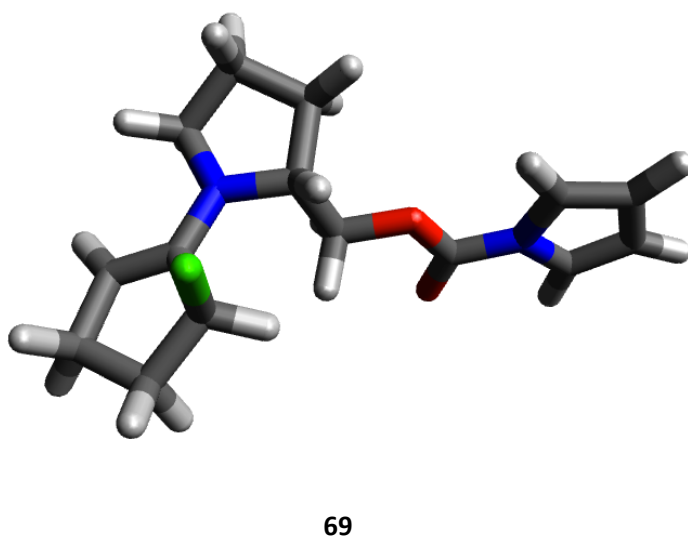
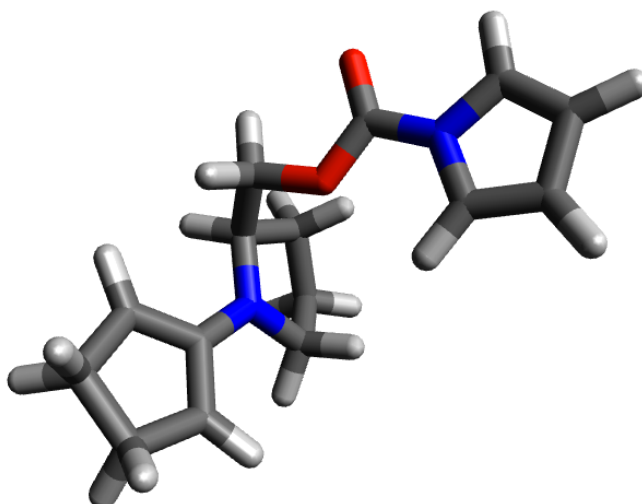


FIGURE 85: OPTIMISED GEOMETRY FOR CHLORIDE

Figure 85 shows the ground state geometry of the chloride, **69**. The equilibrium geometry shows an extended formation with the rings held distant from each other. Upon abstraction of the chloride ion from **69** the equilibrium geometry undergoes relatively minor changes, Figure 86. There was no apparent complex formation between the π fragment and the empty p orbital produced.



70

FIGURE 86: OPTIMISED GEOMETRY FOR AMINO ALLYL CATION

This lack of interaction between the aminoallyl system and the diene fragment, Figure 86, highlighted the need for a large conformational change from the equilibrium geometry of cation, **70**, to the transition state; this could well be significantly energetically unfavourable. A number of similar molecules were also investigated with two principal parameters to be varied: the length of the flexible linker, and the position at which it is attached to the pyrrolidine ring. This led to a series of molecules shown below in Figure 87.

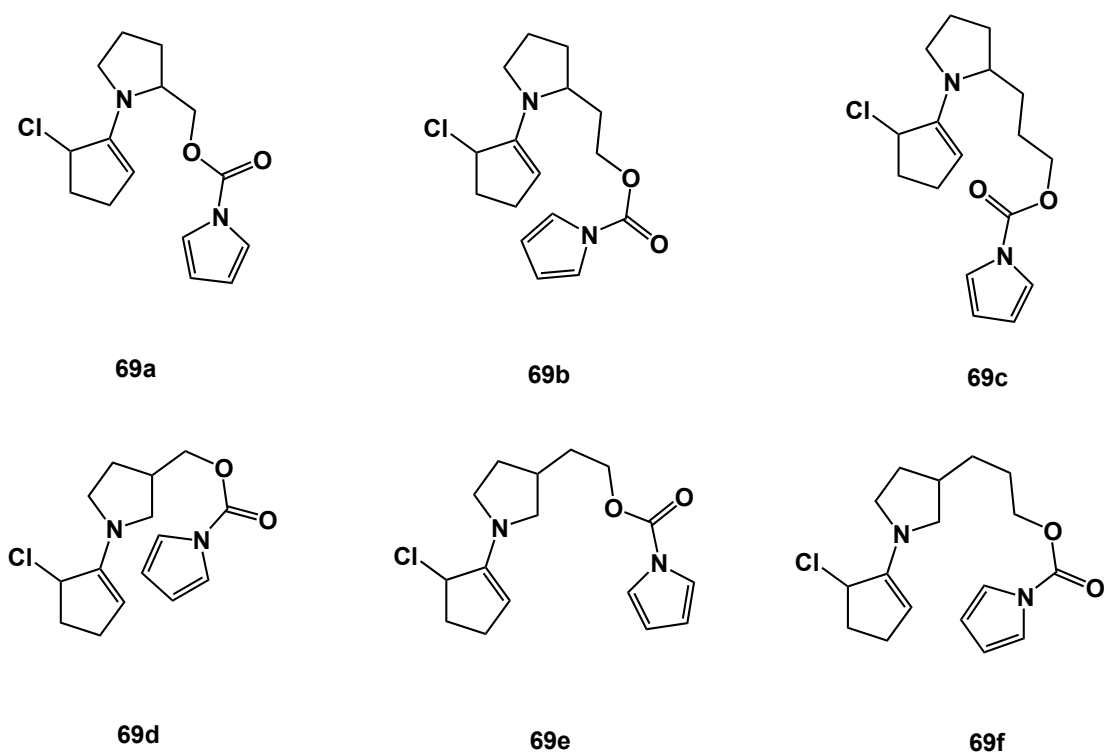


FIGURE 87: PROPOSED STARTING MATERIALS FOR SYNTHESIS OF SECOND GENERATION AMINES

An extensive search was performed for a concerted transition state between the starting material cation and the final product, however in all cases the geometry optimisation collapsed into a stepwise path. This suggests that the reaction proceeds through a stepwise mechanism and that if a concerted pathway exists, it is higher in energy than the stepwise path. Further work on this reaction presumed a stepwise mechanism as predicted here.

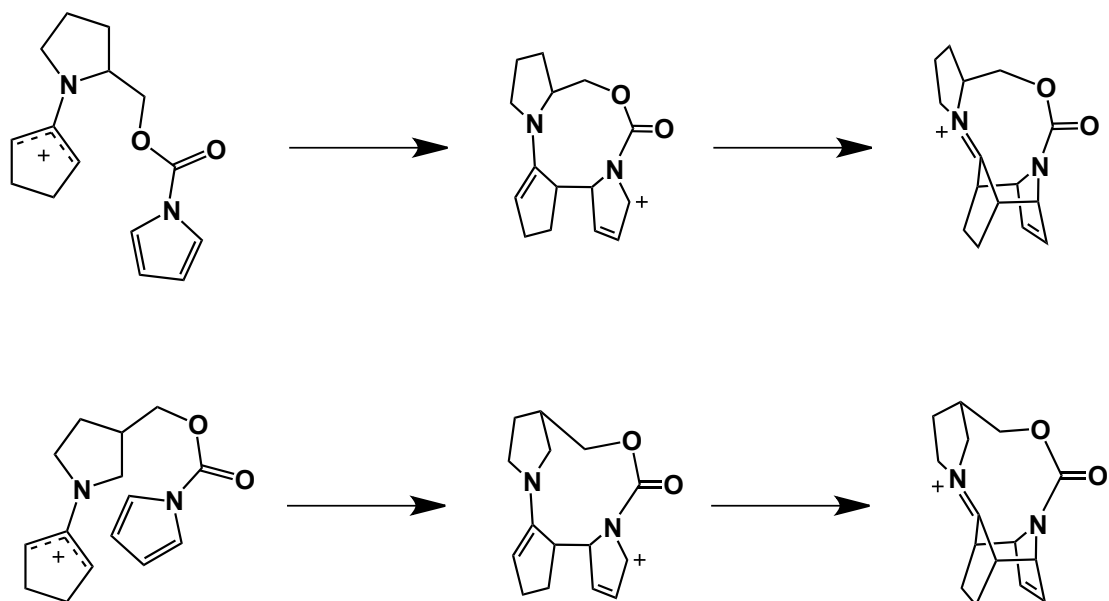


FIGURE 88: PROPOSED MECHANISMS FOR [4+3] CYCLOADDITION

Using the mechanism shown above in Figure 88, each stationary point was calculated for each molecule. This led to a total of 6 potential energy surfaces for comparison. The related thermodynamic quantities are given in Table 20. ΔG_1^\ddagger and ΔG_2^\ddagger are the activation energies of the first and second steps, ΔH_1 the reaction enthalpy of the first step and ΔH the overall reaction enthalpy.

	ΔG_1^\ddagger	ΔH_1	ΔG_2^\ddagger	ΔH
69a	14.42	4.86	2.63	-1.30
69b	12.61	13.53	-1.75 ³	1.84
69c	1.74	-5.02	21.03	-5.80
69d	14.09	5.80	8.35	-1.67
69e	5.44	-0.03	12.38	-0.36
69f	3.17	-3.31	12.58	-4.40

TABLE 20: REACTION PARAMETERS FOR SYNTHESIS OF SECOND GENERATION AMINES (KCAL MOL⁻¹)

³ The calculated negative activation energy is not physically possible. However the error margin typical in such calculations is much larger than the magnitude of the activation energy. This suggests there is small positive activation energy for this step.

POTENTIAL ENERGY SURFACE

As can be seen from Table 20, two of the starting materials substituted in the 2 position of the pyrrolidine have low activation energies for second step, but much higher energies for the first step. The opposite trend is found for two of the three starting materials substituted at the 3 position of the pyrrolidine ring. To determine which starting material is most suitable for the reaction we must not only consider the relative barriers to the desired cycloaddition, but also any other possible reactions.

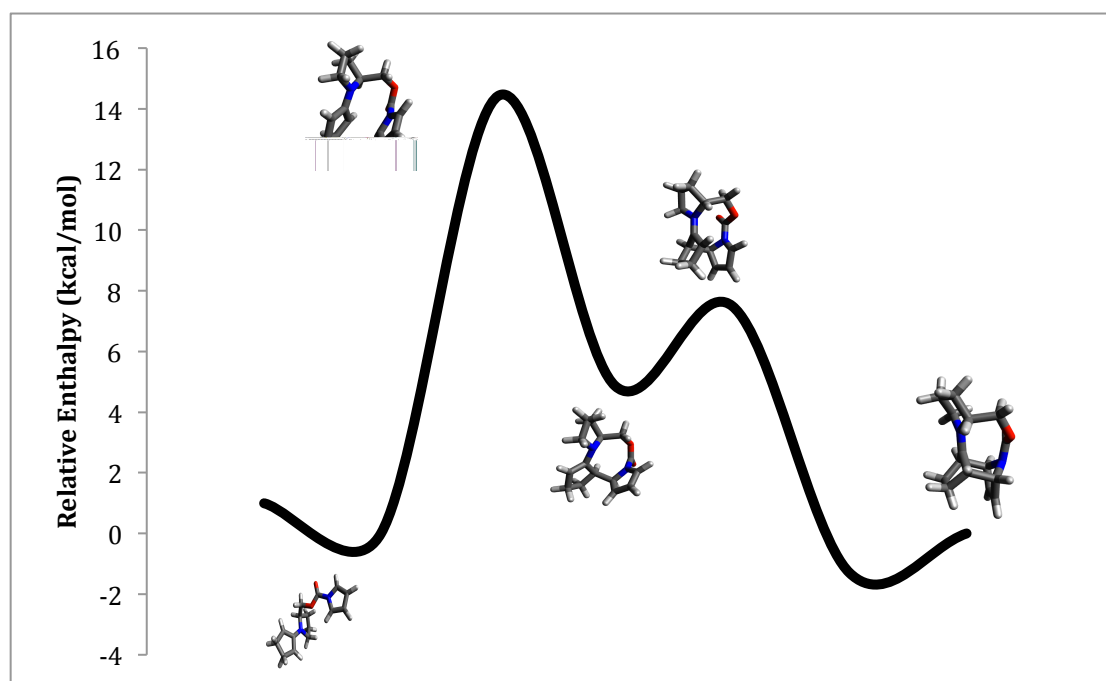


FIGURE 89: REACTION PROFILE FOR SYNTHESIS OF SECOND GENERATION AMINES

With all activation energies less than 22 Kcal mol⁻¹ it would seem there would be no insurmountable barriers to the reaction under normal thermal reaction conditions. One would expect a typical organic reaction with activation energy over 30 Kcal mol⁻¹ to proceed slowly at normal reaction temperatures. It would therefore make sense to select a starting material that is very efficient at the second step to avoid any possibility of proton capture leading to the Friedel-Craft product. This has often been reported as a problem for pyrrole based systems. To this end starting material, **69a**, has been selected as the ideal candidate for synthesis. The potential energy surface that was calculated for the reaction is shown in Figure 89.

CONCLUSIONS

This chapter describes a computational study into the feasibility of the synthesis proposed in Chapter 3. The DFT calculations predict the reaction mechanism will follow a two-step mechanism rather than a concerted reaction, as shown in Figure 88. Neither of the two cycloaddition steps is predicted to have a barrier of over 15 kcal mol⁻¹ and so the reaction is predicted to proceed under normal thermal conditions. This study indicates it would be worthwhile to explore this synthesis experimentally.

CHAPTER 7 – QUANTUM CHEMISTRY INTERFACE - QCI

INTRODUCTION

During this project much work was undertaken using computational chemistry packages such as Gaussian and GAMESS. These packages provide very advanced algorithms for calculating many diverse chemical properties. However it was found during the course of this project that many of the operations carried out were very similar. It soon became obvious that much of the work involved in doing the calculations required for this sort of project was not chemistry but data-handling and analysis.

During discussions with other research groups and students it became clear that computational chemistry has a reputation of having an extremely steep learning curve and that calculating useful chemical data was extremely time consuming. It seemed that these factors were creating a large barrier to entry for many chemists into the field of computational chemistry. Students were often unwilling to expend time learning the Linux command line environment before they could even start formulating plans for useful calculations.

While undertaking the computational work detailed earlier in this report a number of small scripts were written to automate basic tasks and as the work continued the number and complexity of these scripts grew. Before long, it became obvious that such scripts could become useful to the wider chemistry community.

Before embarking on a serious software development project informal discussions were had with a number of my peers, a handful of academic staff and a few undergraduate students. It was through these discussions that a firm specification for the design was developed and is detailed below.

DESIGN REQUIREMENTS

The first, and probably most significant, observation made was the lack of a common format between popular quantum chemistry programs. The lack of this means that a typical computational chemist has to become proficient in the various different programs he or she will use on a daily basis. This can be particularly frustrating when a new user starts to master the art of one program before realising that an important functionality is only provided by a competing program. This has therefore become a key goal in this project: the project must define a common interface between any of the major quantum chemistry programs. We

must design the interface in a modular manner that is agnostic to the underlying program. This interface should take commonly understood chemical structure formats (such as XYZ files) and be capable of producing valid input files for the supported quantum chemistry programs.

A related frustration can be found in the varying outputs of the common quantum chemistry programs. Not only does each program have its own format, but also the output files normally contain masses of data not typically useful to the average user. The interface therefore, must also be capable of parsing these outputs and extracting the most important results from it. This project is not alone in these goals and, as will become apparent when the specific implementation is discussed we do not have to reinvent the wheel in this respect.

The use of batch queuing systems on supercompute clusters is ubiquitous and offers us further opportunity to devolve some tedious work away from the end user. As such the project should understand differing queue systems and should be able to submit jobs directly to the queue. The possibility of tasks such as monitoring the queue for completed jobs and automated resubmission of jobs which do not complete within their allocated time was considered but these tasks were deemed to be better handled by the end user who can make more informed decisions about handling such cases.

Various commercial products, such as WebMO, have already implemented the features discussed above however much more tedious work can be automated if you consider the needs of most organic chemists. Often organic chemists are interested in knowing the relative energies between competing molecular pathways or profiling varying substituents across a base molecule. This typically requires running a number of compute jobs and then doing some basic arithmetic to calculate thermodynamic properties of a reaction. In this respect products such as WebMO start to fall behind, they typically do not understand common usage and do not provide tooling to rapidly create libraries of compute jobs.

As such the project must provide a batch interface to allow operations on groups of jobs simultaneously. This functionality should be accessible by passing a list of jobs to operate on; wildcards will not be supported to avoid minor errors submitting large numbers of jobs to the cluster or doing costly analysis.

The project should understand basic reaction structures and be able to automatically calculate thermodynamic properties such as reaction enthalpies and stepwise activation

energies. The reaction schema should be passed in a human readable format to ensure the interface does not become overly complicated.

As organic chemists often want to study many substituted versions of a base molecule the project should be able to automatically generate new input files from previous jobs and a specified fragment. This will allow rapid generation of a vast number of jobs from a simple base structure. This section of the project will only support fairly small substitution patterns, as generating accurate coordinates for the new molecule becomes progressively harder as the size of the added fragment grows. This part of the project must also avoid altering the base molecule as this will have previously been optimised by a high level calculation.

The final concern that has been raised by many people during discussions around computational chemistry for new users is the lack of a graphical user interface. This, however, will not be included within the requirements as the amount of work required to achieve such a goal is extremely large. A GUI for the interface could be designed on top of a command line version so no effort would need duplicating if at a later date this was deemed worthwhile.

If the above design specifications are followed it should be possible for a student to design a reaction scheme they wish to study and make some simple molecular models in a common format such as XYZ. From this point they can specify some fundamental properties and the level at which they wish to run the calculations. They should then be able to determine the feasibility of the reaction from the thermodynamic properties, this will allow them to determine if further study is worthwhile. If so they can quickly generate large libraries of related molecules without having to generate new XYZ files. Once these jobs have completed they can use the batch mode to quickly analyse all the results and starting drawing chemical conclusions from a plethora of data. As described, this moves the student away from the tedium of many tasks and allows them to focus on the chemical results they get from their calculations.

TECHNOLOGIES USED

The first step in implementing any serious software project is to evaluate the most suitable language in which it should be written. There are many choices of language and a complete discussion of all features of modern languages is far beyond the scope of this report. However this report will briefly discuss the motivations behind choosing Python for this project. As mentioned in the previous section of chapter designing this project in a modular fashion is vital for the success of the final product.

There are various paradigms for designing modular programs; the most common in use today is called object orientated programming. This method works by considering each part of the program as an object that can be created many times, or have many different implementations. Objects have attributes, or data, and methods that act on these data. This encapsulation of data and the methods that act on them allow a programmer to create interfaces between different parts of their program that do not depend on specific implementations of any other part of the program. This will allow us to create objects that know the specific details of one particular quantum chemistry program and can interact with the rest of the program just as any other implementation can. As a fairly modern language Python was built from the ground up with a strong sense of object orientated programming, this means that its features are very easy to exploit. This is especially apparent when comparing to less modern languages such as Perl.

Python also has an extensive standard library. This means that the language already provides many common functions one might wish to access. This often reduces development effort as one does not need to reinvent the wheel and often provides a better implementation that could be quickly provided by the programmer. Common examples of functions used from the standard library include features such as writing a log file and parsing arguments passed from the command line. It is also possible to extend the library of functions available by including new modules.

Python is an interpreted language; this means that the code is run line by line when the program is run. This is in comparison to a language such as C++, which is fully compiled into machine code before any code is run. This can often mean that the program runs slower but development time is normally lower as bugs are easier to catch. The reduction in development time is well worth the additional running time, especially when you consider that the actual compute jobs will normally have running times in the order of hours. The additional seconds added to the analyses of the output is rather trivial in comparison.

The final, and possibly most important, motivation behind choosing Python as the development language is the popularity of it within the rest of the chemistry community. As mentioned above it is possible to extend python through a modular system, there are already many chemistry modules that can be included into Python. The two used in this project are openbabel and cclib, these projects include some complex functionality that has significantly reduced the development effort required to fit the design requirements detailed above. Both projects are released under open source licenses and so are freely available to use within this project.

INTERFACE DESIGN

The next stage in implementation is to design an interface for the user to interact with the program. As the design requirements have already ruled out the possibility of a GUI it is logical to use a command line interface. This is more flexible than designing a new style of input file for the interface and is much more user friendly as well. The first step in designing the interface is to consider how the typical user will use the program. On the basis of the requirements discussed above, it seems that most users will have various projects, which will contain related reactions or jobs, normally differing by substitution pattern, and each of the reactions will contain several individual molecules. As such the program will expect to be passed a:

1. Project Name – an overall name for the project. For example HAbs for a hydrogen abstraction reaction.
2. Job Name – an identifier for the each reaction being studied under a project. This will often be shorthand for a substitution for example 1sOH for an OH group substituted at the 1 position of the parent molecule.
3. Step Name – a name for each molecule in the reaction. For example TS1 for the first transition state.

These 3 names should then allow easy referencing of any specific compute job for example HAbs-1sOH-TS1 would be the full name of the compute job relating to the first transition state of the 1 OH substituted molecule in the hydrogen abstraction project. When passing these names to the command line we should allow passing lists for the batch mode.

There will have to be several modes of operation that allow the user to perform different actions. From the specifications given above there must be a minimum of 4 modes. These are as follows:

1. New – creates program specific input files from the command line options passed
2. Submit – creates the queue file and submits jobs to the queue.
3. Analyse – reads the output of a completed job and prints relevant data
4. Reaction – Takes input of a reaction structure and outputs the reactions thermodynamic data.

There will also need to be various options that can be passed to the program so it can have enough information to properly build or analyse the compute jobs. The full list of options is

specified below, this list might seem overwhelming but the vast majority can be passed a default value from a configuration file (these cases are marked with default in the list).

Chemical Options

1. Charge – The molecules overall charge (default)
2. Multiplicity - The molecules overall multiplicity (default)
3. Transition State – A Boolean flag to set if a molecule should be treated as a transition state (default=false)
4. Symmetry – The molecular point group (only required for GAMESS) (default)

Calculation Options

1. Type – Job type. Currently supported optimisation, frequency and IRC (default=optimisation)
2. Engine – Quantum chemistry program to use. Currently supported Gaussian and GAMESS (default)
3. Basis – The basis set chosen for the calculation
4. Functional – The functional chosen for the calculation (default)
5. PCM – The solvent for a PCM calculation (default)
6. Fragment – Position in which to automatically substitute and the fragment which should be inserted (default=none)
7. XYZ – The file name of molecular coordinates. Accepts .xyz, .mdl and .job (to extract coordinates from previous calculation)

Queue Options

1. Walltime – Maximum execution time (default)
2. Nodes – Number of compute nodes to use (default)
3. CPUs – Number of CPUs to use per node (default)
4. RAM – Amount of RAM to use per node (default)
5. Queue – Name of queue to submit into. (default)

As shown in the above list it is normally only necessary to pass a small number of options for a job. Normally the user will only need to pass the 3 names and a set of coordinates for job creation. The user will often also want to specify a charge and multiplicity but these are normally set to 0 and 1 respectively, in the configuration file.

EXAMPLE CALCULATION

Before discussing the design of the program in depth, it is worth giving a brief example of how a typical user might interact with the program on a basic level. The following example does not use all the features discussed above but allows the reader to better visualise how the final program will work.

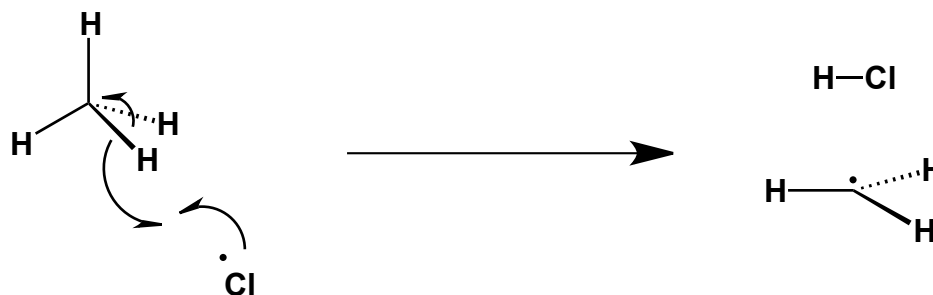


FIGURE 90: EXAMPLE REACTION SCHEME FOR QUANTUM CHEMISTRY INTERFACE

This example, Figure 90, shows the abstraction of a hydrogen atom from methane by a chlorine radical to form HCl and a methyl radical. The coordinate files were built in Avogadro a popular open source program for simple manipulation of molecular representations and then optimised with a molecular mechanics simulation. The input files were then created using the new method, explicitly passing the charge and multiplicity and allowing the remaining options to take their default value in the configuration file, Figure 91.

```
./main.py HAbs H SM --new --charge 0 --mult 1 --xyz methane.xyz
./main.py HAbs H Cl --new --charge 0 --mult 2 --xyz Cl.xyz
./main.py HAbs H Prod --new --charge 0 --mult 2 --xyz methylradical.xyz
./main.py HAbs H TS --new --charge 0 --mult 2 -ts --xyz radTS.xyz
./main.py HAbs H HCl --new --charge 0 --mult 1 --xyz HCl.xyz
```

FIGURE 91: EXAMPLE INVOCATION OF QUANTUM CHEMISTRY INTERFACE

The jobs were then submitted to the queue using the batch version of the submit command, Figure 92.

```
./main.py HAbs H "Cl HCl SM Prod TS" -s
```

FIGURE 92: EXAMPLE JOB SUBMISSION WITH QUANTUM CHEMISTRY INTERFACE

In this example we used the B3LYP functional and a 6-31G(d,p) basis set as these methods are relatively computationally cheap and can be run on commodity hardware for small molecules. Once the jobs have all completed we can analyse the entire set using a batch mode, Figure 93.

./main.py HAbs H "SM Cl TS Prod HCl" -a

FIGURE 93: EXAMPLE ANALYSIS OF REACTION WITH QUANTUM CHEMISTRY INTERFACE

This will display the optimised coordinates and the thermodynamic data for each job, Figure 94.

Job: HAbs-H-SM

CONVERGED

Coordinates:

C	0.00000	-0.00000	0.00000
H	-0.70244	-0.25045	-0.79767
H	-0.55292	0.22750	0.91375
H	0.59010	0.87029	-0.29460
H	0.66525	-0.84734	0.17851

Free energy = -40.498662 kcal mol⁻¹

Enthalpy = -40.475185 kcal mol⁻¹

Entropy = 0.078742 cal/mol-K

Calculated at 298.150000 K

Job: HAbs-H-Cl

CONVERGED

Coordinates:

Cl	0.00000	0.00000	0.00000
----	---------	---------	---------

Free energy = -460.151919 kcal mol⁻¹

Enthalpy = -460.133882 kcal mol⁻¹

Entropy = 0.060496 cal/mol-K

Calculated at 298.150000 K

Job: HAbs-H-TS

CONVERGED

Coordinates:

C	-1.92772	0.00001	-0.00001
H	-0.31300	-0.00001	0.00003
H	-2.09245	-0.58732	-0.89746
H	-2.09260	1.07086	-0.05991
H	-2.09281	-0.48359	0.95729
Cl	1.06807	0.00000	0.00001

Free energy = -500.636127 kcal mol⁻¹

Enthalpy = -500.605561 kcal mol⁻¹

Entropy = 0.102519 cal/mol-K

Calculated at 298.150000 K

Job: HAbs-H-Prod

CONVERGED

Coordinates:

C	0.00001	-0.00003	-0.00000
---	---------	----------	----------

```

H      -0.13822  1.07300  0.00000
H      0.99844  -0.41676  0.00000
H      -0.86029  -0.65609  0.00000

```

Free energy = -39.832940 kcal mol⁻¹

Enthalpy = -39.809076 kcal mol⁻¹

Entropy = 0.080040 cal/mol-K

Calculated at 298.150000 K

Job: HAbs-H-HCl

CONVERGED

Coordinates:

```

H      0.00000  0.00000  -1.21433
Cl     0.00000  0.00000  0.07143

```

Free energy = -460.811942 kcal mol⁻¹

Enthalpy = -460.790750 kcal mol⁻¹

Entropy = 0.071078 cal/mol-K

Calculated at 298.150000 K

FIGURE 94: EXAMPLE OUTPUT FROM CALCULATION ANALYSIS IN QUANTUM CHEMISTRY INTERFACE

The user can now confirm that optimised structures have converged to a sensible geometry by visualising the coordinates in any molecular visualisation software. Once they are happy with the results they can automatically calculate overall reaction thermodynamic properties with the following command, Figure 95.

```
./main.py --reaction HAbs H "SM+Cl=>TS=>Prod+HCl"
```

FIGURE 95: EXAMPLE REACTION ANALYSIS IN QUANTUM CHEMISTRY INTERFACE

This will produce the following output, Figure 96:

Project: HAbs

Reaction SM+Cl=>TS=>Prod+HCl

Substitution: H

Activation energy = 2.200047 kcal mol⁻¹

Reaction enthalpy = 5.798811 kcal mol⁻¹

FIGURE 96: EXAMPLE OUTPUT FROM REACTION ANALYSIS IN QUANTUM CHEMISTRY INTERFACE

The above example shows how a series of calculations can be reduced down to a handful of commands that require little in terms of specialist knowledge about computational chemistry. The use of the program has allowed the user to concentrate on the chemical aspects of calculation rather than the tedious creation of input files.

IMPLEMENTATION DETAILS

As mentioned above Quantum Chemistry Interface (QCI) is written in Python using object-orientated paradigms, this section reports on what advantages this gives us as a

programmer. Furthermore we discuss the templating-based system that allows rapid extension of the program to new computational engines and batch queuing systems.

Each calculation is managed as an object, this allows us to store data related to this job as well as the methods that act on this data. However this is not the beginning of the story; before we start implementing specific job details we must think of the overall structure of the object tree.

The specifications detailed above tell us that we must have a three-layered hierarchy to fully describe how jobs related to each other (Project, Job, Step). Within an object orientated program we can utilise the concept of inheritance to allow the final calculation to make use of all the data and methods associated with the project, job or step.

Once we have defined this structure we can start thinking about what data needs to be stored on each level of the calculation. In our structure, general properties such as information about where files physically sit on the disk drive can be held in higher-level objects and more calculation-specific details such as chemical properties can be stored at lower levels. Most of the initial data stored in the objects are passed to the program on the command line and parsed by a built-in Python library. Later, when we have completed calculations, we can start extracting chemical data from our calculations that is also stored within the same object.

We must also start thinking about what methods are needed to operate on our data. In the first instance, we need methods that will create input files and parse chemical properties from the output files. The parsing of chemical properties has been handled with another Python library, `cclib`, throughout the project and as such this method is completely general and agnostic to the computational engine used in the specific calculation. While modifications to `cclib` have been important during this project it is not deemed relevant to discuss these details during this report.

The generation of input files, however, is necessarily specific per engine, having designed our program structure with object orientated principles we can exploit the power of inheritance. This allows us to define an implementation specific to each engine we wish to support while maintaining a common interface for the rest of the program.

To allow the program to be easily extended or modified in the future a templating-based system has been designed. Each engine has a base input template defined in configuration and the object can be designed to fill in placeholders. The object reads the template and fills in the predefined variables to generate the specific input file for the calculation, the per

engine methods then allow the programmer to ensure that each replaced variable is using the correct format for the template.

For example a Gaussian input file expects its coordinates in the format <Element Symbol> <X> <Y> <Z>, where as the GAMESS input file expects a <Element Symbol> <Atomic Number> <X> <Y> <Z> format. The object for each engine knows these specific implementation details and correctly fills in template to generate a correct input file.

Methods to deal with submission of calculations to the system queue are generally specific to the engine as well and in this implementation they also exploit a similar templating based system

The object graph now has 4 layers and the 4th layer can have many members each representing a different computational engine. It is important to remember that we can initialise many objects of the same type during program run time. This allows us to implement a batch mode capable of operating on many jobs at once.

We have now designed a system capable of generating and analysing basic computational jobs, however we haven't started to look at the advanced features outlined in the requirements.

The automated generation of substituted molecules from a base calculation allows generation of vast libraries of data that allows the chemist to spend more time in analysis of their overall results. There are two sides to this part of the project: first we must analyse the previous results to extract optimised structures to substitute, and secondly we must be able to join new fragments to this base structure in a sensible manner. This job is far from trivial and beyond the simple Cartesian addition it may appear to require at first glance. When adding a fragment to a molecule we must consider the orientation of both parts and the normal bond lengths of the bond we are creating. We could resolve this by enforcing a particular frame on the base molecule but this would likely be disrupted during any optimisation calculation that occurred on the base molecule before substitution. This then suggests we must deal with rotating the frame of reference to allow sensible substitutions to occur. Thankfully once again much of the work has previously been done by another project, namely OpenBabel.

OpenBabel is another program built with object-orientated principles and one of the objects they provide describes a molecule. When we input any molecule to QCI we convert it to an OpenBabel molecule class, this then allows us some access to its methods to perform simple operations on the molecule. In the general sense we create two OpenBabel molecule objects

to represent both the base molecule and fragment, we then are given for free various methods that allow us to operate on them. One such method allows us to replace an atom by another atom and another allows us to reset a bond length to its equilibrium distance. This allows us to deal with cases such as halogen substitution, for example H to Cl. However when we start using more complicated fragments for substitutions then OpenBabel must start using more complicated methods that allow the fragments to rotate and translate to orientate before the connection is made. This is a rather complex procedure for which OpenBabel generally finds a sensible outcome. QCI only has to create a OpenBabel molecule object describing the fragment and call the correct OpenBabel method. The molecule object is generated from a configuration file containing a list of XYZ coordinates and atom numbers.

The second advanced feature is calculation of overall reaction thermodynamics from a series of molecules. Unfortunately no one has done this work for us so we must create our own implementation from scratch. First we must allow the user in input some data to provide the reaction structure, an example of this has been shown in Figure 91. This input must be parsed to create the appropriate step objects containing the individual thermodynamic data. Once again we have reused methods that we have previously designed. Next we need to do the basic arithmetic to calculate the thermodynamics of each step and display this to the user. This requires some complicated looping structures to ensure we can handle any reaction scheme that the user could pass to the program.

Further details on the implementation details can be found with the code comments, see APDENDIX.

EXAMPLE PROJECT

Now we have designed and implemented a complete system for the generation of complicated series of computational jobs it is important to prove its utility. As the program is aimed at new-comers to computational chemistry it was thought a project by an undergraduate student with no pervious experience of computational chemistry would provide a useful metric. The following section details the work and conclusions of an undergraduate student who used QCI to study a series of Diels-Alder reactions. This type of reaction was chosen for a variety of reasons. First and foremost the Diels-Alder reaction is well known among all chemists and its reaction mechanism is understood fairly well even at an undergraduate level. We can also work with molecules small enough that we can run fairly high-level DFT calculations on commodity hardware. Finally we can draw on literature results to validate our final results.



FIGURE 97: REACTION SCHEME FOR DIELS ALDER CALCULATIONS

The base reaction studied was the most basic Diels-Alder reaction, that between ethylene and butadiene. Once this base calculation has completed the student was able to generate a vast number of substituted molecules without manual generation of any files, Figure 97. A small number of jobs failed to converge to a correct stationary point but this was typically due to bad alignment during substitution.

The final results are tabulated below in Table 21. It is important to emphasize an undergraduate student generated all these results with no previous experience in computational chemistry over the course of a weekend (including time for calculations to complete) and that no manual generation or manipulation of files was required.

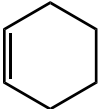
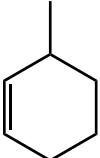
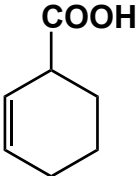
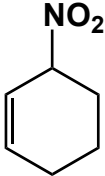
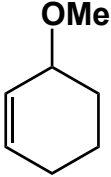
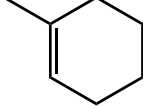
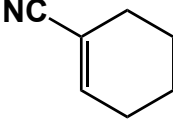
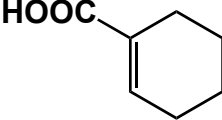
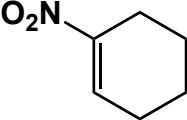
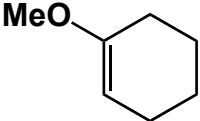
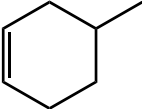
Product	ΔG^\ddagger	ΔH
	20.14	-41.10
	19.62	-43.17
	18.04	-43.14
	15.90	-44.94
	23.51	-41.24
	21.38	-37.92
	19.27	-36.29
	18.74	-38.86
	17.94	-39.75
	20.50	-36.51
	23.12	-38.50

TABLE 21: STUDENT RESULTS GENERATED WITH QUANTUM CHEMISTRY INTERFACE (KCAL MOL⁻¹)

The above results show that it is possible to quickly generate large libraries of calculations, which could then be used to derive chemical interesting data from. This is in stark contrast

to generating the same set of results without the use of Quantum Chemistry Interface, where the student would have to learn a great deal before attempting such a project. This reduction in knowledge and time required to generate data should help all levels of chemists.

CONCLUSIONS

This chapter has presented the development of a tool for exploratory investigation into organic reactions. Its utility as a tool for introducing students to the concepts of computational chemistry was successfully tested with a undergraduate student. The tool was found to be extremely easy to learn, and was capable of rapidly producing a series of useful results. It is clear that this tool is useful as a tool for rapid exploration of a substituted organic reaction but for a serious studies a much more in-depth analysis and likely more complicated calculations than supported by the tool will be required.

EPILOGUE

This thesis has developed a new system for artificial photosynthesis. We have shown it is possible to couple the known chemistries of photochemical water splitting and photochemical CO₂ reduction with a renewable amine. An initial prototype system was developed and has been experimentally shown to both reduce CO₂ and be separately renewed by hydrogenation conditions.

Once the prototype system was developed the work was extended to investigate modifications that could improve the quantum yield. The main focus of this work was stabilization of the formed distonic radical cation. This method was troublesome in the first generation amines so a second base structure was designed specifically to allow radical stabilizing substituents. It was computationally predicted that a phenyl substituted second-generation amine should show improved quantum yields for CO₂ reduction due to reduced electron back transfer. A synthesis to second-generation amines was proposed and reaction mechanism calculations were undertaken to assess the feasibility of this route.

Some synthetic work was undertaken with first generation amines in attempt to remove the oxygen functionality, whilst it was possible to do this the author struggled to purify the resulting products into amines suitable for serious photochemical studies. The author also undertook a synthesis of a DMAP based amine, but time limitations prevented optimization of the synthesis.

To develop this project further any future experimental work must consider undertaking the synthesis of the proposed second-generation amine, or optimizing the synthesis of the DMAP based amines. It is unlikely to be worthwhile expending significant effort on development of first generation amines. Future theoretical work could extend the studies on second-generation amines to determine if the radical stabilization methodology to promote the formation of distonic radical cation has a negative impact on the ability of the amine to transfer a Hydrogen atom to the CO₂ radical anion.

REFERENCES

- [1] J. T. Yates Jr, *Surface Science* **2009**, 603, 1605-1612.
- [2] a) J. S. Hansen, M.; Ruedy, R in *Global Temperature Update Through 2012, Vol. 2013* **2013**; b) J. Hansen, R. Ruedy, M. Sato and K. Lo, *Reviews of Geophysics* **2010**, 48, RG4004.
- [3] S. Levitus, J. I. Antonov, T. P. Boyer, O. K. Baranova, H. E. Garcia, R. A. Locarnini, A. V. Mishonov, J. R. Reagan, D. Seidov, E. S. Yarosh and M. M. Zweng, *Geophysical Research Letters* **2012**, 39, L10603.
- [4] a) R. J. Nicholls and A. Cazenave, *Science* **2010**, 328, 1517-1520; b) J. A. Church and N. J. White, *Geophysical Research Letters* **2006**, 33, L01602.
- [5] a) D. P. Chambers, *Journal of Geophysical Research: Oceans* **2006**, 111, C03010; b) W. R. Peltier, *Global and Planetary Change* **1999**, 20, 93-123; c) B. C. Douglas in *Chapter 3 Sea level change in the era of the recording tide gauge, Vol. Volume 75* Eds.: M. S. K. Bruce C. Douglas and P. L. Stephen), Academic Press, **2001**, pp. 37-64.
- [6] M. B. M. Dyurgerov, M.F, *Institute of Arctic and Alpine Research University of Colorado* **2005**, *Occasional Paper* 58
- [7] a) H. J. Smith, M. Wahlen, D. Mastroianni and K. C. Taylor, *Geophysical Research Letters* **1997**, 24, 1-4; b) J. R. Petit, J. Jouzel, D. Raynaud, N. I. Barkov, J. M. Barnola, I. Basile, M. Bender, J. Chappellaz, M. Davis, G. Delaygue, M. Delmotte, V. M. Kotlyakov, M. Legrand, V. Y. Lipenkov, C. Lorius, L. Pepin, C. Ritz, E. Saltzman and M. Stievenard, *Nature* **1999**, 399, 429-436; c) D. Luthi, M. Le Floch, B. Bereiter, T. Blunier, J.-M. Barnola, U. Siegenthaler, D. Raynaud, J. Jouzel, H. Fischer, K. Kawamura and T. F. Stocker, *Nature* **2008**, 453, 379-382.
- [8] a) N. H. Stern and G. B. Treasury, *The Economics of Climate Change: The Stern Review*, Cambridge University Press, **2007**, p; b) R. K. R. Pachauri, A., *Climate change 2007. Synthesis report. Contribution of Working Groups I, II and III to the fourth assessment report*, IPCC, Geneva, **2007**, p; c) P. A. Smithson, *International Journal of Climatology* **2002**, 22, 1144-1144; d) P. Forster, V. Ramaswamy, P. Artaxo, T. Berntsen, R. Betts, D. W. Fahey, J. Haywood, J. Lean, D. C. Lowe, G. Myhre, J. Nganga, R. Prinn, G. Raga, M. Schultz and R. Van Dorland in *Changes in atmospheric constituents and in radiative forcing, Vol.* Eds.: S. Solomon, D. Qin, M. Manning, Z. Chen, M. Marquis, K. B. Averyt, M. Tignor and H. L. Miller), Cambridge University Press, Cambridge, United Kingdom, **2007**, pp. 129-234.
- [9] J. T. J. Houghton, C.A. , *Climate Change 2001: The Scientific Basis*, CAMBRIDGE UNIVERSITY PRESS, **2001**, p.
- [10] J. D. Hays, J. Imbrie and N. J. Shackleton, *Science* **1976**, 194, 1121-1132.
- [11] T. M. L. Wigley in *The Climate of the Past 10,000 Years and the Role of the Sun, Vol. 236* Eds.: F. R. Stephenson and A. W. Wolfendale), Springer Netherlands, **1988**, pp. 209-224.
- [12] A. Robock and J. Mao, *Journal of Climate* **1995**, 8, 1086-1103.
- [13] S. Rahmstorf, *Nature* **2003**, 421, 699-699.
- [14] S. A. Harris, *Geografiska Annaler: Series A, Physical Geography* **2002**, 84, 1-9.
- [15] C. Lorius, J. Jouzel, D. Raynaud, J. Hansen and H. L. Treut, *Nature* **1990**, 347, 139-145.
- [16] A. A. Lacis, G. A. Schmidt, D. Rind and R. A. Ruedy, *Science* **2010**, 330, 356-359.

- [17] J. F. van Winden, G.-J. Reichert, N. P. McNamara, A. Benthien and J. S. S. Damsté, *PLoS ONE* **2012**, 7, e39614.
- [18] G. MacDonald, *Climatic Change* **1990**, 16, 247-281.
- [19] J. H. Ahn, Melissa; Wahlen, Martin; Brook, Edward J.; Mayewski, Paul A.; Taylor, Kendrick C., *Journal of Glaciology* **2008**, 54, 685-695.
- [20] N. Gilbert, *Nature News* **2012**, Nov.
- [21] J. A. Curry, J. L. Schramm and E. E. Ebert, *Journal of Climate* **1995**, 8, 240-247.
- [22] J. F. B. Mitchell, *Reviews of Geophysics* **1989**, 27, 115-139.
- [23] J. C. Stroeve, J. E. Box, C. Fowler, T. Haran and J. Key, *Remote Sensing of Environment* **2001**, 75, 360-374.
- [24] D. Archer, *Journal of Geophysical Research* **2005**, 110, C09S05.
- [25] E. F. Burgess, J. B. J., *American Journal of Science* **1837**, 32, 1-20.
- [26] S. Arrhenius, *Philosophical Magazine and Journal of Science* **1896**, 41, 237-276.
- [27] R. R. Sussmann, M.; Borsdorff, T., *EGU General Assembly Conference* **2010**, p. 15406.
- [28] S. Solomon, D. Qin, M. Manning, Z. Chen, M. Marquis, K.B. Averyt, M. Tignor, H.L. Miller, *Climate Change 2007: The Physical Science Basis. Contribution of Working Group I to the Fourth Assessment Report of the Intergovernmental Panel on Climate Change* Cambridge University Press, **2007**, p.
- [29] D. Archer, M. Eby, V. Brovkin, A. Ridgwell, L. Cao, U. Mikolajewicz, K. Caldeira, K. Matsumoto, G. Munhoven, A. Montenegro and K. Tokos, *Annual Review of Earth and Planetary Sciences* **2009**, 37, 117-134.
- [30] J. T. Houghton, L. G. M. Filho, B. A. Callander, N. Harris, A. Kattenburg and K. Maskell, *Climate Change 1995: The Science of Climate Change: Contribution of Working Group I to the Second Assessment Report of the Intergovernmental Panel on Climate Change*, Cambridge University Press, **1996**, p.
- [31] T. J. Blasing in *Recent Greenhouse Gas Concentrations.*, Vol. Carbon Dioxide Information Analysis Center, **2013**.
- [32] T. A. G. M. R. J. A. Boden in *Global, Regional, and National Fossil-Fuel CO₂ Emissions*, Vol. Carbon Dioxide Information Analysis Center, Oak Ridge National Laboratory, U.S. Department of Energy, Oak Ridge, Tenn., U.S.A., **2010**.
- [33] G. N. Dutton, J. D.; Elkins, J. W.; Hall, B.; Thompson, T., *American Geophysical Union, Fall Meeting* **2006**.
- [34] C. Norman, S. DeCanio and L. Fan, *Global Environmental Change* **2008**, 18, 330-340.
- [35] D. A. Lashof and D. R. Ahuja, *Nature* **1990**, 344, 529-531.
- [36] N. Nakicenovic, J. Alcamo, G. Davis, B. de Vries, J. Fenhann, S. Gaffin, K. Gregory, A. Grübler, T. Jung, T. Kram, E. La Rovere, L. Michaelis, S. Mori, T. Morita, W. Pepper, H. Pitcher, L. Price, K. Riahi, A. Roehrl, H.-H. Rogner, A. Sankovski, M. Schlesinger, P. Shukla, S. Smith, R. Swart, S. van Rooijen, N. Victor and Z. Dadi, *IPCC Special Report on Emissions Scenarios*, Cambridge University Press, **2000**, p.
- [37] B. Metz, O. Davidson, H. d. Coninck, M. Loos and L. Meyer, *IPCC special report on carbon dioxide capture and storage*, **2005**, p. Medium: X; Size: 440; 423.443 MB pages.
- [38] a) IEA, *CO₂ Emissions from Fuel Combustion 2012*, OECD Publishing, p; b) IEA, *Energy Statistics of OECD Countries 2012*, OECD Publishing, p.
- [39] IEA, *World Energy Outlook 2011*, IEA, **2011**, p.

- [40] B. Parsons, *NREL/CP-500-39955* **2006**.
- [41] N. Bullard in *Renewable energy now cheaper than new fossil fuels in Australia*, Vol. **2013**.
- [42] V. Smil, *General energetics : energy in the biosphere and civilization*, J. Wisley & sons, New York; Chichester; Brisbane [etc.], **1991**, p.
- [43] O. Morton, *Nature* **2006**, 443, 19-22.
- [44] M. Mendelsohn, Lowder, T., Canavan, B. in *Utility-Scale Concentrating Solar Power and Photovoltaics Projects: A Technology and Market Overview*, Vol. U.S. Department of Energy, Office of Energy Efficiency & Renewable Energy, National Renewable Energy Laboratory, **2012**.
- [45] NREL in *Best Research-Cell Efficiency*, Vol. (Ed. NREL), **2013**.
- [46] C. o. A. National Research Council, P. Strategies for Future Hydrogen and N. A. o. E. N. A. o. S. Use in *The hydrogen economy opportunities, costs, barriers, and R & D needs*, Vol. National Academies Press, Washington, D.C., **2004**.
- [47] J. Ramage, *Energy, a guidebook*, Oxford University Press, Oxford Oxfordshire ; New York, **1983**, p.
- [48] A. Rodionov, H. Wilkening and P. Moretto, *International Journal of Hydrogen Energy* **2011**, 36, 2398-2406.
- [49] D. Sofrová, *Photosynthetica* **2001**, 38, 520-520.
- [50] R. Buick, *Philosophical Transactions of the Royal Society B: Biological Sciences* **2008**, 363, 2731-2743.
- [51] D. R. Ort and C. F. Yocum in *Electron Transfer and Energy Transduction in Photosynthesis: An Overview*, Vol. 4 Eds.: D. Ort, C. Yocum and I. Heichel), Springer Netherlands, **1996**, pp. 1-9.
- [52] a) J. F. Allen, *Cell* **2002**, 110, 273-276; b) K. Sauer, *Annual Review of Physical Chemistry* **1979**, 30, 155-178; c) A. S. Raghavendra, *Photosynthesis: A Comprehensive Treatise*, Cambridge University Press, **2000**, p.
- [53] Bensaccount in *Z-scheme*, Vol. 2014 wikipedia, **2005**.
- [54] R. E. Blankenship and R. C. Prince, *Trends in Biochemical Sciences* **1985**, 10, 382-383.
- [55] Y. Umena, K. Kawakami, J.-R. Shen and N. Kamiya, *Nature* **2011**, 473, 55-60.
- [56] P. Glatzel, H. Schroeder, Y. Pushkar, T. Boron, S. Mukherjee, G. Christou, V. L. Pecoraro, J. Messinger, V. K. Yachandra, U. Bergmann and J. Yano, *Inorganic Chemistry* **2013**, 52, 5642-5644.
- [57] A. Arnold and Z. Nikoloski, *Trends in Plant Science* **2011**, 16, 676-683.
- [58] J. M. Berg, J. L. Tymoczko and L. Stryer, *Biochemistry*, W.H. Freeman, **2002**, p.
- [59] R. E. Blankenship, D. M. Tiede, J. Barber, G. W. Brudvig, G. Fleming, M. Ghirardi, M. R. Gunner, W. Junge, D. M. Kramer, A. Melis, T. A. Moore, C. C. Moser, D. G. Nocera, A. J. Nozik, D. R. Ort, W. W. Parson, R. C. Prince and R. T. Sayre, *Science* **2011**, 332, 805-809.
- [60] J. Whitmarsh and Govindjee in *The Photosynthetic Process*, Eds.: G. S. Singhal, G. Renger, S. K. Sopory, K. D. Irrgang and Govindjee), Springer Netherlands, **1999**, pp. 11-51.
- [61] A. Fujishima and K. Honda, *Nature* **1972**, 238, 37-38.
- [62] A. Kudo and Y. Miseki, *Chemical Society Reviews* **2009**, 38, 253-278.

- [63] a) M. G. Walter, E. L. Warren, J. R. McKone, S. W. Boettcher, Q. Mi, E. A. Santori and N. S. Lewis, *Chemical Reviews* **2010**, *110*, 6446-6473; b) S. Chen and L.-W. Wang, *Chemistry of Materials* **2012**, *24*, 3659-3666.
- [64] a) L. J. Minggu, W. R. Wan Daud and M. B. Kassim, *International Journal of Hydrogen Energy* **2010**, *35*, 5233-5244; b) Y. Tachibana, L. Vayssieres and J. R. Durrant, *Nat Photon* **2012**, *6*, 511-518.
- [65] a) J. Tang, J. R. Durrant and D. R. Klug, *Journal of the American Chemical Society* **2008**, *130*, 13885-13891; b) M. Ni, M. K. H. Leung, D. Y. C. Leung and K. Sumathy, *Renewable and Sustainable Energy Reviews* **2007**, *11*, 401-425.
- [66] A. Braun, K. Sivula, D. K. Bora, J. Zhu, L. Zhang, M. Grätzel, J. Guo and E. C. Constable, *The Journal of Physical Chemistry C* **2012**, *116*, 16870-16875.
- [67] a) J. van de Lagemaat and A. J. Frank, *The Journal of Physical Chemistry B* **2000**, *104*, 4292-4294; b) A. Yamakata, T.-a. Ishibashi and H. Onishi, *The Journal of Physical Chemistry B* **2001**, *105*, 7258-7262.
- [68] D. E. Aspnes, *Surface Science* **1983**, *132*, 406-421.
- [69] Z. Zhang, C.-C. Wang, R. Zakaria and J. Y. Ying, *The Journal of Physical Chemistry B* **1998**, *102*, 10871-10878.
- [70] A. Kudo, H. Kato and I. Tsuji, *Chemistry Letters* **2004**, *33*, 1534-1539.
- [71] a) H.-Y. Chen and D. H. Son, *Israel Journal of Chemistry* **2012**, *52*, 1016-1026; b) S. C. Erwin, L. Zu, M. I. Haftel, A. L. Efros, T. A. Kennedy and D. J. Norris, *Nature* **2005**, *436*, 91-94.
- [72] a) Y. Sasaki, H. Nemoto, K. Saito and A. Kudo, *The Journal of Physical Chemistry C* **2009**, *113*, 17536-17542; b) K. Sayama, K. Mukasa, R. Abe, Y. Abe and H. Arakawa, *Journal of Photochemistry and Photobiology A: Chemistry* **2002**, *148*, 71-77; c) D. Wang, Z. Zou and J. Ye, *Chemistry of Materials* **2005**, *17*, 3255-3261.
- [73] H. Tada, T. Mitsui, T. Kiyonaga, T. Akita and K. Tanaka, *Nat Mater* **2006**, *5*, 782-786.
- [74] a) T. Ohno, L. Bai, T. Hisatomi, K. Maeda and K. Domen, *Journal of the American Chemical Society* **2012**, *134*, 8254-8259; b) K. Maeda, T. Takata, M. Hara, N. Saito, Y. Inoue, H. Kobayashi and K. Domen, *Journal of the American Chemical Society* **2005**, *127*, 8286-8287; c) H. Liu, J. Yuan, Z. Jiang, W. Shangguan, H. Einaga and Y. Teraoka, *Journal of Materials Chemistry* **2011**, *21*, 16535-16543; d) H. P. Dasari, K. Ahn, S.-Y. Park, H.-I. Ji, K. J. Yoon, B.-K. Kim, H.-J. Je, H.-W. Lee and J.-H. Lee, *International Journal of Hydrogen Energy* **2013**, *38*, 6097-6103; e) C. Xing, Y. Zhang, W. Yan and L. Guo, *International Journal of Hydrogen Energy* **2006**, *31*, 2018-2024; f) Q. Wang, N. An, R. Mu, H. Liu, J. Yuan, J. Shi and W. Shangguan, *Journal of Alloys and Compounds* **2012**, *522*, 19-24.
- [75] a) H. Oberhofer and K. Reuter, *The Journal of Chemical Physics* **2013**, *139*, -; b) K. Maeda, K. Teramura, D. Lu, N. Saito, Y. Inoue and K. Domen, *Angewandte Chemie International Edition* **2006**, *45*, 7806-7809; c) K. Maeda and K. Domen, *The Journal of Physical Chemistry Letters* **2010**, *1*, 2655-2661.
- [76] a) W. J. Youngblood, S.-H. A. Lee, K. Maeda and T. E. Mallouk, *Accounts of Chemical Research* **2009**, *42*, 1966-1973; b) J. Park and A. Bard, *Electrochemical and Solid-State Letters* **2005**, *8*, G371-G375; c) W. J. Youngblood, S.-H. A. Lee, Y. Kobayashi, E. A. Hernandez-Pagan, P. G. Hoertz, T. A. Moore, A. L. Moore, D. Gust and T. E. Mallouk, *Journal of the American Chemical Society* **2009**, *131*, 926-927.

- [77] a) R. Dholam, N. Patel and A. Miotello, *International Journal of Hydrogen Energy* **2011**, 36, 6519-6528; b) J. J. Sene, W. A. Zeltner and M. A. Anderson, *The Journal of Physical Chemistry B* **2003**, 107, 1597-1603; c) S. T. Martin, C. L. Morrison and M. R. Hoffmann, *The Journal of Physical Chemistry* **1994**, 98, 13695-13704.
- [78] a) T. Ishii, H. Kato and A. Kudo, *Journal of Photochemistry and Photobiology A: Chemistry* **2004**, 163, 181-186; b) A. Kleiman-Shwarsstein, Y.-S. Hu, A. J. Forman, G. D. Stucky and E. W. McFarland, *The Journal of Physical Chemistry C* **2008**, 112, 15900-15907; c) J. W. Liu, G. Chen, Z. H. Li and Z. G. Zhang, *Journal of Solid State Chemistry* **2006**, 179, 3704-3708.
- [79] a) M. A. Khan, S. I. Woo and O. B. Yang, *International Journal of Hydrogen Energy* **2008**, 33, 5345-5351; b) D. W. Hwang, H. G. Kim, J. S. Lee, J. Kim, W. Li and S. H. Oh, *The Journal of Physical Chemistry B* **2004**, 109, 2093-2102.
- [80] S. Y. Reece, J. A. Hamel, K. Sung, T. D. Jarvi, A. J. Esswein, J. J. H. Pijpers and D. G. Nocera, *Science* **2011**, 334, 645-648.
- [81] a) K.-i. Shimizu, S. Itoh, T. Hatamachi, T. Kodama, M. Sato and K. Toda, *Chemistry of Materials* **2005**, 17, 5161-5166; b) C. T. K. Thaminimulla, T. Takata, M. Hara, J. N. Kondo and K. Domen, *Journal of Catalysis* **2000**, 196, 362-365; c) T. Takata, K. Shinohara, A. Tanaka, M. Hara, J. N. Kondo and K. Domen, *Journal of Photochemistry and Photobiology A: Chemistry* **1997**, 106, 45-49.
- [82] a) F. E. Osterloh, *Chemistry of Materials* **2007**, 20, 35-54; b) A. Hameed, M. A. Gondal and Z. H. Yamani, *Catalysis Communications* **2004**, 5, 715-719.
- [83] H. Kato and A. Kudo, *The Journal of Physical Chemistry B* **2002**, 106, 5029-5034.
- [84] H. Yamashita, M. Harada, J. Misaka, M. Takeuchi, Y. Ichihashi, F. Goto, M. Ishida, T. Sasaki and M. Anpo, *Journal of Synchrotron Radiation* **2001**, 8, 569-571.
- [85] a) C. Burda, Y. Lou, X. Chen, A. C. S. Samia, J. Stout and J. L. Gole, *Nano Letters* **2003**, 3, 1049-1051; b) S. Karthik, T. Kong Chhay, K. M. Gopal and A. G. Craig, *Journal of Physics D: Applied Physics* **2006**, 39, 2361; c) J. Hensel, G. Wang, Y. Li and J. Z. Zhang, *Nano Letters* **2010**, 10, 478-483.
- [86] a) N. B. Brookes, G. Thornton and F. M. Quinn, *Solid State Communications* **1987**, 64, 383-386; b) A. Mackor and J. Schoonman, *Recueil des Travaux Chimiques des Pays-Bas* **1980**, 99, 71-72.
- [87] a) Q. Wang, T. Hisatomi, Y. Moriya, K. Maeda and K. Domen, *Catalysis Science & Technology* **2013**, 3, 2098-2103; b) H. Kim, D. Hwang, S. Bae, J. Jung and J. Lee, *Catalysis Letters* **2003**, 91, 193-198; c) V. Reddy, D. Hwang and J. Lee, *Catalysis Letters* **2003**, 90, 39-43.
- [88] a) A. Kudo, H. Okutomi and H. Kato, *Chemistry Letters* **2000**, 29, 1212-1213; b) A. Ishikawa, T. Takata, J. N. Kondo, M. Hara, H. Kobayashi and K. Domen, *Journal of the American Chemical Society* **2002**, 124, 13547-13553; c) M. Machida, S. Murakami, T. Kijima, S. Matsushima and M. Arai, *The Journal of Physical Chemistry B* **2001**, 105, 3289-3294.
- [89] X. Tang and D. Li, *The Journal of Physical Chemistry C* **2008**, 112, 5405-5409.
- [90] L. I. Halaoui, N. M. Abrams and T. E. Mallouk, *The Journal of Physical Chemistry B* **2005**, 109, 6334-6342.
- [91] a) A. Kudo, H. Kato and S. Nakagawa, *The Journal of Physical Chemistry B* **1999**, 104, 571-575; b) H. Kato and A. Kudo, *Catalysis Today* **2003**, 78, 561-569; c) S. Ikeda, M. Fubuki, Y. K. Takahara and M. Matsumura, *Applied Catalysis A: General* **2006**, 300, 186-190.

- [92] a) A. Mukherji, B. Seger, G. Q. Lu and L. Wang, *ACS Nano* **2011**, *5*, 3483-3492; b) H. Hagiwara, K. Kumagae and T. Ishihara, *Chemistry Letters* **2010**, *39*, 498-499; c) A. Mukherji, C. Sun, S. C. Smith, G. Q. Lu and L. Wang, *The Journal of Physical Chemistry C* **2011**, *115*, 15674-15678.
- [93] a) K. T. Maeda, K.; Saito N.; Inoue, Y.; Kobayashi, H.; Kazunari, D, *Pure Appl. Chem* **2006**, *78*, 2267-2276; b) K. Maeda and K. Domen, *Chemistry of Materials* **2009**, *22*, 612-623; c) K. Maeda, K. Teramura, T. Takata, M. Hara, N. Saito, K. Toda, Y. Inoue, H. Kobayashi and K. Domen, *The Journal of Physical Chemistry B* **2005**, *109*, 20504-20510.
- [94] Y. Lee, H. Terashima, Y. Shimodaira, K. Teramura, M. Hara, H. Kobayashi, K. Domen and M. Yashima, *The Journal of Physical Chemistry C* **2006**, *111*, 1042-1048.
- [95] M. Higashi, R. Abe, A. Ishikawa, T. Takata, B. Ohtani and K. Domen, *Chemistry Letters* **2008**, *37*, 138-139.
- [96] D. G. Nocera, *Accounts of Chemical Research* **2012**, *45*, 767-776.
- [97] U.-P. Apfel and W. Weigand, *Angewandte Chemie International Edition* **2011**, *50*, 4262-4264.
- [98] T. Inoue, A. Fujishima, S. Konishi and K. Honda, *Nature* **1979**, *277*, 637-638.
- [99] C. Hemminger J, R. Carr, J. Lo W and A. Somorjai G in *Photochemical Processes at the Solid-Gas Interface*, Vol. 184 AMERICAN CHEMICAL SOCIETY, **1980**, pp. 233-252.
- [100] a) B. Aurian-Blajeni, M. Halmann and J. Manassen, *Solar Energy Materials* **1983**, *8*, 425-440; b) B. Aurian-Blajeni, M. Halmann and J. Manassen, *Solar Energy* **1980**, *25*, 165-170; c) M. Zafir, M. Ulman, Y. Zuckerman and M. Halmann, *Journal of Electroanalytical Chemistry and Interfacial Electrochemistry* **1983**, *159*, 373-389.
- [101] M. Halmann, V. Katzir, E. Borgarello and J. Kiwi, *Solar Energy Materials* **1984**, *10*, 85-91.
- [102] K. Tennakone, *Solar Energy Materials* **1984**, *10*, 235-238.
- [103] I. O., I. C., S. Y. and I. T., *Photocatalytic reduction of carbon dioxide to methane and acetic acid by an aqueous suspension of metal-deposited TiO₂*, Elsevier, Amsterdam, PAYS-BAS, **1993**, p. 269-271.
- [104] a) I. H. Tseng, W.-C. Chang and J. C. S. Wu, *Applied Catalysis B: Environmental* **2002**, *37*, 37-48; b) H.-C. Yang, H.-Y. Lin, Y.-S. Chien, J.-S. Wu and H.-H. Wu, *Catalysis Letters* **2009**, *131*, 381-387; c) Y. Li, W.-N. Wang, Z. Zhan, M.-H. Woo, C.-Y. Wu and P. Biswas, *Applied Catalysis B: Environmental* **2010**, *100*, 386-392; d) J. C. S. Wu and H.-M. Lin, *International Journal of Photoenergy* **2005**, *7*, 115-119.
- [105] H. Yamashita, H. Nishiguchi, N. Kamada, M. Anpo, Y. Teraoka, H. Hatano, S. Ehara, K. Kikui, L. Palmisano, A. Sclafani, M. Schiavello and M. A. Fox, *Research on Chemical Intermediates* **1994**, *20*, 815-823.
- [106] a) Y. Kohno, T. Tanaka, T. Funabiki and S. Yoshida, *Chemical Communications* **1997**, 841-842; b) K. Sayama and H. Arakawa, *The Journal of Physical Chemistry* **1993**, *97*, 531-533.
- [107] O. Ozcan, F. Yukruk, E. U. Akkaya and D. Uner, *Applied Catalysis B: Environmental* **2007**, *71*, 291-297.
- [108] T.-V. Nguyen and J. C. S. Wu, *Solar Energy Materials and Solar Cells* **2008**, *92*, 864-872.
- [109] Y.-J. Yuan, Z.-T. Yu, J.-Y. Zhang and Z.-G. Zou, *Dalton Transactions* **2012**, *41*, 9594-9597.

- [110] C. Wang, R. L. Thompson, J. Baltrus and C. Matranga, *The Journal of Physical Chemistry Letters* **2009**, *1*, 48-53.
- [111] L. Jia, J. Li and W. Fang, *Catalysis Communications* **2009**, *11*, 87-90.
- [112] P.-W. Pan and Y.-W. Chen, *Catalysis Communications* **2007**, *8*, 1546-1549.
- [113] B. Srinivas, B. Shubhamangala, K. Lalitha, P. Anil Kumar Reddy, V. Durga Kumari, M. Subrahmanyam and B. R. De, *Photochemistry and Photobiology* **2011**, *87*, 995-1001.
- [114] O. K. Varghese, M. Paulose, T. J. LaTempa and C. A. Grimes, *Nano Letters* **2009**, *9*, 731-737.
- [115] P. Salvador, *Journal of Applied Physics* **1984**, *55*, 2977-2985.
- [116] J.-M. Lehn and R. Ziessel, *Proceedings of the National Academy of Sciences* **1982**, *79*, 701-704.
- [117] a) P. Kurz, B. Probst, B. Spingler and R. Alberto, *European Journal of Inorganic Chemistry* **2006**, *2006*, 2966-2974; b) H. Hori, F. P. A. Johnson, K. Koike, O. Ishitani and T. Ibusuki, *Journal of Photochemistry and Photobiology A: Chemistry* **1996**, *96*, 171-174.
- [118] K. Koike, H. Hori, M. Ishizuka, J. R. Westwell, K. Takeuchi, T. Ibusuki, K. Enjouji, H. Konno, K. Sakamoto and O. Ishitani, *Organometallics* **1997**, *16*, 5724-5729.
- [119] a) Y. Hayashi, S. Kita, B. S. Brunshwig and E. Fujita, *Journal of the American Chemical Society* **2003**, *125*, 11976-11987; b) D. H. Gibson and X. Yin, *Journal of the American Chemical Society* **1998**, *120*, 11200-11201; c) D. H. Gibson, X. Yin, H. He and M. S. Mashuta, *Organometallics* **2002**, *22*, 337-346; d) B. P. Sullivan and T. J. Meyer, *Organometallics* **1986**, *5*, 1500-1502.
- [120] H. Takeda, K. Koike, H. Inoue and O. Ishitani, *Journal of the American Chemical Society* **2008**, *130*, 2023-2031.
- [121] a) A. H. A. Tinnemans, T. P. M. Koster, D. H. M. W. Thewissen and A. Mackor, *Recueil des Travaux Chimiques des Pays-Bas* **1984**, *103*, 288-295; b) E. Fujita, D. J. Szalda, C. Creutz and N. Sutin, *Journal of the American Chemical Society* **1988**, *110*, 4870-4871; c) E. Fujita, C. Creutz, N. Sutin and D. J. Szalda, *Journal of the American Chemical Society* **1991**, *113*, 343-353; d) T. Ogata, S. Yanagida, B. S. Brunshwig and E. Fujita, *Journal of the American Chemical Society* **1995**, *117*, 6708-6716; e) E. Fujita, L. R. Furenlid and M. W. Renner, *Journal of the American Chemical Society* **1997**, *119*, 4549-4550; f) E. Fujita and D. J. Szalda, *Inorganica Chimica Acta* **2000**, *297*, 139-144.
- [122] S. Matsuoka, K. Yamamoto, T. Ogata, M. Kusaba, N. Nakashima, E. Fujita and S. Yanagida, *Journal of the American Chemical Society* **1993**, *115*, 601-609.
- [123] a) E. Kimura, S. Wada, M. Shionoya, T. Takahashi and Y. Litaka, *Journal of the Chemical Society, Chemical Communications* **1990**, 397-398; b) E. Kimura, X. Bu, M. Shionoya, S. Wada and S. Maruyama, *Inorganic Chemistry* **1992**, *31*, 4542-4546; c) E. Kimura, S. Wada, M. Shionoya and Y. Okazaki, *Inorganic Chemistry* **1994**, *33*, 770-778.
- [124] a) B. Gholamkhash, H. Mametsuka, K. Koike, T. Tanabe, M. Furue and O. Ishitani, *Inorganic Chemistry* **2005**, *44*, 2326-2336; b) S. Sato, K. Koike, H. Inoue and O. Ishitani, *Photochemical & Photobiological Sciences* **2007**, *6*, 454-461.
- [125] T. Dhanasekaran, J. Grodkowski, P. Neta, P. Hambright and E. Fujita, *The Journal of Physical Chemistry A* **1999**, *103*, 7742-7748.
- [126] S. Matsuoka, T. Kohzaki, C. Pac, A. Ishida, S. Takamuku, M. Kusaba, N. Nakashima and S. Yanagida, *The Journal of Physical Chemistry* **1992**, *96*, 4437-4442.

- [127] S. Tazuke and N. Kitamura, *Nature* **1978**, 275, 301-302.
- [128] R. D. Richardson and B. K. Carpenter, *Journal of the American Chemical Society* **2008**, 130, 3169-3180.
- [129] B. K. Carpenter, *The Journal of Physical Chemistry A* **2006**, 111, 3719-3726.
- [130] R. D. Richardson in *Studies on CO₂ reduction with amines*, Vol. Cardiff University, **2009**.
- [131] S. F. Nelsen and J. T. Ippoliti, *Journal of the American Chemical Society* **1986**, 108, 4879-4881.
- [132] R. D. Richardson, E. J. Holland and B. K. Carpenter, *Nat Chem* **2011**, 3, 301-303.
- [133] S.-j. Jin, J.-R. Choi, J. Oh, D. Lee and J. K. Cha, *Journal of the American Chemical Society* **1995**, 117, 10914-10921.
- [134] a) M. Harmata, *Advanced Synthesis & Catalysis* **2006**, 348, 2297-2306; b) M. Harmata, C. B. Gamlath and C. L. Barnes, *Tetrahedron Letters* **1993**, 34, 265-268.
- [135] J. Oh, C. Ziani-Cherif, J.-R. Choi and J. K. Cha, *Org. Synth.* **2002**, 78, No pp. given.
- [136] C. J. Cramer, *Essentials of Computational Chemistry: Theories and Models*, Wiley, **2005**, p.
- [137] M. Born and R. Oppenheimer, *Annalen der Physik* **1927**, 389, 457-484.
- [138] S. T. Epstein, *The Variation Method in Quantum Chemistry*, Academic Press, **1974**, p.
- [139] C. Møller and M. S. Plesset, *Physical Review* **1934**, 46, 618-622.
- [140] C. D. Sherrill and H. F. Schaefer III in *The Configuration Interaction Method: Advances in Highly Correlated Approaches*, Vol. Volume 34 Eds.: J. R. S. M. C. Z. Per-Olov Löwdin and B. Erkki), Academic Press, **1999**, pp. 143-269.
- [141] J. Čížek, *The Journal of Chemical Physics* **1966**, 45, 4256-4266.
- [142] J. A. Pople, M. Head-Gordon and K. Raghavachari, *The Journal of Chemical Physics* **1987**, 87, 5968-5975.
- [143] a) W. Kohn and L. J. Sham, *Physical Review* **1965**, 140, A1133-A1138; b) P. Hohenberg and W. Kohn, *Physical Review* **1964**, 136, B864-B871.
- [144] A. D. Becke, *Physical Review A* **1988**, 38, 3098-3100.
- [145] C. Adamo and V. Barone, *The Journal of Chemical Physics* **1998**, 108, 664-675.
- [146] R. Gleiter, W.-D. Stohrer and R. Hoffmann, *Helvetica Chimica Acta* **1972**, 55, 893-906.
- [147] a) X. L. Huang and J. J. Dannenberg, *The Journal of Organic Chemistry* **1991**, 56, 5421-5424; b) I. Janovský, W. Knolle, S. Naumov and F. Williams, *Chemistry – A European Journal* **2004**, 10, 5524-5534.
- [148] M. L. Coote, C. Y. Lin, A. L. J. Beckwith and A. A. Zavitsas, *Physical Chemistry Chemical Physics* **2010**, 12, 9597-9610.
- [149] H. Zipse in *Radical Stability—A Theoretical Perspective*, Vol. 263 (Ed. A. Gansäuer), Springer Berlin Heidelberg, **2006**, pp. 163-189.
- [150] G. P. F. Wood, D. Moran, R. Jacob and L. Radom, *The Journal of Physical Chemistry A* **2005**, 109, 6318-6325.
- [151] a) M. Baer, *Theory of chemical reaction dynamics*, CRC Press, **1985**, p; b) B. E. Fernandez-Ramos A, BC Garrett, and DG Truhlar, *Variational Transition State Theory with Multidimensional Tunneling.*, Wiley, **2007**, p. 125-232.
- [152] a) B. K. Carpenter, *Journal of the American Chemical Society* **1983**, 105, 1700-1701; b) O. M. Gonzalez-James, X. Zhang, A. Datta, D. A. Hrovat, W. T. Borden and D. A. Singleton, *Journal of the American Chemical Society* **2010**, 132, 12548-12549; c) E.

- M. Greer, C. V. Cosgriff and C. Doubleday, *Journal of the American Chemical Society* **2013**, *135*, 10194-10197.
- [153] E. Wigner, *Physical Review* **1932**, *40*, 749-759.
- [154] a) D. G. Truhlar and B. Garrett, *J Chim Phys* **1987**, *84*, 365-369; b) B. C. Garrett and D. G. Truhlar, *The Journal of Chemical Physics* **1983**, *79*, 4931-4938.
- [155] B. C. Garrett, T. Joseph, T. N. Truong and D. G. Truhlar, *Chemical Physics* **1989**, *136*, 271-293.
- [156] A. D. Isaacson, D. G. Truhlar, S. N. Rai, R. Steckler, G. C. Hancock, B. C. Garrett and M. J. Redmon, *Computer Physics Communications* **1987**, *47*, 91-102.
- [157] a) E. Clemmensen, *Berichte der deutschen chemischen Gesellschaft* **1913**, *46*, 1837-1843; b) M. Huang, *Journal of the American Chemical Society* **1946**, *68*, 2487-2488; c) M. Huang, *Journal of the American Chemical Society* **1949**, *71*, 3301-3303.
- [158] a) J. Spieler, O. Huttenloch and H. Waldmann, *European Journal of Organic Chemistry* **2000**, *2000*, 391-399; b) D. Stead, P. O'Brien and A. J. Sanderson, *Organic Letters* **2005**, *7*, 4459-4462; c) V. Haridas, S. Sadanandan, Y. K. Sharma, S. Chinthalapalli and A. Shandilya, *Tetrahedron Letters* **2012**, *53*, 623-626; d) J. P. Hermet, D. W. Porter, M. J. Dearden, J. R. Harrison, T. Koplin, P. O'Brien, J. Parmene, V. Tyurin, A. C. Whitwood, J. Gilday and N. M. Smith, *Org Biomol Chem* **2003**, *1*, 3977-3988.
- [159] H. H. Szmant, *Angewandte Chemie International Edition in English* **1968**, *7*, 120-128.
- [160] a) N. J. Kishner, *Russ. Phys. Chem. Soc.* **1911**, *43*, 582; b) L. Wolff, *Justus Liebigs Annalen der Chemie* **1912**, *394*, 86-108.
- [161] N. D. Zelinsky and B. A. Kasansky, *Berichte der deutschen chemischen Gesellschaft (A and B Series)* **1927**, *60*, 1101-1102.
- [162] A. N. De Belder, Weigel, R., *Chem. Ind. (London)* **1964**, 1689.
- [163] B. M. Trost and I. Fleming in *Comprehensive Organic Synthesis - Selectivity, Strategy and Efficiency in Modern Organic Chemistry, Volumes 1 - 9*, Vol. Elsevier, pp. 327-343.
- [164] J. Fried and J. A. Edwards, *Organic reactions in steroid chemistry*, Van Nostrand Reinhold Co., **1972**, p.
- [165] M. L. Di Vona and V. Rosnati, *The Journal of Organic Chemistry* **1991**, *56*, 4269-4273.
- [166] S. Yamamura, M. Toda and Y. Hirata in *Modified Clemmensen Reduction: Cholestane*, John Wiley & Sons, Inc., **2003**.
- [167] F. J. C. Martins, A. M. Viljoen, M. Coetzee, L. Fourie and P. L. Wessels, *Tetrahedron* **1991**, *47*, 9215-9224.
- [168] M. Naruse, S. Aoyagi and C. Kibayashi, *Journal of the Chemical Society, Perkin Transactions 1* **1996**, 1113-1124.
- [169] J. Long and G. Skirrow, *Transactions of the Faraday Society* **1962**, *58*, 1403-1408.
- [170] A. D. Baxter, F. Binns, T. Javed, S. M. Roberts, P. Sadler, F. Scheinmann, B. J. Wakefield, M. Lynch and R. F. Newton, *J. Chem. Soc., Perkin Trans. 1* **1986**, 889-900.
- [171] P. R. Story and M. Saunders, *Journal of the American Chemical Society* **1960**, *82*, 6199-6199.
- [172] a) R. Matrisciano and W. H. Snyder, *J. Chem. Eng. Data* **1971**, *16*, 490-491; b) P. R. Story, *J. Org. Chem.* **1961**, *26*, 287-290; c) R. W. Jordan, M. P. Le and W. Tam, *Eur.*

- J. Org. Chem.* **2008**, 80-86; d) F. I. Carroll, L. E. Brieady, H. A. Navarro, M. I. Damaj and B. R. Martin, *J. Med. Chem.* **2005**, 48, 7491-7495; e) A. D. Baxter, S. M. Roberts, F. Scheinmann, B. J. Wakefield and R. F. Newton, *J. Chem. Soc., Chem. Commun.* **1983**, 932-933; f) M. Franck-Neumann and M. Sedrati, *Bull. Soc. Chim. Fr.* **1976**, 1476.
- [173] P. R. Story and S. R. Fahrenholtz, *Org. Synth.* **1964**, 44, No pp. given.
- [174] S. C. Clarke and B. L. Johnson, *Tetrahedron* **1968**, 24, 5067-5074.
- [175] a) E. J. Corey, J. A. Katzenellenbogen, S. A. Roman and N. W. Gilman, *Tetrahedron Letters* **1971**, 12, 1821-1824; b) B. Franzus and E. I. Snyder, *J. Am. Chem. Soc.* **1965**, 87, 3423-3429.
- [176] a) H. M. R. Hoffmann, *Angewandte Chemie International Edition in English* **1984**, 23, 1-19; b) C. J. Cramer and S. E. Barrows, *The Journal of Organic Chemistry* **1998**, 63, 5523-5532.
- [177] a) P. Pérez, L. R. Domingo, M. José Aurell and R. Contreras, *Tetrahedron* **2003**, 59, 3117-3125; b) C. J. Cramer, M. Harmata and P. Rashatasakhon, *The Journal of Organic Chemistry* **2001**, 66, 5641-5644; c) D. I. Rawson, B. K. Carpenter and H. M. R. Hoffmann, *Journal of the American Chemical Society* **1979**, 101, 1786-1793.
- [178] J. H. Rigby* and F. C. Pigge in *[4 + 3] Cycloaddition Reactions*, John Wiley & Sons, Inc., **2004**.
- [179] G. Prié, N. Prévost, H. Twin, S. A. Fernandes, J. F. Hayes and M. Shipman, *Angewandte Chemie International Edition* **2004**, 43, 6517-6519.
- [180] M. Harmata and C. B. Gamlath, *The Journal of Organic Chemistry* **1988**, 53, 6154-6156.
- [181] M. Harmata and P. R. Schreiner, *Organic Letters* **2001**, 3, 3663-3665.
- [182] M. Harmata, S. Elahmad and C. L. Barnes, *The Journal of Organic Chemistry* **1994**, 59, 1241-1242.
- [183] A. J. Cohen, P. Mori-Sánchez and W. Yang, *Chemical Reviews* **2011**, 112, 289-320.
- [184] J. A. Sáez, M. Arnó and L. R. Domingo, *Organic Letters* **2003**, 5, 4117-4120.
- [185] a) D. A. Singleton, S. R. Merrigan, B. R. Beno and K. N. Houk, *Tetrahedron Letters* **1999**, 40, 5817-5821; b) S. Kong and J. D. Evanseck, *Journal of the American Chemical Society* **2000**, 122, 10418-10427; c) S. Yamabe and T. Minato, *The Journal of Organic Chemistry* **2000**, 65, 1830-1841.
- [186] a) M. Arnó, M. T. Picher, L. R. Domingo and J. Andrés, *Chemistry – A European Journal* **2004**, 10, 4742-4749; b) J. A. Sáez, M. Arnó and L. R. Domingo, *Tetrahedron* **2005**, 61, 7538-7545.
- [187] a) M. J. Aurell, L. R. Domingo, P. Pérez and R. Contreras, *Tetrahedron* **2004**, 60, 11503-11509; b) L. R. Domingo, M. J. Aurell, P. Pérez and R. Contreras, *Tetrahedron* **2002**, 58, 4417-4423.
- [188] a) P. K. Chattaraj and D. R. Roy, *Chemical Reviews* **2007**, 107, PR46-PR74; b) J.-L. Calais, *International Journal of Quantum Chemistry* **1993**, 47, 101-101.
- [189] R. G. Parr and R. G. Pearson, *Journal of the American Chemical Society* **1983**, 105, 7512-7516.
- [190] R. G. Parr, L. v. Szentpály and S. Liu, *Journal of the American Chemical Society* **1999**, 121, 1922-1924.
- [191] a) H. Mayr and A. R. Ofial, *Journal of Physical Organic Chemistry* **2008**, 21, 584-595; b) H. Mayr and A. R. Ofial, *Pure and applied chemistry* **2005**, 77, 1807-1821.

APPENDIX 1 – EXPERIMENTAL DETAILS

GENERAL EXPERIMENTAL

Glassware used for moisture-sensitive chemistry was dried in an oven before use, and also under reduced pressure with a heat-gun if required. Oxygen sensitive reactions were performed on a Schlenk line and bubbler under a nitrogen atmosphere. Sensitive reagents were handled with syringe or cannula depending on volume. Unless otherwise stated all reactions were stirred magnetically, solvents removed using a rotary evaporator at the automatically selected pressure and dried on a high vacuum line (<1 mbar).

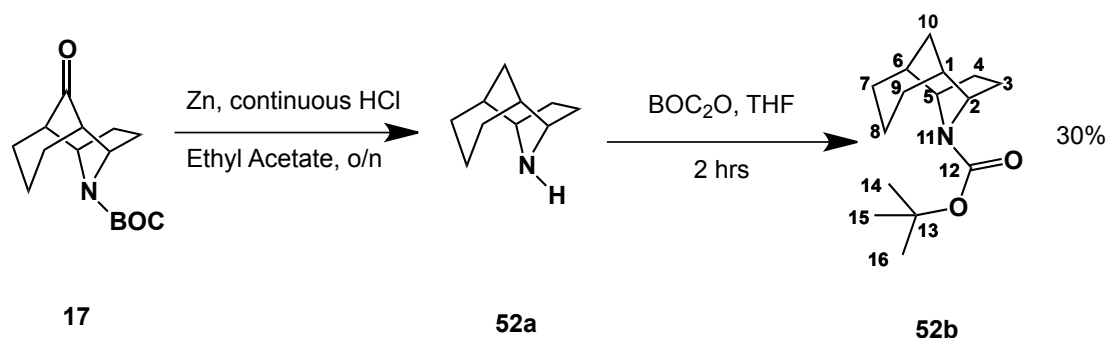
All reagents were purchased from Aldrich, Acros or Alfa Aesar. THF, ether and DCM were dried using a M-Braun SPS-800 solvent purification system. Other anhydrous solvents were either purchased from Acros over molecular sieves, or dried following standard procedures before use. Ether refers to diethyl ether, and petrol to petroleum ether 40-60 fraction. Triethylamine was distilled over calcium hydride, freeze-thaw degassed three times and stored under nitrogen. Pyridine was distilled over calcium hydride and stored under nitrogen. Butyl Lithium (both *n* and *t*), phenyl magnesium bromide, Tebbe reagent, and DIBAL were purchased as a solution from Aldrich (concentrations listed in experimental details). NMR solvents were used as received except CDCl₃ that was stored over alumina. All aqueous solutions were saturated unless otherwise stated.

¹H and ¹³C NMR spectra were obtained using a Bruker DPX 400 or DPX 500 spectrometer (operating at the correct frequency for the required nucleus) and were referenced to the internal solvent peak. All values for *J* are in Hz and δ values are reported in ppm downfield from TMS. Infrared spectra were recorded using a Perkin-Elmer 1600 Series IR spectrometer; samples were prepared as thin films on NaCl plates. Frequencies are reported in cm⁻¹. Low resolution GC/MS spectra were obtained on a Perkin-Elmer Autosystem XL-GC / TurboMass GC/MS with a Supelco fused silica capillary column (30m x 0.32 mm x 0.3 μ m). High resolution mass spectra were obtained on a Water LCT Premier XE MS. MS *m/z* values are reported in g mol⁻¹.

Thin-layer chromatography was performed using Merck 60 F₂₅₄ aluminum-backed plates. They were visualised under UV light (254 nm), anisaldehyde stain, permanganate stain or ceric ammonium molybdate stain. These stains were prepared by the standard procedures.

Column chromatography was performed under increased pressure using silica gel (60Å, 35-70 μ m). Columns were packed using a slurry of starting solvent and silica gel and loaded by careful addition of a concentrated solution of crude mixture in the starting solvent. Photochemical reactions were performed with a Photochemical Reactors Ltd water-jacketed medium pressure mercury vapour lamp.

TERT-BUTYL 11-AZATRICYCLO[4.3.1.1^{2,5}]UNDECANE-11-CARBOXYLATE



A 500 mL 3-necked flask was equipped with a magnetic stirrer, a 250 mL dropping funnel, a gas tube adapter and a stopper. The flask was then charged with concentrated sulphuric acid (250 mL), and the dropping funnel with concentrated hydrochloric acid (150 mL). The round bottom flask was connected to a gas bubbler filled with concentrated sulphuric acid via a latex tube. Separately a 250 mL 2-necked round bottom flask was equipped with a magnetic stirrer bar and a gas tube adapter connected to a solid sodium hydroxide filled gas drying tube. This flask was then charged with ketone **17** (7g, 26.4 mmol) and ether (150 mL). The dry $\text{HCl}_{(g)}$ generator was then connected to the reaction vessel through a fritted glass gas delivery tube. With rapid stirring in both flasks a very slow addition of $\text{HCl}_{(l)}$ to the sulphuric acid was started, the rate was controlled to allow approximately one gas bubble per second to form in the gas bubbler. The reaction setup was allowed to run at room temperature for 18 hours before the apparatus was carefully purged with nitrogen and the excess acid from the $\text{HCl}_{(g)}$ generator was diluted and disposed of. The reaction mixture was then added to a large volume of water in a 1L conical flask, this was carefully quenched with addition of aqueous sodium hydroxide (10%), as the reaction mixture became more basic a large volume of zinc salts formed, addition of a large excess of sodium hydroxide solid caused the resolution of these salts. The reaction mixture was then extracted with THF (5 x 100 mL), the combined organic extracts were washed with brine and then dried over sodium sulphate and the solution was concentrated under reduced pressure yield a crude oil (3.6 g, 23.8 mmol, 90.2%). Next BOC anhydride (7g, 32 mmol) was added to the solution with rapid stirring. The mixture was stirred for 2 hours at room temperature before addition of aqueous sodium bicarbonate solution. The mixture was then stirred for 15 minutes before

separation of the layers and extraction of the aqueous layers with ether (3 x 50 mL). The combined organic extracts were then washed with brine and dried over sodium sulphate before the solvent was removed under reduced pressure. The crude product was purified by column chromatography (1:10 → 1:1 Ethyl Acetate:Hexane) to yield a orange tinted clear oil (2.01 g, 8.00 mmol, 30.03%)

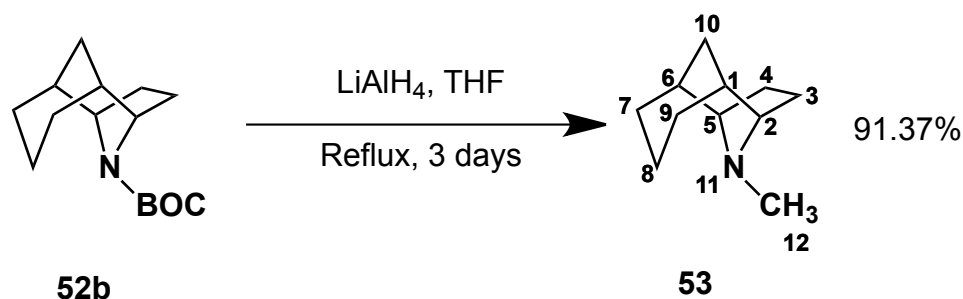
δ_{H} (400 MHz; CDCl_3) = 1.22-1.27 (m, 3 H, C-8 + C-10), 1.45 (br s, 1 H, C-1 or C-6), 1.47 (s, 9 H, C-14 + C-15 + C-16), 1.55 (br s, 1 H, C-1 or C-6), 1.62-1.65 (m, 4 H, C-7 + C-9), 1.78 (m, 4 H, C-3 + C-4), 1.95-2.01 (m, 1 H, C-8), 4.25 (br s, 1 H C-2 or C-5), 4.34 (br s, 1 H, C-2 or C-5)

δ_{C} (125 MHz; CDCl_3) = 153.37 (C-12), 78.68 (C-13), 58.79 (C-2 or C-5), 57.40 (C-2 or C-5), 34.35 (C-3 + C-4), 30.90 (C-14, C-15, C-16), 28.63 (C-1 + C-6), 26.83 (C-7 + C-9) 18.58 (C-10)

m/z = 251.1882, 195.1217, 167.0939, 150.1278, 123.1029, 114.0463, 79.0525, 68.0474, 57.0655 (Calculated: 251.1885)

IR (thin film) ν = 1477.21 (s), 1521.08 (s), 167.25 (br), 2342.12 (s), 2361.41 (s), 2400.46 (s), 2853.65 (s), 2878.72 (s), 2907.16 (s), 2938.02 (s), 2977.07 (s), 3019.01 (s)

11-METHYL-11-AZATRICYCLO[4.3.1.1^{2,5}]UNDECANE



A 250 mL round bottom flask was equipped with a magnetic stirrer bar and then charged with LiAlH_4 (3.7 g, 97.5 mmol) and THF (125 mL) was added under an inert atmosphere. The flask was then cooled to 0°C and a solution of carbamate **52b** (2.00 g, 7.96 mmol) was added dropwise with rapid stirring. The reaction mixture was brought to reflux and held at this temperature for 3 days. The reaction was then cooled to 0°C before quenching the reaction with water (3.7 mL), aqueous sodium hydroxide solution (3.7 mL, 10%), and finally water (11.1 mL). The white solids that formed were stirred with additional THF (25 mL) before filtration and washing with THF (3 x 25 mL). The combined organic extracts were then dried over sodium sulphate and the solvent removed under reduced pressure to yield a clear oil of the title compound (1.2 g, 7.2 mmol, 91.37%)

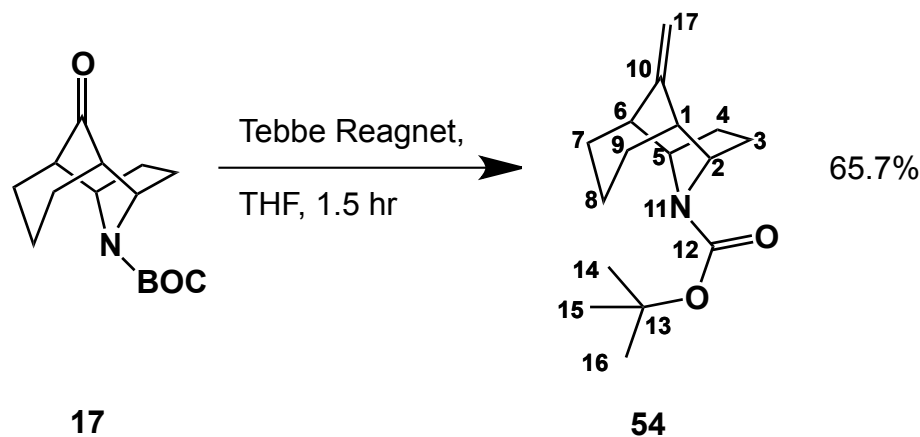
δ_{H} (400 MHz; CDCl_3) = 1.06 (m, 2 H, C-10), 1.38 (dtt, 1 H, $J=12.7, 7.7, 2.6$, C-8), 1.46 (m, 4 H, C-7 + C-9), 1.65 (m, 2 H, C-3- H_{eq} + C-4- H_{eq}), 1.72-1.78 (m, 2 H, C-3- H_{ax} + C-4- H_{ax}), 1.89-1.96 (m, 2 H, C-1 + C-6), 2.09 (s, 3 H, C-12), 2.64 (dtt, 1 H, $J=12.8, 7.1, 2.9$, C-8), 3.00-3.02 (m, 2 H, C-2 + C-5)

δ_{C} (125 MHz; CDCl_3) = 68.2 (C-12), 41.5, 35.8, 30.3, 26.2, 24.9, 20.8

m/z = 165.1518, 137.1196, 94.0644, 83.0728, 82.0649, 58.0393 (Calculated: 165.1527)

IR (thin film) ν = 1124.78 (s), 1209.63 (s), 1335.95 (s), 1444.9 (s), 1463.71 (s), 2793.38 (s), 2844.97 (s), 2916.32 (br)

TERT-BUTYL 10-METHYLENE-11-AZATRICYCLO[4.3.1.1^{2,5}]UNDECANE-11-CARBOXYLATE

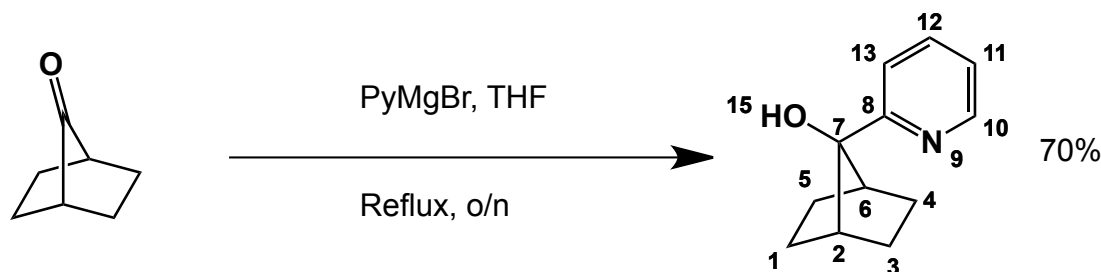


A 25 mL round bottom flask was equipped with a magnetic stirrer bar and charged with carbamate **17** (265 mg, 1 mmol) and THF (10 mL) and then flushed with nitrogen. The reaction mixture was cooled to -40°C and Tebbe reagent solution (2 mL, 1 mmol, 0.5 M in toluene) was added dropwise. The reaction mixture was then stirred for 30 minutes, allowed to slowly warm to room temperature and stirred for an additional hour. The reaction mixture was then diluted with THF (5 mL), cooled to -10°C and aqueous sodium hydroxide (1 mL, 15%) and stirred for 15 minutes. The reaction mixture was then filtered through Celite, washed with ether (3 x 10 mL) and dried over sodium sulphate. The solvent was then removed under reduced pressure to yield an orange solid. The solid was triturated with pentane (3 x 10 mL), filtered, washed with additional pentane and the solvent removed under reduced pressure to yield an orange solid (173 mg, 0.657 mmol, 65.7%)

δ_{H} (400 MHz; CDCl_3) = 1.30-1.37 (m, 3 H, C-8 + C-7 + C-9), 1.44 (s, 9 H, C-14 + C-15 + C16), 1.49-1.50 (m, 2 H, C-7 + C-9), 1.75-1.85 (m, 4 H, C-3 + C-4), 1.90-1.92 (m, 1 H, C-8), 2.15-2.17 (m, 2 H, C-1 + C-6), 4.21-4.32 (m, 2 H, C-2 + C-5), 4.69 (s, 2 H, C-17)

δ_c (125 MHz; $CDCl_3$) = 153.8 (C-12), 150.5 (C-10), 107.5 (C-17), 78.9 (C-2 + C-5), 59.4 (C-6 + C-1), 45.6 (C-8), 30.1 (C-7 + C-9), 28.6 (C-14 + C-15 + C-16), 18.8 (C-3 + C-4)

(1*R*,4*S*)-7-(PYRIDIN-2-YL)BICYCLO[2.2.1]HEPTAN-7-OL



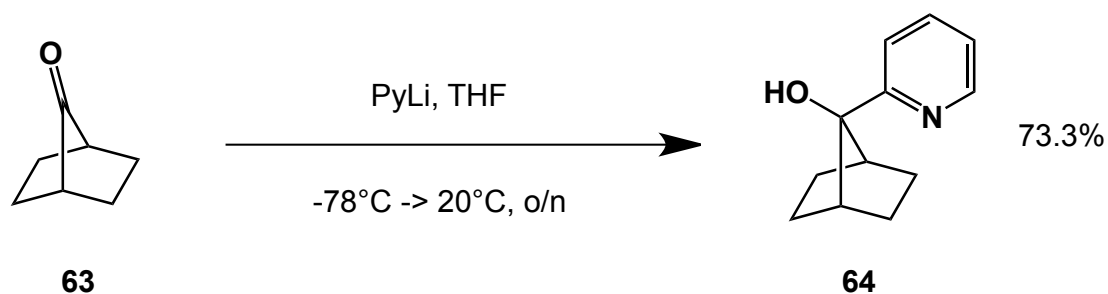
63

64

A 100 mL Schlenk tube was equipped with a magnetic stirrer bar, vacuum purged and filled with nitrogen. The flask was then charged with ketone 63 (330 mg, 3 mmol) and THF (25 mL). In a separate Schlenk tube *n*BuLi (1.2 mL, 3 mmol, 2.5M THF) was slowly added to a -78°C solution of 2-bromo-pyridine (0.28 mL, 0.47 g, 3 mmol) in THF with rapid stirring. The reaction mixture was stirred for 15 minutes before addition of $MgBr_2$ in THF (0.55 g, 10 mL) and stirred for another 15 minutes. Next the prepared 2-grignard-pyridine solution was slowly added to the reaction mixture. This caused a yellow colour to form. The reaction was then allowed to slowly warm to room temperature, and stirring continued overnight. The reaction was cooled to 0°C and quenched with careful addition of water (1 mL). The reaction mixture was then filtered and washed with ether (10 mL). The mixture was then separated and the combined organic extracts were washed with brine and dried over sodium sulphate to yield the crude product as an off white solid (397 mg, 2.1 mmol, 70%). Further purification was possible with column chromatography (1:10 hexane:ethyl acetate) but high losses were seen presumably due to cohesion of the pyridine moiety to the surface of the silica.

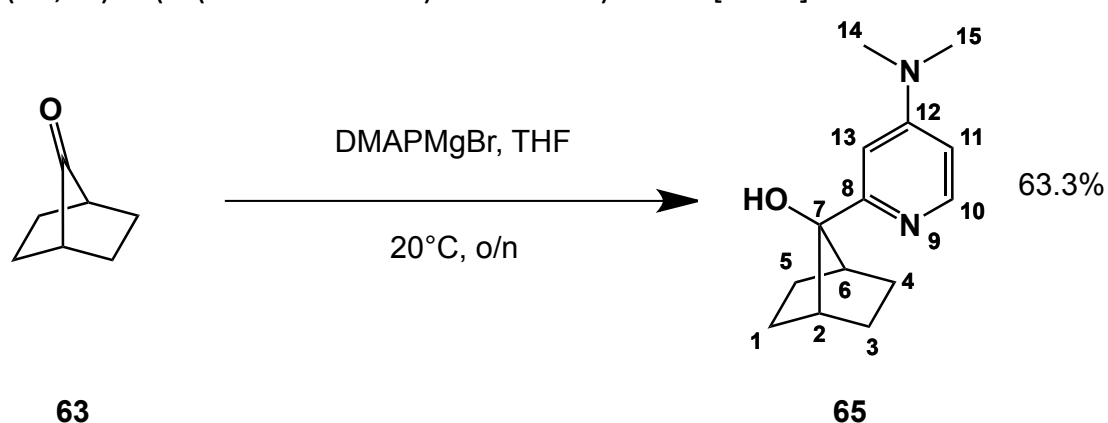
δ_H (400 MHz; $CDCl_3$) = 1.31 (q, 2H, $J=6.81$, C-2 + C-6), 1.48 (t, 4 H, $J=6.60$, C-1- H_{ax} + C-4- H_{ax} + C-4- H_{ax} + C-5- H_{ax}), 2.21- 2.23 (m, 2 H, C-1- H_{eq} + C-5- H_{eq}), 2.49 (m, 2 H, C-1- H_{eq} + C-5- H_{eq}), 7.21 (dd, 1 H, $J=7.51$, 4.86, C-13), 7.46 (dt, 1 H, $J=7.87$, 1.02, C-11), 7.70 (dt, 1 H, $J=7.70$, 1.83, C-12), 8.60 (dd, 1 H, $J=4.84$, 1.78, C-10)

δ_c (125 MHz; $CDCl_3$) = 161.9 (C-8), 149.1 (C-10), 136.6 (C-12), 122.3 (C-11 or C-13), 121.4 (C-11 or C-13), 88.7 (C-7), 53.4 (C-2 + C-6), 28.6 (C-3 + C-4), 27.4 (C-1 + C-5)



A 100 mL Schlenk tube was equipped with a magnetic stirrer bar, vacuum purged and filled with nitrogen. The flask was then charged with ketone 63 (330 mg, 3 mmol) and THF (25 mL) and the reaction was cooled to -78°C . In a separate Schlenk tube nBuLi (1.2 mL, 3 mmol, 2.5M THF) was slowly added to a -78°C solution of 2-bromopyridine (0.28 mL, 0.47 g, 3 mmol) in THF with rapid stirring. The reaction mixture was stirred for 15 minutes. Next the prepared 2-lithio-pyridine solution was slowly added to the reaction mixture. This caused a yellow colour to form. The reaction was then allowed to slowly warm to room temperature, and stirring continued overnight. The reaction was cooled to 0°C and quenched with careful addition of water (1 mL). The reaction mixture was then filtered and washed with ether (10 mL). The mixture was then separated and the combined organic extracts were washed with brine and dried over sodium sulphate to yield the crude product as an off white solid (410 mg, 2.2 mmol, 73.3%). Further purification was possible with column chromatography (1:10 hexane:ethyl acetate) but high losses were seen presumably due to cohesion of the pyridine moiety to the surface of the silica. Spectroscopic data as above.

(1R,4S)-7-(4-(DIMETHYLAMINO)PYRIDIN-2-YL)BICYCLO[2.2.1]HEPTAN-7-OL

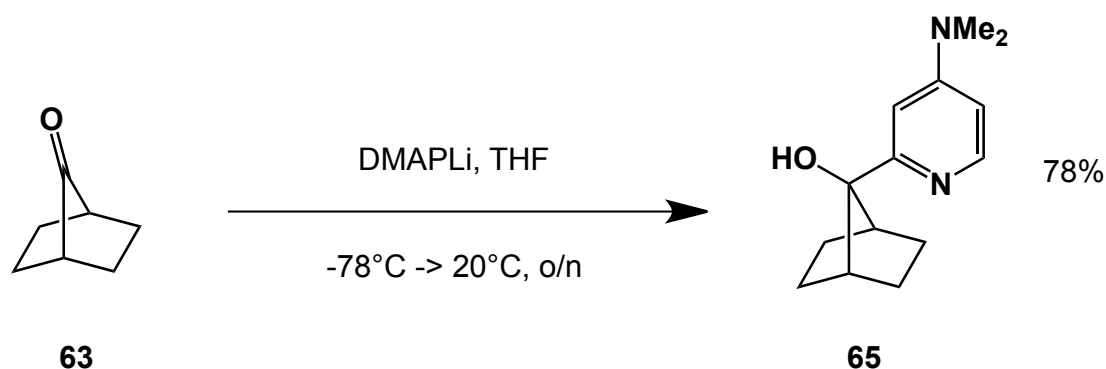


A 100 mL Schlenk tube was equipped with a magnetic stirrer bar, vacuum purged and filled with nitrogen. The flask was then charged with ketone 63 (330 mg, 3 mmol) and THF (25 mL). In a separate Schlenk tube nBuLi (1.2 mL, 3 mmol, 2.5M THF) was slowly added to a -78°C solution of 2-bromo-DMAP (0.61g, 3mmol) in THF with rapid stirring. The reaction

mixture was stirred for 15 minutes before addition of MgBr_2 in THF (0.55 g, 10 mL) and stirred for another 15 minutes. Next the prepared 2-grignard-DMAP solution was slowly added to the reaction mixture. This caused a yellow colour to form. The reaction was then allowed to slowly warm to room temperature, and stirring continued overnight. The reaction was cooled to 0°C and quenched with careful addition of water (1 mL). The reaction mixture was then filtered and washed with ether (10 mL). The mixture was then separated and the combined organic extracts were washed with brine and dried over sodium sulphate to yield the crude product as an off white solid. The crude product was then recrystallised from ether to yield a pure product as brown tinted crystals (441 mg, 1.9 mmol, 63.3%).

δ_{H} (400 MHz; CDCl_3) = 1.28 (q, 2 H, $J=5.9$, C-1- H_{ax} + C-5- H_{ax}), 1.43 (q, 2 H, $J=6.44$, C-3- H_{ax} + C-4- H_{ax}), 1.56 (d, 2 H, $J=8.03$, C-1- H_{eq} + C-5- H_{eq}), 2.21 (d, 2 H, $J=7.74$, C-3- H_{eq} + C-4- H_{eq}), 2.48 (d, 2 H, $J=1.94$, C-2 + C-6), 2.83 (s, 6 H, C-14 + C-15), 6.19 (d, 1H, $J=2.59$, C-11), 6.51 (s, 1 H, C-13), 8.00 (d, 1 H, $J=5.99$, C-10)

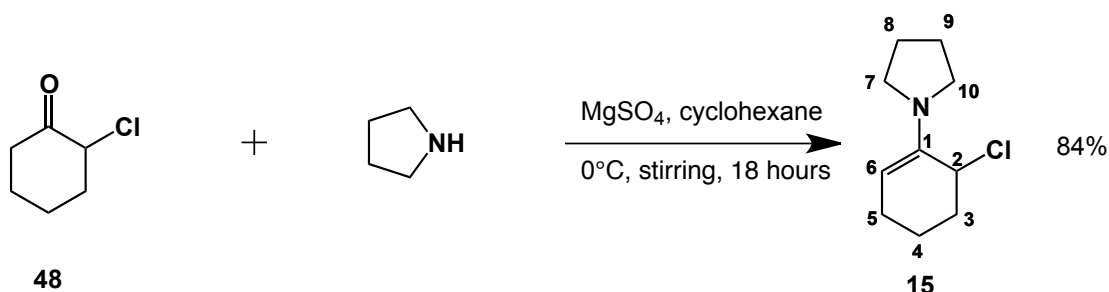
δ_{C} (125 MHz; CDCl_3) = 161.7 (C-8), 154.9 (C-10), 149.1 (C-12), 105.3 (C-11 or C-13), 103.9 (C-11 + C-13), 88.9 (C-7), 42.0 (C-2 + C-6), 39.2 (C-14 + C-15), 28.6 (C-3 + C-4), 27.7 (C-1 + C-5)



A 100 mL Schlenk tube was equipped with a magnetic stirrer bar, vacuum purged and filled with nitrogen. The flask was then charged with ketone **63** (330 mg, 3 mmol) and THF (25 mL). In a separate Schlenk tube $n\text{BuLi}$ (1.2 mL, 3 mmol, 2.5M THF) was slowly added to a -78°C solution of 2-bromo-DMAP (0.61g, 3mmol) in THF with rapid stirring. The reaction mixture was stirred for 15 minutes. Next the prepared 2-lithio-DMAP solution was slowly added to the reaction mixture. This caused a yellow colour to form. The reaction was then allowed to slowly warm to room temperature, and stirring continued overnight. The reaction was cooled to 0°C and quenched with careful addition of water (1 mL). The reaction mixture was then filtered and washed with ether (10 mL). The mixture was then separated and the combined organic extracts were washed with brine and dried over sodium sulphate to yield

the crude product as an off white solid. The crude product was then recrystallised from ether to yield a pure product as brown tinted crystals (524 mg, 2.3 mmol, 78.0%). Spectroscopic data as above.

6-CHLORO-1-PYRROLIDINOCYCLOHEXENE^[135]

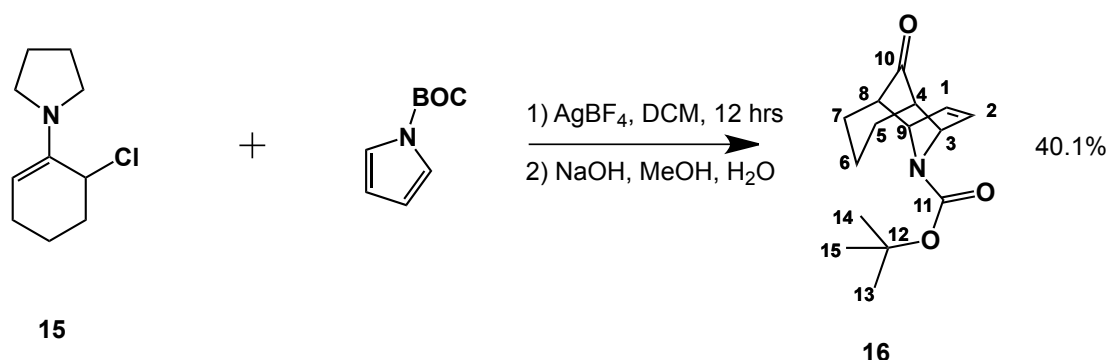


A 2L three necked round bottom flask was equipped with an overhead stirrer bar, a 250 mL dropping funnel and a stopper in the third neck. The flask was then charged 2-chlorocyclohexanone (63.5g, 478.9 mmol), anhydrous magnesium sulphate (315 g) and cyclohexane (350 mL). The mixture was stirred while being cooled to 0°C. Once the 2-chlorocyclohexanone was fully in solution the dropping funnel was charged with pyrrolidine (80 mL, 974.1 mmol) and slow addition occurred over a 3 hour period ensuring the mixture was maintained at 0°C throughout. Once addition was complete the reaction mixture was monitored for loss of starting material by GCMS, with further pyrrolidine was slowly added (3 x 10 mL). After complete consumption of the starting material the mixture was quickly filtered and washed with hexane (3 x 150 mL) and then returned to an ice bath to maintain the low temperature. The combined filtrate and washings were then reduced under reduced pressure. It was necessary to maintain a low temperature throughout to avoid formation of the double addition product. This produced the final product as an orange oil (76.06 g, 289.1 mmol, 84%) that could be used directly in the next step.

δ_{H} (400 MHz; CDCl_3) = 1.60 (m, 1 H, C-4), 1.75 (m, 4 H, C-8 + C-9), 1.80 (m, 1 H, C-4), 1.85 (m, 1 H, C-5), 1.90 (m, 1 H, C-3), 2.05 (m, 1 H, C-3), 2.15 (m, 1 H, C-5), 2.90 (m, 2 H, C-10 or C-7), 3.10 (m, 2 H, C-10 or C-7), 4.35 (t, 1 H, C-2, $J=0.4$), 4.60 (t, 1 H, C-6, $J=0.6$)

δ_{C} (125 MHz; CDCl_3) = 17.1 (C-4), 22.8 (C-5), 24.6 (C-8 + C-9), 32.6 (C-3), 47.2 (C-7 + C-10), 56.3 (C-2), 97.8 (C-6), 142.0 (C-1)

TERT-BUTYL 10-OXO-11-AZATRICYCLO[4.3.1.1^{2,5}]UNDEC-3-ENE-11-CARBOXYLATE^[132]



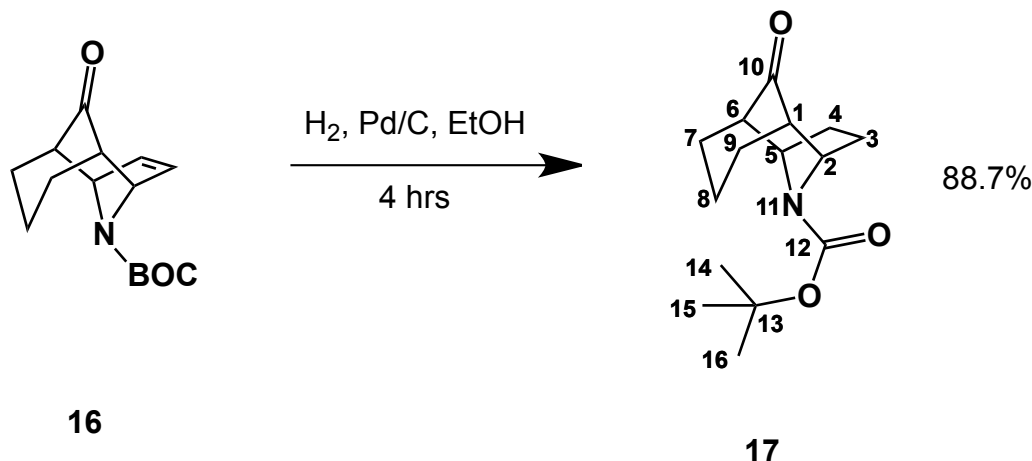
A 2L three necked round bottom flask was equipped with an overhead stirrer bar, a 500 mL dropping funnel and a stopper in the third neck. The flask was then charged with silver tetrafluoroborate (100g, 484 mmol) and covered in aluminium foil to prevent photooxidation. Then the flask was vacuum purged before addition of dichloromethane (500 mL) and N-Boc pyrrole (137 mL, 819.3 mmol) under a nitrogen atmosphere. The reaction mixture was then cooled to -78°C in an acetone/dry-ice bath before slow addition of enamine **15** (76g, 409 mmol) in a solution of dichloromethane (150 mL) with rapid stirring of the reaction mixture. The addition of the enamine occurred over a period of 4 hours, once complete the reaction mixture was allowed to warm slowly to room temperature with continued stirring overnight. The reaction mixture was then filtered through Celite and washed with additional dichloromethane (3 x 100mL) to yield a black oil of the immonium salt. This oil was now added to a 1L single neck flask along with methanol (300 mL), deionised water (300 mL) and sodium hydroxide (45 g) the reaction mixture was stirred for 4 hours at room temperature and a dark orange colour developed. The reaction mixture was then extracted with Ether (5 x 150 mL), the combined washings were dried with brine and then sodium sulphate. The dry solvent was then concentrated under reduced pressure to yield a dark orange oil. This oil was then purified with flash column chromatography on silica gel with a 1:2 ethyl acetate : hexane eluant to yield (43.09g, 163.6 mmol ,40.1%) as a clear orange crystal.

δ_{H} (400 MHz; CDCl_3) = 1.35 (m, 1 H, C-6- H_{eq}), 1.42 (s, 9 H, C-12) 1.95 (m, 1 H, C-6- H_{ax}), 2.05 (m, 2 H, C-5- H_{eq} + C-7- H_{eq}), 2.22 (m, 2 H, C-5- H_{ax} + C-7- H_{ax}), 2.45 (br d, 2 H, C-4 + C-8, $J=9$), 4.80 (s, 2 H, C-3 or C-9), 4.90 (s, 2 H, C-3 or C-9), 6.15 (s, 1 H, C-1 or C-2, $J=22$), 6.21 (s, 1 H, C-1 or C-2, $J=22$).

δ_c (125 MHz; $CDCl_3$) = 18.3 (C-6), 27.6 (C-13+C-14+C-15), 28.8 (C-7), 29.8 (C-5), 50.1 (C-8), 50.2 (C-4), 60.7 (C-3), 61.7 (C-9), 79.3 (C-12), 134.8 (C-2), 135.9 (C-1), 152.0 (C-11), 214.2 (C-10).

IR (thin film) ν = 1168.65 (w), 1205.29, 1253.5, 1287.25 (w), 1321, 1346.07, 1443.46, 2929.34 (s), 3078.8 (w), 3432.67 (w).

TERT-BUTYL 10-OXO-11-AZATRICYCLO[4.3.1.1^{2,5}]UNDECANE-11-CARBOXYLATE^[132]



A Parr hydrogenator was charged with enone 16 (5.27g, 20 mmol), 5% palladium on charcoal (270 mg) and ethanol (150 mL). The reaction chamber was then sealed and degassed under moderate vacuum before introduced of hydrogen gas at 4 bar. The reaction mixture was then stirred for 4 hours with the built in mechanical stirrer the reaction was monitored for consumption of starting material by TLC. After complete consumption of the starting material the reaction mixture was filtered through Celite and concentrated under reduced pressure to yield a weakly coloured orange oil (4.70g, 17.7 mmol, 88.7%)

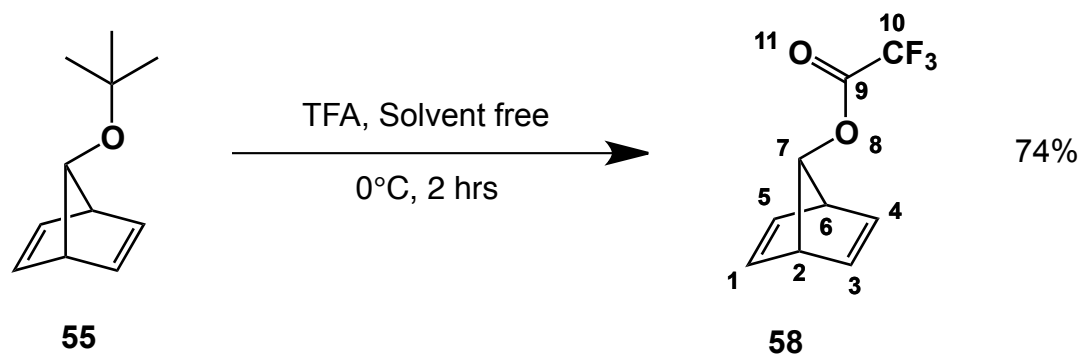
δ_H (400 MHz; $CDCl_3$) = 1.20 (m, 1 H, C-8- H_{eq}), 1.43 (s, 9 H, C-14 + C-15 + C-16), 1.77 (m, 4 H, C-3 + C-4), 1.85 (m, 1 H, C-8- H_{ax}), 2.05 (m, 2 H, 2 x C-7- H_{aq} or 2 x C-9- H_{eq}), 2.15 (m, 2 H, 2 x C-7- H_{aq} or 2 x C-9- H_{eq}), 2.30 (br s, 1 H, C-1 or C-6), 2.35 (br s, 1 H, C-1 or C-6), 4.40 (br s, 1 H, C-2 or C-5), 4.40 (br s, 1 H, C-2 or C-5).

δ_c (125 MHz; $CDCl_3$) = 18.4 (C-8), 26.8 (C-7 or C-9), 27.4 (C-7 or C-9), 28.5 (C-14 + C-15 + C-16), 31.50 (C-4), 31.55 (C-3), 53.6 (C-2), 53.8 (C-5), 58.4 (C-1), 59.4 (C-6), 79.9 (C-13), 153.6 (C-10), 217.6 (C-12)

IR (thin film) ν = 1105.01 (s), 1152.26 (s), 1255.43 (s), 1308.46 (s), 1416.46 (s), 1695.12 (s), 1970.89 (w), 2359.48 (w), 2974.66 (s), 3516.56 (m)

HRMS (m/z) = 265.1674, 209.1230, 192.1028, 165.1161, 137.1192, 94.0675, 68.0470

(1R,4S)-BICYCLO[2.2.1]HEPTA-2,5-DIEN-7-YL 2,2,2-TRIFLUOROACETATE^[172A]

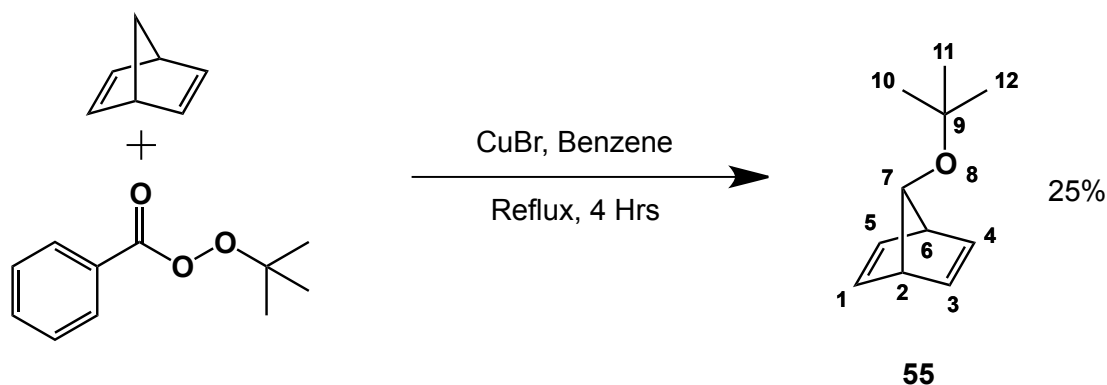


A 100 mL round bottom flash was equipped with a magnetic stirrer bar, then charged with ether **55** (1.00 g, 6.1 mmol) and cooled to 0°C in an ice bath. Once the temperature stabilised trifluoroacetic acid (10 mL, 130.6 mmol) was added in a single portion and the reaction mixture was stirred for 2 hours. The reaction mixture was carefully quenched by slow addition of solid sodium carbonate until pH paper indicated a neutral reaction mixture. Then the reaction mixture was extracted with ether (3 x 50 mL) and the combined washings were dried with brine, followed by anhydrous sodium sulphate. Finally the solvent was removed under reduced pressure to yield an orange oil of 7-norbornadienyl trifluoroacetate (0.92g, 4.51 mmol, 74%). The mixture needed no further purification for use in the next steps.

δ_{H} (400 MHz; CDCl₃) = 3.74 (dq, 2H, J=4.17, 2.05, C-2 + C-6), 4.72 (s, 1H, C-7), 6.63-6.64 (m, 2 H, C-3 + C-4), 6.76-6.78 (m, 2 H, C-1 + C-5)

m/z = 204.0393, 175.0363, 127.0357, 93.0693, 91.0527, 66.0430 (Calculated: 204.0398)

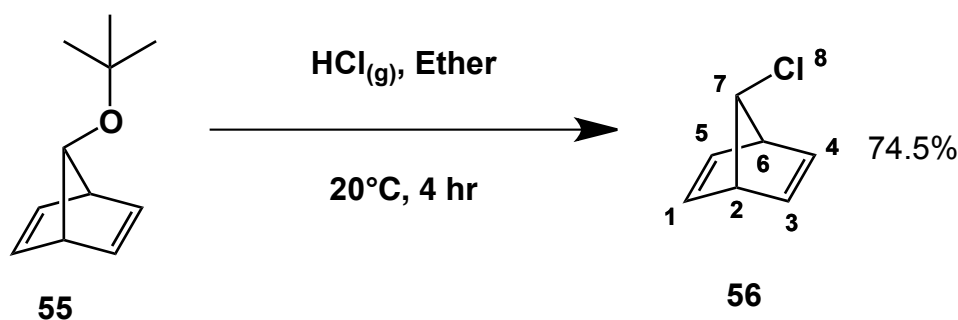
(1*R*,4*S*)-7-(*TERT*-BUTOXY)BICYCLO[2.2.1]HEPTA-2,5-DIENE^[173]



A 2L three-necked flask was equipped with an overhead mechanical stirrer, a dropping funnel and a gas line adapter and flushed with nitrogen. Then the flask was charged with norbornadiene (300g, 3.26 mol), cuprous bromide (0.6g, 4.5 mmol) and benzene (500 mL) and flushed again with nitrogen. The reaction mixture was then brought to reflux and slow addition of a *t*-butyl perbenzoate solution (245g, 1.26 mol, 12.6M in benzene) was started. The reaction mixture immediately turns blue from green. After around 1 hour addition of the *t*-butyl perbenzoate was complete and the reaction mixture was kept at reflux for another 30 minutes. Then the reaction mixture is cooled to room temperature and transferred into a separatory funnel. The reaction mixture is then washed with brine (3 x 200 mL), 10% sodium hydroxide solution (3 x 200 mL), brine (1 x 200 mL) and dried over sodium sulphate. At this stage infrared spectroscopy was used to test the reaction mixture for the presence of peroxides. Once a lack of peroxides was confirmed the reaction mixture was distilled, first to remove solvent and then to extract the desired product. The reaction mixture was rapidly distilled under reduced pressure (265 millibar) and benzene was recovered at around 45°C. After complete removal of benzene the pressure was lowered to (20 millibar) and the product was collected between 80-85°C. This yielded 7-*t*-butyoxynorbornadiene (51 g, 25%) as a clear oil.

δ_{H} (400 MHz; CDCl_3) = 1.160 (s, 9 H, C-10 + C-11 + C-12), 3.41-3.42 (m, 2 H, C-2 + C-6), 3.796 (d, 1 H, $J=0.68$, C-7), 6.60-6.62 (m, 2 H, C-1 + C-5), 6.66 - 6.67 (m, 2 H, C-3 + C-4)

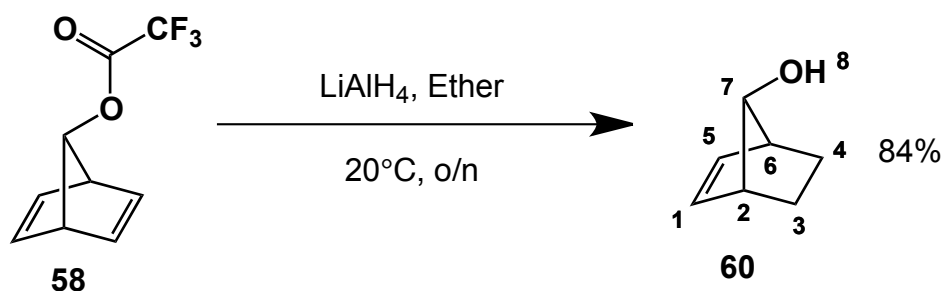
(1*S*,4*S*)-7-CHLOROBICYCLO[2.2.1]HEPTA-2,5-DIENE^[172E]



A 500 mL 3-necked flask was equipped with a magnetic stirrer, a 250 mL dropping funnel, a gas tube adapter and a stopper. The flask was then charged with concentrated sulphuric acid (250 mL), and the dropping funnel with concentrated hydrochloric acid (150 mL). The round bottom flask was connected to a gas bubbler filled with concentrated sulphuric acid via a latex tube. Separately a 100 mL 2-necked round bottom flask was equipped with a magnetic stirrer bar and a gas tube adapter connected to a solid sodium hydroxide filled gas drying tube. This flask was then charged with ether 55 (1.10g, 6.6 mmol) and ether (50 mL). The dry $\text{HCl}_{(g)}$ generator was then connected to the reaction vessel through a fritted glass gas delivery tube. With rapid stirring in both flasks a very slow addition of $\text{HCl}_{(g)}$ to the sulphuric acid was started, the rate was controlled to allow approximately one gas bubble per second to form in the gas bubbler. The reaction setup was allowed to run at room temperature for 4 hours before the apparatus was carefully purged with nitrogen and the excess acid from the $\text{HCl}_{(g)}$ generator was diluted and disposed of. The reaction mixture carefully quenched with aqueous sodium carbonate (10%) until pH paper indicated neutrality. The mixture was then separated and the aqueous phase was extracted with ether (3 x 25 mL), the combined organic extracts were then washed with brine and dried with sodium sulphate. The solvent was then removed under reduced pressure to yield 7-chloronorbornadiene (0.62 g, 4.92 mmol, 74.5%).

δ_{H} (400 MHz; CDCl_3) = 3.67 (dq, 2 H, $J=415, 2.03$, C-2 + C-5), 4.23 (t, 1 H, $J=1.17$, C-7), 6.66 – 6.68 (m, 2 H, C-1 + C-5), 6.78 – 6.80 (m, 2 H, C-3 + C-4)

(1*R*,4*S*,7*S*)-BICYCLO[2.2.1]HEPT-2-EN-7-OL^[172B, c]

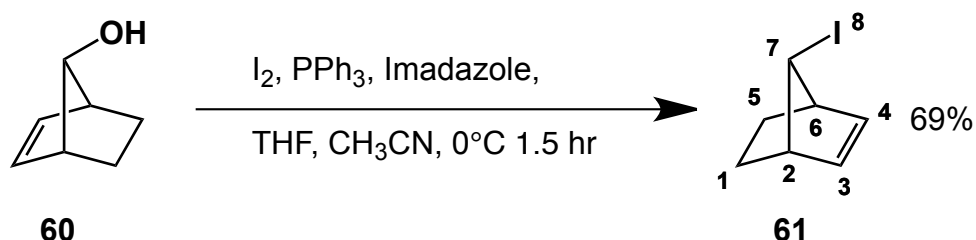


A oven dried 250 mL single necked round bottom flask was equipped with a magnetic stirrer bar and charged with LiAlH_4 (0.42g, 10.8 mmol) and purged with nitrogen. The flask was then filled with dry ether (50 mL) under an inert nitrogen atmosphere. The reaction mixture was cooled to 0°C and trifluoroacetate 58 solution in ether (1.20g, 3.8 mmol, 2 mL ether) was slowly injected into the reaction vessel. The reaction was stirred for 10 minutes at 0°C before being allowed to warm to room temperature, stirring was then continued overnight. The reaction mixture was again cooled to 0°C and then quenched first with water (0.42 mL), then 3M NaOH (0.42 mL) and finally water (1.3 mL). The reaction was then filtered to remove aluminium salt solids and then extracted with ether (3 x 50 mL) the solvent removed under reduced pressure. This yielded a crude oil that was purified by gradient column chromatography (Ethyl Acetate/Pentane 0:1 \rightarrow 1:1) to yield a colourless oil (0.62g, 5.7 mmol, 84%)

δ_{H} (400 MHz; CDCl_3) = 1.04 (tt, 2 H, $J=7.67, 3.66$, C-3- H_{ax} + C-4- H_{ax}), 1.74 (br s, 1 H, OH), 1.82 (m, 2 H, C-3- H_{eq} + C-4- H_{eq}), 2.55 (m, 2 H, C-2 + C-6), 3.59 (br s, 1 H, C-7), 5.98-6.00 (m, 2 H, C-1 + C-5)

δ_{C} (125 MHz; CDCl_3) = 134.3, 82.3, 45.7, 21.1

(1*R*,4*S*,7*R*)-7-iodobicyclo[2.2.1]HEPT-2-ENE^[172c]



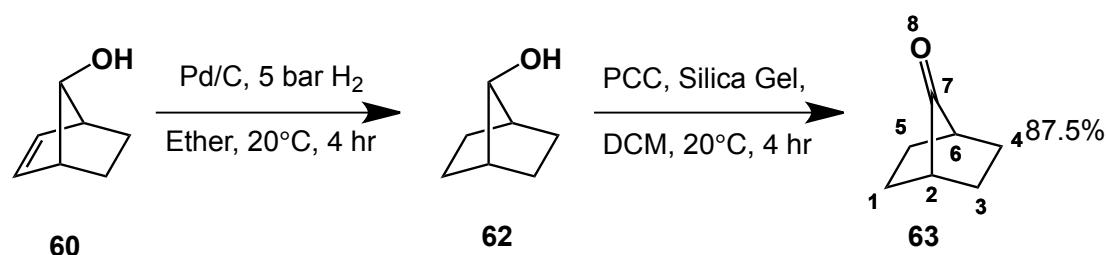
A 500 mL round bottom flask was oven dried and then equipped with a magnetic stirrer bar, the flask was the charged with PPh_3 (28.5 g, 57 mmol), imidazole (15.7g, 232 mmol), THF (50

mL), CH₃CN (200 mL). The reaction mixture was then cooled to 0°C before I₂ (55 g, 217 mmol) was added, this mixture turned red-brown and was stirred for 15 minutes. Next a solution of alcohol 60 (6.2g, 57 mmol) in CH₃CN (25 mL) was syringed into the reaction vessel with rapid stirring. The reaction was then allowed to warm slowly to room temperature over 2 hours, over which time a white precipitate formed. The reaction was then quenched by addition of water (20 mL) and then diluted with hexane (50 mL). The aqueous layer was extracted with 10% CH₂Cl₂ in hexane and the combined organic layers were washed with saturated sodium thiosulphate, water then brine before drying over sodium sulphate. The solvent was removed under reduced pressure to yield a crude product still containing much triphenylphosphine oxide. The crude product was purified with column chromatography eluted with hexane to yield the syn-7-iodonorborene. (8.65 g, 39.3 mmol, 69%)

δ_{H} (400 MHz; CDCl₃) = 1.13-1.17 (m, 2 H, C-1-H_{eq} + C-5-H_{eq}), 2.13-2.17 (m, 2 H, C-1-H_{ax} + C-5-H_{ax}), 2.88 (d, 2 H, J=1.4, C-2 + C-6), 3.88 (t, 1 H, J=1.6, C-7), 6.01-6.03 (m, 2 H, C-3 + C-4)

δ_{C} (125 MHz; CDCl₃) = 134.9, 48.7, 39.5, 22.2

(1*S*,4*S*)-BICYCLO[2.2.1]HEPTAN-7-ONE^[172D]



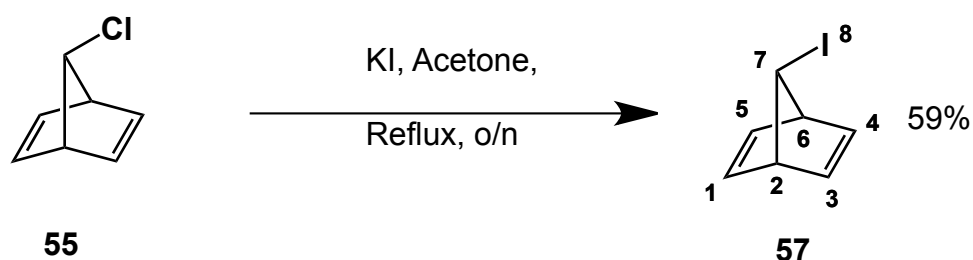
A Parr hydrogenator was charged with alcohol 60 (8.3g, 75.45 mmol), 5% palladium on charcoal (0.25g) and ether (100 mL). The reaction chamber was then sealed and degassed under moderate vacuum before introduced of hydrogen gas at 5 bar. The reaction mixture was then stirred for 4 hours with the built in mechanical stirrer the reaction was monitored for consumption of starting material by TLC. After complete consumption of the starting material the reaction mixture was filtered through Celite and carefully concentrated under reduced pressure. The solvent was not completely removed to prevent undue losses through evaporation of the volatile product. A second round bottom flask was charged with a large magnetic stirrer bar, silica gel (50 g) and PCC (28.3g, 131.3 mmol) and DCM (150 mL) and stirred until a consistent reaction mixture was achieved. Then norbornen-7-ol in ether (75.45 mmol) was added in a single portion and the reaction mixture was stirred for 4 hours. The mixture was then filtered and washed with DCM and the solvent carefully removed

under reduced pressure. Finally the crude product was purified by column chromatography (10% ether in pentane) to yield the title compound as a clear oil (7.12g, 66.0 mmol, 87.5%)

δ_{H} (400 MHz; CDCl_3) = 1.55-1.57 (quintet, 4 H, $J=5.9$, C-1- H_{ax} + C-3- H_{ax} + C-4- H_{ax} + C-5- H_{ax}), 1.87 – 1.89 (m, 4 H, C-1- H_{eq} + C-3- H_{eq} + C-4- H_{eq} + C-5- H_{eq}), 3.42 (m, 2 H, C-2 + C-6)

δ_{C} (125 MHz; CDCl_3) = 217.6 (C-7), 37.8 (C-2 + C-6), 24.2 (C-1 + C-3 + C-4 + C-5)

(1*S*,4*S*)-7-IODOBICYCLO[2.2.1]HEPTA-2,5-DIENE^[172F]



A 50 mL round bottom flask was equipped with a magnetic stirrer bar, and charged with chloride 55 (0.9 g, 7 mmol), acetone (15 mL) and sodium iodide (5.2 g, 35 mmol). The flask was then fitted with a reflux condenser and purged with nitrogen. The reaction was heated to reflux with stirring and held at reflux for 18 hours. Next the reaction was allowed to cool to room temperature and filtered through a fritted glass funnel and washed with a small volume of acetone (25 mL). The solvent was removed under reduced pressure to yield a crude brown solid. The solid was then triturated with ether (3 x 50 mL), the combined organic extracts were then washed with saturated sodium thiosulphate, dried with brine and dried with anhydrous sodium sulphate. The solvent was then removed under reduced pressure to yield 7-iodonorbornadiene as a clear oil (0.9g, 4.12 mmol, 59%).

δ_{H} (400 MHz; CDCl_3) = 3.34 (m, 2 H, C-2 + C-6), 4.55 (t, 1 H, $J=1.17$, C-7), 6.71 – 6.74 (m, 2 H, C-1 + C-5), 6.84 – 6.89 (m, 2 H, C-3 + C-4)

i

APPENDIX 2 – QUANTUM CHEMISTRY INTERFACE SOURCE CODE

MAIN.PY

```
#!/usr/bin/python
import logging
import classes
import argparse
from ConfigParser import SafeConfigParser
```

```
def main():
    """Quantum Chemistry Interface - Designed to simplify the use of QC packages
```

Quantum Chemistry Interface has been designed to simplify quantum chemistry calculations for organic chemists, it provides a common interface to quantum chemistry packages, automatically handles creating input file and reading output files, furthermore it is capable of automatically calculating reaction thermodynamic quantities given basic reaction path info. QCI understands the PBS system so is ideal for use on many clusters

When the script is run you must call it with the 3 positional arguments described below, these tell the script how to name your job, and where the files relating to each job are found. Both the job and step names can accept a list of names to automatically create batch jobs. Warning: Batch modes can rapidly create a large number of job, be careful if there is limits to job submission on your cluster.

Furthermore you must provide a flag indicating which mode the script should run in. Currently the options are new (creates a new job, no batch mode), submit (submits jobs to the queue), analyze (extracts data from jobs), reaction, (extracts thermochemistry for reactions)

It is envisioned that the project name should hold a broad description of a series of calculations, the job name should hold a description of the substitution pattern, and the step name should hold a description of the reaction step.

For example in a series of calculations studying H atom loss from substituted methane molecules you might start with the starting material, methane.

```
projectName: - Hloss
jobName: - H
stepname: - SM
```

```
qci Hloss H SM -n -c 0 -m 1 -x methane.xyz
```

The values not specifically passed are taken from the config file
Next you would calculate the transition state for loss of H atom

```
projectName: - Hloss
jobName: - H
stepName -HlossTS
```

```
qci Hloss H HlossTS -n -ts -c 0 -m 1 -x HlossTS.xyz
```

Notice we have to explicitly tell qci we are looking for a TS state
Next we need to make the product job for methyl radical

```
projectName: - Hloss
jobName: - H
stepName: - Product
```

```
qci Hloss H Product -n -c 0 -m 2 -x methylradical.xyz
```

We have now created the input files for this reaction, we can submit to the queue using a batch mode by passing a list of stepnames

```
qci Hloss H "SM HlossTS Product" -s -w 4:00:00
```

This will submit the jobs we created in the previous commands.

Once this jobs are complete we can analyse the job to check the geometry has converged to the correct structure, again we can use a batch mode here

```
qci Hloss H "SM HlossTS Product" -a
```

This will print the most important information from the output file
If all the jobs have finished correctly, and frequency calculations were requested it is now possible to calculate reaction parameters.

```
qci Hloss H "SM HlossTS Product+H" -re
```

Reaction mode requires a list of reaction steps, it is assumed that odd numbered steps are starting materials and products, and that even steps are transition states connecting them. If a step has more than one molecule you ask qci to sum their enthalpies by giving a list separated by + signs, with no spaces.

Positional Args:

```
projectName -- Set name of project
jobName -- Set name of job. Accepts a list of names for batch modes
stepName -- Set name of Step. Accepts a list of name for batch modes
```

Optional Args:

Modes:

```
new/-n -- Creates inputfile files from options selected
submit/-s -- Creates pbsfile and submits job to queue. Batch mode
analyse/-a -- Reads output file with cclib to extract chemical data.
Batch mode
reaction/-re -- Calculates thermodynamics quantities for reaction
given list in form "SM TS Prod TS2 Prod2 ... TSN
ProdN" where each word is a step name
```

Chemical Options:

```
tstate/-ts -- Mark job as a transition state. Default = False
charge/-c -- Set charge for molecule. Default from config file
mult/-m -- Set multiplicity for molecule. Default from config file
basis/-b -- Set basis set for calculation. Default from config file
functional/-f -- Set functional for system. Default from config file
xyz/-x -- Set location to read .xyz file for coordinates. No default
pcm/-p -- Set PCM simulation on and select solvent. Default = false
type/-t -- Set type of job, currently either OPT and FREQ.
Default = OPT
engine/-e -- Set which QC package to use for calculation.
Default from config file
```

PBS Options:

```
walltime/-w -- Set allowed execution time. Default from config file
nodes/-n -- Set number of nodes to be used. Default from config file
cpus/-cp -- Set number of cpus per node. Default from config file
ram/-r -- Set amount of ram per node. Default from config file
queue/-q -- Set queue for job. Default from config file
```

"""

```
logging.basicConfig(filename='qcloc.log', level=logging.DEBUG)
logging.info('Started')
```

```
confparser = SafeConfigParser()
confparser.read('conf/qcloc.conf')
```

```
argparser = argparse.ArgumentParser(
    description='Quantum Chemistry Interface', version='0.1')
argparser.add_argument('projectName', action='store',
    help='Set name of project')
argparser.add_argument('jobName', action='store',
    help= ('Set name of job. Accepts a list '
    'of names for batch modes'))
argparser.add_argument('stepName', action='store', help=
    ('Set name of Step. Accepts a list '
    'of name for batch modes'))

argparser.add_argument('--new', '-n', action='store_true', default=False,
    help='Creates inputfile files from options selected')
argparser.add_argument('--submit', '-s', action='store_true', default=False,
```

```

        help= ('Creates pbsfile and submits'
              'job to queue. Batch mode'))
    argparser.add_argument('--analyse', '-a', action='store_true',
                           default=False, help= ('Creates pbsfile and submits '
                                                  'job to queue. Batch mode'))
    argparser.add_argument('--reaction', '-re', action='store_true', default=False,
                           help=('Calculates reaction thermochem given reaction'
                                  'profile in stepname in form of'
                                  'SM TS Prod1+Prod2'))
    argparser.add_argument('--irc', '-irc', action='store_true', default=False,
                           help='Checks if IRC jobs give correct SM + Prod')

    argparser.add_argument('--fragment', '-fr', action='store',
                           default=None, help= ('Automatically substitute'
                                                  'atom with fragment. pass'
                                                  'as "AtomNo Frag"'))
    argparser.add_argument('--tstate', '-ts', action='store_true',
                           default=False, help= ('Flag to mark job as a '
                                                  'transition state. Default = False'))
    argparser.add_argument('--charge', '-c', action='store',
                           default=confparser.get('default_options','charge'),
                           help= ('Set charge for molecule. Default from config'
                                  'file'), type=int)
    argparser.add_argument('--mult', '-m', action='store',
                           default=confparser.get('default_options', 'mult'),
                           help=('Set multiplicity for molecule. Default'
                                  'from config file'), type=int)
    argparser.add_argument('--basis', '-b', action='store',
                           default=confparser.get('default_options','basis'),
                           help=('Set basis set for calculation. Default'
                                  'from config file'))
    argparser.add_argument('--functional', '-f', action='store',
                           default=confparser.get('default_options','functional'),
                           help=('Set functional for calculation. Default'
                                  'from config file'))
    argparser.add_argument('--xyz', '-x', action='store', help=
        ('Set location to read .xyz file for coordinates.'
         'No default'))
    argparser.add_argument('--symmetry', '-sym', action='store',
                           default=confparser.get('default_options','sym'),
                           help=('Molecular point group. Default'
                                  'from config file'))
    argparser.add_argument('--pcm', '-p', action='store', default=None, help=
        ('Set PCM solvent simulation on and select solvent.'
         'Default = false'))
    argparser.add_argument('--type', '-t', action='store', default='OPT',
                           choices=('OPT', 'FREQ', 'IRC'), help=('Set type of job, '
                                                                  'currently supported'
                                                                  'OPT and FREQ.'
                                                                  'Default = OPT'))
    argparser.add_argument('--engine', '-e', action='store',
                           default=confparser.get('default_options','engine'),
                           choices=('GAU','GAMESS'), help=('Set which quantum '
                                                             'chemistry packake to '
                                                             'use for calculation. '
                                                             'Default from config '
                                                             'file'))

    argparser.add_argument('--walltime', '-w', action='store',
                           default=confparser.get('default_options','walltime'),
                           help=('Set max allowed excution time. Default '
                                  'from config file'))
    argparser.add_argument('--nodes', '-no', action='store',
                           default=confparser.get('default_options','nodes'),
                           help=('Set number of nodes to be used.'
                                  'Default from config file'))
    argparser.add_argument('--cpus', '-cp', action='store',
                           default=confparser.get('default_options','cpus'),
                           help=('Set number of cpus per node. Default '
                                  'from config file'))
    argparser.add_argument('--ram', '-r', action='store',

```

```

        default=confparser.get('default_options','ram'),
        help=('Set amount of ram per node. Default'
              'from config file'))
    argparser.add_argument('--queue', '-q', action='store',
        default=confparser.get('default_options','queue'),
        help='Set queue for job. Default from config file')

args = argparser.parse_args()

#Call subroutines for making Gaussian new jobs
if args.new is True:
    if args.engine == 'GAU':
        try:
            if args.fragment is not None:
                j = classes.gau_step(args.projectName, args.jobName, args.stepName,
                    ts=args.tstate,charge=args.charge,
                    mult=args.mult,xyz=args.xyz,
                    fragatom=args.fragment.split()[0],
                    frag=args.fragment.split()[1] )
            else:
                j = classes.gau_step(args.projectName, args.jobName, args.stepName,
                    ts=args.tstate,charge=args.charge,
                    mult=args.mult,xyz=args.xyz)
        except IOError, error:
            exit("IOError: %s for job %s-%s-%s" % (error, args.projectName, args.jobName, args.stepName))
        try:
            j.write_inputfile(args.basis, args.functional, args.nodes,
                args.cpus, args.ram, args.pcm, args.type)
            print 'Wrote inputfile for: %s-%s-%s' % (args.projectName, args.jobName, args.stepName)
        except IOError, error:
            exit("IOError: %s for job %s-%s-%s" % (error, args.projectName, args.jobName, args.stepName))
    elif args.engine == 'GAMESS':
        try:
            if args.fragment is not None:
                j = classes.gamess_step(args.projectName, args.jobName, args.stepName,
                    ts=args.tstate,charge=args.charge,
                    mult=args.mult,xyz=args.xyz,
                    fragatom=args.fragment.split()[0],
                    frag=args.fragment.split()[1] )
            else:
                j = classes.gamess_step(args.projectName, args.jobName, args.stepName,
                    ts=args.tstate,charge=args.charge,
                    mult=args.mult,xyz=args.xyz)
        except IOError, error:
            exit("IOError: %s for job %s-%s-%s" % (error, args.projectName, args.jobName, args.stepName))
        try:
            j.write_inputfile(args.basis, args.functional, args.nodes,
                args.cpus, args.ram, args.pcm, args.type,
                args.symmetry)
            print 'Wrote inputfile for: %s-%s-%s' % (args.projectName, args.jobName, args.stepName)
        except IOError, error:
            exit("IOError: %s for job %s-%s-%s" % (error, args.projectName, args.jobName, args.stepName))

#Call subroutines for sumbitting jobs
if args.submit is True:
    for job in args.jobName.split():
        for step in args.stepName.split():
            if args.engine == 'GAU':
                j = classes.gau_step(args.projectName, job, step)
            elif args.engine == 'GAMESS':
                j = classes.gamess_step(args.projectName, job, step)
            try:
                j.write_pbsfile(args.walltime, args.nodes,
                    args.cpus, args.queue)
            except IOError, error:
                exit("IOError: %s for job %s-%s-%s" % (error, args.projectName, job, step))
            j.submit_job()

#Call subroutines for Analysing job
if args.analyse is True:
    for job in args.jobName.split():

```

```

for step in args.stepName.split():
    if args.engine == 'GAU':
        j = classes.gau_step(args.projectName, job, step)
    elif args.engine == 'GAMESS':
        j = classes.gamess_step(args.projectName, job, step)
    try:
        j.analyse_job()
        print j
    except IOError, error:
        exit("IOError: %s for job %s-%s-%s" % (error, args.projectName, job, step))

#Call subroutines for calculating reaction parmeters
if args.reaction is True:
    print 'Project: %s' % args.projectName
    print 'Reaction %s' % args.stepName
    print
    for job in args.jobName.split():
        enthalpies = []
        print 'Substitution: %s' % job
        print
        for step in args.stepName.split('=>'): #Makes a list of anthaplies
            step = step.strip()
            jobs = []
            for sub in step.split('+'):
                sub = sub.strip()
                if args.engine == 'GAU':
                    jobs.append(classes.gau_step(args.projectName, job, sub))
                elif args.engine == 'GAMESS':
                    jobs.append(classes.gamess_step(args.projectName, job, sub))
            try:
                jobs[-1].analyse_job()
            except IOError, error:
                exit("IOError: %s for job %s-%s-%s" % (error, args.projectName, job, sub))
            try:
                enthalpies.append(sum(a.enthalpy for a in jobs))
            except AttributeError:
                exit("AttributeError: Missing Enthalpy for job %s-%s-%s" % (a.projectName, a.jobName, a.stepName))

        activation = []
        reaction = []
        total_reaction = 0
        for count in xrange(0, len(enthalpies)-2, 2):#calcautes thermochem
            activation.append(enthalpies[count+1] - enthalpies[count])
            reaction.append(enthalpies[count+2] - enthalpies[count])
        total_reaction = enthalpies[-1] - enthalpies[0]

        for count in xrange(len(activation)):#outputs therochem
            if len(activation) > 1:
                print "Reaction Number: %d" % (count+1,)
                print "\tActivation energy = %f kcal mol-1" % (float(activation[count])*float(627.509),)
                print "\tReaction enthalpy = %f kcal mol-1" % (float(reaction[count])*float(627.509),)
                print
            if len(activation) > 1:
                print "Total reaction enthalpy = %f kcal mol-1" % (float(total_reaction)*float(627.509),)
                print
logging.info('Finished')

if args.irc is True:
    jobs = []
    for job in args.jobName.split():
        for step in args.stepName.split():
            if args.engine == 'GAU':
                jobs.append(classes.gau_step(args.projectName, job, step))
            elif args.engine == 'GAMESS':
                jobs.append(classes.gamess_step(args.projectName, job, step))
        try:
            jobs[-1].analyse_job()
        except IOError, error:
            exit("IOError: %s for job %s-%s-%s" % (error, args.projectName, job, step))
    print "Optimized Starting Material Coordinates"
    print jobs[0].format_coords(jobs[0].mol)

```

```

        print "IRC Starting Material Coordinates"
        print jobs[1].format_coords(jobs[1].irccoords[0])
        print
        print "Optimized Product Coordinates"
        print jobs[2].format_coords(jobs[2].mol)
        print "IRC Product Coordinates"
        print jobs[1].format_coords(jobs[1].irccoords[-1])

#run if not being imported
if __name__ == '__main__':
    main()

```

CLASSES.PY

```

#!/usr/bin/python
from ConfigParser import SafeConfigParser
from string import Template
import logging
import os
import re
import math
import subprocess
import cclib
import pybel
import openbabel
import numpy

class project(object):
    """Superclass for projects

    Currently holds projectName and makes folder if required
    Attributes:
        projectName: A string holding the project name
    """

    def __init__(self,name):
        """Makes project superclass
        Makes folder is required"""
        self.projectName = name
        try:
            os.makedirs(os.path.join('jobs',self.projectName))
            self.exists = True
        except OSError:
            self.exists = True

class job(project):
    """Superclass for jobs inherits from project superclass

    Currently holds jobName and makes folder if required
    Attributes:
        jobsName: A string holding the job name
    """

    def __init__(self,name,projectName):
        """Job Class: subclass of project
        makes job folder if required
        """
        super(job, self).__init__(projectName)
        self.jobName = name
        try:
            os.makedirs(os.path.join('jobs',self.projectName,self.jobName))
            self.exists = True
        except OSError:
            self.exists = True

class step(job):

```

```

"""Superclass for step inherits from job superclass
Holds methods independant of engine choice and calculation
paramaters. Methods include analyse_job (calls cclib to extract data from
outputfiles), remove_pbsfile (deletes old pbs file), submit_job (calls qsub
with pbf file), make_xyz (returns a list of coords given xyz file),
find_h_spheres (finds H atoms not within 1.2 angstroms from a heavy atom
for pcm)
Attributes:
stepName: A string for holding step name
ts: A booleanfor holding transition state data
charge: An int holding charge for calculation
mult: An int holding mutiplicity for calculation
xyz: A file handler for an xyz file in read mode
coords: A list of lists holding coordinates
h_spheres: A list of ints holding atom numbers for H atoms
            needing H spheres in PCM model
energy: A float holding SCF energy
enthalpy: A float holding enthalpy
freeenergy: A float holding gibbs free energy
entropy: A float holding entropy
"""

def __init__(self, projectName, jobName, stepName, **kwargs):
    """Init method for step superclass, many attributes are made here.

    Makes attributes, calling engine specific methods where needed. There
    should definitely be some checking here that subclasses correctly
    implement the methods that will be used here! Also makes step folder if
    needed

    Attributes:
    projectName: String for project name
                  (passed up to project superclass)
    jobName: String for job name (passed up to job superclass)
    stepName: A string for holding step name
    **ts: A boolean for holding transition state data
    **charge: An int holding charge for calculation
    **mult: An int holding mutiplicity for calculation
    **xyz: A file handler for an xyz file in read mode
    **fragatom: An int holding atom number to be subsituted
    **frag: A string holding fragment name
    """
    super(step, self).__init__(jobName, projectName)

    self.stepName = stepName

    logging.debug("starting init:- %s-%s-%s"
                  % (self.projectName,self.jobName,self.stepName))

    if 'ts' in kwargs:
        self.ts = kwargs.get('ts')
        logging.debug('ts is %s' % self.ts)
    if 'charge' in kwargs:
        self.charge = int(kwargs.get('charge'))
        logging.debug('charge is %s' % self.charge)
    if 'mult' in kwargs:
        self.mult = int(kwargs.get('mult'))
        logging.debug('mult is %s' % self.mult)
    if 'xyz' in kwargs:
        self.mol = self.make_xyz(kwargs.get('xyz'))
    if 'fragatom' in kwargs and 'frag' in kwargs:
        self.mol = self.replace_atom_by_frag(self.mol, kwargs.get('fragatom'), kwargs.get('frag'))
    self.h_spheres = self.find_h_spheres()

    logging.debug('h_spheres is %s' % self.h_spheres)

    try:
        os.makedirs(os.path.join('jobs', self.projectName,
                                  self.jobName, self.stepName, 'checkpoint'))
        logging.debug('Step does not exisit, creating folder')

```



```

        self.exists = True
    except OSError:
        self.exists = True

    logging.debug('finished init: - %s-%s-%s'
                  % (self.projectName,self.jobName,self.stepName))

def __del__(self):
    """Log job name when removing object"""
    logging.debug("Removing step object %s-%s-%s"
                  % (self.projectName, self.jobName, self.stepName))

def __str__(self):
    """Return basic info as string representation of step"""
    lines = []
    lines.append("Job: %s-%s-%s"
                  % (self.projectName,self.jobName,self.stepName))
    if hasattr(self, 'converged'):
        lines.append('CONVERGED')
    if hasattr(self, 'mol'):
        geom = self.format_coords(self.mol)
        lines.append("Coordinates:")
        lines.append(geom)
    if hasattr(self, 'freeenergy'):
        lines.append("Free energy = %f kcal mol-1" % self.freeenergy)
    if hasattr(self, 'enthalpy'):
        lines.append('Enthalpy = %f kcal mol-1' % self.enthalpy)
    if hasattr(self, 'entropy'):
        lines.append('Entropy = %f cal/mol-K' % (self.entropy*1000,))
    if hasattr(self, 'temperature'):
        lines.append('Calculated at %f K' % self.temperature)
    lines.append(' ')
    lines.append(' ')
    return "\n".join(lines)

def replace_atom_by_frag(self, mol, atomno, frag):
    """Replaces a given atom with a given fragment"""

    t = cclib.parser.utils.PeriodicTable()
    atom = [x for x in mol if x.idx == int(atomno)]
    neighbour = [x for x in openbabel.OBAtomAtomIter(atom[0].OBAtom)][0]
    bond = [x for x in openbabel.OBAtomBondIter(atom[0].OBAtom)][0]

    if frag == "CH3":
        atom[0].OBAtom.HtoMethyl()

    elif frag in ('F', 'Cl', 'Br', 'I'):
        atom[0].OBAtom.SetAtomicNum(t.number[frag])
        bond.SetLength(neighbour, bond.GetEquibLength())

    else:
        mol.OBMol.DeleteAtom(atom[0].OBAtom)
        with open('conf/frags/%s.def' % frag, 'r') as def_file:
            new_atoms = []
            count = 0
            for line in def_file:
                split = line.split()
                new_atoms.append(mol.OBMol.NewAtom())
                new_atoms[-1].SetAtomicNum(t.number[split[0]])
                new_atoms[-1].SetVector(float(split[1]), float(split[2]), float(split[3]))
                if count > 0:
                    mol.OBMol.AddBond(new_atoms[-2].GetIdx(), new_atoms[-1].GetIdx(), 1)
                count += 1
            openbabel.OBBUILDER.Connect(mol.OBMol, neighbour.GetIdx(),new_atoms[0].GetIdx())

    return mol

def analyse_job(self):
    """Method for extracting useful data from output files

```

Uses an external module, cclib, for the parsing of outfile. More info about cclib can be found at http://sourceforge.net/apps/mediawiki/cclib/index.php?title=Main_Page Currently modded version of cclib is required to extract thermochemistry data, however hopefully this is be included in the trunk soon. This method will extract optimised coordinates from finished jobs, and final coordinates from jobs that do not seem to have finished correctly, they are stored in coords (an engine specific formatted string). Also extracts thermochemistry data from freq calculations for use in calculating reaction paramaters.

Attributes:

coords: A string of engine specific formatted coordinates
 energy: A float holding SCF energy
 enthalpy: A float holding enthalpy
 freeenergy: A float holding gibbs free energy
 entropy: A float holding entropy

Returns:

True if no failues occur

Throws:

IOError: Cant open outfile with cclib

"""

try:

```
outfile = cclib.parser.clopen(os.path.join(os.getcwd(), 'jobs',
                                          self.projectName, self.jobName,
                                          self.stepName, '%s-%s-%s.out'
                                          % (self.projectName,
                                             self.jobName,
                                             self.stepName)))
```

```
outfile.logger.setLevel(logging.ERROR)
```

```
data=outfile.parse()
```

except (IOError, AttributeError):

```
e = 'Job: %s %s %s' % (self.projectName, self.jobName, self.stepName)
```

```
raise IOError, e
```

final = None

self.converged = False

if (hasattr(data,'geovalues') and hasattr(data,'geotargets'))

and hasattr(data,'atomnos')):

```
final = 0
```

```
count = 0
```

```
t = cclib.parser.utils.PeriodicTable()
```

```
#look for converged step (final)
```

```
for step in data.geovalues:
```

```
if all(a < b for (a,b) in zip(step,data.geotargets)):
```

```
self.converged = True
```

```
final=count
```

```
count += 1
```

```
#gets converged geom or final (should be same for complete jobs)
```

```
if self.converged is True:
```

```
self.mol = pybel.Molecule(cclib.bridge.makeopenbabel(data.atomcoords[final-1], data.atomnos, charge = data.charge,
mult = data.mult))
```

```
else:
```

```
self.mol = pybel.Molecule(cclib.bridge.makeopenbabel(data.atomcoords[-1], data.atomnos, charge = data.charge,
mult = data.mult))
```

if hasattr(data,'scfenergies') and self.converged is True:

```
self.energy = data.scfenergies[final]
```

```
logging.debug("extracted converged scf: -%s-%s-%s"
```

```
% (self.projectName,self.jobName,self.stepName))
```

elif hasattr(data,'scfenergies'):

```
self.energy = data.scfenergies[-1]
```

```
logging.debug("extracted finial scf: -%s-%s-%s"
```

```
% (self.projectName,self.jobName,self.stepName))
```

```
#gets thermochemistry
```

```
if hasattr(data, 'enthalpy'):
```

```
self.enthalpy = data.enthalpy
```

```
logging.debug("extracted enthalpy: -%s-%s-%s"
```

```

        % (self.projectName,self.jobName,self.stepName))
if hasattr(data, 'freeenergy'):
    self.freeenergy = data.freeenergy
    logging.debug("extracted free energy: -%s-%s-%s"
        % (self.projectName,self.jobName,self.stepName))
if hasattr(data, 'entropy'):
    self.entropy = data.entropy
    logging.debug("extracted entropy: -%s-%s-%s"
        % (self.projectName,self.jobName,self.stepName))
if hasattr(data, 'temperature'):
    self.temperature = data.temperature
    logging.debug("extracted temp: -%s-%s-%s"
        % (self.projectName,self.jobName,self.stepName))

if hasattr(data, 'irccoords'):
    self.irccoords = []
    for geom in data.irccoords:
        self.irccoords.append(pybel.Molecule(cclib.bridge.makeopenbabel(geom, data.atomnos, charge = data.charge, mult =
data.mult)))
if hasattr(data, 'ircenergies'):
    self.ircenergies = data.ircenergies
if hasattr(data, 'rxcoord'):
    self.rxcoord = data.rxcoord

return True

def submit_job(self):
    """Submit job using pbs file

    calls qsub to submit job to PBS.Should return success boolean and throw
    relevant exceptions"""

    pbsfile = '%s-%s-%s.pbs' % (
        self.projectName, self.jobName, self.stepName)
    wdir = os.path.join(os.getcwd(), 'jobs', self.projectName, self.jobName, self.stepName)
    subprocess.call(['qsub', pbsfile], cwd=wdir)
    logging.debug("pbsfile: %s \n wdir: %s" % (pbsfile, wdir))

def make_xyz(self, cfile):
    """return a pybel molecule from a filename string

    Takes a string (passed as a command line argument) holding a filename. This file
    has to be either an .xyz or .mdl file (extension matters). The file is parsed by
    openbabel to extract the first molecule in the file.
    Can also take ".job" is a virtual file that references previous jobs. The respective output
    files are parsed for geometries and were possible an optimised geometry is used, otherwise
    the final geometry is used
    Returns:
        firstmol: A pybel molecule
    Throws:
        IOError: Cant read given file"""
    if ".xyz" in cfile:
        try:
            firstmol = pybel.readfile('xyz',cfile).next()
            return firstmol
        except IOError:
            error = "Cant open .xyz file"
            raise IOError, error
    elif '.mdl' in cfile:
        try:
            firstmol = pybel.readfile('mdl',cfile).next()
            return firstmol
        except IOError:
            error = "Cant open .mdl file"
            raise IOError, error
    elif '.job' in cfile:
        names = cfile[:-4].split('-')
        j = step(names[0],names[1], names[2])
        try:

```

```

        j.analyse_job()
        firstmol = j.mol
        return firstmol
    except IOError:
        error = "Cant open .job output file for analysis"
        raise IOError, error
    else:
        error = "File type not supported currently"
        raise IOError, error

def make_distance_matrix(self, mol):
    """Takes pybel molecule and makes a complete distance matrix"""
    i = 0
    j = 0
    output = numpy.empty((len(mol.atoms), len(mol.atoms)))
    for atomi in mol:
        for atomj in mol:
            distance = math.sqrt( math.pow(atomi.coords[0]-atomj.coords[0],2) +
                                   math.pow(atomi.coords[1]-atomj.coords[1],2) +
                                   math.pow(atomi.coords[2]-atomj.coords[2],2))
            output[i,j] = distance
            output[j,i] = distance
            j += 1
        i += 1
        j = 0
    return output

def find_h_spheres(self):
    """Make list of H atoms needing pcm spheres

    Takes an openbabel molecule and finds H atoms that are over
    the threshold define in the conf file away from a heavy atom
    This is used to produce a list of H atoms that will require PCM
    spheres added in g03"""

    spheres = []
    #Loops over H atoms
    for Hatom in self.mol:
        lowest = 1000
        if Hatom.atomicnum == 1:
            for heavyatom in self.mol:
                if heavyatom.atomicnum != 1:
                    distance = math.sqrt( math.pow(Hatom.coords[0]-heavyatom.coords[0],2) +
                                           math.pow(Hatom.coords[1]-heavyatom.coords[1],2) +
                                           math.pow(Hatom.coords[2]-heavyatom.coords[2],2))
                    lowest = min(lowest, distance)
            if lowest > 1.15:
                #adds H atoms further than threshold to list for H spheres
                spheres.append(Hatom.idx)

    return spheres

class gau_step(step):
    """Class for Gaussian steps: subclass of step.

    Specific details on how to write gaussian inputfiles and pbs files

    Methods implemented:
    write_inputfile (generates input file based on definition file)
    write_pbsfile (generates pbs file based on definition file)
    format_coords (formats a pybel molecule to a gaussian formatted string)
    """

    def __init__(self, projectName, jobName, stepName, **kwargs):
        """Makes gaussian step class
        most initiation done in superclass"""
        super(gau_step, self).__init__(projectName, jobName, stepName, **kwargs)
        logging.debug("Making gaussian-step object %s" % self.jobName)
        logging.debug("Full gaussian step name %s-%s-%s"
                      % (self.projectName, self.jobName, self.stepName))

```

```

def write_inputfile(self, basis, functional, nodes, cpus, ram, pcm, type):
    """Writes gaussian specific input files.

    Checks for exisitance of input file and fails if exists otherwise writes
    a gaussian specific inputfile to the relevant location based on the
    definition file and args passed
    Args:
        basis: Set basis set for calculation. Default from config file
        functional: Set functional for calculation. Default from config file
        nodes: Set number of nodes to be used. Default from config file
        cpus: Set number of cpus per node. Default from config file
        ram: Set amount of ram per node. Default from config file
        pcm: Set PCM simulation on and select solvent. Deafult = false
        type: Set type of job, currently allowed OPT and FREQ. Default = OPT
    """

    # handles pcm models and any spheres that need adding on H atoms
    if pcm is None:
        pcm_string = ""
        sphere_string = ""
    else:
        pcm_string = 'SCRF=(PCM, SOLVENT=%s)' % pcm
        sphere_string = ""
        if len(self.h_spheres) > 0:
            pcm_string = 'SCRF=(PCM, SOLVENT=%s, READ)' % pcm
            sphere_string = 'sphereonh = '
            for atoms in self.h_spheres:
                sphere_string = sphere_string + "%d ," % atoms
            sphere_string = sphere_string[:-2]

    #Implement more job types here
    if type == 'OPT':
        type_string = 'OPT FREQ'
        if self.ts is True:
            type_string = 'OPT=(CalcFC, TS, NOEIGEN) FREQ'
    if type == 'FREQ':
        type_string = 'FREQ'
    if type == 'IRC':
        type_string = 'IRC=(CalcFC, MaxPoints=10)'

    #open job and definition file
    with open(os.path.join('jobs', self.projectName, self.jobName, self.stepName,
        '%s-%s-%s.inp' % (self.projectName, self.jobName,
            self.stepName)), "w") as inputfile:
        with open('conf/gaussian_input.def', 'r') as def_file:
            content = def_file.read()

            #This is where template definition is held
            d = dict(projectName = self.projectName, jobName = self.jobName,
                stepName = self.stepName, nodes = nodes, cpus = cpus,
                ram = ram, functional = functional, basis = basis,
                PCM = pcm_string, type = type_string, charge = self.charge,
                mult = self.mult, xyz = self.format_coords(self.mol),
                sphere_string = sphere_string)
            inputfile.write(Template(content).safe_substitute(d))

def write_pbsfile(self, walltime, nodes, cpus, queue):
    """Writes gaussian specific pbs files.

    Checks for exisitance of pbs file and fails if exists otherwise writes
    a gaussian specific pbs file to the relevant location based on the
    definition file and args passed
    Args:
        walltime: Set max allowed excution time. Default from config file
        nodes: Set number of nodes to be used. Default from config file
        cpus: Set number of cpus per node. Default from config file
        queue/-q -- Set queue for job. Default from config file
    """

```

```

with open(os.path.join('jobs', self.projectName, self.jobName, self.stepName,
    '%s-%s-%s.pbs' % ( self.projectName, self.jobName, self.stepName)),
    'w') as pbsfile:
    with open('conf/gaussian_pbs.def', 'r') as def_file:
        content = def_file.read()

    #template file definition here
    d = dict(projectName = self.projectName, jobName = self.jobName,
        stepName = self.stepName, nodes = nodes, cpus = cpus,
        walltime = walltime, queue = queue)
    pbsfile.write(Template(content).safe_substitute(d))

def format_coords(self, mol):
    """Produces a Gaussian specific coordinate string

    Takes a openbabel molecule and produces a string specific to
    gaussian input files"""

    formatted = []
    t = cclib.parser.utils.PeriodicTable()
    for atom in mol:
        formatted.append("%s \t %10.5f \t %10.5f \t %10.5f" % (t.element[atom.atomicnum], atom.coords[0], atom.coords[1],
atom.coords[2]))
    return "\n".join(formatted)

class gamess_step(step):
    """Class for Gamess steps: subclass of step.

    Specific details on how to write gaussian inputfiles and pbs files

    Methods implemented:
    write_inputfile (generates input file based on definition file)
    write_pbsfile (generates pbs file based on definition file)
    format_coords (formats a pybel molecule to a gaussian formatted string)
    """

    def __init__(self, projectName, jobName, stepName, **kwargs):
        """Makes Gamess step class
        most initiation done in superclass"""
        super(gamess_step, self).__init__(projectName, jobName, stepName, **kwargs)
        logging.debug("Making Gamess-step object %s" % self.jobName)
        logging.debug("Full Gamess step name %s-%s-%s"
            % (self.projectName, self.jobName, self.stepName))

    def write_inputfile(self, basis, functional, nodes, cpus, ram, pcm, type, sym):
        """Writes Gamess specific input files.

        Checks for existance of input file and fails if exists otherwise writes
        a Gamess specific inputfile to the relevant location based on the
        definition file and args passed
        Args:
        basis: Set basis set for calculation. Default from config file
        functional: Set functional for calculation. Default from config file
        nodes: Set number of nodes to be used. Default from config file
        cpus: Set number of cpus per node. Default from config file
        ram: Set amount of ram per node. Default from config file
        pcm: Set PCM simulation on and select solvent. Deafult = false
        type: Set type of job, currently allowed OPT and FREQ. Default = OPT
        """

        extras = []

        #Implement more job types here
        if type == 'OPT':
            type_string = 'OPTIMIZE'
            if self.ts is True:
                type_string = 'SADPOINT'
            extras.append('$STATPT HESS=CALC HSEND=.TRUE. $END')

```

```

        else:
            extras.append('$STATPT HSEND=.TRUE. $END')
    if type == 'FREQ':
        type_string = 'HESSIAN'
    if type == 'IRC':
        type_string = 'IRC=(CalcFC, MaxPoints=10)'

    #BASIS sets
    if basis == '6-31G(d,p)':
        basis = "GBASIS=N31 NGAUSS=6 NDFUNC=1 NPFUNC=1"
    if basis == '6-31G':
        basis = "GBASIS=N31 NGAUSS=6"
    if basis == '6-31+G(d,p)':
        basis = "GBASIS=N31 NGAUSS=6 NDFUNC=1 NPFUNC=1 DIFFSP=TRUE"
    if basis == 'STO-3G':
        basis = "GBASIS=STO NGAUSS=3"

    #SCF type
    if int(self.mult) > 1:
        scf = "ROHF"
    else:
        scf = "RHF"

    #Turn ram into mwords
    if ram[-2:] == 'mb':
        ram = int(ram[:-2])/8
    elif ram[-2:] == 'gb':
        ram = (1000*int(ram[:-2]))/8

    if sym.upper() == "DNH 4":
        sym += '\n'
    if len(self.mol.atoms) == 2:
        lastatom = [x for x in self.mol][-1]
        self.mol.OBMol.DeleteAtom(lastatom.OBAtom)

    #open job and definition file
    with open(os.path.join('jobs', self.projectName, self.jobName, self.stepName,
        '%s-%s-%s.inp' % (self.projectName, self.jobName,
            self.stepName)), "w") as inputfile:
        with open('conf/gamess_input.def', 'r') as def_file:
            content = def_file.read()

            #This is where template definition is held
            d = dict(projectName = self.projectName, jobName = self.jobName,
                stepName = self.stepName, ram = ram, functional = functional,
                basis = basis, scf = scf, type = type_string,
                charge = self.charge, extras = "\n".join(extras),
                mult = self.mult, xyz = self.format_coords(self.mol), sym = sym)
            inputfile.write(Template(content).safe_substitute(d))

def write_pbsfile(self, walltime, nodes, cpus, queue):
    """Writes Gamess specific pbs files.

    Checks for existance of pbs file and fails if exists otherwise writes
    a gaussian specific pbs file to the relevant location based on the
    definition file and args passed
    Args:
        walltime: Set max allowed excution time. Default from config file
        nodes: Set number of nodes to be used. Default from config file
        cpus: Set number of cpus per node. Default from config file
        queue/-q -- Set queue for job. Default from config file
    """

    with open(os.path.join('jobs', self.projectName, self.jobName, self.stepName,
        '%s-%s-%s.pbs' % ( self.projectName, self.jobName, self.stepName)),
        "w") as pbsfile:
        with open('conf/gamess_pbs.def', 'r') as def_file:
            content = def_file.read()

```

```

#template file definition here
d = dict(projectName = self.projectName, jobName = self.jobName,
        stepName = self.stepName, nodes = nodes, cpus = cpus,
        walltime = walltime, queue = queue)
pbsfile.write(Template(content).safe_substitute(d))

def format_coords(self, mol):
    """Produces a Gamess specific coordinate string

    Takes a openbabel molecule and produces a string specific to
    gaussian input files"""

    formatted = []
    t = cclib.parser.utils.PeriodicTable()
    for atom in mol:
        formatted.append("%s \t %10.1f \t %10.5f \t %10.5f \t %10.5f" % (t.element[atom.atomicnum], atom.atomicnum,
atom.coords[0], atom.coords[1], atom.coords[2]))
    return "\n".join(formatted)

```